TOWARDS DEVELOPING A VIABLE CIRCUIT FOR BENEFICIATING ULTRAFINE CHROME AND PGM TAILINGS TO RECOVER CHROMITE

NATHAN TOGARA MUDZANAPABWE

STUDENT NUMBER 419893

SUPERVISOR: Prof V. SIBANDA

A thesis submitted to the Faculty of Engineering and the Built Environment, University of the Witwatersrand, Johannesburg, in fulfilment of the requirements for the degree of Doctor of Philosophy (PhD) in the field of Mineral Processing.

May 2025

DECLARATION

I declare that this thesis is my own unaided work. It is being submitted for the Degree of Doctor of Philosophy to the University of the Witwatersrand, Johannesburg. It has not been submitted before for any degree or examination to any other University.

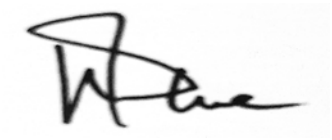

Signature of Candidate

11th day of May 2025

ABSTRACT

Tharisa minerals is one of the operations that generates ultrafine tailings from its Platinum Group Metals (PGM) and chrome spiral recovery circuits that treat Middle Group (MG) chromitites package in the Western limb of the Bushveld Igneous Complex (BIC). The tailings generated by the process at Tharisa had a grind of 80% passing 75µm, of which about 50% was below 25µm. This work therefore aims at investigating the potential to recover chrome from such tailings using different approach. The mineralogical examination performed by TESCAN Integrated Mineral Analyzer (TIMA) an equivalent of Quantitative Evaluation of Minerals by Scanning Electron Microscopy (QEMSCAN), electron probe microanalysis, X-ray diffraction as well as wet chemical assay analysis by Inductively Coupled Plasma Optical Emission Spectroscopy (ICP-OES) revealed that the bulk of the mineral in this feed material contained 9% Cr_2O_3, and the rest of gangue material being SiO_2, Al_2O_3, MgO and CaO. In terms of mineral makeup, the feed material comprised of feldspar accounting for 41.7% of the mass followed by Enstatite-ferrosilite accounting for 29.2% of the mass. Chromite contributed 18% by mass and the balance were minor oxides. The chromite mass percentage increased as the particle size decreased from 106µm to 25µm indicating why conventional gravity equipment would not be effective in recovering this chrome. The degree of liberation of the particles in the feed was found to be 90% on average and the liberation increased as the particle size decreased. In terms of chrome deportment, it was found that chromite mineral is the only source of Cr whereas Fe which is an element making chromite with Cr was contributed by enstatite-ferrosilite, chromite and amphibole minerals.

Bulk samples were used to investigate the effect of process variables on separation capabilities of three unit of separation specifically chosen to recover ultrafine chrome. These units are: (i) a wide radius shallow trough angle M1T53 spiral originally designed for ultrafine feed like coal, (ii) an L300 Wet High Intensity Magnetic Separator (WHIMS) belt magnet of 1.5mx0.3m dimensions fitted with a 1.3mm thick rubber belt rotating over a 9000 Gauss magnet cassette and (iii) a Holman-Wilfley Model 800 laboratory shaking table capable of handling ultrafine feed.

Results from single units' separation tests showed that for optimum recovery and grade attainment, the spiral requires a slurry of density 1.52t/m^3, feed rate of 0.83t/h per start and concentrate cutter position set at 80 mm from the centre pole. The most significant factor among the three factors was concentrate cutter position followed by feed rate. For magnetic

separation, the optimum slurry density was 1.38t/m3 feeding at 0.81 t/h at a belt speed of 0.5m/sec and fluidisation water of 74.4ml/sec. Of these factors, the most significant one was feed-rate followed by fluidisation water. For shaking table separation, the deck angle was the most significant factor, and the operating level was 4°. It was also found that wash water was important in terms of its effect on tailings grade. The optimum slurry density for the shaking table was 1.34t/m^3, feed rate was 500ml/min (0.01428t/h) and wash-water was 140ml/sec per deck.

For full circuit design, results from single unit tests placed the spiral as the first or rougher unit for recovery purposes. The magnet was suitable for lower grade streams hence it was placed as a scavenger of spiral middlings and tailings. The shaking table had the best upgrade as well as highest grades but was poor in mass yield. For these reasons, the shaking table was placed as the last or cleaner unit of the circuit to treat smaller high-grade streams and produce final grade. From this, two complete circuit configurations were set up to compare their effectiveness. The first configuration consisted of the spiral as the first unit producing concentrate of grade 14.41% Cr_2O_3 from a feed of 10.68% Cr_2O_3 with the middlings and tailings assaying 8.97% and 9.31% Cr_2O_3 respectively. The middlings and tailings were processed on the magnet and the magnetic fraction sent to a separate shaking table. The combined final concentrate from separate shaking tables (configuration 1) assayed 40.59%Cr_2O_3 at an overall yield and recovery of 5.81% and 19.01%, respectively.

The second configuration consisted of only two concentration stages, i.e. the spiral separation and shaking table separation of the two size fractions, -25µm and +25µm. These two streams were fed to the spirals separately and the spiral concentrates fed to the shaking table separately. The fine spiral concentrate was processed on the shaking table at lower slurry density of 1.34t/m3 and lower feed rate of 0.150t/h compared to single units shaking table results. The combined final concentrate from the +25 µm and -25 µm circuits assayed 40.07% Cr_2O_3 at a yield and recovery of 7.00% and 29.28%, respectively. The better performance of circuit configuration 2 is due to the treatment of narrow size fractions separately a requirement for most gravity separation processes.

Configuration 2 was chosen as the better circuit for this investigation. The costing of configuration 2 showed that the capital cost would be R718,376,073 with an operating cost of R128,716,294 per annum and annual production of metallurgical chrome of 259,512 tons, the net present value of the project is R2,550.5 million and a payback period of 11 months. From

a technical and economic point of view the chosen circuit is viable and it is a terrific opportunity for the operation that is currently losing this ultrafine material to the Tailings Storage Facility.

PUBLICATIONS

Work is under publication embargo.

DEDICATION

This work is dedicated to my two daughters Takudzwa Gayle and Tavonga Chrissie, who have the privilege of inheriting a good name. This is for you all. I honour and give praise to the Almighty God who predestined this long before the idea came to me.

ACKNOWLEDGEMENTS

I would like to acknowledge the following people without whom this work would not have been possible:

My supervisor, Prof Vusumuzi Sibanda for his solid guidance, and thorough technical rigour during the last few years as we sought to add to the body of metallurgical knowledge. I hope my final offering has done justice to his critical yet balanced feedback, patience, and commitment to seeing the research through.

Mr Hans van Wyk Tharisa Minerals Chief Technical Officer who granted permission, authorised, and subsequently funded the research.

My mentor, Mr Peter Chennells, Managing Director of Arxo Metals who helped develop the scope of this research and continuously provided encouragement and technical insights throughout the research period.

Dr Alan Shemi for selflessly giving of his time, insights, and knowledge in the use of Design Expert software during the planning and analysis phases of my experimental work.

Tharisa Minerals Research and Development team for giving up their weekends to assist with sample collection, preparation, and analysis.

My family who graciously allowed me to monopolise the family study room and, in the process, missed out on many family activities, outings and downtimes believing that this work was for a greater cause. I am grateful for their generosity.

TABLE OF CONTENTS

LIST OF FIGURES

LIST OF TABLES

ABBREVIATIONS/NOMENCLATURE/LIST OF SYMBOLS

ABBREVIATIONS

AACE	American Association of Cost Engineers
ANOVA	Analysis of Variance
BMA	Bulk Mineral Analysis
BPS	Bright Phase Search
BSE	Back scattered electrons
C.V	Coefficient of Variation
CapEx	Capital Expenditure
CRM	Certified Reference Material
DIC	Direct and Indirect Costs
DOE	Design of Experiments
DPC	Direct Plant Costs
EDS	Energy Dispersive Spectroscopy
EDX	Energy Dispersive X-rays
ESD	Equivalent Spherical Diameter
ICP-OES	Inductively couples Plasma Optical Emission Spectroscopy
ICQ	Instrument Quality Control
MG	Middle Group
NPV	Net Present Value
O/F	Overflow
O/S	Oversize
OpEx	Operational Expenditure
PGE	Platinum Group Elements
PGM	Platinum Group Metals
PMA	Particle Map Analysis
PSD	Particle Size Distribution
RD	Relative Density
SEM	Scanning Electron Microscopy
SG	Specific Gravity

TCI	Total Capital Invested
TDC	Total Depreciable Costs
TIMA	TESCAN Integrated Mineral analyser
TSF	Tailings storage facility
U/F	Underflow
U/S	Undersize
UG	Upper group
UP	Upper group
WHIMS	Wet High Intensity Magnetic Separation
XRD	X-ray Diffraction
XRF	X-ray Fluorescents

SYMBOLS

μm	micrometre
α	angle
ρ	particle density
λ	separation parameter
η	fluid viscosity
T	friction parameter
θ	angle of inclination
R^2	Coefficient of determination

CHAPTER 1: INTRODUCTION

1.1 Background

Chromite recovery, whether from primary or secondary sources, has traditionally been accomplished mainly through conventional gravity methods like spiral concentration and jigging. There is, however, a huge amount of chromite that is lost to ultrafine tailings in the chrome concentration industry. This is due to the poor recovery response associated with the methods currently deployed, especially at particle size lower than about 75µm. It is reported that about 25% of the mineral value of chromite is lost as slimes during the processing of many chrome ores (Murthy *et al., 2*011). This potential source of chromite, which sits in many slimes dams and dumps, represents a huge opportunity especially in areas where rich chromite ore is fast dwindling. The main purpose of this study is to investigate several separation techniques, including novel ones, in the processing and recovery of chrome from slimes, to develop an effective process of ultrafine chromite recovery from slimes during the processing of chromite ore. In addition, the success in recovery of ultrafine chromite has an environmental spinoff as it will imminently reduce the slimes dam footprint and lessen the environmental legislation compliance pressure, which the chrome mining businesses are experiencing. The success of this investigation will have an impact on chrome and PGM processing as they both generate excessive amounts of the ultrafine tailings containing chromite.

Currently, the recovery of normal size chromite is done using gravity-based processes, which combine spiral separators, cyclones, and thickeners. This route has however been found to be inefficient when it comes to recovery of the ultrafine size fraction. Das & Sarkar (2018) pointed out that for most conventional gravity separation methods or equipment that use the difference in settling velocity to attain separation, the effectiveness or efficiency decreases as the particle size reduces.

The conventional gravity separators are mostly effective in the recovery of fine to coarse sizes (75 µm to 500 µm). Below 75 µm, the conventional methods do not achieve the intended separations as the fluid viscous forces become dominant relative to the gravity (Bornman *et al,* 2020). In cases where the gravity separation unit has capability to handle the particle size less than 75 µm, i.e. shaking tables, the capacity of these units does not satisfy commercial throughputs. It is the intention of this research to investigate a viable combination of re-designed gravity, centrifugal and magnetic separators in processing ultrafine chrome tailings,

and potentially develop a commercially viable process to effectively concentrate ultrafine chrome. This will effectively open a new opportunity for the exploitation of ultrafine waste material as well as lean ultrafine chromite resources. For the purposes of this research, ultrafine size particles will be defined as anything below 75 μm.

1.2 Problem Statement

The conventional methods of beneficiating chromite from either primary chrome ore sources or from by-product tailings from PGMs processing involves crushing and milling to liberate the value mineral from the gangue. These processes and unit operations invariably introduce overgrinding due to the nature of the chromite mineralogy, indiscriminate methods of comminution as well as increased mechanization (Murthy and Tripathy, 2020). The over-ground material sometimes contains prominent levels of chromite, which eventually report to ultrafine tails/slimes after failure of the conventional processes to recover the chromite contained in the ultrafine size fraction. The conventional methods including spirals, jigs, tables, and hydro cyclones are most effective at coarser particle sizes (>75μm) where gravity forces are still more dominant relative to fluid and viscous forces. In the ultrafine size ranges, these pieces of equipment are rendered ineffective and inefficient to recover the ultrafine chromite. This problem is contributing to the accumulation of ultrafine chromite on the tailings facilities, with environmental implications. The inability of the current mineral processing methods to effectively recover ultrafine chromite also prevents the exploitation of marginal ores and/or refractory ores whose liberation entails reducing the particle size to the ultrafine range. With dwindling chrome resources, there is need for effective and efficient methods to recover ultrafine chromite, and this will create opportunities to exploit marginal ores without running away from unavoidable overgrinding. The aim of this research is to investigate, evaluate and develop commercially viable methods of beneficiating ultrafine chromite fines in the chrome recovery processes.

1.3 Research Objectives

a) To characterise the ultrafine tailings arising from a chrome and Platinum Group Metals (PGMs) beneficiation operations at Tharisa Minerals (Pty) Ltd in terms of mineralogical, physical properties and assay by size.
b) To investigate the influence of feed preparation units such as screens and densifiers on upgrading the ultrafine feed material.

c) To investigate the recovery, grade and yield response of the ultrafine chromite and associated gangue components in the ultrafine tailings on spirals, magnets, shaking table classifiers individually and in permuted combinations using three levels of variables like (i) feed-rate (ii) solid/liquid ratio and (iii) solids concentration, (iv) splitter position and (v) dressing water.
d) To investigate the impact of mineralogical and physical properties of the ultrafine chrome feed material on the processing response parameters such as yield, recovery, and product grade.
e) To establish correlations of processing response parameters such as yield, recovery, and product grade to the process variables for singular separation units and combinations of separation units
f) To develop a high-level economic evaluation of the optimum flow sheet.

1.4 Thesis Layout Flowchart

The following section and flowchart depict the thesis layout as it was executed. The layout of the thesis is divided into three main sections comprising of 9 chapters. The first section is made up of Chapter 1 and Chapter 2.

Chapter 1 presents the background to the motivation for the research, the problem statement and research objectives. To support the chapter 1 in this section is Chapter 2.

Chapter 2 explores and presents the literature available on the beneficiation of ultrafine particles in particular chrome. The literature also covers operation of separation equipment in the recovery of fine chrome from PGM and chrome operations.

The second main section contains three chapters.

Chapter 3 presents the methodology of feed material characterization. The concepts covered are chemical assaying through XRF and ICP-OES, X-Ray diffraction analysis for phase identification, particle size distribution and size by assay analysis. Liberation characteristics and mineral associations as well as grain size distribution is also covered in this chapter.

Chapter 4 presents the results of all the tests covered in chapter 3 and implication of the results on the research questions.

Chapter 5 presents the gravity and magnetic separation equipment test methodology as part of equipment screening for suitability determination. The main pieces of equipment compared are

spirals, magnets and shaking tables. The second part of chapter 5 presents results of the equipment comparison, and the results forms the basis for full circuit design for the recovery of ultrafine chrome.

The last major section is comprised of four sections.

Chapter 6 presents the methodology on how the tested pieces of equipment were arranged to build a full circuit. Chapter 7 presents the results of the full circuit tests in terms of product yield, recovery, product grade as well as waste streams analysis. Chapter 8 is an economic evaluation of the full circuit from a financial feasibility point of view. The project key numbers in determining the viability of the circuit are presented and discussed. Chapter 9 constitute the conclusion and recommendations of the research. The following diagram presents the thesis flow process as described above.

CHAPTER 2: LITERATURE REVIEW

2.1 World Sources of Chrome

In 2008, South Africa, India, Kazakhstan, and Zimbabwe accounted for 70% of the world's production of chromite and in terms of proven resources, South Africa and Zimbabwe hold about 90% of chrome in the world (Murthy *et al*, 2011). It is for this reason that efforts to produce viable solutions for the beneficiation of ultrafine are important for South Africa and Zimbabwe.

2.1.1 Zimbabwean Chrome Sources

Zimbabwe is the only country that exploits both stratiform and podiform deposits. Stratiform deposits occur in parallel seams in large layered igneous rock complexes and extensive bands with little deformation, while podiform deposits occur in highly folded ultramafic peridotites and serpentinites with small pod-shaped bodies characterised by extreme deformation (Murthy *et al*, 2011).

2.1.2 South African Chrome Sources

In South Africa, chrome is hosted in the Bushveld Igneous Complex (BIC), which is a large geological intrusive body within the earth's crust that has been tilted and eroded and now outcrops around what appears to be the edge of a geological basin that is almost 350km long (Steenekamp, 2015). The BIC is divided into eastern, western, and northern lobes, which are sometimes called limbs. The chromite deposits in the BIC occur as stratiform layers of massive chromitite, and the layers of significance are all present in a lower portion of the BIC known as the critical zone. The chrome layers are grouped together in three groups based on their proximity to each other. The Lower Group (LG) consists of seven chromitite layers, the Middle Group (MG) consists of four main chromitite layers and the Upper Group (UG) consists of two chromitite layers (Kinnaird *et al*, 2002). The Merensky reef, which overlays the UG2 layer by some distance, is the uppermost layer of economic interest in the critical zone. The Merensky reef comprises predominantly Pyroxenite, with only a few thin chromite stringers towards its base. The thickness of the individual chromitite layers (LG, MG, and UG) can vary from a few centimetres to well over 2 metres but on average they are in the order of 1 metre thick. There is a general trend to these layers of chrome in relation to depth underneath the surface. The average chrome content and the Cr/Fe ratio of the individual layers decrease upwards while the

PGM content increases in the same direction. The chromitite seam of the Middle Group (MG) contain relative intermediate concentrations for both Chrome and PGE mineralisation, but it displays a general decrease in grain size from the lowermost layers towards the uppermost layers (Steenekamp, 2015). Traditionally, the Lower Group layers have been exploited for chrome production while the Merensky and Upper Groups (UG) have been exploited for PGE. Chrome and PGE concentrations in the Middle Group (MG) have been considered marginal for economic exploitation. In their report, Kinnaird *et al.* (2002) gave the average in-situ chrome content of the three main layers as 46-47% Cr_2O_3, 44-46%Cr_2O_3 and 43%Cr_2O_3 for LG6, MG and UG2 layers, respectively. There are however some deposits where the chrome content for MG can go as low as 18 – 25% Cr_2O_3. In their paper on characterisation of chromite Middle Group seams (Maruli & Nheta, 2020), found that chromite phases in the ore are remarkably similar in all Middle group seam layers. They also determined that the six end-member compositions that combine to form chromite are hercynite ($FeAl_2O_4$), spinel ($MgAl_2O_4$), Fe-chromite ($FeCr_2O_4$), magnesiochromite ($MgCr_2O_4$), magnetite (Fe_3O_4), and magnesioferrite ($MgFe_2O_4$). In terms of particle size, their report showed that particle size of the grains in the ore ranged between 20 to 418µm, with majority being between 150µm and 200µm indicating that the ore can be fairly liberated at 80µm to achieve high % recovery of chromite. The lower end of the grain size (i.e., 20µm) range and the marginal ore deposits with low chrome content and fine grain texture are the ones in which ultrafine generation is encountered to sufficiently liberate the ore for beneficiation.

2.2 Chromite Concentration Methods

The beneficiation of chromite from its parent ore is governed by the exploitation of physical, magnetic, and physico-chemical characteristics of the different mineral components making the ore. The most popular of the methods used is gravity separation that utilises the differences in the density between the value mineral and gangue minerals within the ore.

2.2.1 Common Gravity Separation Methods

Gravity separation relies on the difference in specific gravities of the minerals within an ore matrix. The methods are generally of low capital and operating costs and are also environmentally friendly due to lack of chemicals and excessive heat requirements (Falconer, 2003, Burt, 1999). Agacayak *et al*, (2007) wrote about test-work in which a combination of gravity separation equipment was tested on a low-grade ore in Turkey to beneficiate ultrafine chrome. The simplistic view of gravity separators is based on the principle of a particle

immersed in a fluid, which is either air or liquid. A particle suspended in the fluid experiences forces that determine which way and how fast it moves through the fluid as shown in Figure 2.1 (Drzymala, 2007). F_c is the weight of the particle due to force of gravity g, F_o is the resistance or drag force that the fluid imposes on the particle and F_b is the force of inertia or buoyancy force, and these forces balance when the particle reaches terminal velocity, i.e.

Equation 2.1 $$Fc + Fo + Fb = 0$$

The drag force Fo due to viscous resistance and for a particle of diameter d travelling at a velocity V in a fluid of viscosity η is given as:

Equation 2.2 $$Fo = 3\pi\eta dv$$

$Fo = 3\pi\eta dv$The force of gravity acting on a spherical particle of diameter d is given as

Equation 2.3 $$Fc = {\rho z\pi d\text{^}3g}/{6}$$

Where the $\boldsymbol{\rho}_z$ is the density of the particle.

The buoyance force (which is equivalent to the weight of the displaced fluid) on a particle of diameter d travelling down in a fluid of density $\boldsymbol{\rho}_c$ is given by the formula.

Equation 2.4 $$Fb = {\rho c\pi d\text{^}3g}/{6}$$

where $\boldsymbol{\rho}_c$ is the density of the medium or fluid.

The terminal velocity of the particle is then given as:

Equation 2.5 $$v = \frac{gd^2(\rho z - \rho c)}{18\eta}$$

where η is the fluid viscosity.

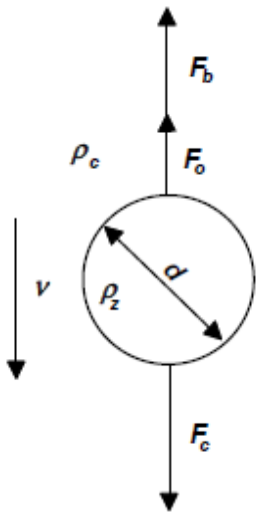

Figure 2.1: Forces acting on a particle settling a medium (Drzymala, 2007)

The separation of two particles in a fluid is based on their difference in settling velocity. Those that settle fast migrate to the bottom and those that settle slower sit on top. The relationship between two mineral particles can be expressed as a ratio between the diameter of particle *a* and particle *b,* and this ratio is called the free-settling ratio (Drzyamala, 2007, Wills and Finch, 2016),

Equation 2.6 $$\frac{da}{db} = ((\rho_b-\rho_f))/((\rho_a-\rho_f))^n$$

where ***da*** is the diameter of particle **a** and ***db*** is the diameter of particle b, while $\boldsymbol{\rho}_a$, $\boldsymbol{\rho}_b$ and $\boldsymbol{\rho}_f$ are the densities of solid particle ***a***, solid particle ***b*** and of fluid *f* respectively.

This ratio determines the susceptibility to separation of the two minerals under consideration.

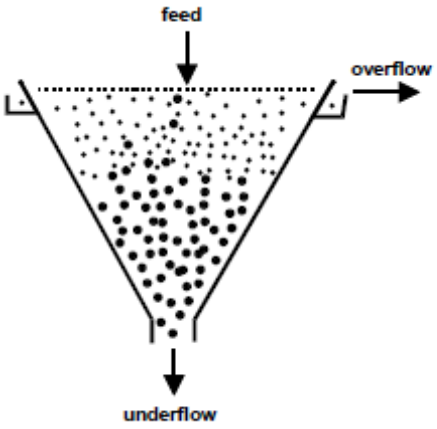

Figure 2.2: Stationary cone classifier (Drzyamala, 2007)

2.2.1.1 Cone Classifier

Figure 2.2 shows an example of a gravity separator called a stationary cone classifier, in which the feed is fed at the top and the heavy particles settle at the bottom while the light particles exit the unit as the overflow with water at the top (Drzyamala, 2007). Wills and Finch (2016) noted that classification by horizontal current action takes place radially from the feed pipe to the overflow lip. They also observed that the main difficulty in operation of such a device is the balancing of the sand discharge and deposition rates; it is virtually impossible to maintain a regular discharge of sand through an open pipe under the influence of gravity.

2.2.1.2 Elutriator

Another example of a gravity separator is an elutriator, which is cylindrical in shape. Water is fed into this separator near the bottom and the slurry enters close to the midpoint of the unit. Particles meet an upward current of water as they are introduced into the separating unit. The lighter particles whose settling velocity is lower than the velocity of rising water current are pushed upwards to the overflow launder, while the heavy particles sink to the bottom and get discharged as the underflow (see Figure 2.3).

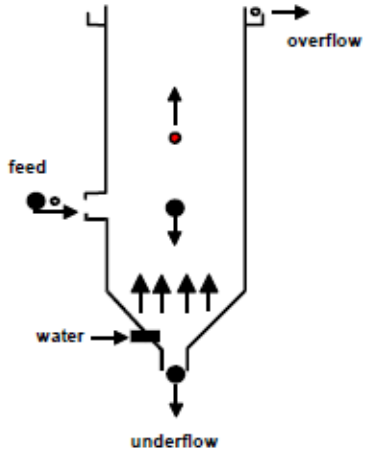

Figure 2.3: Vertical classifier -elutriator (Drzyamala, 2007)

The two separating or classifying units (Stationary cone settler and an Elutriator) represent almost a free-settling scenario when the proportion of solids in the pulp is less than 15%.

Another gravity separation mechanism involves thin stream separation. In the separators that apply this mechanism, separation utilises stratification of particles during movement in a suspension. The stratification can be either vertical (Figure 2.4) or horizontal (Figure 2.5) and the ability for particles to stratify depends on particle properties like size, density, shape and friction between particles and the walls and the shape of the separator (Drzyamala, 2007).

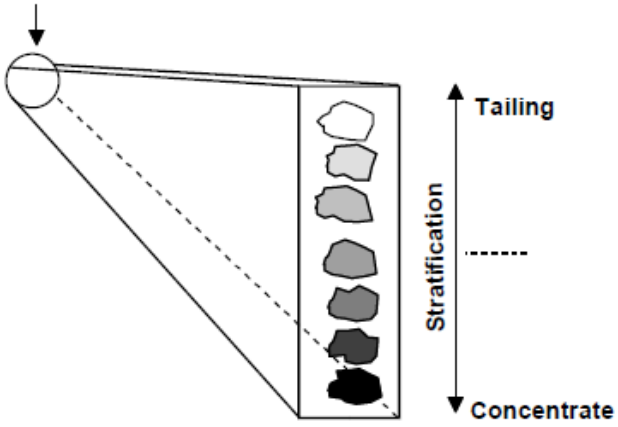

Figure 2.4: Vertical separation (Drzyamala, 2007)

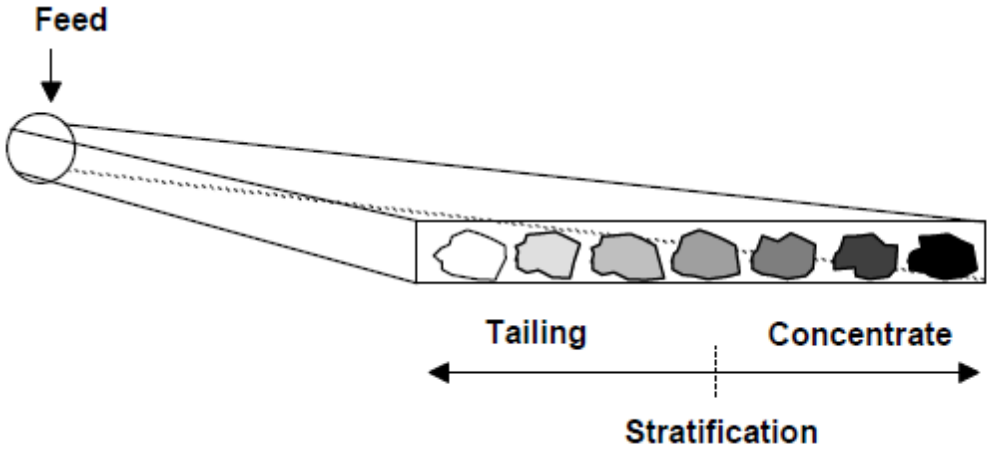

Figure 2.5: Horizontal separation (Drzyamala, 2007)

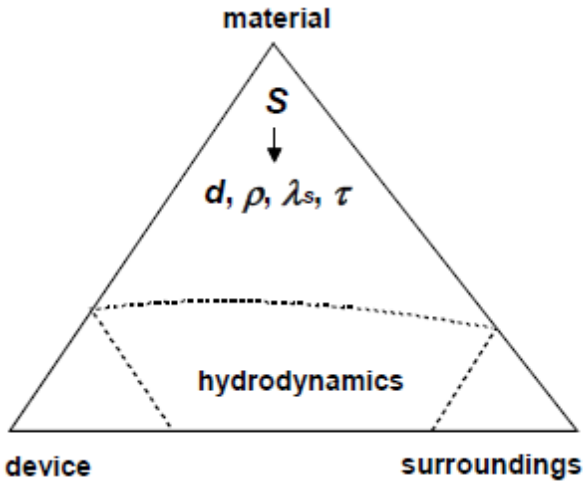

Figure 2.6: Main parameter of separation in a thin layer: S-stratification (Drzyamala, 2007)

The main separation parameter S depends on particle size d, particle density ρ, shape λs and friction against particles and walls of separator τ (Figure 2.6). Separation parameter S together with device and surroundings determine the extent of stratification.

2.2.1.3 Jigging

Jigging is one of the methods that falls under the stratification gravity separation methods. Jig concentrators accomplish the separation of particles based on their specific gravity. A jig is an open tank filled with water and equipped with a horizontal screen in the water bath. At the bottom of the tank is an opening that allows the heavy particles to escape. In jigging, a slurry

with particles of comparable size after crushing and screening is introduced into the water tank, and pulsing of the water is achieved by either a diaphragm or pistons in the tank itself moving relative to the slurry. Upon pulsing, the particles are suspended in the water and as the pulse is cut, the bed collapses and the heavier particles settle on the bed formed on the screen. The settling of the particles is according to the response of each particle to the gravitational energy or force (Brożek and Surowiak, 2007). Those particles with higher specific gravity settle faster than those with lower specific gravity. This results in the separation of particles according to density. The heavy particles will be collected at the bottom while the light particles will be washed by cross-current at the top of the screen bed and collected as either tails or concentrate depending on the density of mineral of value. The jigs can handle a wide particle size range of between 75µm and 10mm, however, with the respective feed into a specific jigging process having a narrow particle size range.

The main advantage of jigs is their ability to separate coarse particles effectively, thus reducing the need for fine grinding. Jigs are also open bath machines and that makes it easy to inspect the process and to adjust settings. There are however some notable disadvantages of jigs, which limit their application in gravity separation. Jigs are not suitable for the recovery of fines i.e. < 75µm. The jig screen easily blinds and therefore needs periodic cleaning. One other drawback of jigs is that they require a lot of water per unit ton of material, but this water is easily recoverable. This aspect makes jigs less suitable for water scarce locations (Falconer, 2003).

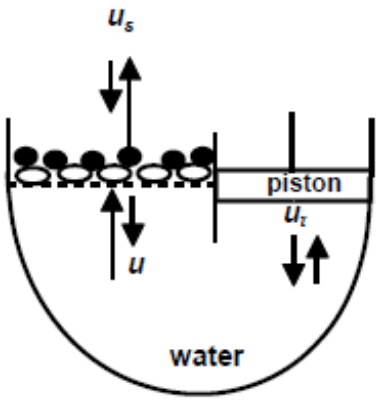

Figure 2.7: Pulsating jig separator (Drzyamala, 2007)

2.2.1.4 Sluice Box

Pinched sluice is another family of gravity separation techniques. It is an inclined slope over which slurry-containing particles of different specific gravity flows. The typical % solids in

sluice slurries should be between 50-60% (Wills and Finch, 2016). Along the plane of the sluice box, segregation occurs due to the gravitational, frictional forces as well as narrowing of the sluicing deck called “pinching.” Heavy particles migrate to the bottom and are taken off through the slots, while light fine particles pass over the slots and discharge at the downstream end. Pinched sluices have an advantage in that the equipment is open for visual inspection, adjustment, and cleaning. It can take slurries of higher density such as 60% solids, resulting in low volume pump requirements. However, the pinched sluices require large space, they have low upgrade ratio of only 3 to 1, they have low recovery of fines and low tolerance to slimes.

2.2.1.5 Spirals Separation

Spirals are among the newer generation of methods that are enjoying widespread application in modern mineral processing establishments. The spiral is an inclined spiralling channel with a complex cross section wrapped around a central column. The heavies will be remarkably close to the central column while the lights are furthest from the central column (Dallaire *et al*, 1978). The middlings are made up of mineral particles whose characteristics are in between the heavies or concentrate and the lights or tailings as shown in Figure 2.8 below. The new generation of spirals were developed in the early 1980s. The construction material for spiral is normally fiberglass and polyurethane, a departure from the original cast iron or rubber tyres. These have modified profiles and concentrate cutters. In most cases, the modified profiles and cutters eliminate the need for wash water in modern day operations.

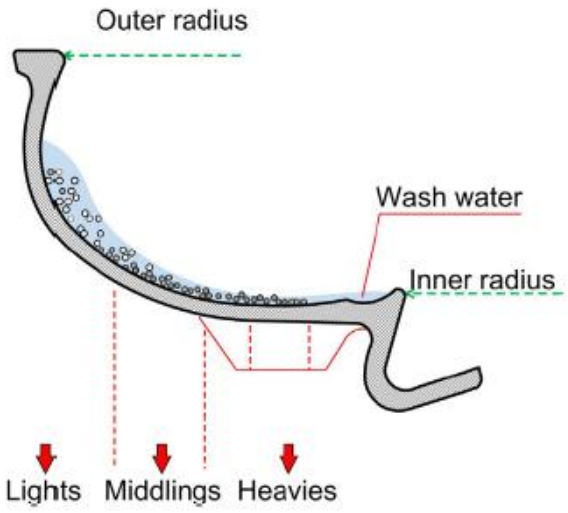

Figure 2.8: Cross section of spiral stream (Wills and Finch, 2016)

To effect separation, there is a combination of gravitational and centrifugal forces acting upon particles of different specific gravities. This combination of gravitational and centrifugal forces produces a secondary flow which is perpendicular to the primary flow, and this pulls heavies from outside along the floor surface of spiral while the lights are lifted from inside to the outside as shown in Figure 2.9. Surkov *et al.* (2008) mentioned that particle motion under the gravitational and centrifugal forces does not depend on particle density alone but also on its size and shape, with large particles being affected more than smaller ones. This causes the fine dense particles to separate from the light particles. These forces together with lower slurry density normally used, produce a greater upgrade ratio of 5 to 1, which is higher compared to other gravity separation methods. Spirals also produce better recovery of fines, making them a more versatile piece of equipment for fines recovery in mineral processing. However, Izerdem and Ergun (2018) contend that spirals are more effective around the 300-micron sizes. When the sizes go down to minus 40 microns the effectiveness of spirals, especially as single recovery units drop significantly. They also found that the upgrade ratio and recovery are higher at coarser particle sizes when size-by-size grade ratios on the concentrate and other products was analysed.

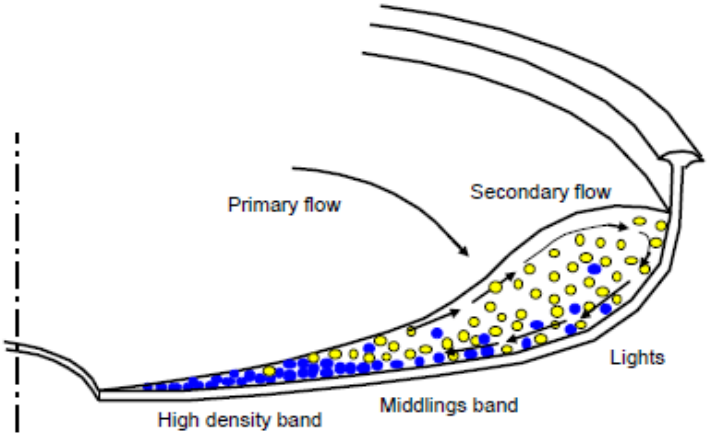

Figure 2.9: Schematic diagram of the primary and secondary flows in a spiral concentrator (Palmer and Vadeikis, 2010)

The forces on the individual particles which gives rise to the flow pattern given in Figure 2.9 is shown in Figure 2.10, which depicts two particles, a heavy and a light one. There are four forces acting on the particle and depending on whether it is heavy or light, the particle's stable position as it rolls down the helix is determined. For a heavy particle, liquid pressure (F_n) forces together with horizontal component of the gravity forces $F_{c(x)}$ is higher than the sum of

horizontal component of the centrifugal force ($F_{o(x)}$) and friction force (F_t). The resultant effect is that the particle moves down the slope towards the inside according to the equations below.

Equation 2.7 $$F_n + F_c(x) > F_t + F_o(x)$$

With the relationship of Equation 2.7 above, the resultant separation force F_w is denoted as

Equation 2.8 $$F_n + F_c(x) > F_t + F_o(x)$$

For the light particle, the opposite is true. Liquid pressure (F_n) forces together with horizontal component of the centrifugal force ($F_{o(x)}$) are higher than the friction force (F_t) together with horizontal component of the gravity forces ($F_{c(x)}$) as depicted by Equation 2.9. The resultant effect is that the lights move up the slope toward the outside until some equilibrium is reached, and the separation occurs following the above balance of forces (Eq. 2.10).

Equation 2.9 $$F_n + F_o(x) > F_t + F_c(x)$$

The resultant force that moves the light particles is represented by Equation 2.10.

Equation 2.10 $$F_n + F_o(x) > F_t + F_c(x)$$

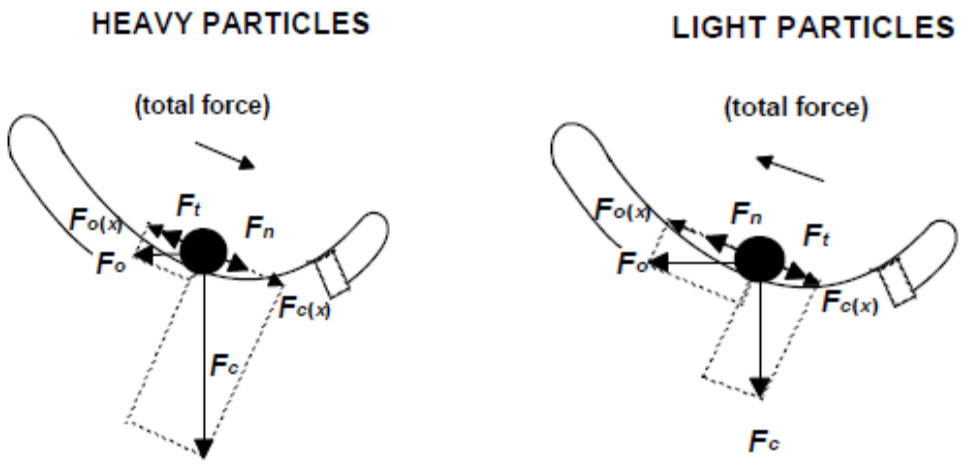

Figure 2.10: Forces effecting a particle in a spiral separator (Drzyamala, 2007).

There is a lot of work done on the utilization of spirals in the beneficiation of fine to ultrafine size particles. De Andrade *et al.* (2014) reported work done on new spiral design (LC3) for coal fines processing as well as for heavy mineral sector. LC3 was developed specifically for

enhancing the separation of ultra fine coal, and recent work has shown that the LC3 model spiral achieves good operational efficiency when beneficiating spiral feed down to 40 microns, resulting in improved plant yield.

The LC3 spiral was developed by Mineral Technologies - A Downer Company for enhancing the separation of ultrafine coal. It has 8 turns with continuously changing trough profiles equipped with 2 slide style reject splitters at turns 4 and 6. It is made in either single, twin, and triple start and the surface is manufactured in a highly wear-resistant polyurethane (De Andreda *et al*, 2014). The process parameters of the LC3 spiral are given in Table 2.1 below.

Table 2.1: Process parameters for the LC3 Mineral Technologies Spiral

Capacity	Up to 3.0 t/h per start (optimal separation at 1.0 to 2.0 t/h/start)
Pulp Density	20 to 40% solids (typically 30 to 35 solids)
Size Range	Particle size range 0.1 – 1.5mm (ideally 0.2 – 1.0mm)
Pulp Volume	Optimal performance 4.0 – 5.0 m^3 /h per start (up to 6.0 m^3 /h)

The operating capacity that extends to fines recovery is opening opportunities in the processing of fine tailings material. The success of the LC3 in the separation of ultrafine coal led to the development of the FM1 by Mineral Technologies, but with focus on the heavy minerals sector. These spirals can handle a pulp density of between 30 to 55% solid content and a feed rate of 0.6 to 2 t/h per single start. The particle size processed can go down as low as 30µm and up to 150µm (De Andrade *et al*, 2014). This spiral was tested in a study at Exxaro Namakwa Sands, (Ramsaywok *et al*, 2010) and it was observed that the performance of spiral is negatively affected by the increasing quantity of slimes that are below 63µm in the feed. It was observed that for every 1% increase in slime content, a 5% reduction is zircon recovery was observed in the process. Kari *et al.* (2006) also observed similar behaviour in the processing of minerals sands with slime during spiral separation test-work. For this reason, it may be prudent to de-slime the feed before feeding onto the spirals but when operating a process aimed at recovery of ultrafine material, chrome de-sliming may result in reduced chrome recovery since the ultrafine fraction in chrome feed is a main contributor to the slimes. Spirals possess some notable advantages over other gravity separation methods.

These advantages include:

- Openness for visual inspection, adjustment, and cleaning.
- High upgrade ratio resulting in fewer stages in circuit.
- Ability to tolerate moderate to large variations in slurry feed density.
- Low footprint when used as triple starts with large diameters.
- Better slimes and oversize tolerance compared to other gravity separation units.
- No wash water required.

These advantages result in spirals being generally preferred over competitor methods and equipment. Spirals do not come without some disadvantages as well. Sivamohan and Forssberg (1985) outlined the principles of spiral concentration. As a flowing film concentration process, spiral separation happens through vertical stratification of the flowing film down the spiral conduit. This vertical stratification is related to sorting processes of hindered settling, interstitial trickling and the attainment of minimum potential energy and Bagnold forces. Through these processes, separation of fine particles take place. They noted that for separation, the following performance characteristics are at play. They noted that velocity of particle flow is determined by pitch of helix while deep angles provide high capacities, grade, and low recovery. Shallow angles are suitable for operations involving small specific gravity difference and fine particle sizes. They also noted that larger diameter spirals are effective in treating fine material. They also noted that maximum recovery of spirals is attained at low federate and high % solids. Szpyrka *et al.* (2017) presented work on the impact of spiral geometrical parameters on the density separation of various fine-grained materials. They compared the performance of three spiral separators; Krebs 2.85, Reichert LD-4 and Reichert LG-7 which had different geometrical parameters such as number of turns, slope of the sluice, width and shape of the sluice, diameter of the spiral number of separating slots and number of product collection boxes. The best performing spiral was Reichert LD-4 because of high number of helixes promoting longer residence time. It also had collection points halfway the height of spiral and this allowed better separation of the remaining material after collection of concentrate mid-way down the spiral.

The following are some of the disadvantages which make spirals not so easy to operate (MacHunter *et al*., 2003; Kohmuench, 2000).

- Relatively high specific gravity cut points (>1.7 SG)
- Relatively low unit throughput
- The need for multi-stage processing

- Limited acceptable feed size range.
- The need for multiple feed points requiring even distribution.
- The use of water at the cleaning stages renders the process a bit expensive.

The variables that affect the performance of a spiral can be divided into two categories as shown in Table 2.2.

Table 2.2: Variables Affecting the Spiral Performance

Design variables	Operating variables
• Spiral diameter • Spiral pitch • Spiral angle • Number of starts • Number of turns • Separating surface material • Number of cutters	• Slurry feed rate • Slurry density • Wash water addition • Cutter position • Feed size distribution

2.2.1.6 Shaking Tables Separation

The shaking tables are a group of gravity separating units that utilises the impact of various forces on the particles to be separated. In principle, the particles are subjected to three main forces, namely gravity, table thrust and slurry flow. Fitzpatrick *et al.* (2016) summarised the variables that affect the performance of a shaking table as shown in Table 2.3.

Table 2.*3*: Variables affecting the shaking table performance (Fitzpatrick, 2016)

Design variables	Operating variables
• Size and shape of deck • Differential acceleration • Riffle pattern • Deck surface characteristics, including roughness	• Pulp feed rate • Pulp density • Wash water addition rate • Cutter position • Stroke frequency and length • Table tilt and end elevation

Ansari (1997) contends that the shaking table provides the best chance of recovery of fine particles because the table has a tilting frame and a small settling zone, both of which are conducive for the recovery of fine particles. On the contrary, though, the mass of the small particle is low and for efficient operation, the separation of minerals of relatively high-density differential is normally limited to particles above 20µm size (Ansari, 1997). This assertion needs testing as the material may behave differently in the presence of clean wash water such as that used in the shaking table after another separation process such as magnetic separation. The principle of operation of a shaking table is governed by the motion of particles of different specific gravity and size moving in a slurry across an inclined table that oscillates backwards and forwards at right angles to the slope (Falconer, 2003). There riffles hold back the particles, which are closest to the deck surface in the process of stratification where particles seek to lower the potential energy (Figure 2.11). With this motion, the fine high specific gravity particles migrate closest to the deck and are discharged at the uppermost part of the deck, while the low specific gravity courser particles move close to the surface of the slurry and ride over the riffles, discharging over the lowest edge of the table. In essence, the riffles act as miniature jigs where there is localized stratification. Shaking table separation process involves *thin film* and *flowing film* concentration mechanisms. In the *thin film* flow mode, the thickness of the flow and the particle size are of similar magnitude, while in the *flowing film* mode the film is much thicker in comparison to the particle size (Burt and Mills, 1984). One of the distinguishing characteristics between *thin film* concentration and *flowing film* is that the rate of shear is relatively low in *thin film* while there is substantial shear in *flowing film*. When considering the beneficiation of ultrafine particles on a shaking table, the mechanism is predominantly *flowing film* since the average particle size will be significantly lower than the slurry flow thickness.

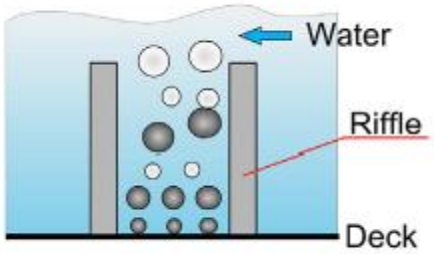

Figure 2.11: Vertical stratification between shaking table riffles (Wills and Finch, 2016)

Considering the self-arrangement of the particles on an incline in a laminar flow slurry, the sequence of the particles is shown in Figure 2.12.

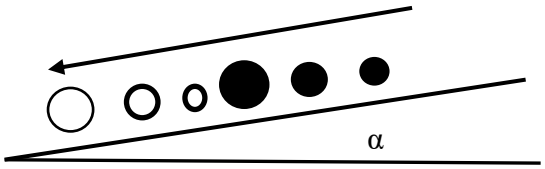

Figure 2.12: Particle arrangement down the shaking table slope (Burt and Mills, 1984)

At the bottom of the slope there will be coarse lights, and, in the middle, coarse heavies mixed with fine lights. At the top there will be fine heavies and in the riffle pocket these will be at the bottom. This sequencing gives rise to the general top view arrangement of the shaking table shown in Figure 2.13 and the product particle profile given in Figure 2.14. Burt and Mills (1984) produced flow and thickness relationships on inclined surfaces. The volume of fluid W is given as;

Equation 2.11 $$W = (\rho s g sin\alpha x^3)/3\eta$$

where W is volume of flow

ρ_s is the fluid density

g is acceleration due to gravity

α is the angle of inclination

η is the fluid dynamic viscosity

x is the thickness of the stream

The thickness x of the stream is given as;

Equation 2.12 $$x = \left(3W/\rho s g sin\alpha\right)^{0.33}$$

These two equations show that x increases with increase in rate of flow at constant slope and increases with decrease of slope angle at constant rate of flow. There is, however, another factor according to Burt and Mills (1984), which determines the separation of mineral particles flowing on an inclined plane. This factor is the critical angle for sliding motion for various minerals and sizes and it gives the minimum angle below which motion by sliding cannot occur.

Depending on the shape characteristics of the particles, there may be rolling instead of sliding. This also depends on where the force is applied on the particle. It is important to pay attention to the shape of the particle as this, to some extent determines the separation potential of two minerals, which may have different shapes due to mineralogical differences.

If the forces are applied at the centre of gravity, rolling will occur before sliding if the coefficient of friction μs exceeds the values shown in Table 2.4.

Table 2.4: Coefficient of friction and resultant movement of various particles of different shapes (Burt and Mills, 1984)

All forces at the Centre of gravity	Motion mode	Slide ←			slide or roll ↔		roll →
	μs	1.732	1.0	0.577	0.414	0.268	0.158
	Shape						
	Sides	3	4	6	8	12	20
Fluid force applied ¾ up	μs	1.20	0.69	0.40	0.29	0.185	0.110
	Motion mode	slide →		slide or roll ↔		roll →	

Particle shape therefore has a considerable influence on the separation efficiency as there may be particles in the slurry which do not roll easily across the deck because they are flat in profile. Even though they may have lower density, these particles will stick to the deck and get carried down to the concentrate discharge. For this reason, characterisation of table feed with respect to particle shape will reveal the particle susceptibility to separation. Similarly, dense spherical particles may also move easily due to rolling and report to tails.

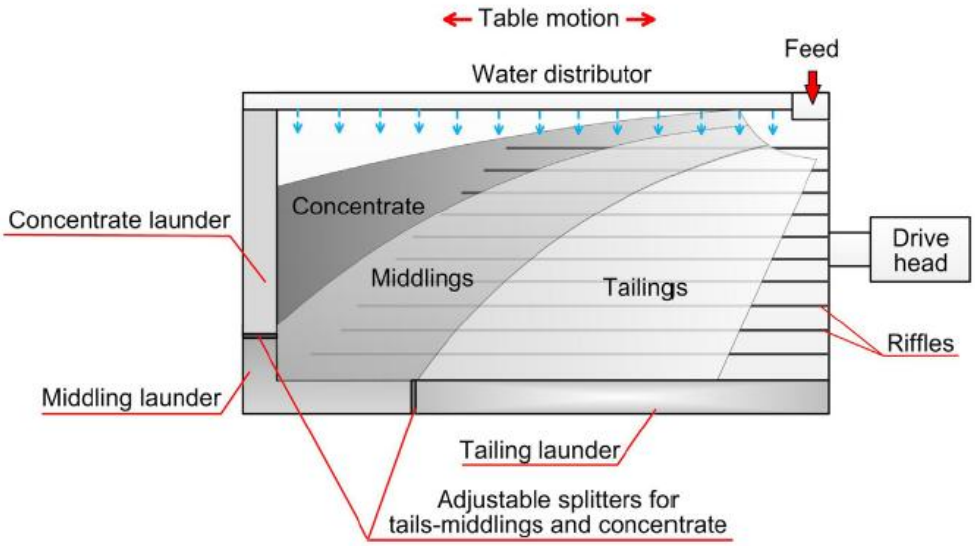

Figure 2.13:Horizontal stratification of the shaking table showing product zones (Wills and Finch, 2016)

The middlings zone in Figure 2.14 may be made up of the particles that behave uncoordinated with other particles of same density due to the shape factor. However, middlings that make the bulk of this zone are due to poor liberation and these particles are identifiable through a mineral liberation analysis.

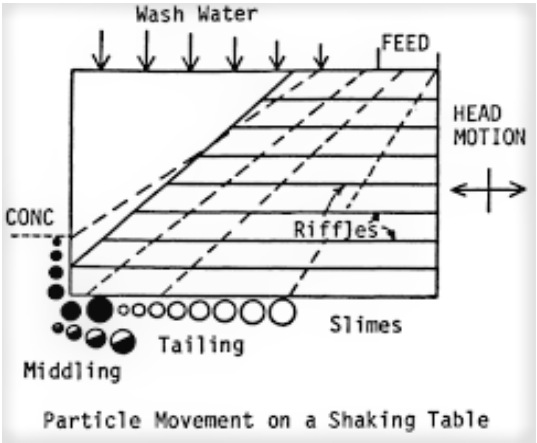

Figure 2.14: Product arrangement on partially riffled shaking table (Burt and Mills, 1984)

Cicek *et al*, (2010) did some work on low-grade chromite ore where a shaking table and a Multi-Gravity Separator (MGS) were used in combination. Finer particles of less than 0.1mm were sent to the MGS while the coarse particles (+0.1mm) were sent to the shaking table. The middling from the shaking table was milled before combining it with MGS feed. A combined

average concentrate grade from both the shaking table and MGS of 50.4% Cr_2O_3 and a combined recovery of 84.7% was realised from an original feed of 9.3% Cr_2O_3.

Makgokgoa (2019) investigated the recovery of chrome from chrome slimes using a shaking table. In the study, slurry density measured as percent solids was varied from 20% to 30%, and the recovery of the chrome to the concentrate was found to increase from about 10% to about 35%. The increase of the slurry density has the effect of slowing down slurry speed over the shaking table and allows for time to effect separation.

2.2.2 Magnetic Separation Methods

Magnetic separation is a method that is used to separate minerals with dissimilar magnetic properties. Generally, minerals are classified as ferromagnetic, paramagnetic, or diamagnetic. The difference between these classes is the strength of response of the minerals to the magnetic field they are subjected to. Since minerals are an assemblage of different constituents with different properties in terms of density, crystal structure as well as magnetic susceptibility, magnetic separation is one of the oldest ways of concentrating minerals based on differing magnetic properties of the constituent components (Dworzanowski, 2010 and Abubakre, 2007). Chromite is one of the minerals that can be separated from gangue by using magnetic separation. Chromite is paramagnetic and as such, it needs slightly higher magnetic field intensity (approximately 8000–15000 Gauss) to separate it from the gangue components.

Magnetic susceptibility is a measure of the magnetic response of a material to an external magnetic field. It has been reported that exceptionally fine particles are often viewed as non-magnetic because they require extremely high magnetic field strength to recover (Dworzanowski, 2010). This is because the magnetic force F acting on a particle is proportional to the sum of mass susceptibility $\boldsymbol{x}$ and particle mass $\boldsymbol{m}$ in a relationship given below.

Equation 2.13 $$F \propto \boldsymbol{x}\, m^3$$

For paramagnetic minerals like chromite, wet magnetic separation is usually used for separation of magnetic minerals from non-magnetic gangue.

2.2.2.1 Competing Forces on particles

During wet magnetic separation process, there are competing forces that act on the particles to effect separation. These are magnetic field forces, gravitational forces and drag forces. In the

slurry, the hydrodynamic forces produce the drag force that is related to slurry velocity and density (Dworzanowski, 2010). As the slurry density increases, the viscosity increases, and this gives rise to entrapment of the non-magnetic particles in magnetic particles and vice-versa. This means that the effect of hydrodynamic force becomes more prominent at higher solids percentage.

There is also another force at play during slurry magnetic separation. This force is called magnetic flocculation, and it is defined as the agglomeration of ferromagnetic particles because of internal magnetic forces. For exceptionally fine particles, the coercive forces are higher than in coarse particles and this causes the fine particles to form aggregates of higher tensile strength than coarser particles. This kind of force introduces a problem whereby the entrapment of magnetic and non-magnetic material affects the separation and hence grade of product. The use of fluidization water alleviates this problem to some extent.

2.2.2.2 Feed Preparation

For wet magnetic separation, four main factors are considered to have an impact on the performance of the separation process. These factors are;

i. Slurry density
ii. Particle size distribution
iii. Proportion of magnetic material in the feed solids
iv. Distribution of slurry to the magnetic separator (effective length of magnetic surface).

In terms of the slurry, the points to consider are volumetric capacity, viscosity, and magnetic flocculation. Low slurry density results in low capacity as well as low magnetic flocculation. On the other hand, higher slurry density increases the viscosity that in turn increases particle entrapment.

2.2.2.3 Feed Particle Size Distribution

In general, the particle size distribution of feed material into separation devices depends on the preceding crushing and milling processes aimed at achieving adequate liberation. Normally the top size of magnetic separation is determined by the need for the particles to pass through the gap between drum and tank without disturbing the collected film. Decreasing the particle size results in the reduction of magnetic susceptibility hence recovery reduction. This means there needs to be a balance of top and bottom size for effective separation using the magnetic method.

Belt magnets are more tolerant to the particle size than drum magnets and the problem of choking the gap is less significant in belt magnets.

2.2.2.4 Proportion of magnetic material in feed solids

The capacity of a magnetic separation process is proportional to the magnetic content in the solids. Ideally, the rougher part of the process demands that the % solids be 30 to 45 % of the slurry, while for the cleaner stages the % solids can go down to 20 to 30 %.

2.3 Challenges of Fine Particle Processing for the Mining Industry

The liberation of the mineral values in the ore body depends on how finely disseminated the mineral value is in the host rock. This invariably results in the generation of ultra fines during liberation which present a problem during processing as ultrafine particles form slimes that are difficult to treat by the methods developed for the coarser fraction. There are two sources of slimes, (i) primary slimes resulting from accumulation of fine mineral values in most of the ore bodies due to weathering and decomposition of certain rock components, and (ii) secondary slimes, which depend on the liberation size, and the natural breakage characteristics of the ore and to some extent on the method of milling used. It is usually the primary slimes that present more problems to the process engineer rather than the secondary slimes (Ansari, 1997). The reason for this difficulty is that in most cases, the primary slimes have been altered significantly (weathering and decomposition of certain rock components) because of climatic changes. In the study of utilisation potential of low-grade chrome ore by Singh *et al.* (2014), it was shown that there is a relationship between percentage liberation of the ore and its particle size. In this work, it was shown that for low grade chrome, the liberation is inversely proportional to particle size. This adds complexity to the efforts of trying to recover fine chrome at the ultrafine sizes especially using gravity methods.

To develop a suitable process technology for recovering metal values from fine size ranges, (Ansari, 1997) produced size classification categories for fine particles.

Fines – particles below 100µm size

Exceptionally fine – particles below 20µm size

Ultra fines – particles less than 5µm size

Colloids – particles less than 1µm size

Super colloids – particles less than 0.2µm size

Each size class has an associated technique or techniques that are more suitable for the recovery of mineral values contained therein (Singh *et al., 2*014). Efforts have been made to determine the effective range of application of conventional mineral process techniques as a function of particle size. It is evident that the upper size is governed by the dominance of gravitational forces, which influences the separation process at course size while the lower size limit is determined by the principles of separation on which the process under consideration operates (Ansari, 1997). As can be seen from Figure 2.15, out of 23 main mineral separation techniques, only six are effective at minus 75µm particle size range. These six are hydro cyclones, tilting frames, mozley tables, high intensity wet magnets, matrix magnets, and froth flotation.

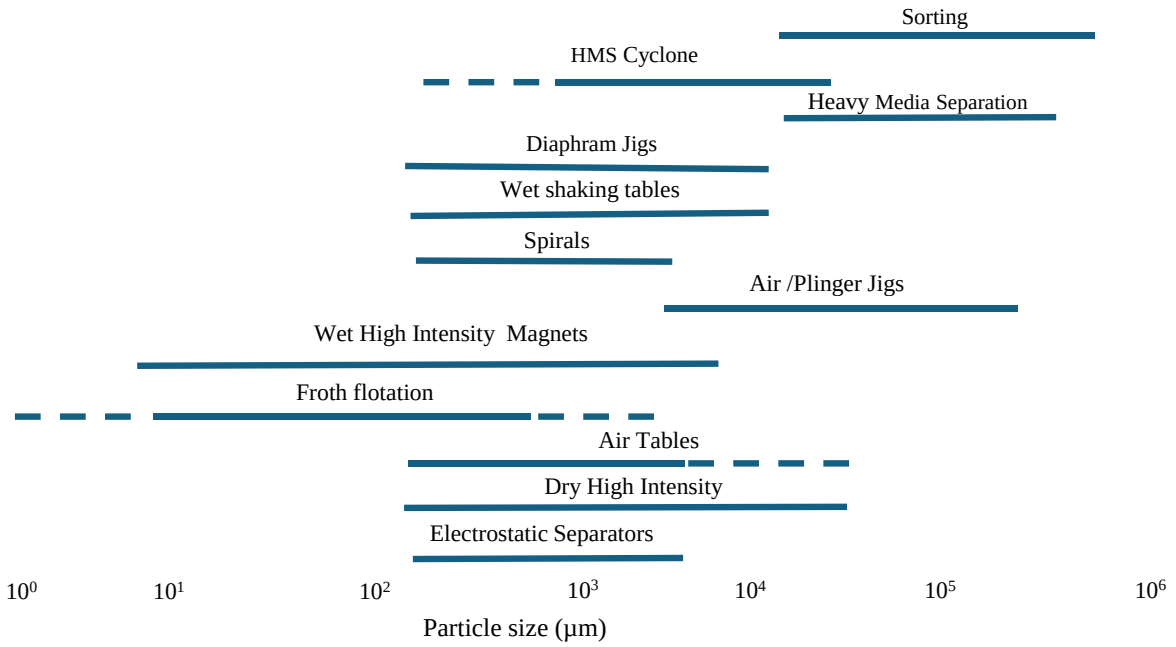

Figure 2.15: Effective range of application of conventional mineral processing techniques (Burt, 2005).

In gravity separation methods, Burt (2005) points out that the choice of equipment and technique to use for separation of the value mineral depends on size range, capacity, and efficiency. In general, slimes are a problem because they have a small mass, high surface area and a high surface energy. Small mass leads to low particle momentum such that they can be washed away easily. Small particles are also predisposed to hetero-coagulation where different particles in that size range coagulate regardless of their mineralogy. In flotation processes, the small particles are associated with low probability of collision with a bubble leading to lower

recoveries. The high surface area of exceptionally fine particles leads to a high dissolution rate in leaching reagents and adsorption of copious quantities of chemicals.

The techniques that can be used in the beneficiation of the slimes of exceptionally fine particles are summarized in Figure 2.16.

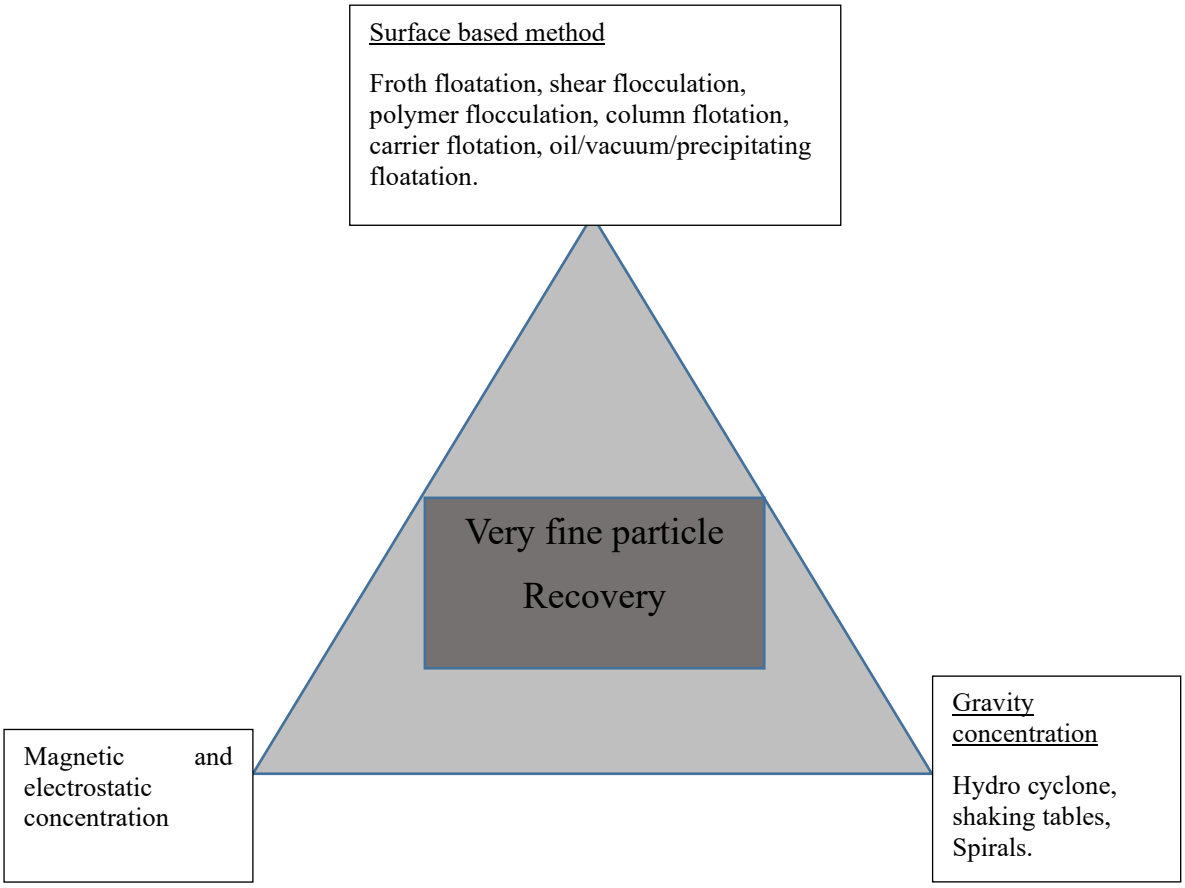

Figure 2.16: Typical methods that can be applied in the recovery of fine particles (Sivamohan and Forssberg, 1990)

2.4 Industry Efforts in Fine Chrome Beneficiation

The recovery of chrome from chrome and PGM mining tailings is now receiving significant attention from most chrome processing organisations in Africa and globally. This is because of two reasons, (i) the environmental implications of millions of tons of mining waste in tailing facilities that still has value in them and (ii) the dwindling of rich resources necessitating the turn of attention to the leaner grade ores and tails from PGM processes. As a result, huge efforts are being applied by minerals engineers to find ways of beneficiating fine to ultrafine chrome from tails already produced as well as current arisings from either chrome or PGM processes.

In the minerals processing industry, especially chrome industry, definitions for size and grades tend to vary and there is no universal agreement on the definition of ultrafine chrome or low-grade chrome ore. The reason for this is that for operations using predominantly conventional gravity methods and equipment, ultrafine may be particles of size below 100µm whereas for recently developed methods and processing units, ultrafine size could mean 53µm and less. In a comparable way, when assessing chrome grade, there is no universal definition of low-grade chrome. In the South African Bushveld Igneous Complex (BIC), there are three main formations, which host chrome at different content. The Lower Group (LG), which occurs at the bottom of the three systems, has the highest chrome of the three systems. The Middle Group (MG), which is found above the LG, has slightly lower chrome than the LG. Above the MG is the Upper Group (UG), and this has the lowest chrome content of the three systems (Kinnaird *et al*, 2002). Even on the same system, there is always a difference in chrome content between the seams. When looking at the LG and MG systems, the chrome content varies such that the MG sometimes records chrome grades as low as 18% to 25% while the LG has chrome contents as high as 40 to 45%. These differences may lead to the difficulty of defining low and high chrome grades. Exploitation of low grades or lean ores leads to significant amount of work to recover fine chrome. In all these efforts, various methods and equipment have been and are being tested with the main objective of improving the recovery of chrome and rejecting the tails containing as little chrome as possible. Spirals concentrators, centrifuge type concentrators, magnetic separators, shaking tables and flotation are some of the processes and equipment that have been considered for distinct types of ores. These have been tried as single units but predominantly as combinations of processes.

2.4.1 Use of Spiral Separators in Fine Chrome Beneficiation

Conventional spirals have been designed to treat material in the 75µm to 1000µm size range (Sethabi, 2019). New spiral designs that have recently been developed can tolerate finer particle sizes. Mineral Technologies – A Downer Company specialising in specialty mineral processing equipment, has produced a new type of spiral called FM1 that is more effective in the treatment of less than 75µm size range (Henderson, 2003). This spiral has the capability to treat and beneficiate fines between 30µm to 150µm effectively because of its profile, which is a shallow troughs and wide diameter. This profile causes material to slow down, forming a lamellar profile with the resultant effect of better separation of the ultrafine material (Richards, 2000). This spiral has more turns to allow for higher residence time for separation of concentrate from the gangue material. The only drawback experienced on these kinds of spirals is that their

throughput is slightly reduced because of the need to form lamellar profile, which prevents back mixing once separation has happened. To counter the throughput constraint, the double and triple start options have been designed so that the throughput is increased per unit area of footprint.

Izerdem and Ergun (2018), did some comprehensive test-work on spirals where the main objective was to investigate the impact of size-by-size processing of chrome ore of 5.5% feed grade. The feed material was screened at 425µm, 300 µm, 212 µm, 150 µm, 106 µm, 75 µm and 53µm and these fractions were treated separately through the spirals. By doing this, the effect of size on density was removed so that minerals and gangue particles were only separated based on their density differences. The test was carried at three feed rates, C1, C2 to C3 with C1 representing the highest feed rate while C3 the lowest of the three. The circuit was made up of two main branches i.e. cleaner circuit and scavenger circuit. The cleaner circuit constituted of three levels of spiral concentration – Rougher (SP1), Cleaner 1(SP2) and Cleaner 2 (SP3) spirals. The scavenger circuit (SP4) was made up of only one scavenger spiral set, scavenging from the tailings of the Rougher, Cleaner 1, and Cleaner 2 of the main circuit as shown in Figure 2.17. The concentrate from each of the three feed rates was subjected to particle size distribution analysis by screening into seven size fractions (minus 425µm, minus 300µm, minus 212µm, minus 150µm, minus 106µm, minus 75µm and minus 53µm).

The distinct size fractions were then analysed for mass yield, recovery, grade, and separation efficiency. From the feed rate test results (Table 2.5), it was noted that the highest feed rate (C1) produced the lowest recovery (40.55%), and the lowest feed rate (C3) produced the highest recovery (63.86%). This is because an increased feed rate to the spiral results in a greater part of the additional flow volume reporting to the outside of the trough, carrying some mineral particles in that flow and reducing their chance of recovery (Holland-Batt and Holtham, 1991; Holtham, 1992). This is especially true for fine to ultrafine particles where the hydrodynamic forces are more prominent than the gravity forces resulting in loss of recovery for ultrafine particles. In this work, it was also reported that the grade was highest on the intermediate feed rate. The intermediate feed rate promotes higher selectivity which results in the most upgrade of the feed into the concentrate.

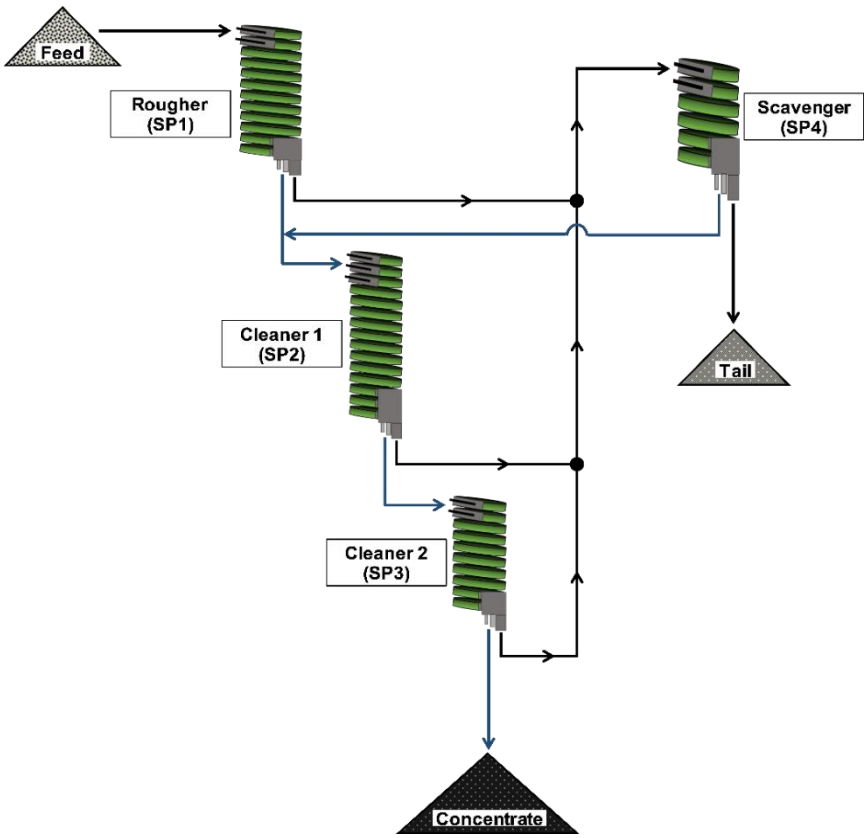

Figure 2.17: Flowsheet of the spiral concentrator process (Izerdem *et al*, 2018).

Table 2.5: Spiral performance comparison between three levels of feedrate (Izerdem *et al*, 2018)

TEST RESULTS	C1	C2	C3
Weight (%)	5.20	5.83	9.06
Grade (%)	42.90	46.76	39.09
Recovery (%)	40.55	51.57	63.86
Feed Grade (%)	5.50	5.28	5.54

When the three concentrates from the three feed rates were screened on screens from 425µm down to 53µm, it was found that the highest grade was between 200µm and 300µm size fractions, with the intermediate feed rate C2 having the highest grade between 150µm and 425µm. The mass distribution shows that the most predominant size fractions in the concentrates is between 150µm and 300µm (Figure 2.18). It is interesting to note that all fractions below 106µm had exceptionally low concentrate grades compared to that of the average for combined concentrate. This observation shows that the separation efficiency below 106µm becomes exceptionally low. There is therefore a need to look at ways of treating the

size fractions separately if the recovery and separation efficiency at these low particle sizes must improve.

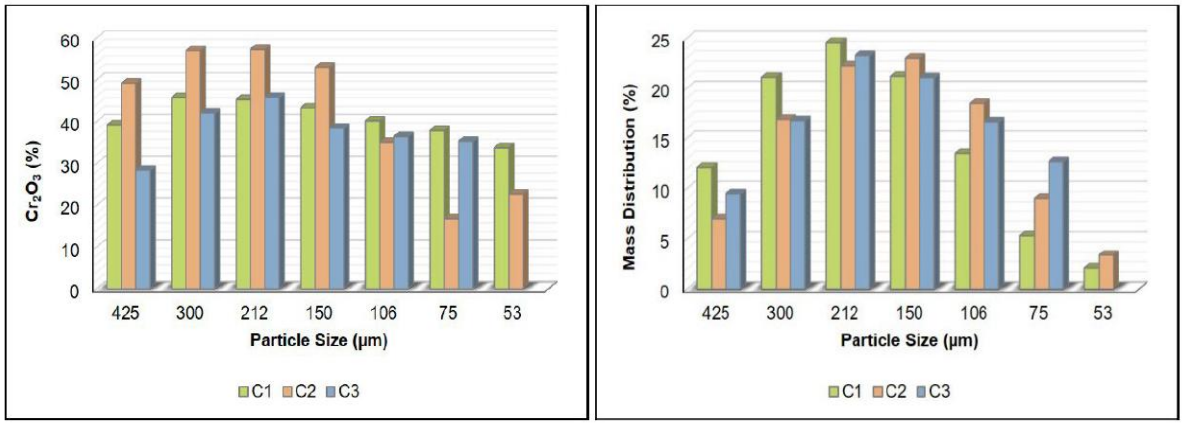

Figure 2.18: Size-by-size grade and mass distribution trends for all three feed rates (Izerdem *et al.*, 2018).

An analysis of the size-by-size separation efficiencies and recoveries in Figure 2.19 below showed that for particles below 53µm, the recovery and efficiency dipped to below 20 % and even down to 5% at high feed rates (C1). The drop in efficiency and recovery below 53µm is because the hydrodynamic forces become more pronounced than gravity forces on the particles such that separation according to gravity is impeded. It was also observed that for size fraction above 200-300µm, the efficiency and recovery also dipped. The reason for this dip at coarse particle size ranges is due to Bragnold forces that cause the coarse particles to be flushed to the outside of the trough preventing settling (Izerdem, 2018, Holtham, 1990, 1992,). This negatively affects the efficiency of separation hence recovery as well.

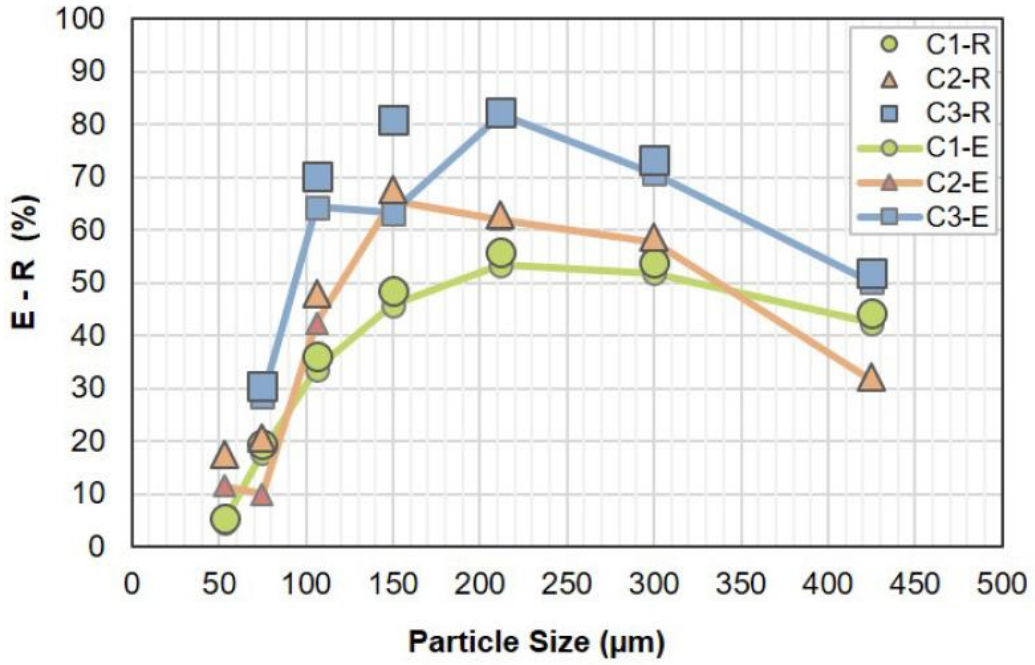

Figure 2.19: The size-by-size recovery and the separation efficiency values of the concentrates

In other work, Agacayak *et al.* (2007) performed some tests using Humphrey spirals on tailings of an abandoned mine. The test was part of scouting tests on various separation techniques used in the concentration of chrome ores. The particle two size ranges -0.3+0.212mm and -0.212+0.106mm were used and the feed grade for these two sizes were 47.55% Cr_2O_3 and 48.35% Cr_2O_3 respectively. The % solids of the slurry tested was 25% for both tests. The results of the two tests showed that the coarser size fraction gave better overall results in terms of concentrate grade and recovery compared to the finer size fraction. These results show that at finer size fraction, some of the liberated chrome particles may be swept by high flow velocity wash water resulting in poor recovery.

Like the work done by Agacayak *et al.* (2007), Aras and Taner (2023) also investigated the possibility of beneficiating a chrome ore with unwanted gangue material using gravity separation methods. The methods investigated were jigs, Reichert spirals, shaking tables and multi-gravity separator (GMS). For these spiral tests, two size fractions -2+1mm and -1+0.5mm were separately run and produced concentrate of grades 39.31%Cr_2O_3 and 45.10% Cr_2O_3 respectively. The finer size fraction also produced better concentrate recovery at 71.56% while the coarse size fraction chrome recovery was 43.87%. Flanagan and Dias (2023) investigated the possibility of upgrading metallurgical chrome tailings to foundry grade chrome sand. The metallurgical chrome tailings had a grade of about 15% Cr_2O_3 and particle size range

of 1 mm to 0.1 mm, with 80% passing 0.4 mm. The process involved taking the metallurgical chrome tailings and classify it to remove fines, then use High intensity magnetic separator the tailings of which was run on spiral separator. The products of the magnetic separator and spiral separator were combined to form the final product. From this test, the realised that magnetic separator is a silica rejection unit while the spiral was functioning as the chrome recovery unit for the misplaced chromite in the magnetic separator tailings. In the process, they also found that the % of magnetics in the concentrate was inversely proportional to the magnetic field strength. Jenkins and Hayslip (1965) reported similar behaviour of the chromite streams when they carried out tests to remove silica from foundry chrome. In their tests they found that silica rejection was achieved more by wet gravity concentration than by high intensity magnetic separation.

In contrast to the coarse material tested by the earlier investigators discussed above, Tripathy *et al.* (2010) investigated the concentration of fine chromite using spirals. The material used was the tailings fraction of fine circuit of chrome beneficiation plant. In terms of the grade of the tailings, the material contained 21.96% Cr_2O_3, 20.7% Fe_T, 14.68 Al_2O_3, 29.59% SiO_2, 4.52% MgO and particle size distribution of about 80% passing 100µm. A five turn single start spiral was used with feed rate varying between 1.2 and 3 m^3/hr, while the feed pulp density (in solids %) ranged from 10 to 30% and the splitter position ranging between 12 and 16 cm.

From the results, they plotted response surface plots between two variables of spiral concentrator against the independent parameters. The independent parameters presented against concentrate grade and recovery were pulp density, feed rate and splitter position. The results showed that splitter position has the major influence on grade and recovery. Recovery was shown to directly proportional to splitter position whilst concentrate grade was inversely proportional to splitter position. In terms of the effect of pulp density and federate on grade, it was found that higher feed rate favours lower grades whilst pulp density changes had insignificant effect on grade. Lower pulp density favoured better recovery than higher density. It must be noted that higher pulp density and higher feed rate have similar effects.

Tripathy *et al.* (2019) used spirals and magnetic separation to enhance the Cr/Fe ratio of a concentrate. In this test, they used two models of spirals HG10i and FM1 whose process parameters were slightly different. Both spirals had 8 turns and were fed at 0.9-2.3 m3/h and the pulp density between 15 and 30%. HG10i had a spiral length of 2.84m, trough diameter of 580mm and pitch of 350mm while FM1 had a length of 3.12m, trough diameter of 685mm,

and trough pitch of 360mm. Three concentrates (coarse-14% passing 100µm, fine-40% passing 100µm and ultrafine-95% passing 100µm) were processed on these spirals. In terms of the grades of the concentrates, the coarse analysed 49.9% Cr_2O_3, the fine analysed 53.7% Cr_2O_3 and ultrafine analysed 42.9% Cr_2O_3. In terms of the FM1 spiral, it was found that for coarse concentrate processing, the concentrate grade decreases with increase in slurry pulp density at both slurry flowrates while separation efficiency was poor at higher than 20% pulp density. Higher separation efficiency was observed at higher slurry flow rates of 2.3m^3/h. This is due to the enhancement of centrifugal forces at high flowrates.

For the HG10i spiral model it was reported that the optimum separation was at pulp density above 20% for coarse concentrate processing. They reported that the HG10i is more suitable for iron rejection due to lower diameter trough and with minimum pitch in the design which facilitated enhanced separation.

Overall, the work revealed that between the two spirals FM1 which is the wide diameter spiral gave the best results in ultrafine concentrate cleaning or upgrading. It also must be noted that the liberation of the chrome particles was in the fine particle size concentrate, and this also had the highest Cr/Fe ratio. These results shed some light on the key considerations like liberation and whether the gangue material to be rejected is either silica-based or iron-based. This specific characteristic is also considered when one compares gravity and magnetic separation of chrome tailings.

Alaee *et al.* (2025) performed a study on the development of a prototype spiral separator for processing of low-grade chromite. In their study, they noted that previous researchers like Meng *et al.* (2023), and Sudikondala et al. (2022) identified six different forces acting on spiral particles and these forces are gravity, centrifugal, drag, lift, friction, and Bagnold forces. These are influenced by fluid flow speed, flow rate, particle size, shape, and dimensions as well as particle density according to Kianoush *et al.* (2024). Honaker and Forrest (2003) noted that the fluid flow stability changes and is different across the inner, middle, and outer trough as the trough length increases. Boucher et al. (2016), found that increase in slurry density and volume feed increases the tendency of heavy materials to move towards outer wall in the process reduce the efficiency. It means that there must be an optimum density of slurry and feed rate to avoid remixing of chromite particles during spiral separation.

Boisvert et al., 2023, 2024 noted that unlike other gravity separators like shaking tables, a complex fluid flow regime occurs on the surface of spiral separator. For thin fluid flow, the

depth of the flow in the surface troughs is less than 1cm and the flow speed at the centre of the spiral is close to zero. This flow speed increases as one goes outwards. Ankireddy *et al*, 2024, and Boucher *et al.* (2016), noted that during secondary flow pattern, heavy particles like chromite rich particles are directed to the centre while water and light particles move to the outside. As the speed of the slurry flow increases down the slope and heavy particles accumulate in the inner part, shear forces increase gradually beyond a certain point and this shear force can disperse the heavy particles from this area as noted by Ankireddy *et al., 2*024 and Sudikondala *et al.* (2022). This observed phenomenon makes it very crucial for accurate calculation of the number of turns a spiral must have to avoid mixing of concentrated product. One key consideration is the movement of particles that is influenced by three sliding processes-rolling, sliding and saltation according to Martin-Gill and Flores, (2024). Linking all the information from other researchers, Alaee *et al.* (2025) tested a chromite samples of grade 11.59% Cr_2O_3, liberated at 300 µm and solids concentration of 50% on a spiral separator. They produced a concentrate of 58.60% Cr_2O_3 and a tailings stream of 4.78%. At this particle size range, water addition assisted in producing high quality concentrate yielding a recovery of 85% compared to 60% of conventional spirals.

2.4.2 Use of Magnetic Separators in Fine Chrome Beneficiation

Magnetic separation has been used in chrome beneficiation especially in combination with other separators like spirals and shaking tables. Diverse types of magnets and magnetic strengths used have been based on whether the material under separation is ferromagnetic, paramagnetic, or diamagnetic. Since chrome is largely paramagnetic, chrome magnetic separation is generally done using high intensity magnets in wet environment (WHIMS). Drum permanent magnets are in use in most applications, however there is growing interest in belt magnets because of the ease with which they can be operated. Use of drum magnets for chrome separation has experienced a drawback because chrome sticks onto the drum surface such that the efficiency drops significantly after a few tons of running.

There are several other magnetic separators that have been in use in the minerals industry. Their application depends on the type of material being treated and the capital and operational costs that are sustainable for those applications. Dry high intensity separators are some of the types of magnets used, they come in the following types: induced roll magnetic separator, lift roll magnetic separator, cross-belt magnetic separator and rare earth roll magnetic separator. Tripathy *et al*, (2017) reviewed the application of these types of magnets on dry feed material.

It was observed that the efficiency of separation is a function of particle size, roll speed, feed rate, and magnetic susceptibility of the material. The drawback of dry magnetic separation is the generation and difficulty of containing the dust and that is why wet processes have an advantage over dry processes. Therefore, a gap exists in investigating the applicability of wet magnetic separation at ultrafine sizes. Generally, at particle sizes less than 30μm the efficiency of magnets drops significantly because hydrodynamic forces are more powerful than magnetic forces, and to counter this limitation, a process called floc magnetic separation (FMS) has been studied (Roy, 2012). This process aims at agglomerating the fine magnetic particles so that their sizes increase before feeding on to a magnetic separator. Sodium oleate at a pH of 9.5 has been used with particularly satisfactory results on iron ore fines. The effect of sodium oleate is that it makes the fine particles hydrophobic which causes them to coalesce into bigger particles, that can withstand the hydrodynamic forces in wet magnetic separation. An almost similar method is used for a magnetic carrier to recover chromite from serpentine at ultrafine sizes. The use of dodecyl amine (DDA) at higher pH was reported to separate chromite from gangue of predominantly serpentine (Ucbas *et al*, 2013). Once the chromite has been separated from serpentine, a further process to upgrade the concentrate like flotation or shaking table can follow.

Rao et al. (1996) did some work on two Indian chrome ores trying to improve the grade as well as the Cr:Fe ratio using magnetic separation. Of the two samples, one was hard, lumpy, and rich in Cr2O3 while the other was friable soft and fine ore. Before separation on the magnet, the materials were washed on a spiral classifier to remove fines. A dry belt magnetic separator was used for upgrading the Cr: Fe ratio. Initially the samples A and B had Cr/Fe ratios of 1.91 and 1.85, respectively. At the end of magnetic separation, the grade for A had increased from 48.3% to 55.4% and Cr/Fe ratio increased to 3.15 while that for B had increased from 47.3% to 53.4% and Cr/Fe ratio increased to 2.99. The reason for the difference in the response to magnetic separation of the two ores is that A was associated with $Fe(Al, Cr)_2O_3$ whole B was associated with FeO $(Cr, Al)_2O_3$. Such variation influenced the magnetic properties and separation characteristics of the two samples.

Tripathy *et al.* (2019) performed magnetic separation testwork on ferruginous chromite concentrates to improve Cr/Fe ratio. They carried out the test on magnetic separator with magnetic field strength varying between 0.4T to 1.3T. The chromite streams were split into coarse, fine, and ultrafine. The coarse fraction's grind was 95% passing 900μm and 25% passing 180μm while the fine fraction had a grind of 95% passing 500 μm and 25% passing

80µm. The ultrafine fraction's grind was 95% passing 100 µm and 25% passing 30 µm. One observation was that as the magnetic field strength increases, the recovery of the magnetic fraction increased as well. The Chromite grade, Cr:Fe ratio and enrichment ratio all increased with magnetic strength until 1.1T where they all fell as the strength reached 1.3T. The reason for this is the recovery to concentrate of the iron-bearing gangue at high magnetic field strength of coarse and fine fractions. The trends changed for the ultrafine fraction where the Cr:Fe and enrichment ratios did not increase with strength until 1.3T. The poor capture was due to inefficient capture of small magnetic particles as well as the abundance of hematite and geothite in the ultrafine material. A comparison of the magnetic method with spiral gravity method showed that magnetic separation is less efficient in iron bearing gangue mineral compared to spirals. From these results, it was shown that WHIMS can be used for increasing the chromium oxide recovery but does not result in an increase in Cr:Fe ratio and upgrade. Spirals are more efficient in Cr:Fe ratio than WHIMS. To this end, knowledge of the iron-bearing gangue content in the material is vital to determine which method is most effective.

2.4.3 Use Shaking Table and Multi-Gravity Separators in Fine Chrome Beneficiation.

Shaking tables have been used as part of a combination of equipment for the separation of chrome. The main disadvantage of shaking tables is that their capacity is a huge limitation, and this is why they are mostly used as the last piece of equipment in the recovery circuit that process a low volume to achieve desired grade of concentrate. Most conventional shaking tables have been designed for sands (+75µm and -150µm). Below 75µm, the separation becomes difficult because hydrodynamic forces are more dominant than gravity and frictional forces. The main parameters influencing the separation of chrome on the shaking table have been found to be the pulp density, feed rate, particle size, wash water flow rate, table tilt angle, stroke characteristic and cutter position (Tripathy *et al*, 2010). In studying the separation factors using a shaking table, Zhao *et al.* (2013) looked at several factors and observed that the most prominent one was the shape factor ahead of density, granularity, and size. This is one area, which requires further investigation during the application of shaking tables in chrome separation. Seifelnasr *et al.* (2012) studied the separation of low-grade Sudanese ore and realised that among other factors, feed size range was important. Narrow size range of particles produced better results than wide size range in table separation. For this reason, Seifelnasr *et al.* (2012) proposed de-sliming as a prerequisite for shaking table separation and treating the

slimes separately from the fines. One other challenge of use of shaking tables is their high consumption of clean water, and water recovery needs to be done effectively.

Aras and Taner (2023) tested on a laboratory scale shaking table two samples with particle size of -0.5mm + 0.3mm and -0.3mm + 0.106mm. The -0.5 mm fraction feed grade was 36.38% Cr_2O_3 while the -0.3mm fraction feed grade was 36.46%Cr_2O_3. The finer fraction stream achieved a concentrate recovery of 94.29% while the coarse fraction stream achieved a concentrate recovery of 92.31%. The difference in recovery between the two samples is liberation factor. At coarse fraction fractions, the chromite particles are not fully liberated and hence have some gangue influence. It is be noted however that the feed grade of this work is much higher than the lean tailings which are sitting on most tailings' facilities. In comparison to other separators, the shaking table still had superior performance compared to spirals, and multi-gravity separator. In another work Agacayak (2007) tested shaking table on five distinct size fractions (-1+0.5mm, -0.5+0.3mm, -0.3+0.212mm, -0.075+0.053mm, -0.053+0.038mm). The head grades of these samples were all above 39% Cr_2O_3 and concentrate grades ranged from 43% Cr_2O_3 to 55% Cr_2O_3. The recovery increased from about 51% on the finest fraction peaking at 92% for the -0.5+0.3mm fraction but dipping down to 85% on the coarsest fraction. The reason for this behaviour is two-fold, where at coarse size fractions the liberation hinders recovery while at the finest fraction the recovery is negatively affected by the hydrostatic flow pressure that washed even chromite particles.

Another option that is gaining traction for ultrafine mineral recovery is application of enhanced forces higher than gravity i.e. Multi-gravity Separators (MGS). Nzeh *et al.* (2023) wrote a review on the state of art literature on Gravity separation techniques. They noted that there is more research needed especially in the comparison of enhanced gravity separators with conventional techniques. The centrifugal forces generated in the MGS range from 8 to 20xG. It is believed that coupled with the rocking motion of the drum, there is enhanced separation effect. It has been argued that MGS perform better than shaking tables for fine particles. However, MGSs main drawback is the capacity, which is the lowest compared to other methods (Majumder and Barnwal, 2007, and Das and Sarkar-2018). Aras and Taner (2023) and Rath *et al.* (2017) investigated the chromite ore beneficiation possibilities with different gravity concentrators. The material was sourced from Tokat province in Turkey for a technical investigation. This material did not qualify as ultrafine or low grade since it assayed 35.46% Cr_2O3. The equipment that was used in the investigation were, Jigs, Reichert spirals, Shaking table and Multi gravity separator (MGS). The material was crushed and milled into size

fractions aligned with the specific gravity separation unit. The jig was fed with material of size -3.35mm+2mm, and for spirals two size fractions -2+1mm and -1+0.5mm were prepared. The shaking tables were also fed with two size fractions, -0.5+0.3mm and -0.3+0.106mm. The last size fraction -106µm was processed in the multi gravity separator. From the 4 gravity separators, the best results were obtained with the shaking table achieving a grade of 46.43% Cr_2O_3 from a feed grade of 36.38% Cr_2O_3 and a recovery of 92.31%. The spiral managed to reach a grade of 39.31%Cr_2O_3 at a recovery rate of 43.87%. The Jig manged to produce a concentrate of grade 38.35% Cr_2O_3 with a recovery of 92.04%. The grade attained by the MGS was only 34.21% Cr_2O_3 with a recovery of 85.14%. One thing to note about this test-work and result is that each separation unit had its own size fraction and the success and or failure to attain desired grade and recovery was due to either poor liberation or too much ultrafine material hindering the efficient separation of chromite from gangue. Modification of circuit with recirculation streams would improve the results which failed to attain targeted levels.

Cicek *et al.* (1998) carried out test-work on the fine chromite tailings of Karagedik plant in Turkey. The head sample assayed 12.10%Cr_2O_3 with MgO and SiO_2 being the major oxides at 32.50% and 29.25%, respectively. The particle size distribution of this head sample was between 1000µm and 106µm. The -106 µm in this sample was 46.38% by mass and 77.26% chrome mass. The sample was screened at 106 µm and the course was discarded because of poor chrome content of 5.23% Cr_2O_3. This is the mass which was used to run on the MGS for ultrafine chrome recovery. The -106µm was screened down into size fraction down to 10µm for characterization. The overall grade of this -106 µm was 20.55% Cr_2O_3 and was run on the MGS. The factors which were being monitored were drum tilt angle, drum rotational speed, wash water and pulp density. Of these parameters, it was found that drum tilt angle and drum rotational speed were the most dominant operational parameters while the other two had milder effects on Grade and Recovery (Rao *et al*, 2017). When fractional recovery was evaluated, it was found that the -10µm fraction achieved the lowest recovery of 43.12%. The highest recovery was in the -53+38µm fraction followed by -75+53µm with 84.50%. The -106+75µm fraction achieved a recovery of 80.46%. These numbers gave an indication of what an MGS can achieve

2.4.4 Use of Flotation and Flocculation in Fine Chrome Beneficiation.

As the efforts to recover ultrafine chrome pick up pace, other methods are also being investigated and evaluated. Considerable work has been done on the flotation of ultrafine chromite feed materials. Flotation apparently introduces chemicals into the process, and this is one of the concerns when compared to gravity methods which are more environmentally friendly. Seifelnasr and Tamam (2011) studied the flotation of Sudanese chrome ore in which they tested use of long chain fatty acid as a collector at pH of 1.5 to 5 and at a pH of 11. In these studies, sodium silicate was as a dispersant. A study by Nelufhangani (2019) used the same collector and dispersant and used carboxymethylcellulose (CMC) as a depressant for silicate gangue. Promising results have been reported in these respective studies.

Selective flocculation of the chrome fines to separate the chrome from serpentine was studied by Beklioglu and Arol (2004). Starch, which has been discovered to have affinity to iron containing minerals such as magnetite, hematite as well as chrome was used a flocculant, and sodium silicate was used as the dispersant in the study. Favourable results were obtained at a pH of 11.5. These results are particularly important to the work of ultrafine beneficiation since flocculation can be used as a pre-concentration step in spirals, magnetic and shaking table separation processes.

Some flotation work has been done on the beneficiation of UG2 ultrafine chrome (Wesseldijk *et al*, 1999 and Ross *et al*, 2022). In the work by Wesseldijk, sodium isobutyl xanthate (SIBX) and SK5 containing sodium dibutyl dithiophosphate (DTP) were used as collector mixture. Copper sulphate was used as the activator. From the results, it was shown that the presence of copper sulphate at higher pH 10 was more significant than high concentration at low pH. The other flotation work by Ross (2022) in which Flotinor V2711, Flotinor 7253, Lupromin 476, Oleic acid, Na_2SiO_3 and Betafroth 200 were used also yielded satisfactory results. A feed of 16% was upgraded to 42% Cr_2O_3 with a yield of about 11% and recovery of 24%. One thing to note is that for successful chrome flotation, desliming is overly critical as removes slimes that compete for reagents with the chrome particles.

2.5 Literature Review Conclusion

Literature has shown that separation and concentration of chromite ores is achieved through use of surface acting methods, such as flocculation and flotation, magnetic forces method used on belt or drum magnets and gravity separation methods. Of these three main processes, chromite recovery has predominantly been carried out using gravity separation techniques and equipment. Some of the equipment used in gravity separation ranges from jigs, spirals, sluice boxes, stationary cone classifiers, elutriators, shaking tables and multi-gravity separators. Each of these pieces of equipment has its operating parameter window where it is most effective. The application of the equipment depends principally on nature of the material to be beneficiated or processed as well as the processing capacity and cost of procurement and running such. Besides design parameters of equipment, material operating variables such as particle density, particle size and shape, liberation and association, slurry density and feed rate have an influence on the efficiency of separation of chromite. Literature has shown that separation of fine to ultrafine chromite ores and tailings is difficult on certain pieces of equipment than others. To mitigate the difficulties of separation ultrafine chromite, literature has shown that circuits which utilises a combination of methods and pieces of equipment have been successful. From literature, spirals, cone settlers and shaking tables have successfully been used at commercial level of chrome ore and tailings retreatment. In terms of capital investment per unit throughput, the spiral is more attractive since it has lowest footprint area per unit production. The shaking table has high capital requirements and operating costs due to moving parts, but they have the attraction of achieving some of the best upgrades utilising wide size range of feed. The magnets use different feed characteristic to effect separation of gangue from chromite particles, able to process at high tonnage per hour but they are also expensive to install and run.

Since the main objectives of this work is to develop a viable circuit for beneficiation of ultrafine chrome tailings, three pieces of equipment were chosen. A modified design of spiral able to treat fine particles was chosen to form part of the circuit. This spiral design reduces the effect of hydrodynamic forces and magnify gravity and centrifugal forces by using low angle and wide troughs. A shaking table was also chosen for this investigation due to its robust capability in treating wide range of chromite material achieving also high upgrades. The third unit that was chosen is a belt magnet separator. It was chosen to augment separation capacity due to its capability to separate based on magnetic properties. Its use deals with the material where gravity separation has limitations.

CHAPTER 3: MATERIALS AND METHODS

3.1 Introduction

The understanding of the performance of separating or beneficiation circuits in mineral processing invariably involves deep understanding of the nature of the feed material from its mineralogical associations, liberation characteristics, particle size distribution, grain size and even sometimes shape.

The feed material for the test-work in this study were the final tails from an operating chrome and PGM processing plant. As part of the investigation, this feed material was characterised in terms of particle size distribution, chemical composition, and mineralogical makeup. The following sections describe the feed material characterisation tests that were carried out to address the research questions.

3.2 Feed Material Characterisation

The test-work feed sample was collected by sampling the final tailings over a period of 5 days to accumulate a representative sample for characterisation. A vezin sampler was used to collect a daily sample from the main tail stream that is pumped to the tailings storage facility (TSF). The daily samples collected over a period of 5 days were composited to make one homogeneous sample from where representative samples were taken for different characterisation analysis.

3.2.1 Head Chemical Assays

A portion of the homogenised sample was used for head assay analysis to give the chemical composition of the feed material. Two methods were used to get the head chemical assay of the feed sample. The first method was X-Ray Fluorescence (XRF) where the components were analysed as oxides, and the second method was the Inductively Coupled Plasma Optical Emission Spectroscopy (ICP-OES) where the components were analysed as elements.

3.2.1.1 X-Ray Fluorescence Sample Preparation

The sample was ground/pulverized first in a swing mill to particle size of 100% <75µm and then followed by mixing it with a binding aid in a swing mill again for 2 minutes to ensure total blending. The blended mix was then pressed in an aluminum cup die at a pressure of 6 bars, for 10 sec to produce a homogeneous sample pellet. The binding aid used was a cellulose wax

mixture and was combined with the sample in a proportion of 10% binder to 90% sample mass. The sample was analyzed for 1 minute before the results were reported on the screen.

3.2.1.2 X-Ray Fluorescence Principles and Method

The X-Ray fluorescence measurements were performed using Epsilon 4 XRF machine supplied by Panalytical and run on Epsilon software V2VLTU. The principle of operation of an XRF was described in detail by van Niekerk (2010) in his thesis on method development and validation using X-Ray fluorescence Spectroscopy. X-rays are electromagnetic waves of a short wavelength found between gamma and ultraviolet region of the electromagnetic spectrum. The wavelength is between about 10^{-5}A and 100 A. These X-rays are produced in an X-ray tube using tungsten filament (cathode and negative) which is heated to incandescence by an electron current passing through the external filament terminals. The hot W filament produces a cloud of electrons, which are accelerated along a focusing tube on a target material that is regarded as an anode and is positive. In most case the material for the anode is rhodium. This anode is made of copper block covered in a thin film of Rhodium. The purpose of the copper is to conduct heat away from the electron-beam focusing point. High energy electrons produced by the tungsten filament are accelerated towards Rh target due to the potential difference between the cathode and the anode.

This process releases energy in the form of primary X-Rays since they come from the rhodium tube during the process of relaxation, where inner electrons return to their original energy state. For the analysis, the sample is bombarded with the primary X-Ray photons and if the photons have enough energy, the photos will be absorbed by the inner electrons in the sample atoms which will expel electrons from their atomic orbital and leaves the atoms in an excited state. The emitted radiation is unique such that copper fluorescence looks vastly different from zinc fluorescence and from fluorescence of any other element in the periodic table.

The XRF Measurement settings used for the work are given below.

Binder used	CH18H36N2O5
Tube kV setting	20.000
<Cr-Co> kV	20.000
<Cr-Co> uA	500
<Fe-Si> kV	5.000
<Fe-Si> uA	2000.
Measurement time(s)	30

3.2.1.3 The ICP-OES Method and Operational Principles

Inductively Coupled Plasma Optical Emission spectroscopy (ICP-OES) is an analytical technique used to determine how much of certain elements are in a sample. The instrument was supplied by Agilent Technologies through Chemetrix and the Model used was 5110 with ICP Expert software 76.3.12735. The ICP-OES principle uses the fact that atoms and ions can absorb energy to move electrons from the ground state to an excited state. In ICP-OES, the source of that energy is heat from an argon plasma that operates at 10,000 Kelvin, generated at the end of quarts torch by a cooled induction coil through which a high frequency alternating current flows. As a result of this an alternate magnetic field is induced which accelerates electrons into a circular trajectory.

3.2.1.4 ICP-OES Sample Preparation and Introduction

The collected and dried samples were received at the analytical section for sample preparation. A 10-way splitter was used and % Relative Standard Deviation (RSD) of splitter was checked and verified with the original sample to ensure optimum operation is achieved. The % RSD target was less than 5%. For every sample analysed on the ICP, two splitter sample cups of opposite sides were taken as a representative sample of the bulk sample, and it was then sent for milling to a size fraction of 95% passing 75µm. A 10% v/v H_2SO_4 was used for digesting the milled sample and then fused with Na_2O_2. After doing the prechecks including verification that the flowrate of the liquid sample was set at 1.5 – 2 ml/min, the sample was ready for reading. The instrument was calibrated with calibration solutions ranging from 0ppm to 350ppm and the calibration curve correlation coefficient is supposed to be 0.999% or 1 and must be linear. An instrument quality control (IQC) was read and a target of 120ppm for all elements, with 5% limit up or down was attained before reading the sample. The liquid sample was pumped into the nebulizer, which turns the liquid into a fine aerosol using a stream of argon gas. This aerosol passes into the spray chamber, where larger droplets are removed from the aerosol. The rest of the aerosol continues into the plasma torch. Reporting of results was done once both Instrument Quality Control (IQC) and Certified Reference Material (CRM) passed, which are used to validate the results.

The conditions set for analysis of the ICP-OES are given below.

Replicate Count	3
Pump speed (rpm)	15
Sample Uptake Time(s)	16

Rinse time (s)	10
Read Time (s)	10
RF Power (KW)	1.4
Stabilization Time (s)	15
Viewing mode	Radial
Viewing Height (mm)	9
Nebulizer Flow (L/min)	0.78
Plasma Flow (L/min)	15
Aux Flow (L/min)	1.2

3.2.2 X-ray Diffraction

The other portion of the homogenised sample was split into five size fractions, +106µm, -106+75µm, -75+53 µm and -53+25µm and -25µm. Each of the five size fractions were pulverised and analysed using an X-ray diffractometer to determine the relative mineral abundances, which are expressed as the actual mass % of the crystalline phases identified.

The X-RD machine used was a Paralytical X'pert Pro employing Fe filtered Co-Kα radiation. Mineral identification and quantification were done using the Panalytical HighScorePlus software with Pan-ICSD database. The abundance of each phase was determined by the Rietveld refinement method and those minerals in percentages greater than >3 % were identified. The measurement conditions for the machine used are given below.

3.2.2.1 Measurement conditions

Detector:	Pixel detector, Scintillation detector
Goniometer Radius [mm]	240,00
Specimen Length [mm]	10,00
Anode Material	Co
Measurement Temperature [°C]	25,00
Automatic sample loader:	Max 45 samples
Material	Powders, pellets, thin films, or bulk materials
Sample Holders:	Aluminium, (15 mm×20 mm×1.8mm)

3.2.2.2 Machine Settings

Max X-Ray power:	45 kV and 40 mA
Source of X-Rays:	Cu Kα, 1.54 Å wavelength
Sample stage:	Fixed, with X-Ray source & Detector rotation
Angular range:	$5° < 2\theta < 110°$
Scan Axis	Gonio
Start Position [2θ]	4,5042
End Position [2θ]	74,9922
Step Size [2θ]	0,0080

3.2.3 TESCAN Integrated Mineral Analyzer (TIMA)

The TESCAN Integrated Mineral Analyzer (model TIMA-G4) supplied by TESCAN is used to measure mineral or phase abundance, size by size liberation, mineral associations, and grain size automatically on multiple samples of grain mounts, thin sections, or polished sections. The physical principle of TIMA is based on the interaction of a focused beam of accelerated electrons with a mineralogical (or other material) sample. Bombardment of the sample surface by electrons generates distinct types of signals. The most important for automated mineralogy are back-scattered electrons (BSE), due to their sensitivity for contrast in mean Z (atomic number) of individual phases and characteristic X-ray radiation for analysing chemical composition. Combining these two signals enables imaging (visualization) and analysis of the sample surface. Stepping of the electron beam over an equally spaced regular grid allows analysis of relatively large samples, while up to 4 Energy-dispersive X-ray (EDX) detectors make the acquisition of spectra amazingly fast. Minerals (or phases) are identified from their typical spectra at each measurement point to create two-dimensional mineral or phase maps. Maps are analysed further to extract distribution and texture information. TESCAN's unique technology is based on a completely integrated EDX system, which performs full spectrum acquisition at amazingly fast scan-speeds. The level of hardware integration of Scanning Electron microscope (SEM) and EDX allows extremely high acquisition speeds for fully automated data collection, resulting in fast, accurate and reliable results.

3.2.4 TIMA sample preparation

Another portion of the head sample (where XRD and chemical analysis samples were taken from) was homogenised on a riffle splitter divided by an even number of compartments. The representative and homogenised material was mixed with high purity graphite to prevent segregation of particles and then mounted in epoxy resin in special cylindrical plastic rings. To avoid air bubbles within the resin, a vacuum chamber was used. After curing and binding of the resin with sample particles, the samples were ground and polished using varied sizes of silicon carbide grinding disks and polishing cloths with diamond paste down to 1 to ¼ micron fineness. The surface of the samples was coated with graphite/carbon to provide an electrically conductive coating that contacts the lip on the sample holder for the purposes of conducting away electrons from the surface thereby allowing accurate analysis. Three measurement modes in built in the TIMA were used for the analysis of samples as outlined in the following sections.

3.2.4.1 Bulk Mineral Analysis (BMA)

This was performed by the linear intercept method where the electron beam is scattered at a predefined point spacing along several lines per field and covering the entire polished section at any given magnification. This measurement provides a robust data set to determine bulk mineralogy and modal proportions. Since the entire block is scanned, an extremely high statistical population is produced. In addition, the random alignment of the particles ensures appropriate sampling. Quantitative modal mineralogy is obtained from the BMA measurement mode. The Bulk Mineral Analysis (BMA) measurement mode identifies the minerals present and determines their relative proportions in mass percent.

3.2.4.2 High resolution Particle Mineral Analysis (PMA) mapping

The electron beam steps through a field over an equally spaced regular rectangular mesh. At each point, the Back-Scattered Electron (BSE) signal intensity is determined. If the BSE signal is above a certain threshold, the beam is retained on this spot until a specific number of counts (1,000 by default) from the spectrometers is collected. The beam then moves to the next point and so on, from left to right. At the end of the line the beam moves rapidly one step down and to the left edge. The procedure is repeated until the whole field is inspected.

The BSE image is used to discriminate individual particles, and a combination of the BSE image and spectroscopic data is used to determine the boundaries between distinct phases. The

advantage of this method is that it resolves the boundary between phases with a similar mean atomic number (which have similar BSE-intensity) but different chemistry.

The spectroscopic data from the measurement points inside each phase are summed. The mean BSE intensity for each grain is also determined. The mean BSE intensity and the combined spectrum is used to classify the grains using the specified classification scheme to determine the mineral.

3.2.4.3 Scanning Electron Microscope -EDS Analysis

The polished samples were taken for SEM-EDS micro-scanning. In this sample, a maximum of 20 chromite grains were identified and analysed using Energy Dispersive Spectrometry (EDS) on the SEM-EDS analyser. The TIMA-X configuration uses four Energy Dispersive X-Ray (EDX) silicon drift detectors (SDD) attached to a TESCAN MIRA (S600) (field-emission gun – FEG) platform, which also includes a backscattered electron detector. The polished sections were mapped for Cr speciation, mineral associations, liberation, exposure, and grain size distribution. The detection limit for this technique is approximately 0.1 mass %. The main constituents of the chromite phase were measured with emphasis on Fe, Cr, Si, Mg, Mn, V, and Al content. The results were used to provide the Cr: Fe ratio which is an important metric in chromite analysis.

3.2.4.4 Chrome Deportment

A total of 4 transverse polished blocks for the various fractions were prepared and analysed by the TIMA Bright Phase Search (**BPS)** measurement mode for the Cr deportment study. The Cr analysis was conducted using the PMA analysis mode on the Tescan-TIMA G4. The Tescan TIMA G4 was used in place of the old QEMSCAN equivalent but utilising the same measurement modes for quantifying mineralogical parameters. The EMPA results were used to compute the Cr/Fe ratio and the presence of other elements in the chromite structure. The other quantitative data that was generated was:

- The grain size distribution of the various Cr-bearing minerals.
- Quantification of the Cr-bearing mineral liberation characteristics.
- Mineral associations.

CHAPTER 4: FEED CHARACTERISATION RESULTS

This section presents results of the different tests which were carried out on the characterisation of the feed material. The feed characterisation tests were aimed at identifying the physical and chemical properties of the feed material that are pertinent to the amenability of the material to separation processes.

4.1 Feed Material Characterisation

The first phase of feed material characterisation involved collection of a representative sample over a seven -day period. The material collected was the final tailings of the chrome and PGM recovery plant. This material is referred to as "feed" in all this work. A Vezin sampler was used for the purposes of collecting the sample in slurry form. The slurry was filtered to remove water and then dried in an oven 110^{o}C for a duration of 12 hours. The dried and cooled sample was prepared for further test-work by breaking the lumps using a steel roller on a flat stainless-steel bench. The sample was homogenised by running it on a rotary splitter and then remix the bulk sample again. After homogenization of the collected sample, the material was split into different lots for different tests. The following specific analysis were performed on the material.

1) Head chemical assay (by XRF and ICP)
2) Particle size distribution.
3) X-ray diffraction for mineral prevalence determination.
4) SEM-EDS Analysis of chrome grains
5) Chrome deportment
6) Grain size distribution
7) Mineral liberation
8) Mineral associations.

4.1.1 Head Chemical Assay

The head chemical assay was performed to determine the content of chrome in the feed as well as the associated minerals making up the bulk of the sample. Two methods were used to determine the head assay of the composited sample. The first method was the XRF technique, and the second method was ICP-OES. Table 4.1 shows the XRF analysis of the material and Table 4.2 shows the ICP-OES analysis of the material under investigation.

Table 4.1 Major elements in the chrome tail by XRF

Elements	METHOD	LDETECTION	UDETECTION	UNITS	**Feed** (Final tails)
Wt. Rec	WGH79	0	0	g	199.2
Al_2O_3	XRF79V	0.05	100	%	17.18
CaO	XRF79V	0.01	100	%	7.32
Cr_2O_3	XRF79V	0.01	100	%	9.01
Fe_2O_3	XRF79V	0.01	100	%	11.21
K_2O	XRF79V	0.01	100	%	0.20
MgO	XRF79V	0.05	100	%	11.66
MnO	XRF79V	0.01	100	%	0.06
Na_2O	XRF79V	0.05	100	%	1.39
P_2O_5	XRF79V	0.01	100	%	0.05
SiO_2	XRF79V	0.05	100	%	42.49
TiO_2	XRF79V	0.01	100	%	0.35
BaO	XRF79V	0.01	100	%	0.03
LOI	XRF79V	-50	100	%	0.45

The XRF results show that the chrome content of the tail sample collected was 9.01%, and that of the other dominant mineral phases in the sample, i.e. those >5% are Cr_2O_3 at 9.01% SiO_2 at 42.49%, Al_2O_3 at 17.18%, MgO at 11.66%, Fe_2O_3 at 11.21%, and CaO at 7.32%.

Table 4.2 shows the feed sample multi element results obtained using the ICP-OES method. From the ICP-OES method, the following results were obtained in comparison to the XRF results: Cr_2O_3-9.01%, SiO_2–44.71%, Al_2O_3-18.61%, MgO-11.49%, Fe_2O_3-11.24% and CaO-6.72 % respectively.

Looking at the results from the two methods, one can see that there is remarkably high correlation between the analysis of the six major oxides of interest even though the methods have differences in suitability of application in various requirements. ICP-OES has a wider spectrum of elements that can be analysed, from metals, non-metals, and rare-earth elements while XRF is most suitable for heavier elements but not effective in light elements. In terms of sensitivity and detection limits, ICP-OES have lower detection limits but high sensitivity hence suitable for trace elements while XRF has higher detection limits and is more suitable for qualitative and semi-quantitative analysis in bulk samples. Given these unique differences and

the correlations of the results show that the sample characteristics are credible, and hance can be worked on as true representation of the feed samples to this research.

To show the correlation between the XRF and ICP-OES results, Figure 4.1 shows how the XRF and ICP-OES results of the six main oxides (Cr_2O_3, SiO_2, Al_2O_3, MgO, Fe_2O_3, and CaO) correlate. The oxides that had some noticeable variances were SiO_2, Al_2O_3 and CaO but not significant enough to discard one result. SiO_2 had a 2.22% between the two methods while Al_2O_3 and CaO had 1.43% and 0.6% variance, respectively. All these are within acceptable chemical analytical errors.

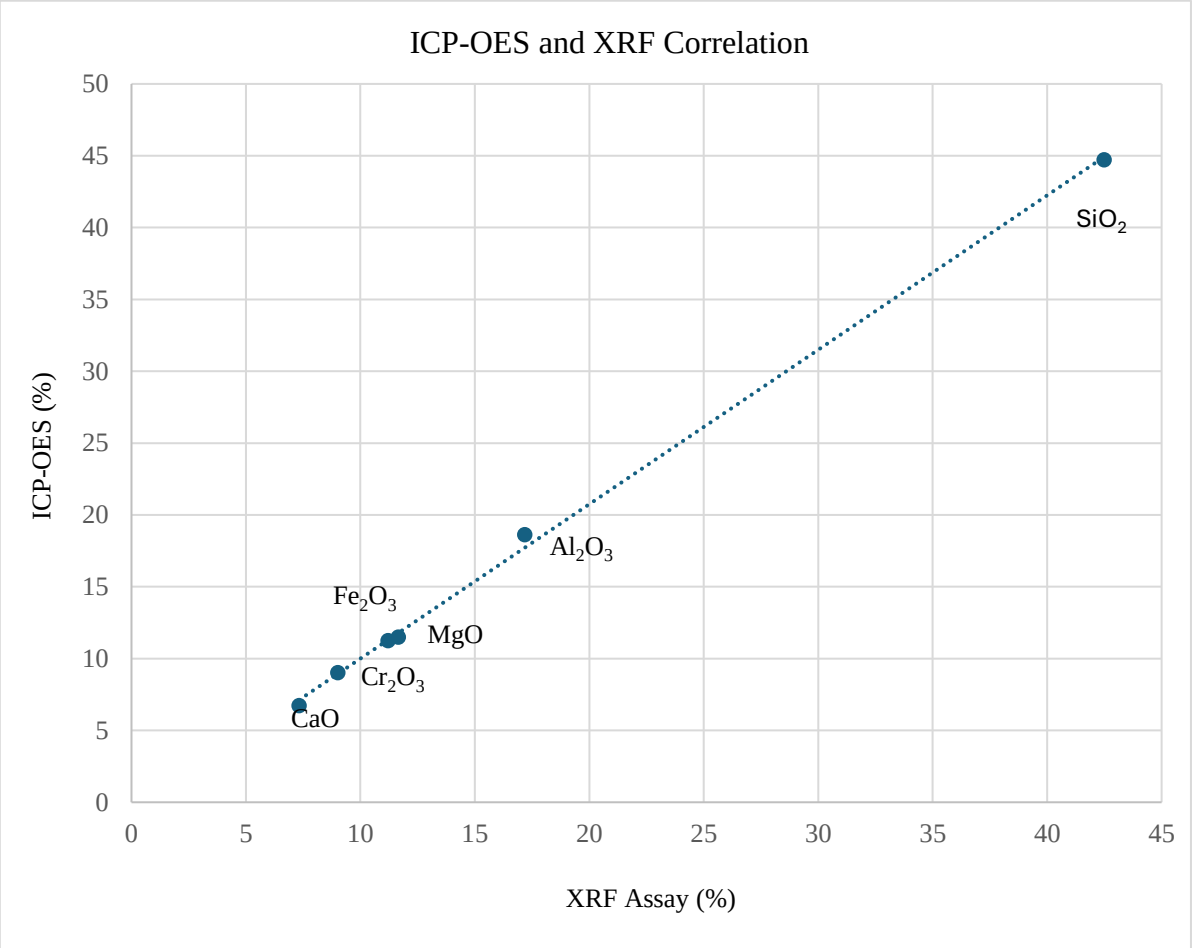

Figure 4.1 XRF-ICP-OES results correlation.

Table 4.2 Multi Element by ICP-OES

Elements	METHOD	LDETECTION	UDETECTION	UNITS	Feed
Si	ICP90A	0.1	30	%	20.9
Al	ICP90A	0.01	25	%	9.85
Fe	ICP90A	0.01	30	%	7.86
Mg	ICP90A	0.01	25	%	6.93
Cr	ICP90A	0.01	25	%	6.17
Ca	ICP90A	0.1	25	%	4.8
Ti	ICP90A	0.01	25	%	0.2
K	ICP90A	0.1	25	%	0.5
P	ICP90A	0.01	25	%	<0.01
S	ICP90A	0.1	25	%	<0.01
As	ICP90A	30	100000	PPM	<30
Ba	ICP90A	10	100000	PPM	99
Cd	ICP90A	10	50000	PPM	<10
Co	ICP90A	10	100000	PPM	105
Cu	ICP90A	10	100000	PPM	70
La	ICP90A	10	100000	PPM	<10
Li	ICP90A	10	100000	PPM	<10
Ni	ICP90A	10	100000	PPM	325
Pb	ICP90A	20	100000	PPM	<20
Sc	ICP90A	5	50000	PPM	<5
Sn	ICP90A	50	50000	PPM	<50
Sr	ICP90A	10	10000	PPM	201
V	ICP90A	10	50000	PPM	564
W	ICP90A	50	50000	PPM	<50
Y	ICP90A	5	50000	PPM	<5
Zn	ICP90A	10	100000	PPM	145

4.1.2 Particle Size Distribution

A part of a representative sample was taken for particle size distribution analysis and Figure 4.2 shows the distribution of the mass across the five size fractions measured. A wet screening method was used to perform particle size distribution on the head sample. The screen sizes selected were 106µ, 75µm, 53µm, 38µm and 25µm. The screening showed that there was little mass in the +38µm size range and a decision was made to combine it with the -53µm size.

The results from the cumulative particle distribution curve show that almost half the mass is in the less than 25µm size range i.e. 49.6 %, while a cumulative 80% of the total mass is below 75µm. Of the 50.4% mass above 25 µm 9.4% is above 106 µm. The cumulative particle size distribution curve is not the typical S-curve for milled product. Because the feed material to this research is a tailings stream of spiral and PGM flotation recovery processes. From 25µm to 75 µm there is fewer particles in this range meaning that the chrome recovery has removed predominantly from this size fraction range.

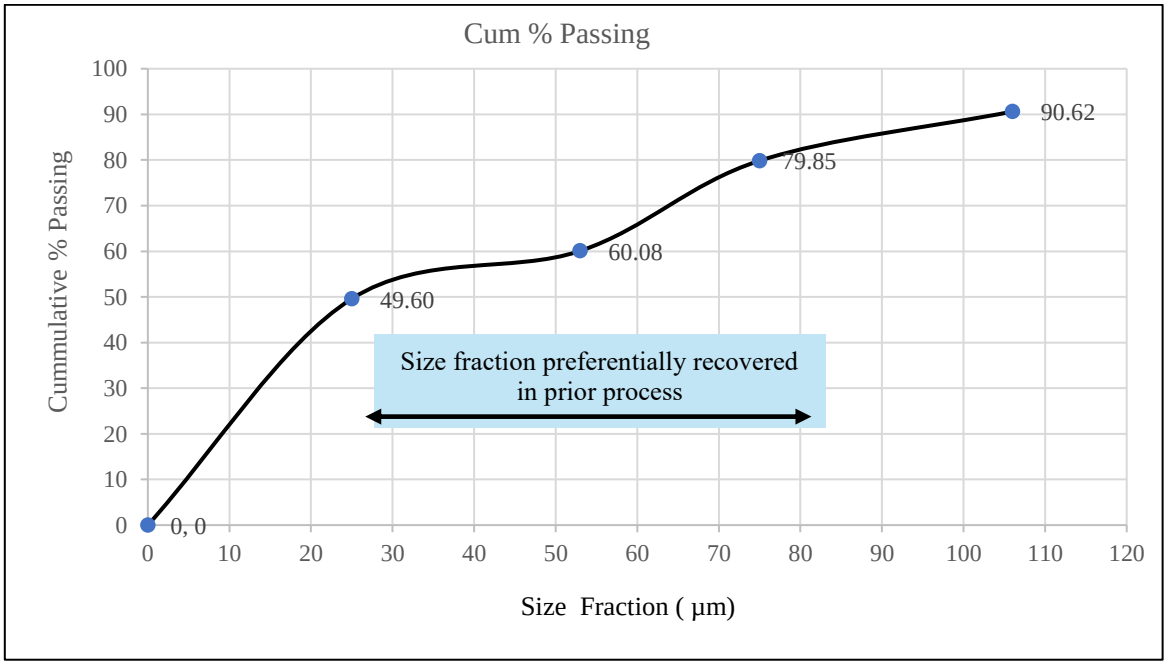

Figure 4.2: Feed Particle Size Distribution

Table 4.3 shows the assays per size fraction indicating the mineral oxides distribution across the particles size fractions that were analysed.

Table 4.3 Fractional distribution of main oxides in the feed material

	Mass	Al_2O_3	CaO	Cr_2O_3	MgO	SiO_2	Fe_2O_3	Cu	Ni	LOI (1050)
Unit	%	%	%	%	%	%	%	ppm	ppm	%
Test feed head	100	17.18	7.32	9.01	11.66	42.49	11.21	70.00	325.00	0.45
Test feed +106um	9.4	18.93	9.49	1.56	10.57	50.26	6.07	55.00	244.50	0.55
Test feed -106/+75um	10.8	17.19	8.23	4.27	12.34	48.00	8.46	105.00	260.00	0.40
Test feed -75um/+53um	19.8	16.41	7.15	8.63	12.10	42.18	11.17	60.00	442.00	0.21
Test feed -53/+25um	10.5	16.59	6.89	10.62	11.73	40.26	12.30	60.00	355.00	0.02
Test feed -25um	49.6	16.44	6.60	11.04	10.96	38.03	12.54	90.00	444.00	0.64

From the fractional chemical analysis, it is evident that Cr_2O_3 and Fe_2O_3 grades increase with decreasing particle size and highest grades of these minerals are found in the -75µm to -25µm fractions. SiO_2 shows an opposite trend as its grade decreases with a decrease in particle size. CaO also shows a decrease in grade as particle size decreases, while the grade of other main minerals i.e. Al_2O_3 and MgO remain largely unchanged as the particle size decrease. This data suggests that +75µm fraction has low chrome content i.e. less than 4.3%, indicating that when that size fraction is screened off, the remainder of the material is upgraded in terms of chrome content and may provide an opportunity of beneficiating a richer material in downstream processes.

4.1.3 X-Ray Diffraction Analysis

Table 4.4 and Figure 4.3 show the relative abundances of the minerals in the distinct size fractions of the feed sample as a % mass of the total crystalline phases identified.

Table 4.4 Mineral abundance per fraction by X-Ray diffraction Analysis

Sample ID	Recombined Head	Test Feed +106µm	Test Feed-106/+75µm	Test Feed - 75/+53µm	Test Feed - 53/+25µm	Test Feed - 25µm
Mass Distribution (%)	100.0	9.4	10.8	19.8	10.5	49.6
Chromite ($FeCr_2O_4$)	18.0	2.9	9.2	20.3	24.6	20.6
Feldspar ($KAlSi_3O_{8)}$	41.7	58.1	47.2	41.7	39.5	37.8
Chlorite $(Mg,Fe)_3(Si,Al)_4O$	1.7	1.3	1.1	1.0	1.0	2.3
Magnetite/Hematite Fe_2O_3/Fe_3O_4	0.1	0.1	0.1	0.1	0.1	0.1
Amphibole ($Mg_7Si_8O_{22}(OH_2)$)	2.1	0.8	0.6	0.6	0.6	3.5
Diopside ($CaMgSi_2O_6$)	2.7	2.5	2.7	2.6	2.6	2.8
Mica-Clay-$AB_{2–3}(X, Si)_4O_{10}(O, F, OH)_2$	0.8	0.9	1.0	0.8	0.7	0.7
Carbonates (CO_3^{2-})	0.2	0.2	0.1	0.2	0.2	0.2
Enstatite-Ferrosilite- $(Mg,Fe)SiO_3$	29.2	31.2	35.8	30.9	28.4	26.9
Ti Oxides (Ti_2O_3)	0.1	0.0	0.0	0.1	0.1	0.1
Quartz ($SiO_{2)}$	0.9	1.3	1.2	1.0	1.0	0.8
Talc $(Mg_3Si_4O_{10}(OH)_2$	1.4	0.4	0.6	0.6	0.8	2.2
Alumosilicates ($xAl_2O_3 \cdot ySiO_2 \cdot zH_2O$)	0.6	0.2	0.2	0.2	0.2	1.1
Other	0.5	0.3	0.2	0.2	0.3	0.9
Total	**100**	**100**	**100**	**100**	**100**	**100**

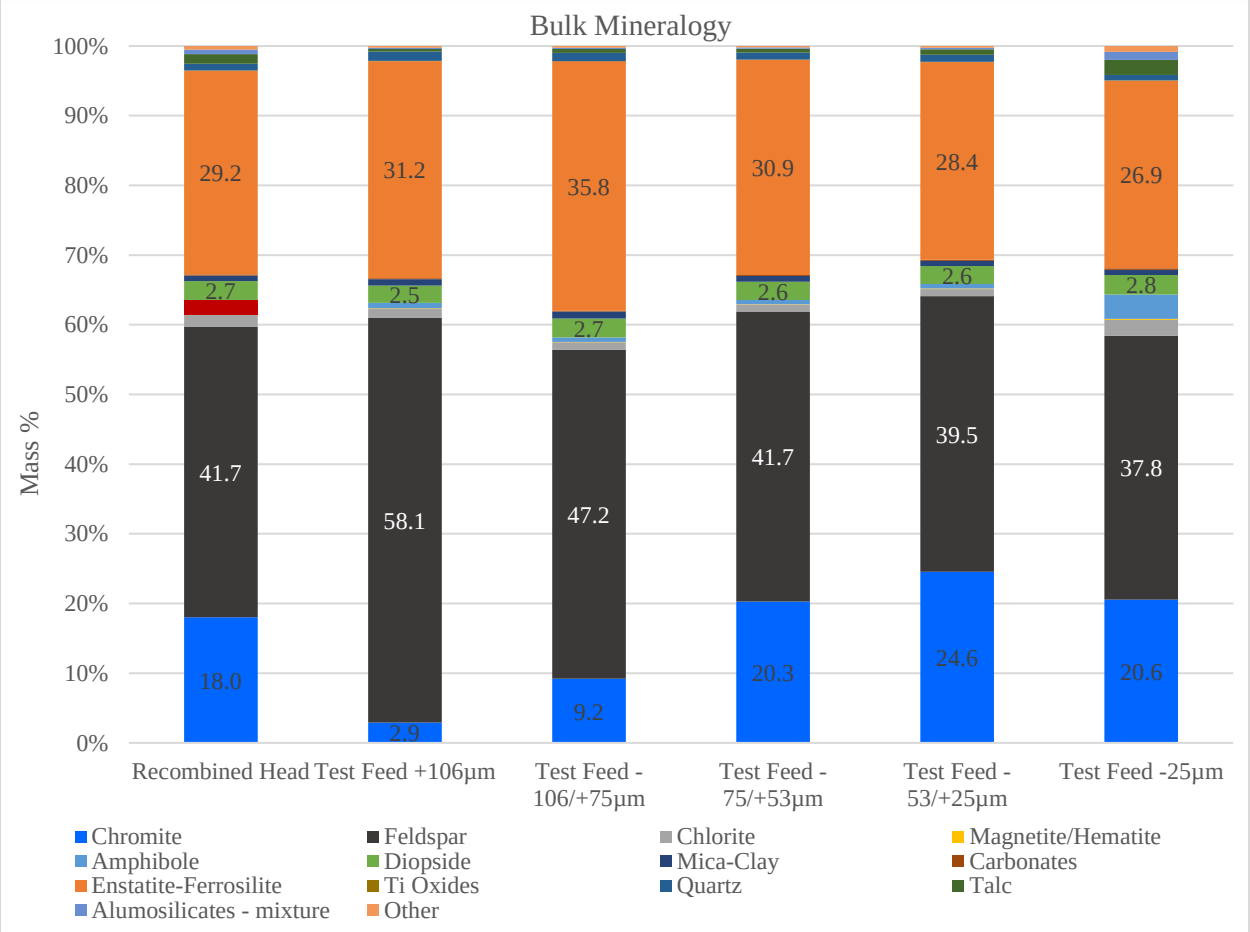

Figure 4.3 Mineral Abundance in the feed and distinct size fractions

The results from Table 4.4 and Figure 4.3 show feldspar as the most predominant mineral in the feed, followed by enstatite-ferrosilite (pyroxene) and then chromite across all the size fraction measured. Chromite, which is the mineral of interest in this study, increases in abundance from +106µm to -53 microns and then slightly dips at -25µm size fraction. This shows that more chromite is found in the fine to ultrafine size fraction, suggesting that the chromite liberates more efficiently at ultrafine grain size in this material. Enstatite-ferrosilite is mostly abundant in the -106+75µm size fraction and reduces as the size decrease from 75µm down to 25µm. Feldspar decreases in amount as the particle size decreases from 106µm down to 25µm. This suggests that enstatite-ferrosilite and feldspar that make up the bulk of the gangue material liberate at a much coarser particle size than chromite.

Figure 4.4 shows the X-ray diffractogram of the feed and size fractions as submitted for mineral abundance evaluation. The patterns confirm that the same minerals in the feed are found in the distinct size fractions.

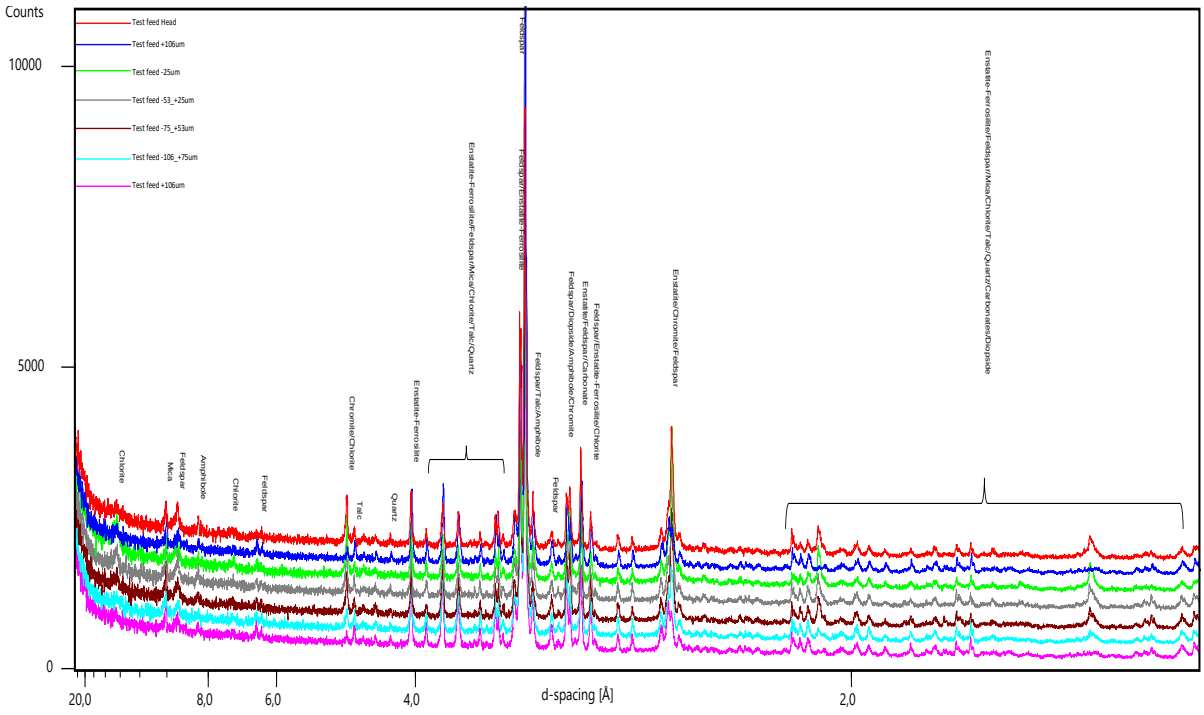

Figure 4.4 X-Ray diffractograms of the Head as well as other size fractions screened from the submitted head sample

4.1.4 SEM-EDS Analysis

The prepared polished sections were analysed by the TESCAN Integrated Mineral Analyzer (TIMA) using the Bulk Modal Analysis (BMA) as the measurement mode and Bright Phase Search method (BPS) for the Cr deportment. This analysis was carried out using Scanning Electron Microscopy (SEM) with Energy Dispersive X-Ray Spectroscopy (EDS). In this mode, the SEM provides the imaging component, while EDS is used for detection. The purpose of this test was to determine the chemical composition of each identified chromite grain. A maximum of 20 chromite mineral grains in each size fraction (from +106µm to 25µm) were analysed with detection limits of around 200 ppm. From this analysis, the Fe:Cr ratio was determined, and the emphasis was put on Fe, Cr, Mg, Mn, Al and O. Results of the SEM-EDS are shown in Table 4.5. Figure 4.5 shows the EDS image of the polished section containing chromite and gangue particles. The lighter particles are chromite particles due to the energy dispersed giving a brighter image. Low molecular mass elements do not disperse as much energy compared to Cr hence the dull colours on the image. The grey particles are predominantly silicates making up the gangue component.

Table 4.5: EDS composition results

Test Feed: All size fractions (+106µm to -25µm)						
Size Fraction	**O**	**Mg**	**Al**	**Cr**	**Fe**	**Cr/Fe Ratio**
+106	26.55%	4.60%	7.45%	36.50%	24.87%	**1:1.47**
-106+75	25.67%	4.75%	7.78%	36.98%	24.80%	**1:1.49**
-75+53	26.36%	4.65%	8.02%	36.09%	24.86%	**1:1.41**
-53+25	26.27%	4.35%	7.13%	36.24%	25.54%	**1:1.42**
-25	26.99%	4.67%	0.36%	36.08%	24.41%	**1:1.48**
Average	**26.37%**	**4.60%**	**7.60%**	**36.38%**	**24.90%**	**1:1.45**

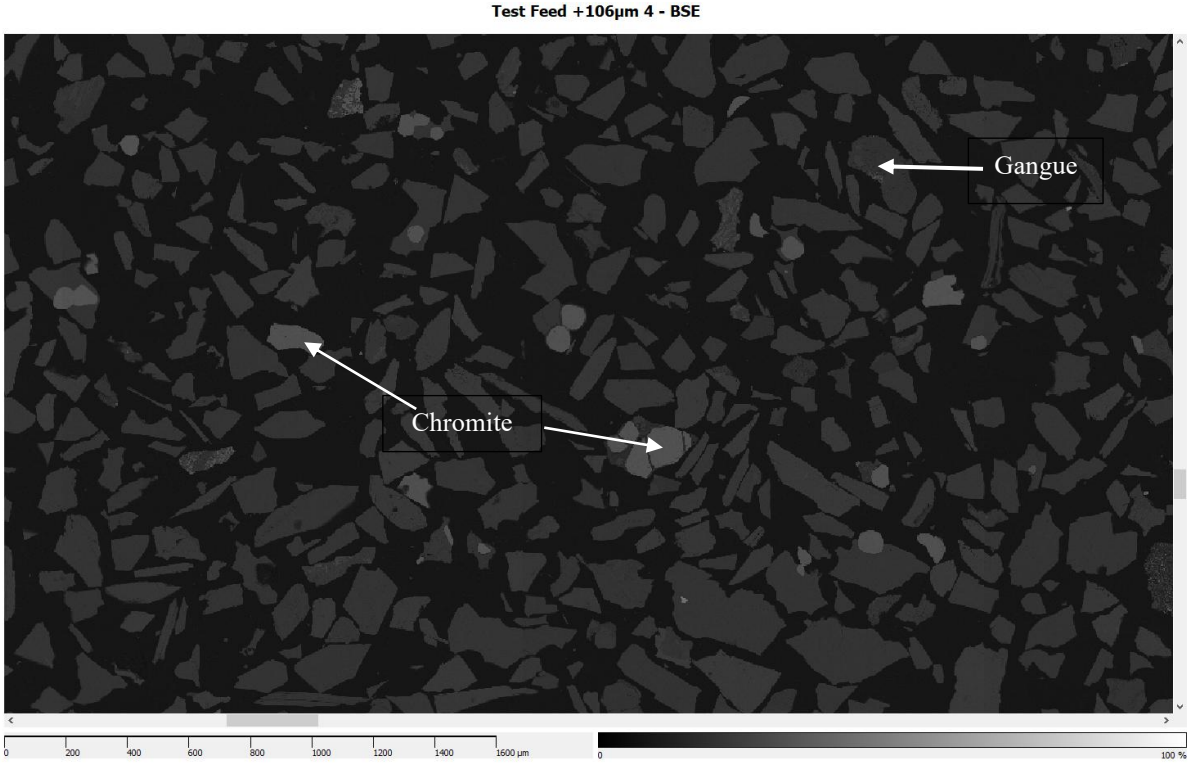

Figure 4.5 EDS Image of a field of chromite and gangue particles

From the results in Table 4.5, the major components in each chromite grain particles are Cr at 36.38%, followed by O_2 at 26.37% and then Fe at 24.90%. Al and Mg contribute 7.60 and 4.60%, respectively. It is important to note that the O represents the oxygen in all the oxides measured by EDS. The average Cr/Fe ratio of all the measured chromite particles is 1.45:1. The Cr/Fe ratio is important in determining the end use of the chromite concentrate. The EDS results of other size fractions are given in the appendix. One notable observation is the absence of Si in chromite grains, while other elements like Al, Mg and Fe are present. This is because

SiO_2 and $FeCr_2O_4$ do not substitute each other in the complex chromite mineral chain. The proportion of each of the components in the grains gives the grain particles their physical properties like density, hardness, lustre, and colour and these are used in minerals separation processes.

4.1.5 Chrome and Iron deportment

The mineral phases that were identified by the XRD method were searched by TIMA in the PMA mode of measurement. Specifically, focus was put on the mineral phases on a planar surface of the mounted specimens measuring the concentration of Cr in each of the phases. The main purpose of this analysis was to determine the mineral phases that are the main sources of Cr and Fe in each specific size fraction. The measurement of the two elements would allow for the determination of Cr/Fe ratio in the ore for the purposes discussed in section 4.1.4. Table 4.6 shows the deportment of the element Cr identified by XRD in chromite in Table 4.4 as a function of particle size fraction. What this table shows is that the chromite mineral phase is the only source of Cr in the sample's distinct size fractions. Similarly, when considering Fe deportment, Table 4.7 shows the deportment of Fe in the different minerals phases as function of size fractions.

Table 4.6 Chrome deportment in the mineral phases

Cr Deportment					
	Test Feed +106µm	**Test Feed -106/+75µm**	**Test Feed -75/+53µm**	**Test Feed -53/+25µm**	**Test Feed -25µm**
Chromite	100%	100%	100%	100%	100%

Table 4.7 Fe Deportment in the mineral phases

Fe Deportment					
	Test Feed +106µm	**Test Feed -106/+75µm**	**Test Feed -75/+53µm**	**Test Feed -53/+25µm**	**Test Feed -25µm**
Chromite	19.8	41.04	63.78	69.32	62.44
Chlorite	3.44	1.93	1.19	1.11	2.59
Magnetite/Hematite	2.02	0.68	0.59	0.76	0.98
Amphibole	2.08	1.02	0.74	0.62	3.68
Diopside	0.27	0.18	0.13	0.12	0.19
Mica-Clay	1.41	1	0.53	0.39	0.3
Enstatite-Ferrosilite	69.99	53.17	32.18	26.59	25.08
Pentlandite	0	0.03	0	0	0
Ti Oxides	0	0	0.03	0.03	0.03
Pyrite	0	0.06	0.01	0.02	0
Talc	0.32	0.49	0.56	0.78	2.9
Other	0.67	0.4	0.26	0.26	1.81
Total	**100**	**100**	**100**	**100**	**100**

Table 4.6 shows that 100% Cr element comes from the chromite mineral, and it is not hosted in any other mineral phase within the ore. This means that there is no other mineral in this feed material that contributes Cr other than the chromite phase itself. The deportment of the element Fe in the minerals phases was also evaluated and the results are given in Table 4.7. The biggest contributor of Fe in the +106µm size fraction is enstatite-ferrosilite, contributing 69.99% followed by chromite that contributes 19.8%. Chlorite, Magnetite/hematite, and amphibole each contributes just below 4% of the Fe. As the particle size fraction decreases, the contribution of Fe from enstatite-ferrosilite also decreases. However, chromite contribution increases from +106µm up to -53µm before slightly dipping in the -25µm size fraction. The other minerals are minor contributors of Fe even in particle size fraction below 106µm.

4.1.6 Minerals Association

Mineral association data is derived from shared boundaries amongst the identified mineral grains. The interpretation from the mineral association data is that the higher the associated percentage is, the greater the degree of boundary sharing between the mineral species. Table 4.8 and Figures 4.6 to 4.10 show the mineral association data and particle maps of all the minerals identified by XRD.

Table 4.8 shows the mineral associations of the feed material under investigation. The feed chromite particles (head sample) have 95.31% free surface area. The balance of 4.69% of the area that is not free and is in contact with feldspar (1.63%), enstatite-ferrosilite (1.14%) and other minerals each contributing less than 1%. It should be noted that pores contribute 0.7% of

the association. When each size fraction is considered, the free surface area increases from +106 µm to -53+25µm size fraction and then dips down at -25µm size fraction. This means that as the chromite particle size decreases the free surface area increases. At -106 µm size fraction and below, the chromite particles' free surface area is above 95% indicating close to full liberation. Figures 4.6 to 4.10 show the shared surface between the chromite particles and gangue particles from 106µm down to -25µm size fraction. What can be inferred from this characteristic is that any surface treatment that can be used on the chrome particles is more effective as the size fraction decreases. This also means that a decision to screen this feed sample at 106µm and treat the fractions separately may yield different results than treating the feed as a whole.

Table 4.8 Mineral Association data for the tested points

Mineral Association	Test Feed +106µm	Test Feed -106/+75µm	Test Feed -75/+53µm	Test Feed -53/+25µm	Test Feed -25µm	Head Sample
Chromite Free surface/Exposed	**71.90**	**96.43**	**98.36**	**98.43**	**97.62**	**95.31**
Feldspar	13.18	0.59	0.27	0.33	0.49	1.63
Chlorite	2.70	0.85	0.29	0.19	0.21	0.53
Magnetite/Hematite	0.04	0.02	0.01	0.00	0.00	0.01
Amphibole	0.57	0.07	0.03	0.03	0.24	0.19
Diopside	0.20	0.04	0.02	0.02	0.03	0.04
Mica-Clay	0.60	0.14	0.05	0.03	0.02	0.09
Carbonates	0.11	0.01	0.01	0.01	0.00	0.01
Enstatite-Ferrosilite	6.01	0.98	0.39	0.39	0.71	1.14
Ti Oxides	0.06	0.03	0.02	0.01	0.00	0.01
Quartz	0.22	0.03	0.01	0.01	0.01	0.03
Talc	0.48	0.04	0.01	0.01	0.04	0.07
Alumino-silicates - mixture	0.66	0.17	0.08	0.06	0.11	0.16
Other	0.19	0.06	0.02	0.02	0.07	0.07
Pores	3.07	0.54	0.43	0.46	0.45	0.70
Total	100.00	100.00	100.00	100.00	100.00	100.00
% Mass Distribution	**9.38**	**10.77**	**19.77**	**10.48**	**49.6**	

4.1.6.1 Mineral Particle Maps

The mineral particle maps were performed on the five samples which were generated from screening the feed into distinct size fractions. The particle size classes that were analysed were +106µm, -106µm+75µm, -75µm+53µm, -53µm+25µm and -25µm. The 38µm class was not included due to too little mass in that fraction to perform all the tests contemplated. As part of the mineral association analysis, the TIMA was put in the Bright Phase Search (BPS) mode.

About more than 3000 grains were analysed by the QEMSCAN particle mineral analyses (PMA) technique on a polished section of each size fraction. The QEMSCAN in PMA mode produced a particle map, depicted in the Figures below, containing textural data such as particle size and shape, and mineral association images. The following table is the key to the mineral identity of the particle maps given below. The main purpose of these particle maps is to show the chromite particle sizes and any associated gangue particles. The maps do not show the relative abundance of the mineral in the matrix, but they show the size and shape of the chrome particles in each size fraction.

Table 4.9: Mineral maps colour key for phase identification

Mineral	Phase Colour
Silicates	
Fe-Ti Oxides	
Chromite	
Other	
Carbonates	

4.1.6.2 +106 µm Mineral Particle Maps

Figure 4.6 below gives the particle map for the +106µm particle size range. The main phase of focus was the chrome particles, showing the shape, size, and any association at this size. The shape of the chrome particles ranges from circular (spherical in 3-D) to angular and elongated. The silicate particles, which are associated with a considerable proportion of the chrome particles, are largely elongated to angular in form. What is interesting to observe is that of all the particles that are associated with each other, it is the silicates that encapsulate the chrome particles and not the other way round.

The bulk of the chromite particles that are still associated with gangue are associated with feldspar at 13% of total surface. This is followed by enstatite-ferrosilite at 6% of the total surface. The total association in this size fraction is about 28 % leaving 71.9 % free chromite surface.

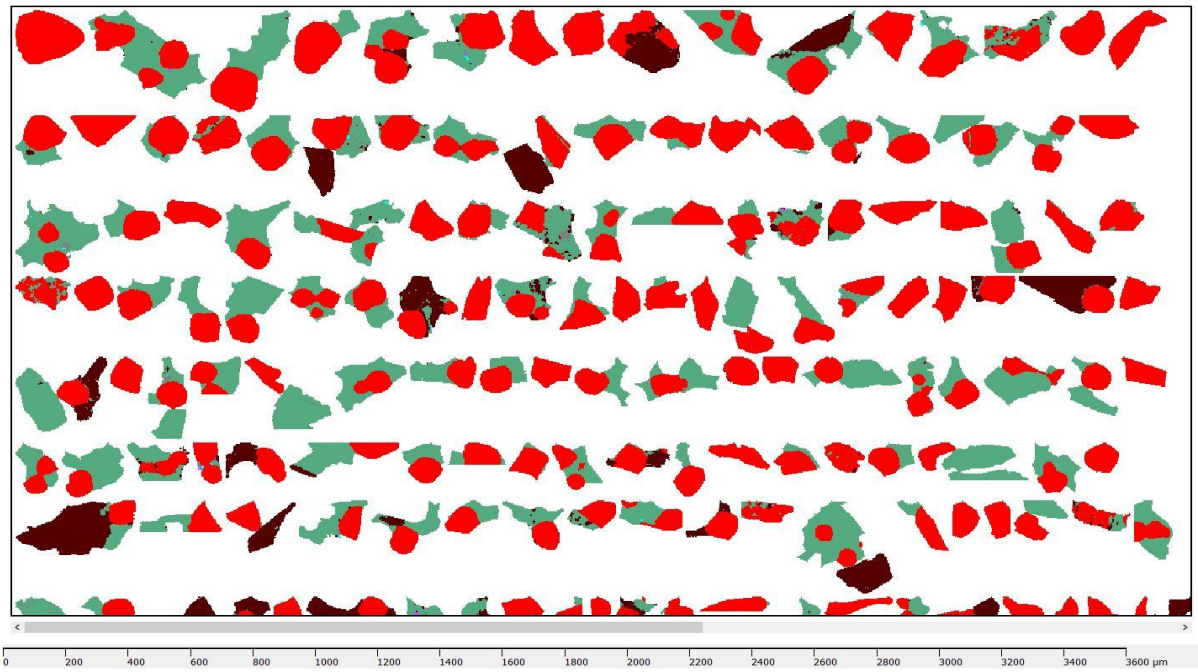

Figure 4.6: Particle map showing mineral association for +106µm size fraction

4.1.6.3 -106µm+75 µm Mineral Particle Maps

The next size fraction to be analysed was the -106 +75 µm. The particle map is shown in Figure 4.7 below. The general shape of the chrome particles is now more angular and elongated compared to the coarser fraction of +106 µm. There is an exceedingly small number of chrome particles that are still associated with gangue particles. Silicates and Fe-Ti oxides are the gangue particles that were found associated with the chrome particles. The average particle size range is between 70µm and 120µm. An interesting observation is that there are some particles that are elongated such that their lengths are larger than the 106µm, but they have been classified as under 106 µm. This means that the aspect ratio of these particles allows them to orient themselves with screen holes and pass through utilising the short dimension to pass through. The association in this size fraction is only 3.5%. This means in terms of separability the particles wholly behave as chromite particles from surface properties and density.

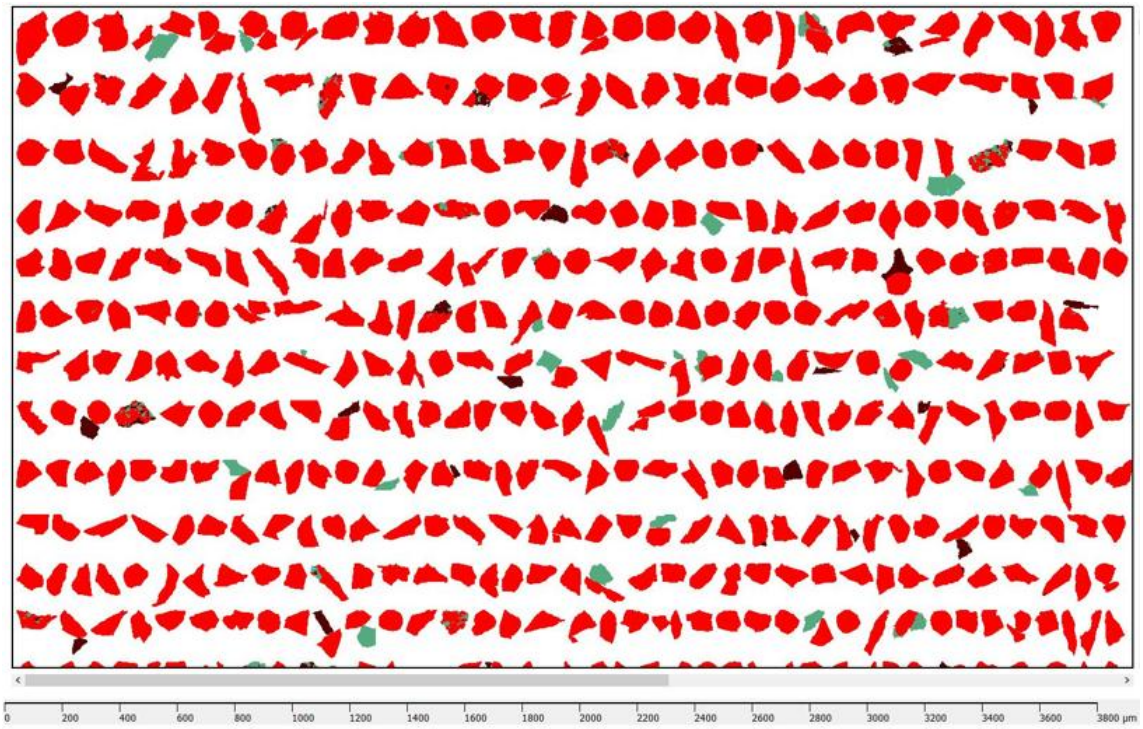

Figure 4.7 Particle map showing mineral association for -106µm + 75µm size fraction

4.1.6.4 -75µm+53µm Mineral Particle Maps

Figure 4.8 is the particle map for the -75µm +53µm size fraction. Of all the particles identified and analysed by the software program, the general shape of the chrome particles is a mixture of rounded and elongated and angular particles. From the map, it is also evident that the gangue particles are smaller than the chrome particles. The chrome particles are almost 100% free from any association with the gangue particles. As observed in Table 4.7, the only surface that is associated with gangue is about 1.7%. The almost flat and elongated particles might present difficulties in gravity separation processes where rolling might aid separation. When the particles are flatter and more elongated the settling under gravity might be compromised because the wide flat face may be perpendicular to force of gravity, and this will make the particle to have an exceptionally low settling velocity.

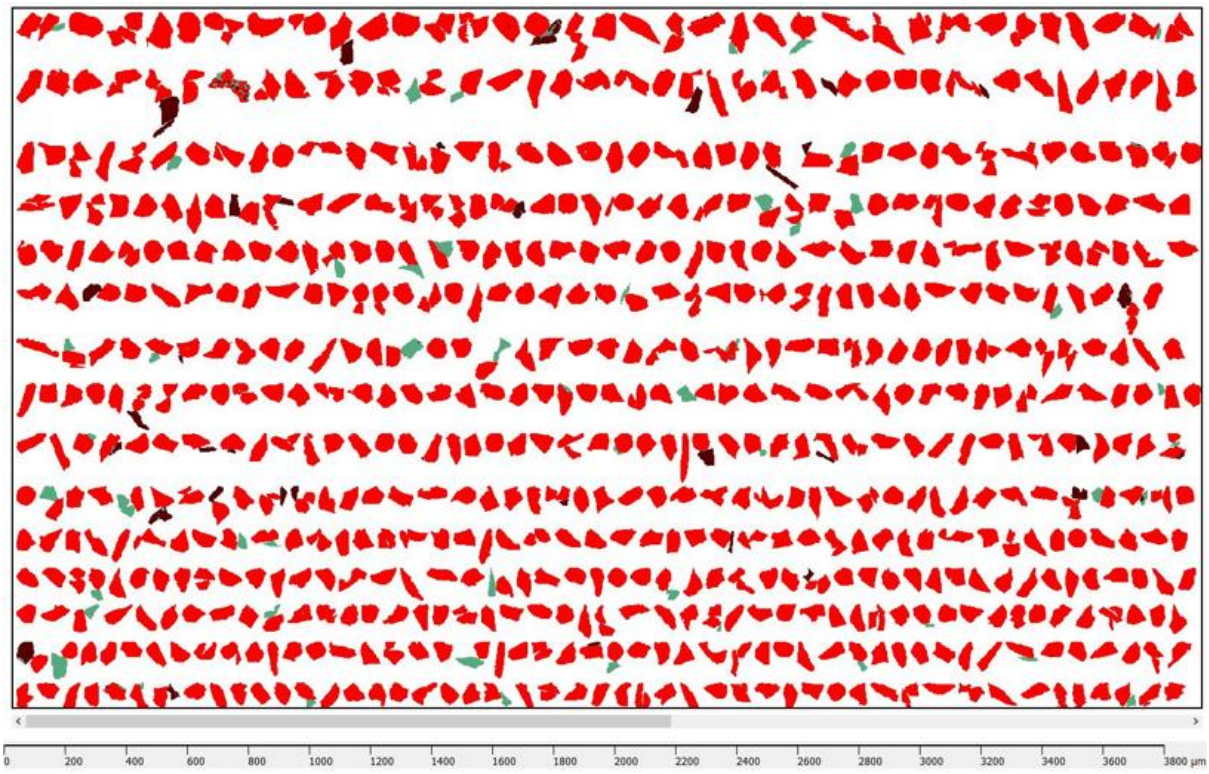

Figure 4.8 Particle map showing mineral association for -75µm + 53µm size fraction

4.1.6.5 -53µm+25µm Mineral Particle Maps

Figure 4.9 below shows the particle map pattern for the fraction -53µm+25µm. It is noticeably clear that this size fraction has more elongated chrome particles than the coarser fractions. A few chrome particles have some associations with gangue in the form of silicates and Fe-Ti oxides. The free surface of the particles from Table 4.7 is given as 98.6%. This means at this size fraction chrome particles are in the fully liberated band of liberation classification. It must be noted that the particle map arranges courser particles of the range on the top side of the map and the fine particles at the bottom portion of the map.

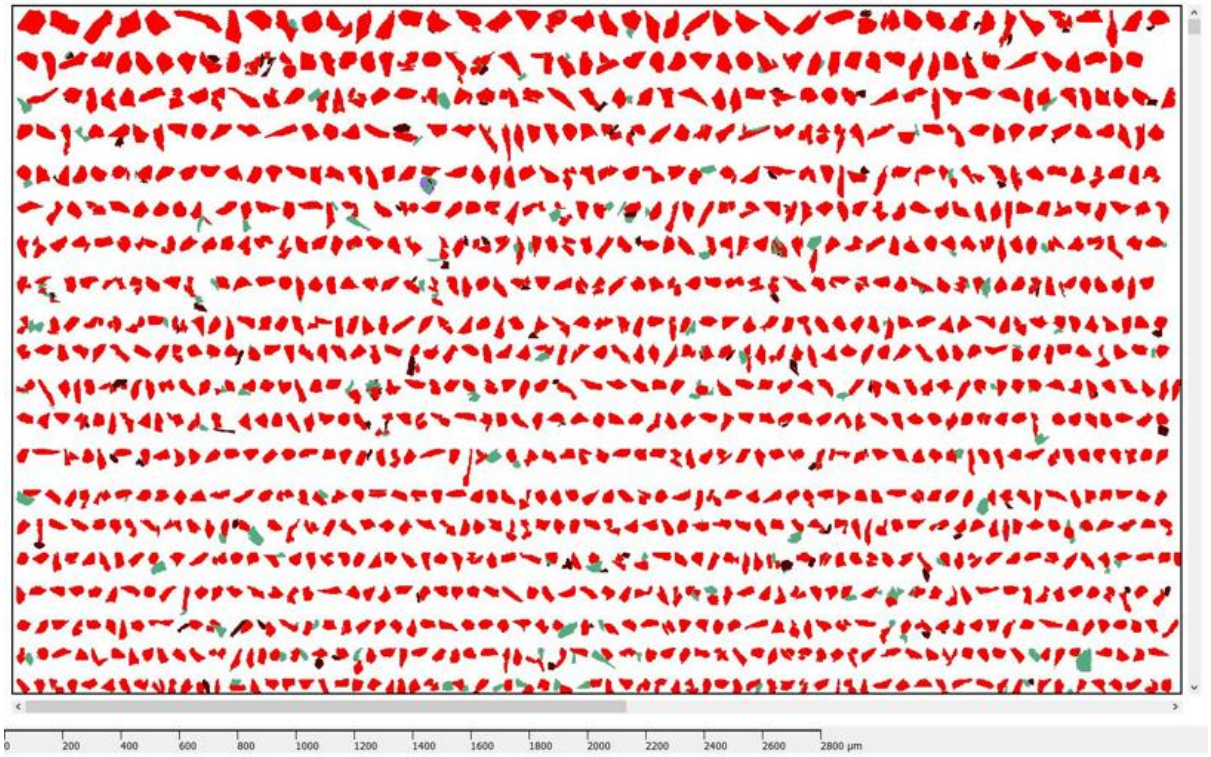

Figure 4.9 Particle map showing mineral association for -53µm + 25µm size fraction

4.1.6.6 -25µm Mineral Particle Maps

The last particle size map is that of the ultrafine material as shown in Figure 4.10 below. The particle shape is also more elongated than the coarser fractions. The particles are remarkably close to being free of any association with other gangue particles. From Table 4.7, the associated surface area is about 2.3%, which is slightly higher than the two coarse fractions above this one. The reason for this slight increase in association is that at this size most of the chrome particles which have been broken from the gangue particle have some remnant of gangue still attached hence the slightly higher associated surface area.

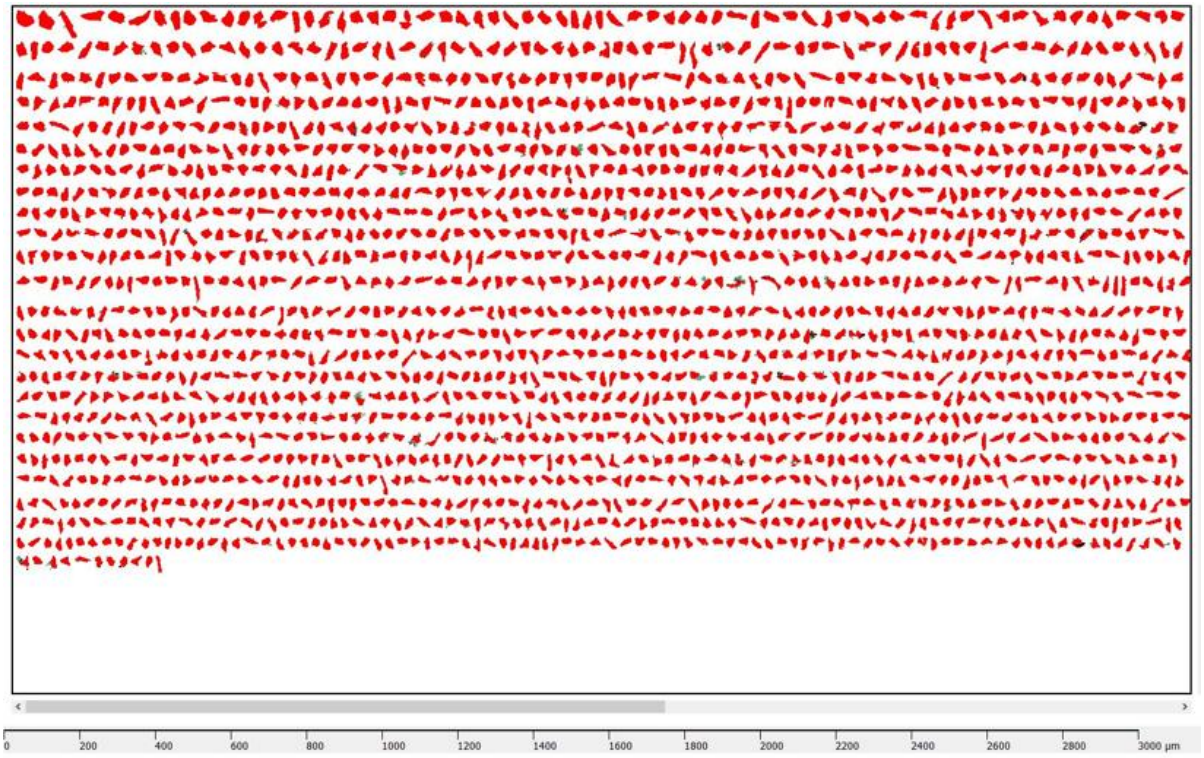

Figure 4.10 Particle map showing mineral association for - 25µm size fraction

4.1.7 Chromite Liberation

Liberation is different from free surface area. The degree of liberation is typically based on the % area of the mineral grain(s) of interest in a particle. When observing particles on a planar polished surface, the area covered by the free value mineral grain in a mineral particle represents the degree of liberation, but this is converted into volume %. Whereas free surface area represents the perimeter of the value mineral grain that is not attached to any particle. Table 4.10 gives the distribution of liberation percentages across the distinct size fractions compared to the feed.

The liberation of mineral particles is usually classified into 5 classes. When fully liberated, a value mineral grain is 100% i.e. it is not attached to any gangue grains. In this test, only 4 classes were considered to indicate the liberation of the grains. Liberated is when particles are between 70% and 100% liberated. This is then followed by high middling with liberation levels between 50% and 70% and low middling between 30% and 50%. The last class that is poorly liberated is referred to as ‘locked’ with only 0 to 30% liberation.

Table 4.10: Liberation of chromite particles in the feed and the five size fractions

Liberation classes	Liberation of Chromite	Head Sample	Test Feed +106µm	Test Feed -106/+75µm	Test Feed -75/+53µm	Test Feed -53/+25µm	Test Feed -25µm
Locked	**<10**	1.0	5.4	0.3	0.1	0.1	0.8
	≥10<20	1.0	6.3	0.6	0.3	0.3	0.6
	≥20<30	1.2	7.7	0.7	0.6	0.5	0.5
Low Middlings	**≥30<40**	1.5	9.4	0.9	0.9	0.8	0.5
	≥40<50	1.3	6.4	1.1	0.9	1.2	0.5
High Middlings	**≥50<60**	1.8	9.6	1.4	1.1	1.5	0.8
	≥60<70	1.4	4.8	1.5	1.2	1.3	0.9
Liberated	**≥70<80**	1.7	5.4	1.6	1.0	1.2	1.3
	≥80<90	2.2	3.0	1.8	1.2	1.3	2.7
	≥90	87.0	41.9	90.0	92.7	91.9	91.6
Total		100.00	**100**	**100**	**100**	**100**	**100**
% Mass Distribution		100	9.38	10.77	19.77	10.48	49.6

Table 4.10 shows that the feed (head) sample has a total of 90.82% of particles in liberated class, with 6.0% of particles in middling class and only 3.2% in locked class. Considering the size fractions from + 106µm down to - 25µm, the liberated particles increase from 50.3% to 95.5%. The middling and locked percentage decreases with decreasing particle size. This indicates that separation of the chromite particles from the gangue should be easier with decrease in particle size based on the degree of liberation. However, this is normally impeded by other physical properties of particles in minerals separation processes.

Figure 4.11 clearly shows the trend of the liberation in volume % against size fraction. The feed material shows that 87 % of the chromite grains are ≥90%-100% liberated, while 3.9% is just under between 70% and 90% liberated. Comparison of the liberation extents between the size fractions shows that the liberated (≥70) particles are 50.3% for the +106µm size fraction and generally increases as the size decreases to -25µm (95.5%). It is also worth noting that the volume of locked particles in the -25µm size range is higher than that in the -75 and 53µm size fractions. The explanation for this unexpected anomaly is rooted in the liberation by milling. Since liberation by milling occurs through cracks and grain boundaries, at exceedingly small sizes the cracks are so small that fracture is more difficult to initiate causing the exceptionally fine mineral grains to remain attached to the gangue.

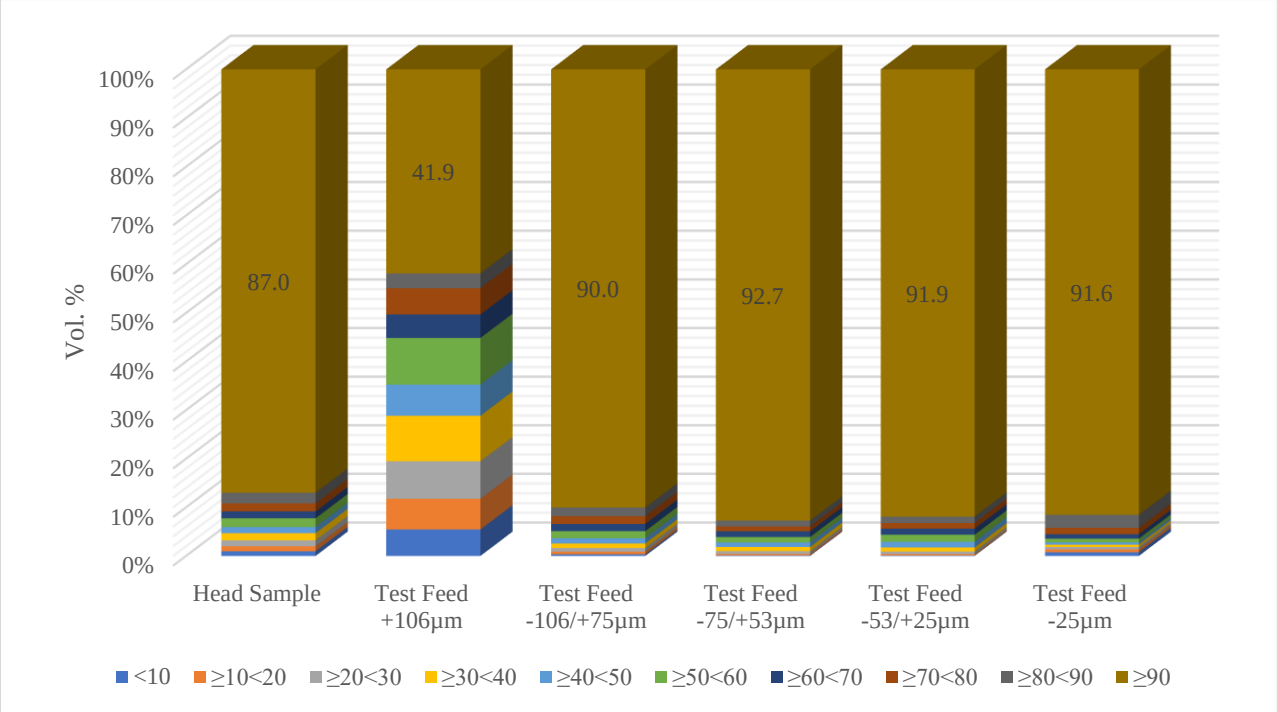

Figure 4.11 Graphical representation of liberation of chromite particles

Figure 4.12 shows the volume % of liberation in terms of the three main broad classes, 'Locked,' 'Middling' and 'Liberated.' The +106µm size fraction has the highest middling and locked classes compared to all the other five size fractions. From a separation perspective, the -106µm size fraction would behave differently from the other four due to its wide spread of grains still locked with the gangue particles. It may require screening off and re-milling to improve liberation.

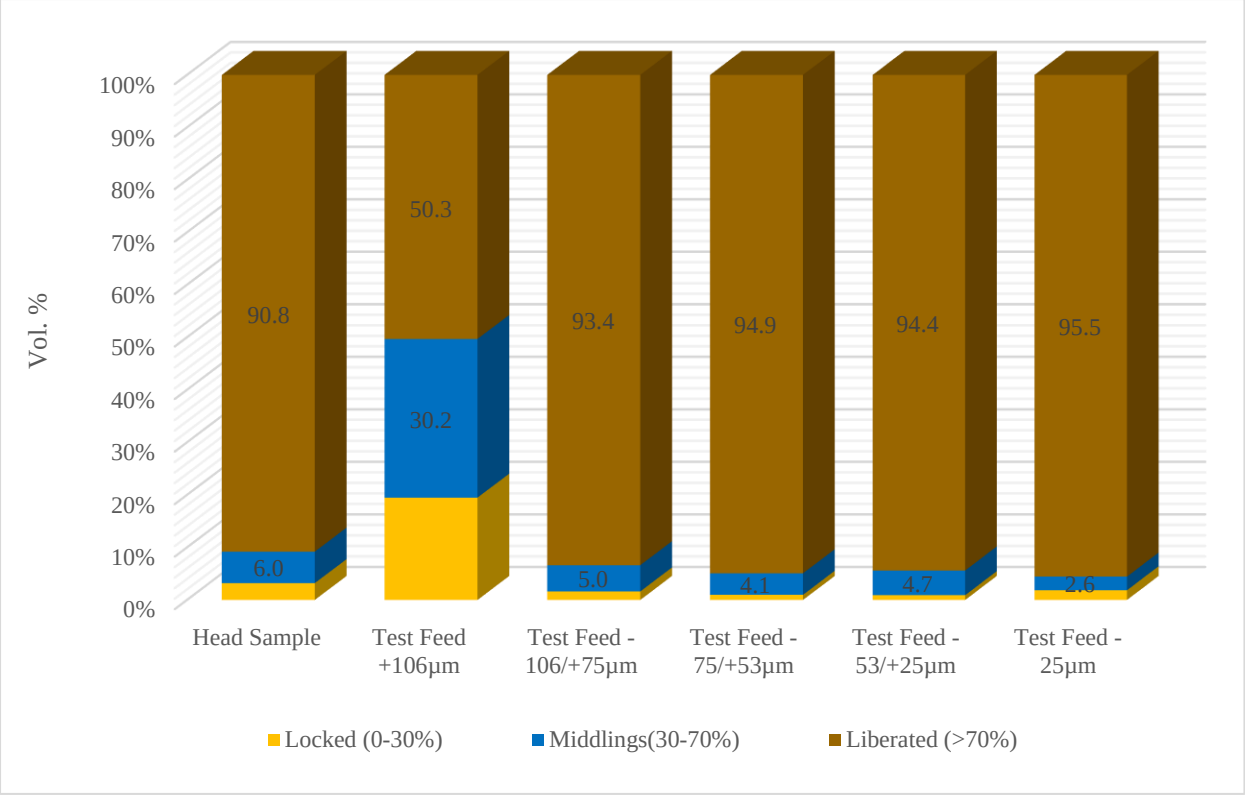

Figure 4.12 Three main liberation classes comparison across the five-size fraction.

4.1.8 Chromite Grain Size Distribution

The mineral grain sizes are presented in terms of equivalent sphere diameter (ESD), which represents the diameter of a sphere of equal volume to the grain measured. The grain size distribution for the feed material shows that in the +106µm fraction, the bulk of the grains are in the 60-100µm ESD. In the -106+75µm size fraction, the bulk of the grains (54.2%) are size ≥20<60µm, while in the -75+53 µm size range the bulk (87%) is also in the ≥20<60µm. In the minus 53 µm size fraction, about 20 % grains are in the ≤20 µm with about 78% between 20 and 60 µm. For the size fraction -25µm, most of the grains are in the <20µm grain size band. This information shows that for this material; chromite grains are predominantly in the size ≤20 µm since this particle size range has the highest mass fraction of 49.6% in the head sample.

Table 4.11: Grain size distribution (GSD) of chromite grains in the feed and distinct size fractions

WGSD Size of Chromite (um ESD)	Head Sample	Test Feed +106µm	Test Feed - 106/+75µm	Test Feed - 75/+53µm	Test Feed - 53/+25µm	Test Feed - 25µm
<20.00	46.6	5.9	4.0	7.0	20.4	84.9
≥20.00<60.00	41.0	23.2	54.2	87.0	78.9	15.1
≥60.00<100.00	10.2	48.7	40.0	6.1	0.7	0.0
≥100.00<150.00	2.1	20.3	1.9	0.0	0.0	0.0
≥150.00<190.00	0.1	1.2	0.0	0.0	0.0	0.0
≥190.00	0.1	0.7	0.0	0.0	0.0	0.0
Total	100.0	**100.0**	**100.0**	**100.0**	**100.0**	**100.0**

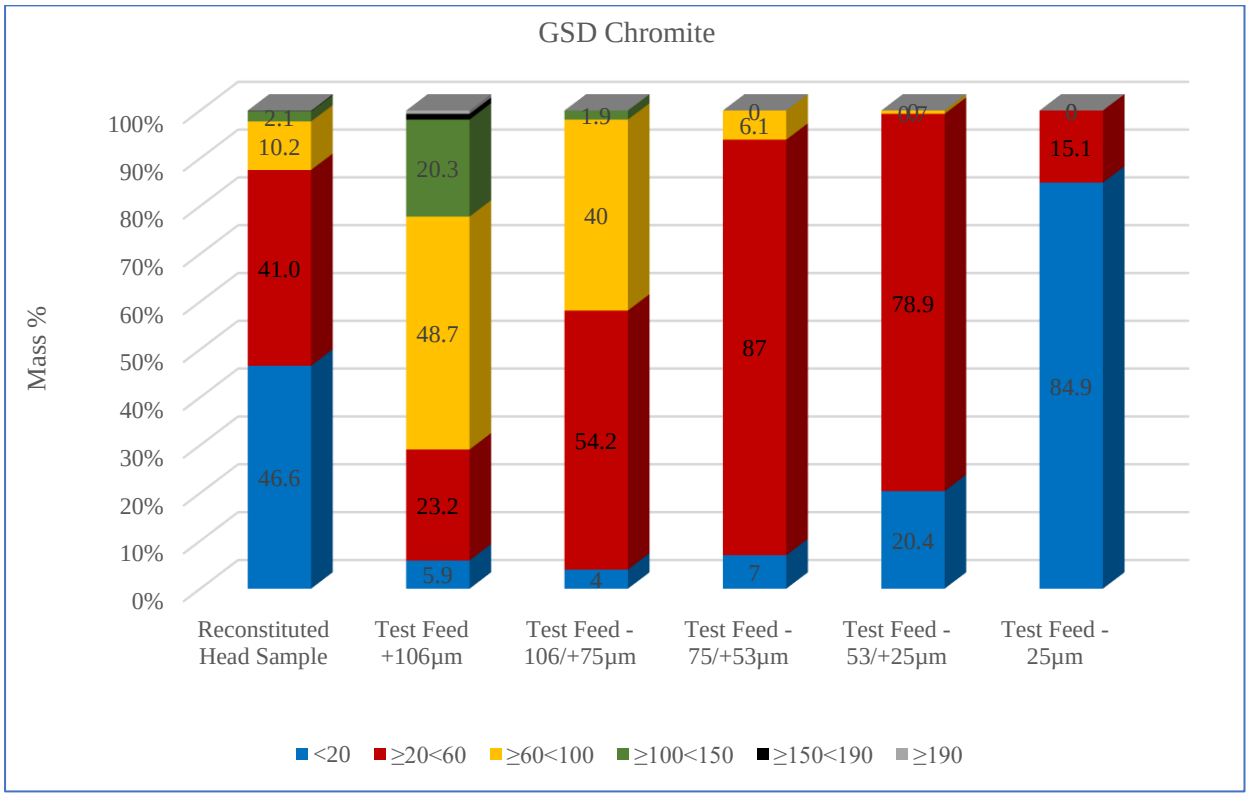

Figure 4.13 Grain size distribution of chromite grains

This data also indicates that at smaller particle sizes the grain sizes increasingly approach the particle size of the material.

4.2 Feed Characterisation Conclusion

The feed characterisation results show that the main components/minerals of the feed under investigation in order of abundance are SiO_2, Al_2O_3, MgO, Fe_2O_3, Cr_2O_3, and CaO collectively

contributing above 98% of the mass. The main components of interest are Cr_2O_3 and Fe_2O_3 and their association with other mineral components determines how well the separation can be achieved.

The main mineral phases in the feed materials are feldspar, pyroxene (enstatite-ferrosilite), chromite, diopside, amphibole and chlorite. The proportion of chrome phase was found to increase as the size fraction decreases from 106 down to 53 µm. However, the trend changes as the amount of chromite at below 25µm is less than that in the -53+25µm. This deportment of the chrome phase makes it possible to achieve a good degree of concentration by only screening out the coarser size fraction i.e. > 106 µm.

It was also established that the chromite mineral is the only source of Cr element, while chromite, pyroxene, and chlorite are the sources of element Fe, according to the deportment analysis. The contribution of these two elements comes more from the finer size fractions of the feed material.

In terms of mineral association, it was observed that the feed material contains a high amount of chromite with free surface area. The free surface area increases with decreasing particle size. At distinct size fractions, the chromite is associated with different mineral phases like feldspar, pyroxene, chlorite, and other lesser amounts of other minerals. It is also possible to determine the contaminants of the chrome in particular size fraction from the association and free surface data. The association data closely correlates with the liberation data. It was shown that the liberation of the chromite grains improves with reduction in particle size. The feed material as is, is well liberated (90% liberated) such that there is no need for further comminution to liberate the chromite grains.

The information from this characterisation test-work can be used to guide the separation process and to infer on the equipment performance based on their separation windows. This can further assist in the selection and positioning of the separation equipment in the circuit. An evaluation of the separation equipment will be assessed in conjunction with the information generated from the feed characterisation studies to design an optimum circuit to recover chrome from the ultrafine feed material.

CHAPTER 5: SEPARATOR PERFORMANCE AND COMPARISON RESULTS

5.1 Introduction

The test-work for developing a circuit for beneficiating ultrafine chrome from chrome and PGM tailings was carried out using a setup that consists of a few conventional processing equipment. The uniqueness of the study is that the conventional pieces of equipment were used under different optimum conditions to address the recovery of ultrafine particles, which are normally not recovered during conventional chrome processing. The features and characteristics of the different pieces of equipment that were deployed in the experimental investigations will be discussed with the view to justifying why they have been selected for the investigation of beneficiation of ultrafine chrome particles. These pieces of equipment were tested singularly and in different combinations to determine the optimum combinations that maximise recovery and grade of the chrome final concentrate product and minimise loss of chrome to the tails. The following sections present the fundamentals of Design of Experiments (DOE) as well as describe the equipment selection, test-work set-up and the scoping tests that were carried out to address the research questions.

5.1.1 Design of Experiments -Background

The concept of DOE is a powerful statistical tool introduced by R Fisher in the 1920s when he was investigating the simultaneous effect of multiple variables on the response variable or objective function (Durakov, 2017, Ranga *et al*, 2014). In the late 1940s, Genuchi Taguchi, a Japanese statistician carried out research with DOE techniques and he applied these to improve the quality of manufactured products. (Durakovic, 2017).

5.1.2 Design of experiments -Fundamental Principles

The fundamental principles in design of experiments are solutions to the problems in experimentation posed by the two types of nuisance factors and serve to improve the efficiency of experiments (Telford, 2007, Montgomery, 2013). The fundamental principles are:

- Randomization
- Replication
- Blocking

- Orthogonality
- Factorial experimentation

The following sections describe in brief what each of the fundamental principles mean.

5.1.2.1 Randomization

Randomization is a method that protects against an unknown bias distorting the results of the experiment. This means that the testing sequence of the baseline and new factors and/or levels should be done in random order.

5.1.2.2 Replication

Replication is repetition of an experiment or observation in the same or similar conditions. It increases the sample size and thereby increasing the precision of an experiment. Replication increases the signal to noise ratio when the noise has its genesis in uncontrolled nuisance variables.

5.1.2.3 Blocking

Blocking is used to remove the effects of a few of the most important nuisance variables. It increases precision by removing the effect of nuisance factor such as batch-to-batch variability. In blocked design, both the baseline and new procedures are applied to samples of material from one batch then to samples of another batch. Looking at the method, blocking is a restriction of complete randomization since both procedures are always applied to each batch.

5.1.2.4 Orthogonality

Factors in an orthogonal experiment are varied and independent of each other. The effects of any factor balance out (sum to zero) the effects of the other factors.

5.1.2.5 Factorial experimentation

This is a method in which the effect due to each factor and/or a combination of factors is estimated. Factorial designs including fractional factorials have increased precision over the types of designs because they have built-in internal replication.

5.1.3 Purpose and Uses of Design of Experiments

The main uses of design of experiments are:

- Discovering interaction among factors

- Screening many factors
- Designing robust products
- System optimization
- Establishing and maintaining quality control

5.1.4 Types of Design of Experiments

According to Telford (2007), there are generally two categories of design of experiments (DOE), classical and modern designs. Classical designs are mostly used to introduce DOE concepts, whereas modern designs are mostly used by industry practitioners in carrying out experiments. Below are short summaries of each type of DOE.

5.1.4.1 Full Factorial Designs

In full factorial design, trials are run at all possible combinations of factor settings. The sample size is the product of the numbers of levels of the factors. For example, a factorial experiment with a two-level factor, a three-level factor and a four-level factor has 2 x 3 x 4 = 24 runs. One characteristic of the full factorial design is that it is expensive in terms of resources and time to run as the sample size grows exponentially with the number of factors. Full factorial design is often used when the number of factors and levels are small.

5.1.4.2 Fractional Factorial Designs (Screening designs)

To reduce the costly effect of the full factorial design, fractional factorial designs, sometimes referred to as screening designs, are among the most popular designs for industrial experimentation where time and costs are critical. They are used in the initial stages of experimentation to narrow down the lengthy list of potentially key factors and interactions to only a few important effects. To get the number of runs, a fractional design builder is used as shown in Table 5.1 below.

Table 5.1: Two-Level Fractional Factorial Design Builder (Danacıoglu and Muluk, 2005)

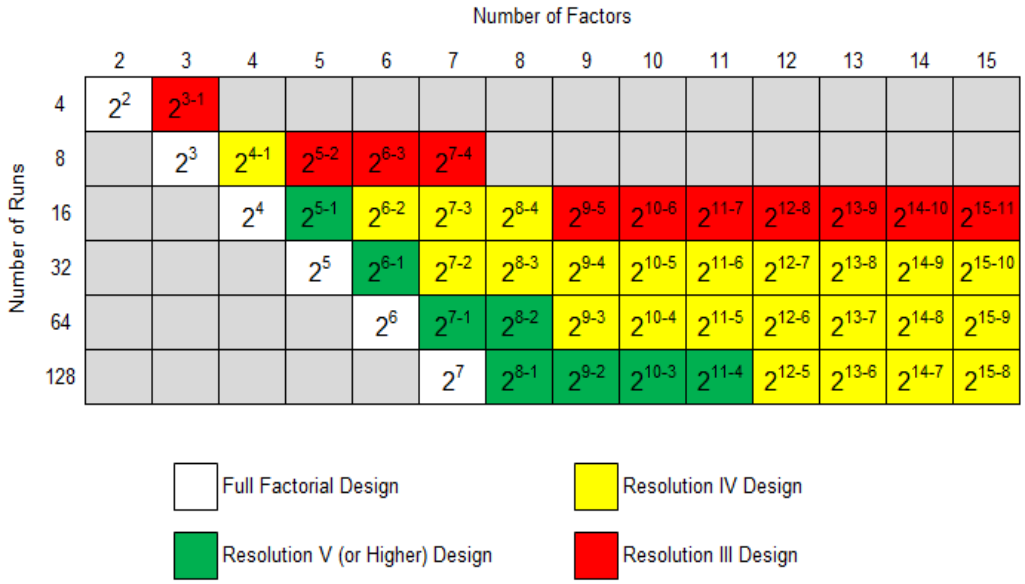

This builder directs the researcher as to the number of runs expected per specific number of factors at two levels. For example, for a two-factor and two-level experiment, the total number of runs is 4. If the number of factors rise to 4, the possible runs are either 8 or 16 depending on the level confidence required.

5.1.4.3 Response Surface Designs

Response surface experiments are typically used in the latter stages of experimentation when the crucial factors have been identified. It usually involves a small number of continuous factors (up to 8) that have been identified as more relevant to the response parameters or variables. One key feature of the response surface designs is that it is used to create and design the curvature in the relationship between the factors and the response. From the curvatures, it becomes easy to determine the optimum points on the surface whether the goal is to minimize or maximize a response. Three levels of the factors are required to estimate the curvature.

5.1.4.4 Mixture Designs

Mixture designs are used when factors are interdependent or have interaction effect and when each component in a mixture is dependent upon the settings of other component settings. A factor's value is its proportion of the mixture, which falls between zero and one. Mixture experiments have three or more factors with the sum of the factor proportions equal to one (100%). Hence, its experimental space is typically triangular and forms a simplex. The goal for mixture design is to optimize a recipe for a mixture of several ingredients.

5.1.4.5 Split Plot Designs

Split plot designs are typically used when an experiment involves hard-to-change variables, i.e., temperature of an industrial oven or the location of a cornfield. In the traditional randomized experiments, all factors are to be tested for each run, which is impractical in this case. Split plot design is a blocked experiment, and these blocks serve as experimental units for a subset of factors. In split plot experiments, treatment is applied to more than one experimental unit because a factor(s) is associated with batch processing, or it is hard or costly to change. As a result, split plot experiments are more practical to be carried out in the industrial world. The advantage of split plot designs is that they enable experiments to be carried out even with the presence of hard-to-change variables.

5.1.4.6 Taguchi Array Designs

Taguchi array designs are used to identify signal factors or control factors, which minimize the effect of noise factors that are typically difficult or expensive to control. They are carried out based on Taguchi's inner and outer array approach. The inner array is made up of control factors to find optimum settings while an outer array is composed of noise factors. Taguchi ensures a robust design in which results are not easily affected by the uncontrolled external variables of a setting. The goal of Taguchi's design is to ensure consistency in output, by finding control factor settings, which generate acceptable responses despite natural environmental and process variability. According to Fraley *et al.* (2021) and Karna & Sahai, (2012), there are some general steps involved in the Taguchi methods. These steps are detailed below.

Step 1 Define the process objectives.

Step 2 Determine the design parameters affecting the process.

Step 3 Create an orthogonal array for the parameter design indicating the number of and conditions for each experiment.

Step 4 Conduct the experiments indicated in the array to collect data on the effect on the performance measure.

Step 5 Complete data analysis to determine the effect of the different parameters on the performance measure.

Under the Taguchi array designs steps, Step 3 is accomplished by selecting an array which is in line with the parameters and the levels at which the parameters will be tested. There are

predefined arrays in the array selector table like the one given below (Table 2.7). These arrays were created using an algorithm developed by Taguchi. The choice of the array to use depends on the time allocation for such a test as well as the budget available for the tests.

Table 5.2: Two-Level Fractional Factorial Design Builder (Danacıoglu and Muluk, 2005)

Orthogonal Array	# of Rows	# of maximum factors	# of Maximum Column			
			2 Levels	3 Levels	4 Levels	5 Levels
L4	4	3	3			
L8	8	7	7			
L9	**9**	**4**		**4**		
L12	12	11	11			
L16	16	15	15			
L16	16	5			5	
L18	18	8	1	7		
L25	25	6				6
L27	27	13		13		
L32	32	31	31			
L32	32	10	1		9	
L36	36	23	11	12		
L36	36	16	3	13		

5.2 Materials: Separation Equipment

The beneficiation of ultrafine material from various tailing streams has been studied (Burt, 2005, Sign, 2014 and Ansari, 1997). The work from these authors generated useful insights on the effective range of application of conventional mineral processing techniques as far as processing ultrafine material is concerned. In this work, a review of different technologies/equipment that have been used to treat ultra fines was done and potential equipment candidates were selected for test-work to investigate the feasibility of developing a viable circuit to beneficiate ultrafine chrome from PGM and chrome tailings.

5.2.1 Background

The feed material for this study was the final tailings of the PGM and chrome processing of a working plant in South Africa. The grade of this feed material was between 8% and 12 % Cr_2O_3. At this grade and at a tailings generation rate of 420 tph, the amount of chrome sent to the tailings storage facility (TSF) translates to about 30240 tonnes of Cr_2O_3 per month. Assuming a feed of average grade 10 % Cr_2O_3 is fed to the proposed circuit with a target to produce a chrome concentrate of grade 40% Cr_2O_3 and if a conservative recovery of 50 % can be attained by reducing the tailings grade of the new arising tailings to about 5.7 % Cr_2O_3, then about 37800 tonnes per month of additional chrome concentrate can be produced if a viable circuit is

developed, which may be substantial in economic terms to warrant investment in the additional plant.

5.2.2 Spiral Separation Equipment

Considerable research and development work has been undertaken by several Original Equipment Manufacturers (OEMs) in South Africa to develop designs of spirals that might be more effective in recovering fine to ultrafine chrome. The type of the spiral that was used for the test-work was a M1T53, which is a wide and shallow angle spiral design recommended for fines recovery and supplied by MET Q South Africa. This is a 5-turn triple start spiral that has a maximum capacity of between 0.8 and 1.2 tons per hour per start depending on the particle size of the material. For the purposes of determining the separation profile, a single-start, 5-turn spiral (Figure 5.1) fitted with a mouth organ splitter was used. Table 5.3 below gives the design parameters of the M1T53 spiral that was used for the test-work. Other spiral designs that were considered were the conventional Multotec's High-flow 3-turn and 5-turn spirals (HX3 and HX5) and these were not used as they exhibited poor recovery of fine chrome.

Table 5.3: Design parameters for M1T53 test spiral used for test-work

Parameter	Value/measurement	Units
Pitch, U	360	mm
Height, H (Centre Column height)	2600	mm
Slope, S (α)	7	degrees
Trough Slope (θ)	9	degrees
Diameter	880	mm
Inner Radius (Centre column diameter)	160	mm
Tonnage per start (max)	1	t/hr

Figure 5.1 Spiral test rig set up comprising of single start 5-turn spiral and triple-start 5-turn spirals

5.2.3 Magnetic Separation Equipment

The second separator that was used in the research test-work is a Wet High Intensity Magnetic separator (L300 model WHIMS) supplied by Malvern Engineering. The strength of the magnet is 9000 Gauss, and the magnets cassettes are made of rare-earth elements. The choice of a high gauss WHIMs was based on its demonstrated ability to recover fine paramagnetic chromite particles. The maximum capacity of the L300 WHIMS is about 3 tonnes per hour. This magnetic separator operates in a counter current mode where the slurry flows down the slope, and the rotating belt moves up the slope capturing magnetic chromite particles that have been pulled by the magnetic field and releasing the particles when the load goes past the magnetic field. Table 5.4 indicates the design parameters for the model L300 WHIMS. Figure 5.2 shows the different components of the generic belt magnet separator and Figure 5.3 is the picture of the actual L300 WHIMS magnetic separator used in the test-work.

Table 5.4: Magnetic separator (Model L300) design parameters

Parameter	Measure	Units
Magnetic pack width	300	mm
Magnetic pack length	1500	mm
Magnet Bed angle	4-10	degrees
Belt linear speed (max)	0.5	m/sec
Belt thickness	1.3	mm
Magnetic Strength	15000	Gauss

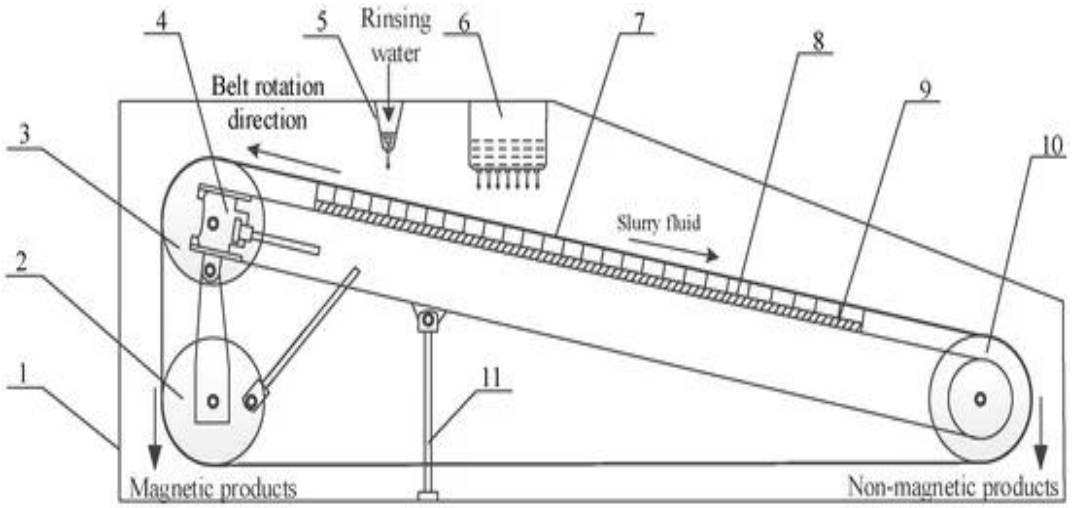

1 - Support frame
2 - Drive wheel
3 - Belt pulley
4 - Belt tension system
5 - Water tank
6 - Feeding box
7 - Belt
8 - Plate magnet
9 - Steel plate
10 - Drive roller
11 – Angle adjustment

Figure 5.2 Flat plate high gradient magnetic separator

Source: Fangping Ye *et al*, (2022)

Figure 5.3 L300 WHIMS used for the test-work.

5.2.4 Shaking Table Separation Equipment

The third separation equipment that was used in the test-work is a Holman-Wilfley Model 800 single deck shaking table. The capacity of the deck is about 75 kg/hr per deck for continuous processing of normal feed sizes but may reduce significantly to about 1-20kg/hr as the size fraction of the particles decreases. The shaking tables can be used to achieve a final grade of the product because of its capability to achieve higher upgrade ratios. Table 5.5 below gives the design parameters of the Holman-Welfley shaking table.

Table 5.5: Holman-Welfley Shaking table design parameters

Parameter	Measure	Units
Deck area	0.8	m^2
Concentrate edge length	640	mm
Tailings edge length	1280	mm
Wash Water requirements	6-12	l/min
Feed dilution	25-30	%
Samples Capacity	1-20	Kg/hr
Continuous Capacity	<75	Kg/hr
Stroke Length	7-11	mm
Stroke Frequency	130-300	rpm
Deck Angle	0-10	degrees

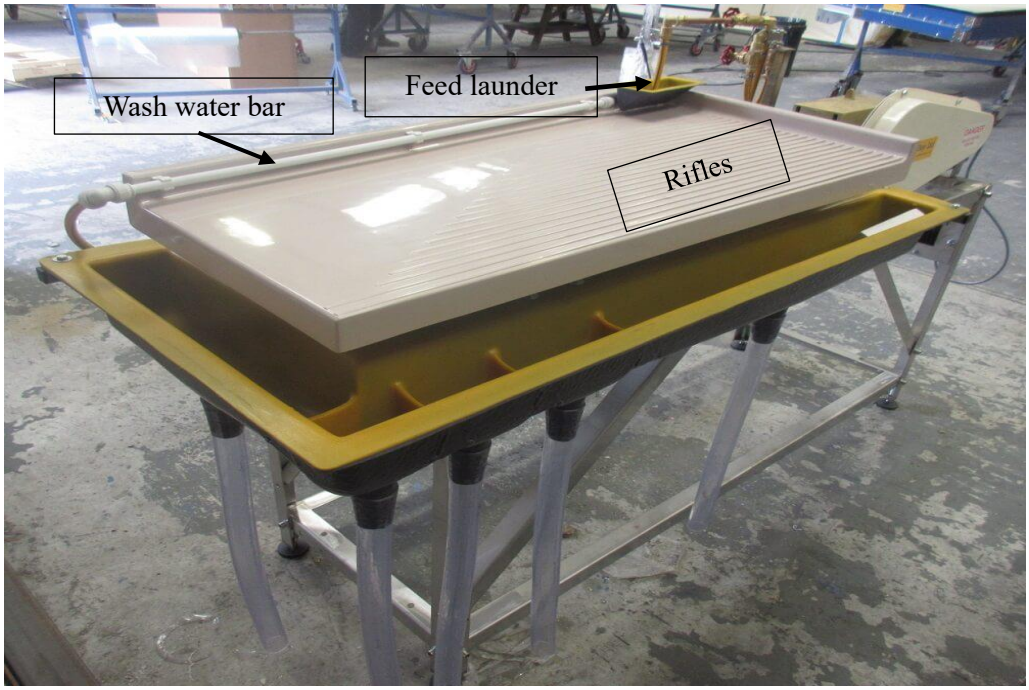

Figure 5.4 Holman-Wilfley Shaking Table Model 800 used for the test-work.

5.2.5 Particle size Screening equipment

A single deck Rhologan MK5 screen was used as part of feed and product classification. This screen can be fitted with distinct size panel depending on the cut size required. The slurry to be screened was introduced at the top into the pan fitted with a stainless-steel mesh of the desired size. The vibrations produced by an eccentric motor at the bottom of the pan together with fluidization water aid the screening process. The capacity of the screen is 0.5 tph and this capacity is dependent on the particle size involved. Dewatering of the slurry streams when required was done by letting the slurry settle and then decant water until the right pulp density is attained.

Figure 5.5 The Rhologan MK5 screen used to screen feed and product material.

5.3 Method: Single Unit Separation Screening Tests

The comparison of the performance of the selected chrome separation equipment was based on a careful selection of factors and response variables that are at play during the separation of ultrafine chromite from the gangue material using each individual separator. The number of factors and the levels at which the factors affect the response variables, and the number of repeat tests determines the confidence of the pattern of cause and effect that comes out of such tests. The selection of factors, the response variables and the number of experimental runs conducted to investigate the cause-and-effect relationships was based on the principle of design of experiments (DOE). The concept of DOE was discussed in section 5.1.1of this chapter.

5.3.1 Single Unit Separation Performance Test using Fractional Factorial Design

The single unit separation tests phase was used to determine the performance of each respective unit in terms of recovery, upgrade ratio achieved, and the grades that can be achieved. This was

done by processing the same feed material (assay, particle size distribution and mineralogy) through each respective unit i.e. the spirals, the belt magnets and shaking table.

The following section present details of the test-work done on each of the test units. The design of experiment method chosen for the separation equipment performance tests is the Fractional Factorial design with two levels and a centre point. For the test on a particular piece of equipment, the number of experimental runs was determined by the number of factors investigated as well as the levels.

5.3.2 Spiral separation performance test-work

The effectiveness of spirals in treating fine to ultrafine chrome feed involved independently varying, slurry pulp density and slurry feed rate and the cutter positions. The dependent variables or objective functions were streams mass yield, stream chrome grade, and an up-grade ratio of the stream that has the highest grade and recovery of the chrome in the streams. The profile of the spiral product streams was determined by using a mouth organ splitter box mounted on the test spiral. Table 5.6 shows the experimental design for running tests on the spiral with three factors at three (two + one centre point) levels each. According to the Fractional Factorial arrays, the experimental matrix has a total of 22 test runs that cover all combinations necessary to get robust data to use in the performance evaluation. The 22 is made up of 16 point representing high and low levels plus 6 centre points.

The spiral separation tests were carried out using the equipment setup shown in Figure 5.6. Of the three factors to be investigated, slurry density was the one that was the most difficult to change because of the need to balance water addition in order not to overshoot the required density. Once the density was attained in tank G, the required volumetric flowrate for that test run as per design experimental matric was set by tuning the variable speed drive of the pump H to feed the spiral distributor A. With the cutter positions set, sampling was commenced to collect timed samples for mass balance calculations. The spiral product streams C were then combined into tank D and pumped back to the feed control tank H. The tank F's purpose was for density correction which was done by adding water. The entire process was repeated until all the runs were completed. The collected samples were weighed to get wet mass before filtering and drying in an oven. After drying, the samples were weighed to get the dry mass which was used to calculate dry feed rate. Part of the mass balance samples were split to get a representative sample for chemical analysis. Mass measurements and chemical assays of all experiments indicated in the experimental matrix in Table 5.4 were recorded.

Table 5.6: Spiral experimental design -3 factors, 2 levels and 6 centre points

Std	Run	Slurry Density (t/m^3)	Slurry Feed Rate (t/h)	Concentrate Cutter Position (mm)
1	4	1.4	0.69	45
2	11	1.4	0.69	45
5	22	1.4	0.97	45
6	8	1.4	0.97	45
9	18	1.4	0.69	106
10	13	1.4	0.69	106
13	21	1.4	0.97	106
14	17	1.4	0.97	106
17	12	1.52	0.83	75.5
18	19	1.52	0.83	75.5
19	6	1.52	0.83	75.5
20	9	1.52	0.83	75.5
21	20	1.52	0.83	75.5
22	2	1.52	0.83	75.5
3	1	1.64	0.69	45
4	10	1.64	0.69	45
7	15	1.64	0.97	45
8	14	1.64	0.97	45
11	3	1.64	0.69	106
12	7	1.64	0.69	106
15	16	1.64	0.97	106
16	5	1.64	0.97	106

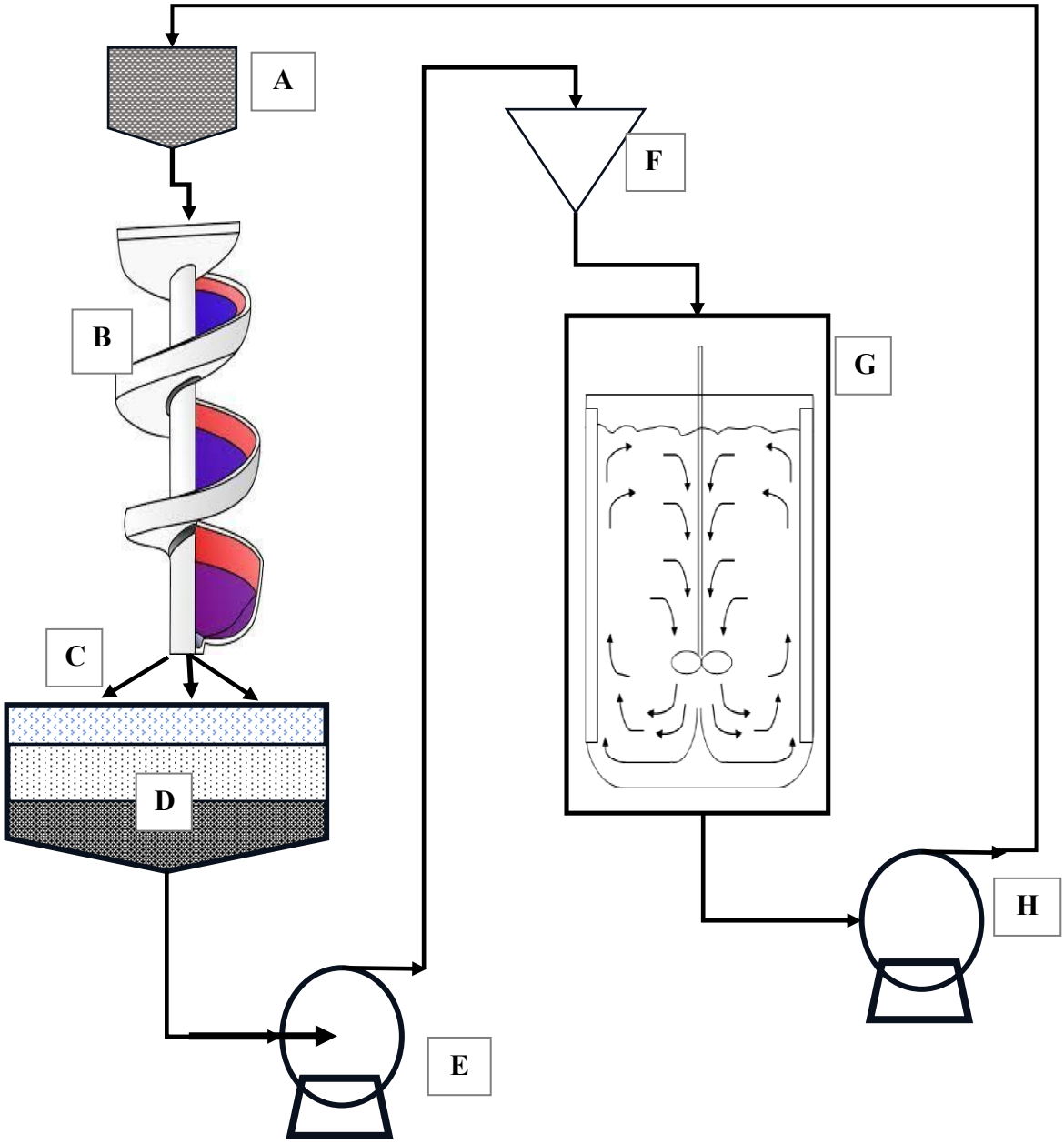

A. spiral feed distributor
B. 5-turn spiral
C. spiral products
D. product remixing tank
E. density control feed pump
F. density control tank
G. spiral feed homogenization tank
H. spiral feed pump (VSD controlled)

Figure 5.6 Spiral tests components set-up

5.3.3 Magnetic Separation Performance Test-Work

The belt magnet was fed with feed material like that used for the spirals test-work in terms of assay, particle size distribution and mineralogy. The independent variables or factors that were investigated in the magnetic separation performance test runs were slurry feed rate, slurry density, belt speed and amount of fluidization water. The equipment design parameters that were kept constant were magnet strength (9000 Gauss), magnet belt thickness (1.3mm), and the magnet angle of inclination (5º). The angle used for these tests was 5º and was previously determined and found to be optimum during tests on a similar but bigger version of the same magnet model (L300 WHIMS). The dependent variables or objective functions were magnetic and non-magnetic stream yields, grade of each stream, upgrade ratio and chrome recovery to two product streams.

Table 5.7 below indicates the conditions for the tests that were investigated, and it also shows the factors and levels that were considered for the evaluation of the belt magnet performance. Figure 5.7 depicts the streams configuration around the magnetic separation unit. The starting point of the circuit was at unit A, the feed homogenization tank fitted with an agitator. This tank could circulate material while adjustments were made to density or feed rate using valve L. Tank M and line K were used for decanting water to densify and then top up tank A. Pump B was a variable speed drive pump to regulate the slurry flow rate as per experimental design.

Timed samples were collected at the magnetic and non-magnetic collection tanks at the top and bottom sides of the magnet. The wet and dry masses were recorded for all experimental runs for the determination of mass balance. Dried samples were split on a sample splitter for chemical assays on the 5110 ICP-OES.

Table 5.7: Belt magnet experimental design

Std	Run	Slurry density (t/m3)	Slurry flowrate (t/hr.)	Belt speed (m/sec)	Fluidization water flow (ml/sec)
6	20	1.6	0.7	0.50	35
16	18	1.6	1.3	0.50	115
4	8	1.6	1.3	0.25	35
2	7	1.6	0.7	0.25	35
10	6	1.6	0.7	0.25	115
12	5	1.6	1.3	0.25	115
8	4	1.6	1.3	0.50	35
14	3	1.6	0.7	0.50	115
21	21	1.49	1.0	0.375	75
18	14	1.49	1.0	0.375	75
20	12	1.49	1.0	0.375	75
22	11	1.49	1.0	0.375	75
17	9	1.49	1.0	0.375	75
19	2	1.49	1.0	0.375	75
15	22	1.38	1.3	0.50	115
7	19	1.28	1.3	0.50	35
5	17	1.38	0.7	0.50	35
11	16	1.38	1.3	0.25	115
1	15	1.38	0.7	0.25	35
3	13	1.38	1.3	0.25	35
9	10	1.38	0.7	0.25	115
13	1	1.38	0.7	0.50	115

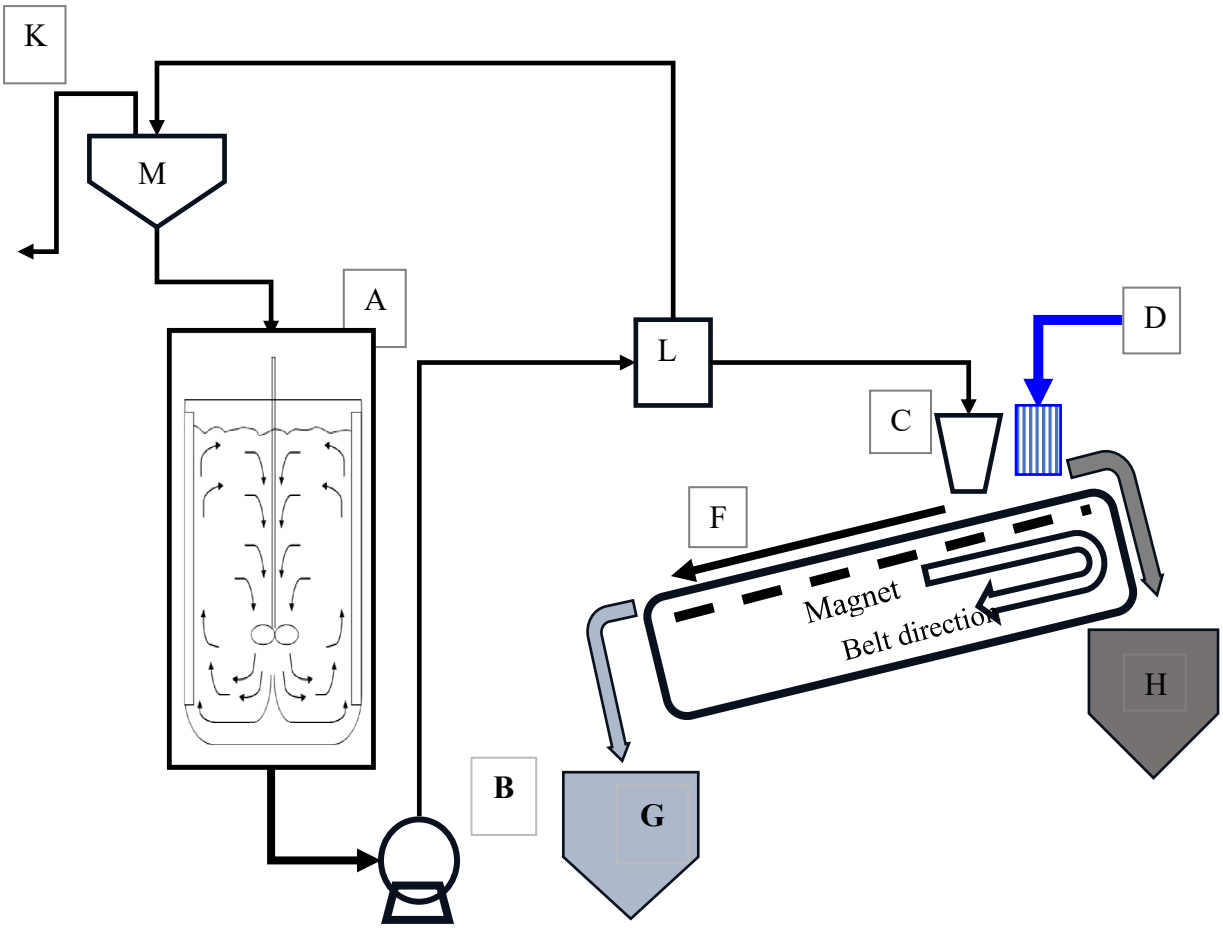

A - Homogenization tank,
B - VSD feed pump,
L - By-pass valve
C - Feed distributor,
D - Fluidization water,

F - Non-magnetic product flow direction
G - Non-magnetic product collection
H - Magnetic product collection,
K - Overflow settled water,
M - Feed top up

Figure 5.7: Belt-magnet equipment test set-up.

The angle on inclination of the belt magnet was set at 5°. This angle was chosen as it was optimum to balance recovery of chrome to the magnetic fraction and upgrade of the concentrate by washing gangue down the slope allowing the process to produce desired grade.

5.3.4 Shaking table separation performance test-work

A Holman-Wilfley single deck shaking table was used to test the performance of a shaking table separator by feeding it with the same feed material used on the spirals and magnet. The independent variables tested were feed rate, slurry density, wash-water flow rate and deck

angle. The dependent variables or the objective functions were streams mass yield, stream grade, upgrade ratio of the highest-grade stream and chrome recovery to various streams. Table 5.8 shows the number of experimental runs planned and the levels per parameter under investigation. The feed rate and wash-water given in table is for a single deck.

Table 5.8: Shaking table experimental design

		Factor 1	Factor 2	Factor 3	Factor 4
Std	**Run**	**Slurry Density (t/m3)**	**Slurry Feed rate (ml/min)**	**Wash Water Flow (ml/sec)**	**Table Deck Angle**
1	13	1.28	300	100	2
2	2	1.4	300	100	2
3	16	1.28	700	100	2
4	1	1.4	700	100	2
5	22	1.28	300	180	2
6	5	1.4	300	180	2
7	10	1.28	700	180	2
8	14	1.4	700	180	2
9	11	1.28	300	100	6
10	3	1.4	300	100	6
11	8	1.28	700	100	6
12	19	1.4	700	100	6
13	9	1.28	300	180	6
14	6	1.4	300	180	6
15	7	1.28	700	180	6
16	21	1.4	700	180	6
20	4	1.34	500	140	4
17	12	1.34	500	140	4
22	15	1.34	500	140	4
18	17	1.34	500	140	4
19	18	1.34	500	140	4
21	20	1.34	500	140	4

Figure 5.8 shows the equipment setup showing the shaking table's possible products depending on the cutter positions and the number of cutters used. Generally, there are three products;

concentrate, middling and tails but the concentrate can also be divided into high- and low-grade streams depending on the separation experienced. Before the experiment could begin, the slurry was made by mixing a proportionate mass of dry feed with water to make a slurry of the required density. Once the feed density was attained, an agitator was switched on for about 30 minutes before starting the pump to feed the deck. All the timed samples were collected, and masses and assays were used to determine the yield, recovery and grades of the streams measured. This information was used to determine the relationship between the independent factors and the response variables as given in Table 5.8.

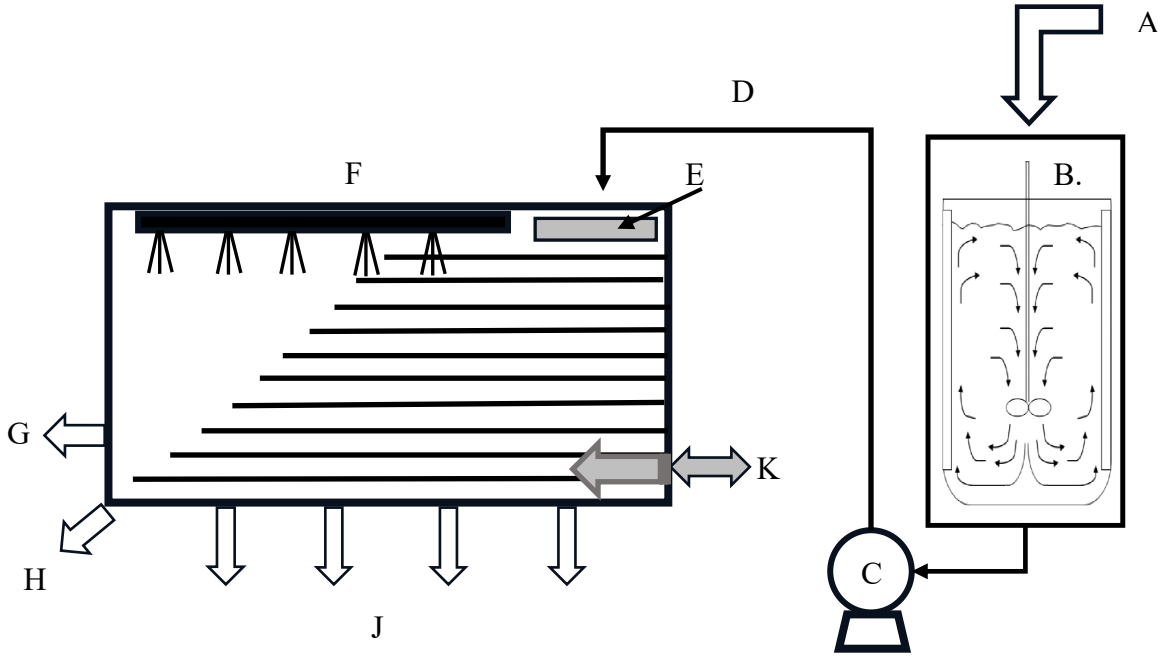

A – Slurry feed
B – Homogenisation tank
C – Variable speed pump
D – Shaking table feed line
E – Slurry feed distribution
F – Wash water distribution
G – Final concentrate stream
H – Middling stream
J – Tailings stream
K – Table drive mechanism

Figure 5.8 Shaking table test set-up showing feed preparation and product streams

The data generated from the preliminary separation performance test-work on the spiral, magnet and shaking table was analysed to determine the possible location of each separation unit in the proposed circuit flowsheet. The data would also demonstrate the factor/s that have the most significant effect on the response variables for all the 3 separators that were investigated.

5.4 Equipment Selection Results and Discussion

The main purpose of the separator equipment performance tests was to determine how each piece of selected equipment for ultrafine chrome recovery responded to an array of independent-dependent factor combinations. Specifically, the main objectives for these tests were to address the following:

i. determine the effect of processing input parameters i.e. slurry specific gravity, flow slurry flowrate, % solids of slurry and equipment input parameters i.e. spiral cutter/splitter positions, magnet fluidization water, magnet belt linear speed, magnet deck angle, shaking table deck angle, shaking table wash water on the dependent/response parameters like concentrate mass yield, recovery of chrome to streams, grade of product streams, upgrade of the concentrate streams.
ii. Evaluate the suitability of each separating unit (spiral, magnet and shaking table) in a circuit as either a roughing unit for recovery, a scavenger unit or cleaning unit for grade attainment.

A few assessment tools were employed for this purpose and the outcome of these assessments are presented in the following sections. It is noted here that for the purposes of this work, there was no effort to change the design of each of the pieces of equipment as part of the scope. The identified pieces were deployed into the design plane without the need to change the design. All efforts were directed to the determination of the performance of each unit under different material conditions as well as operating settings within the design envelop of the unit. For example, the spiral chosen as the test unit was not modified in terms of number of turns, pitch and trough angle and width of the trough. In the same way the magnet magnetic strength and belt thickness were not changed. In an equivalent way, the shaking table's riffles and stroke length were not changed as part of the investigations.

The following section presents the results of the parallel separation tests carried out on each individual separators i.e. spirals, magnetic separator and shaking table using identical fresh feed material. Fractional factorial design array was used to set up the (DOE) experimental matrix to investigate the relative impact of the main independent variables on the response parameters in the separation of chromite feed material on each separator unit. The concept of

Taguchi Main Effect Plots (Periyasamy, 2014, Raykundaliya & Shanubhogue, 2015, Jou *et al*, 2014) will be used as a tool for analysing the results.

5.4.1 Spiral separation tests

The independent parameters (factors) considered on the spiral tests were (i) Slurry Density, (ii) Slurry Flow rate (reported as dry tons unless otherwise specified) and (iii) Concentrate Cutter Position. The response parameters observed and measured as a function of changes in the input parameters (factors) were (i) Mass Yield, (ii) Recovery, (iii) Grade and (iv) Upgrade ratio for the Concentrate and (i) Recovery, (ii) Yield and (iii) Grade of the Tailings stream.

5.4.1.1 Spiral Fractional Factorial Array and Main effect Plots

To evaluate the effect of the independent variables on the dependent parameters, main effects plots of means (average of response parameters per level) graphs were plotted. The highest or lowest average response parameter against the independent (input) parameters at level 1, 2 or 3 indicated the best level to be considered for optimisation tests depending on whether the goal is to maximise or minimise the response parameter value. The independent parameter that has the steepest gradient between two levels has the most prominent effect on the response parameter at those levels.

The matrix shown in Table 5.9 is based on fractional factorial design according to the Design Expert matrix generator. The number of runs depends on the combination of factors and levels under consideration. For this spiral test-work, three factors and two levels were used to run the tests. The number of runs was derived from the expression 2^k where 2 represents the levels and k representing number of factors. In the separation of chrome from gangue material in the spirals, the independent variables which were investigated are relative slurry density (RD-measured in t/m^3), at density of 1.44, and 1.64. The other variable was the feed rate, and this was also investigated at two levels (0.69t/h and 0.97 t/h). The last variable investigated was Concentrate Cutter Position measured from perimeter of the centre column. There were also 6 centre points which were included in the design and the main purpose of the centre point is to determine if there is curvature on the line joining the lower and upper points or values. So, the total number of runs for spiral tests was 2x2x2=8. For a duplicate run, the total number of runs was 16. Adding the 6 centre points brings the total number of runs to 22.

Table 5.9 below shows the matrix with factors and their respective levels. According to the design of experiments terminology, the lower point can be given a code of -1 and the upper

point is given a code of +1. The middle point is given a 0 code for ease of reference. Table 5.8 shows the results of the 22 runs in terms of the target response parameter value against the factor level. For ease of reading, the factor side with lower (-1) points is indicated in green and the upper (+1) points is indicated in orange. The centre points (0) are marked in blue. On the response side, the results have been given a conditional formatting resulting in a heat map in which the concentrate objective function of recovery, grade, yield, and upgrade factor are given a colour green when they are high and transition to yellow, orange, and red at the lowest values. The colour for discard streams (tailings) objective function is the opposite of the concentrate stream where the lowest is coded as green and the highest as red.

Table 5.9: Fractional factorial DOE matrix settings for Spiral Performance Tests

	Factor 1	**Factor 2**	**Factor 3**
Run 1	**Slurry Density (t/m3)**	**Dry Slurry Feed Rate (t/hr.)**	**Concentrate Cutter Position (mm)**
1	1.4	0.69	45
2	1.4	0.69	45
3	1.4	0.97	45
4	1.4	0.97	45
5	1.4	0.69	106
6	1.4	0.69	106
7	1.4	0.97	106
8	1.4	0.97	106
9	1.52	0.83	75.5
10	1.52	0.83	75.5
11	1.52	0.83	75.5
12	1.52	0.83	75.5
13	1.52	0.83	75.5
14	1.52	0.83	75.5
15	1.64	0.69	45
16	1.64	0.69	45
17	1.64	0.97	45
18	1.64	0.97	45
19	1.64	0.69	106
20	1.64	0.69	106
21	1.64	0.97	106
22	1.64	0.97	106

To be able to get the combination of factor levels that give best performance on the response parameters, there must be some ranking mechanism used to produce the optimum combination. This ranking must be advised by the knowledge of the process and the fundamental physical laws that govern the separation of components in the system. For the separation of chromite particles from gangue particles, a measure of upgrading the product stream based on chrome is promoted while depleting the other stream (tail) of chrome. This results in recovery and yield of the target mineral in the upgraded stream. These parameters were used for the evaluation of the separation process.

Table 5.10: Fractional Factorial DOE matrix for Spiral Preliminary tests

Run	Slurry Density	Slurry Feed Rate	Concentrate Cutter Position	Feed Cr_2O_3 Grade	Conc Cr_2O_3 Recovery	Conc Cr_2O_3 Grade	Conc Mass Yield	Upgrade Factor	Tailings Cr_2O_3 Grade	Tailings Cr_2O_3 Recovery	Tailings Mass Yield
	Kg/l	t/h	mm	%	%	%	%	Times	%	%	%
22	1.42	0.97	45	12.67	23.41	23.37	14.66	1.84	13.05	45.62	51.19
15	1.62	0.97	45	12.69	19.19	17.87	13.91	1.41	11.76	38.4	42.3
11	1.42	0.69	45	12.48	23.58	18.28	15.77	1.46	11.27	43.43	47.12
10	1.62	0.69	45	12.65	23.06	18.05	17.46	1.43	12.59	25.42	27.59
21	1.42	0.97	106	12.15	36.04	17.34	29.49	1.43	13.2	50.49	54.3
16	1.62	0.97	106	12.91	36.82	14.11	30.84	1.09	10.92	40.45	43.74
18	1.42	0.69	106	11.99	37.48	14.55	32.04	1.21	11.65	45.19	48.24
7	1.62	0.69	106	12.87	43.67	13.75	38.52	1.07	11.26	27.34	29.45
8	1.42	0.97	45	12.11	19.61	20.91	13.09	1.73	12.97	50.24	54.09
14	1.62	0.97	45	12.94	19.61	20.65	13.71	1.6	12.9	38.05	42.59
4	1.42	0.69	45	12.84	22.52	20.69	15	1.69	13	45.26	47.99
1	1.62	0.69	45	11.62	23.97	18.84	17.8	1.62	12.97	24.69	26.63
17	1.42	0.97	106	12.84	35.32	17.04	28.78	1.33	12.86	50.65	54.67
5	1.62	0.97	106	12.45	38.07	14.38	33.31	1.16	11.53	38.07	40.87
13	1.42	0.69	106	12.38	39.49	16.38	33.11	1.32	12.63	44.28	48.16
3	1.62	0.69	106	11.96	43.54	14.34	38.37	1.2	11.52	28.87	31.67
20	1.52	0.83	75.5	12.64	29.96	15.94	23.35	1.26	11.43	41.61	45.23
19	1.52	0.83	75.5	11.81	30.87	16.15	23.44	1.37	11.14	41.76	45.96
12	1.52	0.83	75.5	12.11	30.3	17.95	23.36	1.48	12.73	41.79	45.42
9	1.52	0.83	75.5	12.22	31.48	18.77	23.71	1.54	12.77	41.15	45.58
6	1.52	0.83	75.5	12.11	32.15	16.46	24.8	1.36	11.74	40.37	43.64
2	1.52	0.83	75.5	12.84	29.73	16.63	22.98	1.3	11.82	41.85	45.5

The following sections analyse the effects of factors and their levels on the response parameters to determine the best factor combinations. The Main Effect Plots concept is based on the Taguchi method of quality improvement (Periyasamy, 2014, Raykundaliya & Shanubhogue, 2015, Jou *et al*, 2014). To get the comparison, the value of the response parameter is determined by taking an average of this response parameter values per level of the factor. This was done for all factor levels and for all response parameter values in all the Spiral runs. According to Design Expert the centre point is to determine if there is curvature on the plane or line joining -1 to +1 points.

5.4.1.2 Main effects plots for Concentrate Yield means

Figure 5.9 shows the relationship between spiral average concentrate yield as a function of the individual factors at the three (-1, +1 and 0) levels. The average concentrate yield is calculated by averaging different yields obtained at one level of a particular factor and various levels of the other 2 factors. It can be seen from Figure 5.9 that as slurry density increases from level 1 to 2 and 3, the concentrate yield increases marginally from 22.74% to 25.49%. A similar pattern is observed for dry slurry flow rate. Concentrate cutter position has the biggest impact on the increase of concentrate yield. All factors demonstrate a positive correlation with concentrate yield. To maximise the concentrate yield, all factor levels must be set on level 3. The average concentrate yield when all the 3 factors are at level 3 is 28.19%. These settings mean that slurry density must be 1.6t/m3, dry feed rate set at 0.97t/h and concentrate cutter position at 106mm.

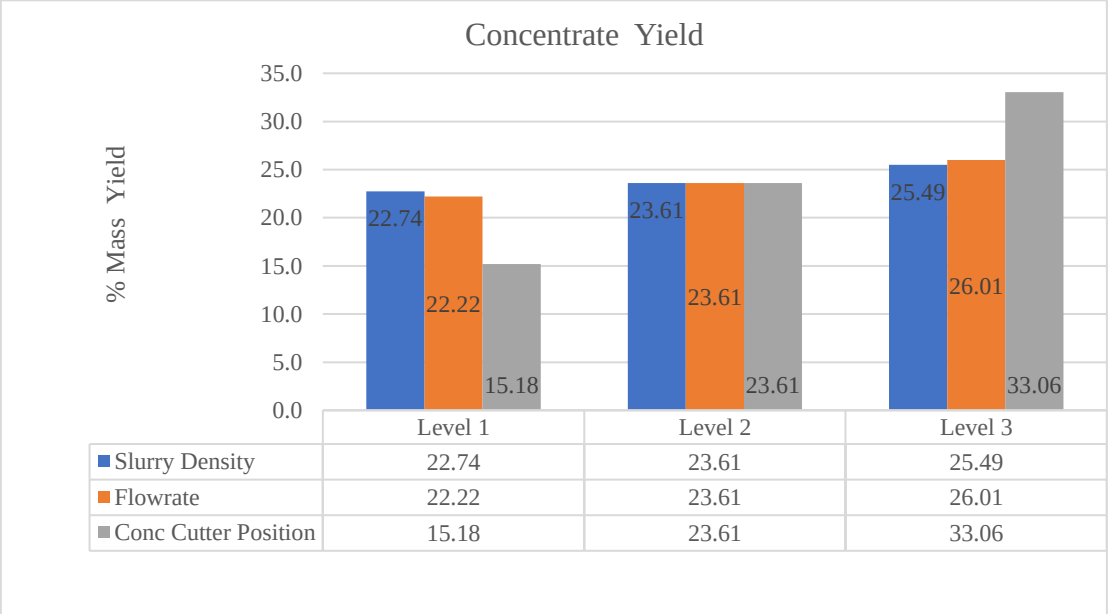

Figure 5.9: Main effects plots for Concentrate Yield

5.4.1.3 Main effects plots for Concentrate Recovery means

Figure 5.10 shows the relationship between the independent variables tested and their effect on concentrate recovery. Since recovery is proportional to yield, the main effect plots for concentrate recovery resemble that of the concentrate yield relationship shown in Figure 5.9. The best levels for maximizing recovery are the same as those for maximizing concentrate yield. At level 3 for all the factors, the average recovery is 33.98%. It must be noted that concentrate cutter position has the biggest impact on recovery as well as shown by the steep gradient of graph between 1 and 3 levels.

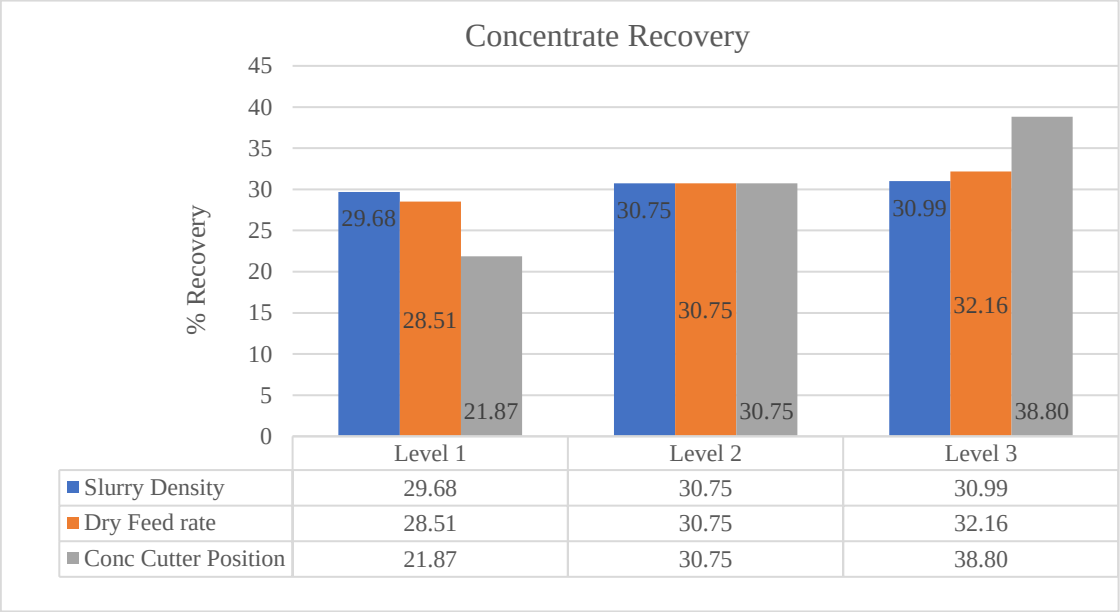

Figure 5.10: Main effects plots for Concentrates Recovery

5.4.1.4 Main effects plots for Concentrate Grade

Like concentrate yield and recovery, the goal on the spiral separation is to maximise the concentrate grade. Figure 5.11 shows the relationship between the factor levels and concentrate chrome grade. There is an overall negative correlation of all factors with the grade of the concentrate from the slopes between levels 1,2 and 3. Concentrate cutter position drops the most from level 1 to 2. The other two factors show marginal changes from level 1 to 3. Level 1 is deemed as the best setting for all three factors for maximizing concentrate grade and the resultant average grade is 18.87% Cr_2O_3.

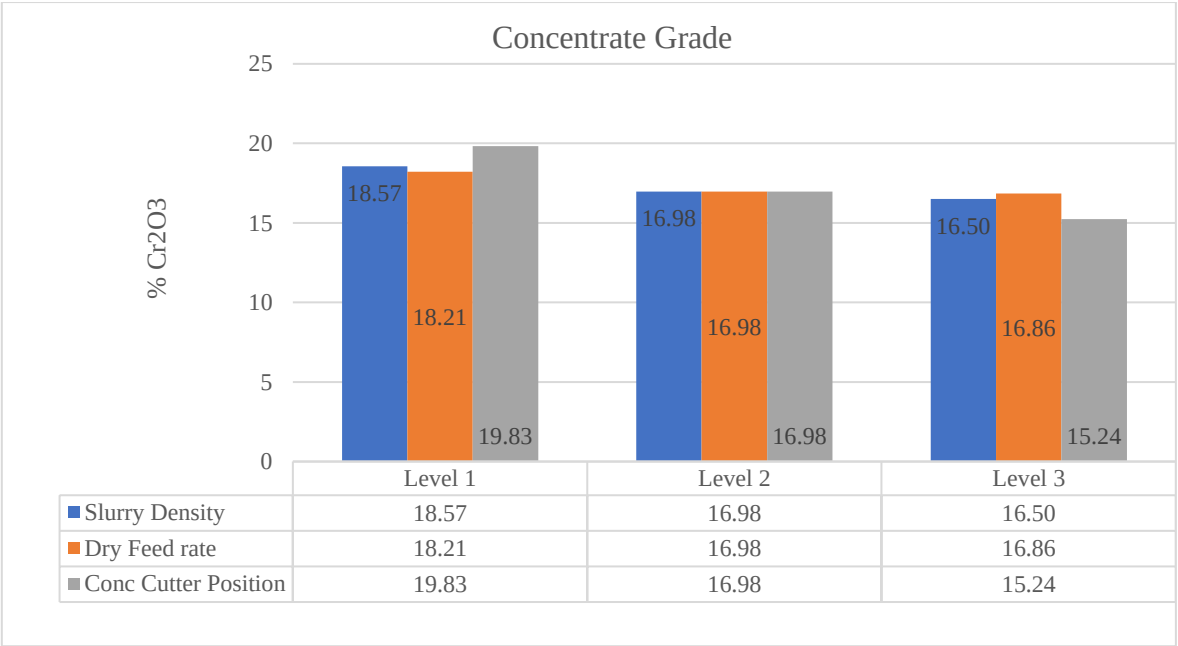

Figure 5.11: Main effects plots for Concentrate Grades

5.4.1.5 Main effects plots for Concentrate Upgrade ratio

The upgrade ratio is one of the key parameters considered in minerals beneficiation. A high upgrade ratio with high recovery shows good selectivity of the separation process. Figure 5.12 indicates that for maximum upgrade ratio of concentrate from the feed, concentrate cutter positions, slurry density and feed rate must be set at level 1. At level 1 the average upgrade ratio was 1.54. The gentle gradient on the graphs of Figure 5.12 between level 1 and 3 suggests that the effect of the three factors on the upgrade ratio is not as influential as their effect on other response parameters like grade, recovery, and yield. However, the concentrate cutter position has the biggest impact on upgrade ratio.

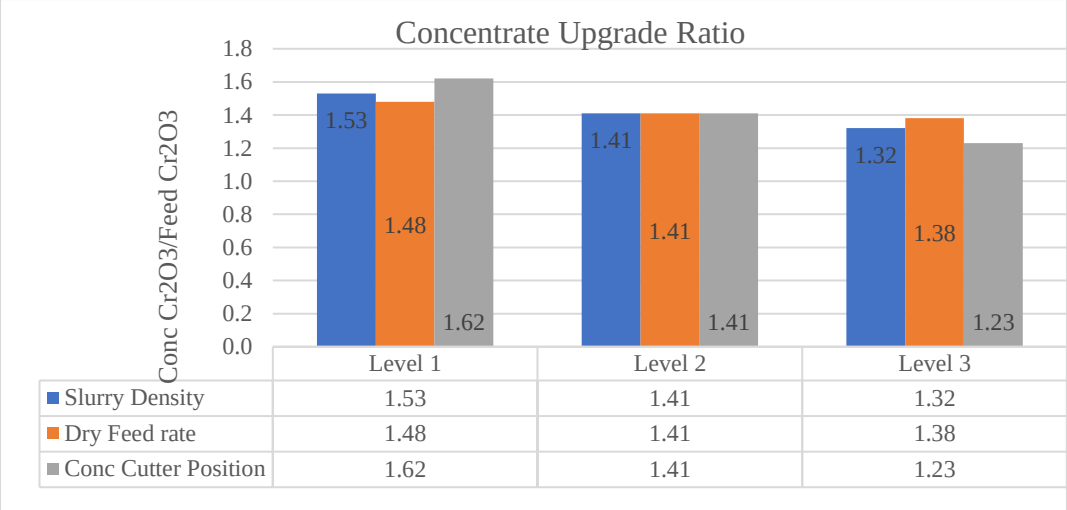

Figure 5.12: Main effects plots for Concentrates Upgrade ratio

5.4.1.6 Main effects plots for Tailings Recovery

In the separation process on the spirals, the aim is to minimise recovery of the chrome mineral to tailings. This drives the requirement to lower the concentration of chromite in the tails (Tail Cr_2O_3 grade) as much as possible to minimise chrome losses. Figure 5.13 shows the relationship between tails recovery as a function of the 3 independent variables. Slurry density has the most prominent effect on tailings recovery than the other two factors. Concentrate cutter position has the least effect. To minimise tails recovery, the slurry density and feed rate must be set at level 3 while concentrate cutter position must be set at level 1. The tailings recovery at these levels was 35.70%.

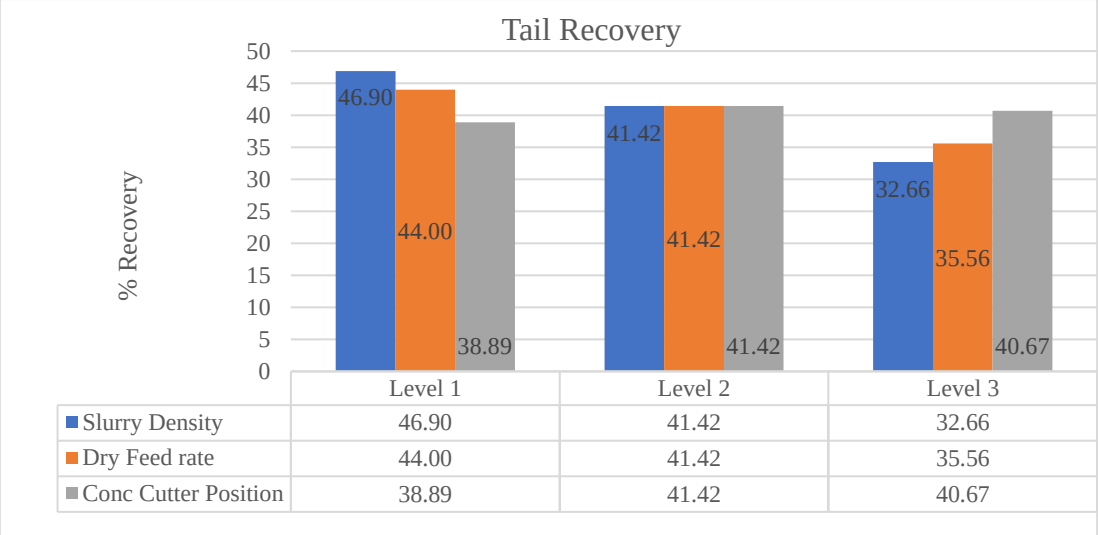

Figure 5.13: Main effects plots for Tail Recovery

5.4.1.7 Main effects plots for Tail Yield

The behaviour of tailings yield resembles that of tailings recovery since they have a direct proportional relationship. From Figure 5.14, slurry density has the prominent effect followed by feed rate and the least being concentrate cutter position. The reason why the slurry density has the most prominent effect is likely because the ultrafine particles, which make 49% of the mass, have lower density and these particles are largely pushed to the edge of the spiral and get lost with tailings, which causes loss of the ultrafine chrome particles when the slurry density is low. If the slurry density is higher, the effect of hydrodynamic forces acting on particles is reduced, and gravity forces become more prominent. This prevents mass loss to the tailings. Minimum tailings yield is achieved by setting the slurry density and feed at level 3 and concentrate cutter position at level 1. The average yield of the tailings was 38.99%.

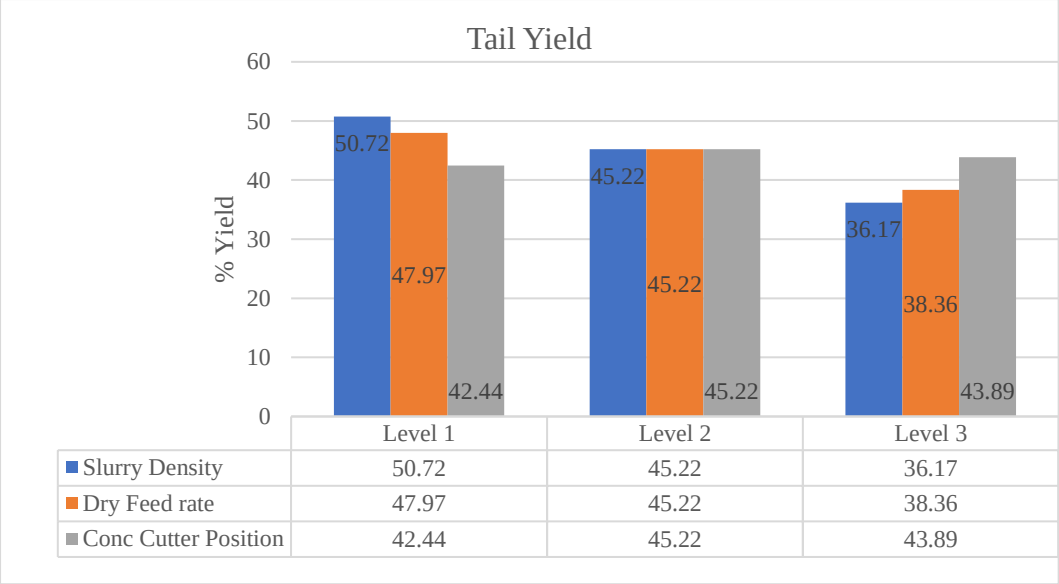

Figure 5.14: Main effects plots for Tail Yield

5.4.1.8 Main effects plots for Tail Grade

From Figure 5.15, to lower the tails grade, feed rate and concentrate position must be set at level 2 while slurry density must be set at level 3. Levels 1 and 3 pushes the tailings grade up. What is also noticeably clear is that there is a steep change from level 1 to level 2 for all three factors but not much change from level 2 to level 3. The tailings grade at the set levels was 11,94%.

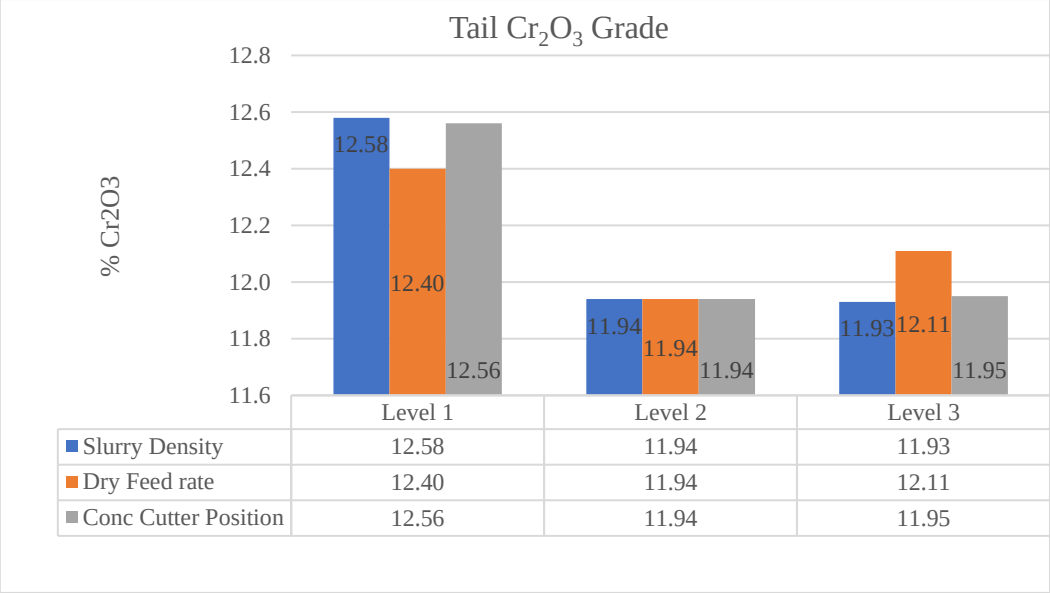

Figure 5.15: Main effects plots for Tail Grade

5.4.1.9 Factor Statistical Analysis

As part of the factor-response relationships, the fractional factorial matrix results were analysed using Design-Expert software by Stat-Ease Inc. The results presented here look at the impact of each of the factors which were being investigated as part of determining the significant factors and their impact. Below is a summary of the results of the equipment performance separation tests of ultrafine chrome on the wide diameter spiral M1T53. Table 5.11 gives the ANOVA analysis for the spiral separation tests for all the 3 factors and 7 responses. For ease of reference, the factors in Table 5.11 are indicated as alphabet A, B, C representing slurry density, feed rate and concentrate cutter position, respectively. In the first row the concentrate recovery is presented showing the intercept point in the first column, slurry density correlation value in the second and feed rate correlation value in the third column and concentrate cutter position correlation in the fourth column. The next 4 columns are for the interaction effects correlation values. Below the response parameter row, comes the p-value row indicating the significance of relationship between the factors and response parameter-concentrate recovery. The p-value indicates the significance of the correlation between the factors and response parameter. Any value below 0.05 indicates significant correlation between the factors. If the p-value is above 0.05 it means the relationship is not significant. Looking at concentrate parameters only in Table 5.11, results suggests that there is a significant correlation between concentrate recovery, yield, grade, and upgrade factor and concentrate cutter position since the p-values are less than 0.05. Feed rate has a significant correlation with concentrate recovery,

yield, and grade while slurry density has a significant correlation with concentrate upgrade factor. There is also an interaction effect of slurry density and feed rate that has a significant correlation with upgrade factor.

On the tailings relationships, slurry density has significant correlation with tailings recovery, yield, and grade while feed rate has significant correlation with recovery and yield but not with tailings grade. Slurry density and feed rate interaction has significant correlation with all three tailings response parameters. An interaction between slurry density and concentrate cutter position, feed rate with concentrate cutter position as well as interaction between the three factors has a significant correlation with tailings mass yield.

Table 5.12 give the statistics of the model fit between the independent variables and response parameters. The statistical parameters under review are standard deviation, mean, Coefficient of Variation (C.V%), R^2, Adjusted R^2, Predicted R^2 and Adequate Precision or Signal to Noise ratio. The fit statistics has generally shown that the model is significant; 5 out of 7 response parameters have C.V % of equal to or below 5% and this model has good fit. The coded and actual equations Tables 5.13 and 5.14 do make sense when values corresponding to the independent variable are substituted. The model has predicted that the most appropriate level settings are slurry density-1.50 t/m3, slurry feed rate-0.83 t/h and concentrate cutter position -50.49mm.

Table 5.11: ANOVA analysis for the Spiral preliminary separation tests

	Intercept	**A**	**B**	**C**	**AB**	**AC**	**BC**	**ABC**
Concentrate Cr_2O_3 Recovery	29.1782	-0.5439	-2.6838	8.5885		1.2579		
p-values		0.0612	0.0444	< 0.0001		0.0026		
Concentrate Cr_2O_3 Grade	17.8033	-0.8039	0.8857	-2.3381				
p-values		0.0612	0.0444	< 0.0001				
Concentrate Mass Yield	22.4536	-0.1643	-2.7903	9.0625	-0.8104			
p-values		0.7063	< 0.0001	< 0.0001	0.0848			
Concentrate Upgrade factor	1.42959	-0.1399	0.0715	-0.2025	-0.0987			
p-values		0.0061	0.0891	< 0.0001	0.0474			
Tailings Cr_2O_3 Grade	12.1312	-0.5877	0.2357		-0.5954			
p-values		0.0443	0.3398		0.0480			
Tailings Cr_2O_3 Recovery	43.7463	-4.149	6.0461		2.6285			
p-values		< 0.0001	< 0.0001		0.0001			
Tailings Mass Yield	47.7775	-3.9860	6.8989	-0.4658	3.0474	-1.0477	-0.9108	-1.2009
p-values		< 0.0001	< 0.0001	0.1815	< 0.0001	0.0196	0.0204	0.0124

Key

A Slurry density
B Feed rate
C Concentrate cutter position

Table 5.12: Fit Statistics for Spiral preliminary tests

	Concentrate Cr_2O_3 Recovery	Concentrate Cr_2O_3 Grade	Concentrate Mass Yield	Concentrate Upgrade Factor	Tailings Cr_2O_3 Grade	Tailings Cr2O3 Recovery	Tailings Mass Yield
Std. Dev.	1.19	1.16	1.07	0.1114	0.6773	1.30	0.9571
Mean	30.45	17.38	23.98	1.42	12.17	40.23	43.72
C.V. %	3.90	6.67	4.46	7.85	5.57	3.24	2.19
R^2	0.9809	0.8170	0.9861	0.8079	0.3266	0.9744	0.9908
Adjusted R^2	0.9764	0.7865	0.9829	0.7627	0.2144	0.9702	0.9862
Predicted R^2	0.9668	0.7274	0.9733	0.6926	-0.0282	0.9593	0.9721
Adeq Precision	40.9384	16.2067	48.8410	13.6535	4.9566	41.7283	47.1572

Table 5.13: Coded Equation

	Concentrate Cr_2O_3 Recovery	Concentrate Cr_2O_3 Grade	Concentrate Mass Yield	Concentrate Upgrade Factor	Tailings Cr_2O_3 Grade	Tailings Cr2O3 Recovery	Tailings Mass Yield
Intercept	**29.18**	**17.80**	**22.45**	**1.43**	**12.13**	**43.75**	**47.78**
A	-0.54	-0.80	-0.16	-0.14	-0.59	-4.15	-3.99
B	-2.68	0.89	-2.79	0.07	0.24	6.05	6.90
C	8.59	-2.34	9.06	-0.20			-0.47
AB			-0.81	-0.09	-0.60	2.63	3.05
AC	1.26						-1.05
BC							-0.91
ABC							-1.20

Key:

A	Slurry density
B	Feed rate
C	Concentrate cutter position
AB	Slurry density and Feed rate interaction
AC	Slurry density and cutter position interaction
BC	Feed rate and cutter position interaction
ABC	Slurry density, feed rate and cutter position interaction

Comparison of the predicted recovery from coded equation and actual equation shows that the Recovery for coded equation for (-1) point was 25.07% compared to 24.57% of the actual equation. The recovery at (+1) point on the coded equation was 35.81% compared to 35.13 of the actual equation. This shows that the model is consistent when using both coded and actual equation.

Table 5.14: Actual Equation

	Concentrate Cr_2O_3 Recovery	Concentrate Cr_2O_3 Grade	Concentrate Mass Yield	Concentrate Upgrade Factor	Tailings Cr_2O_3 Grade	Tailings Cr2O3 Recovery	Tailings Mass Yield
Intercept	70.16	28.52	-42.21	-4.13	-26.53	257.84	464.38
A	-30.48	-6.70	38.67	3.71	24.52	-164.43	-309.03
B	-19.17	6.33	53.39	9.44	55.55	-194.63	-479.30
C	-0.24	-0.08	0.30	-0.01			-2.36
AB			-48.24	-5.88	-35.44	156.46	358.34
AC	0.34						1.66
BC							3.35
ABC							-2.34

Key:

A	Slurry density
B	Feed rate
C	Concentrate cutter position
AB	Slurry density and Feed rate interaction
AC	Slurry density and cutter position interaction
BC	Feed rate and cutter position interaction
ABC	Slurry density, feed rate and cutter position interaction

5.4.2 Response Surface Plots for Spiral performance test results

The Surface plots in the following sections are derived from the Design-Expert software results and design of experiment analysis of the relationship between input or independent factors and their corresponding response or dependent factors. This 3-dimensional plot depicts the variation of the response parameter when the two input factors are changed within the design limits as per the DOE matrix.

5.4.2.1 Response Surface Plot for Effect of Cutter Position and Slurry density on Recovery.

Figure 5.16 below shows the relationship of Cr_2O_3 recovery to the concentrate as a function of concentrate cutter position and slurry density. From the slopes of the concentrate cutter position and slurry density between low (45mm) and high (106mm), and 1.42kg/L and 1.62kg/L respectively, changing the position of cutter has a more significant effect than moving from low density to high density points. The higher cutter position yields higher recovery than the low cutter position. Between concentrate cutter position and slurry density, cutter position is more significant than slurry density. In fact, the p value of the concentrate cutter position is <0.0001 while the p value of slurry density is 0.0612 which is statistically insignificant as given in Table 5.11 above. From this graph the highest point on the recovery axis corresponds to the largest cutter position and highest density. This strong interaction effect was demonstrated by P value of AC on recovery in Table 5.11.

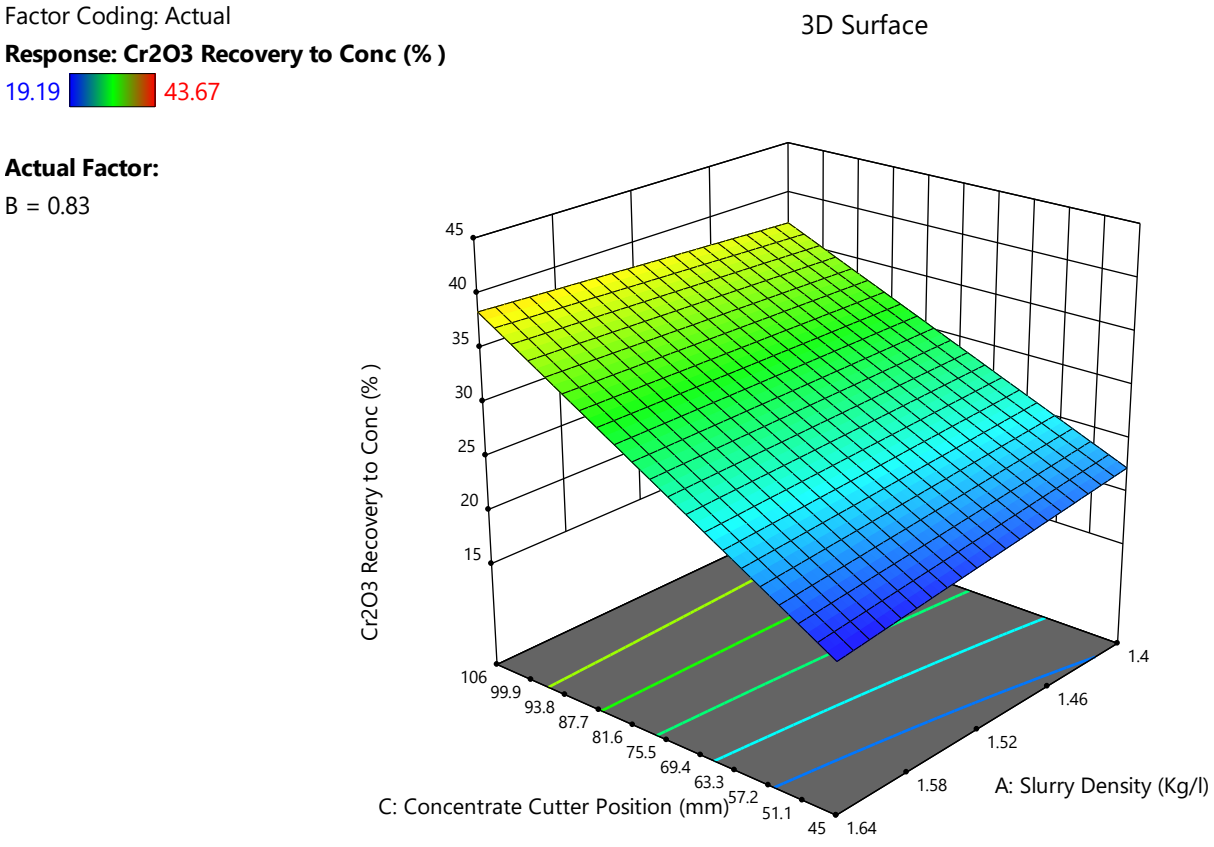

Figure 5.16: Surface plot of Cr_2O_3 Recovery as functions of Concentrate cutter position and Slurry density

5.4.2.2 *Response Surface Plot for Effect of Slurry feed rate and Slurry density on Recovery*

The surface plot for recovery as a function of slurry density and slurry feed rate is shown in Figure 5.17 below. From the slopes of the feed rate and slurry density, it can be seen that feed rate has a more significant effect on recovery of the chrome to the concentrate. The explanation for low feed rate being inversely proportional to recovery is that lower feed rate ensures a more lamella flow to ensure a more efficient separation of ultrafine particles through gravity effect. This is because the feed material has about 49% of its particles less than 25µm in size. From Table 5.11, the p-values of the factors; slurry density and slurry feed rate are 0.0612 and 0.0444, respectively. Also, between these two, slurry density is not a significant factor whereas slurry feed rate is. From Figure 5.17, it is indicated that the design points are above the surface meaning that the relationship between recovery and these two factors is strictly not linear but has maxima point on both slurry density and slurry feed rate.

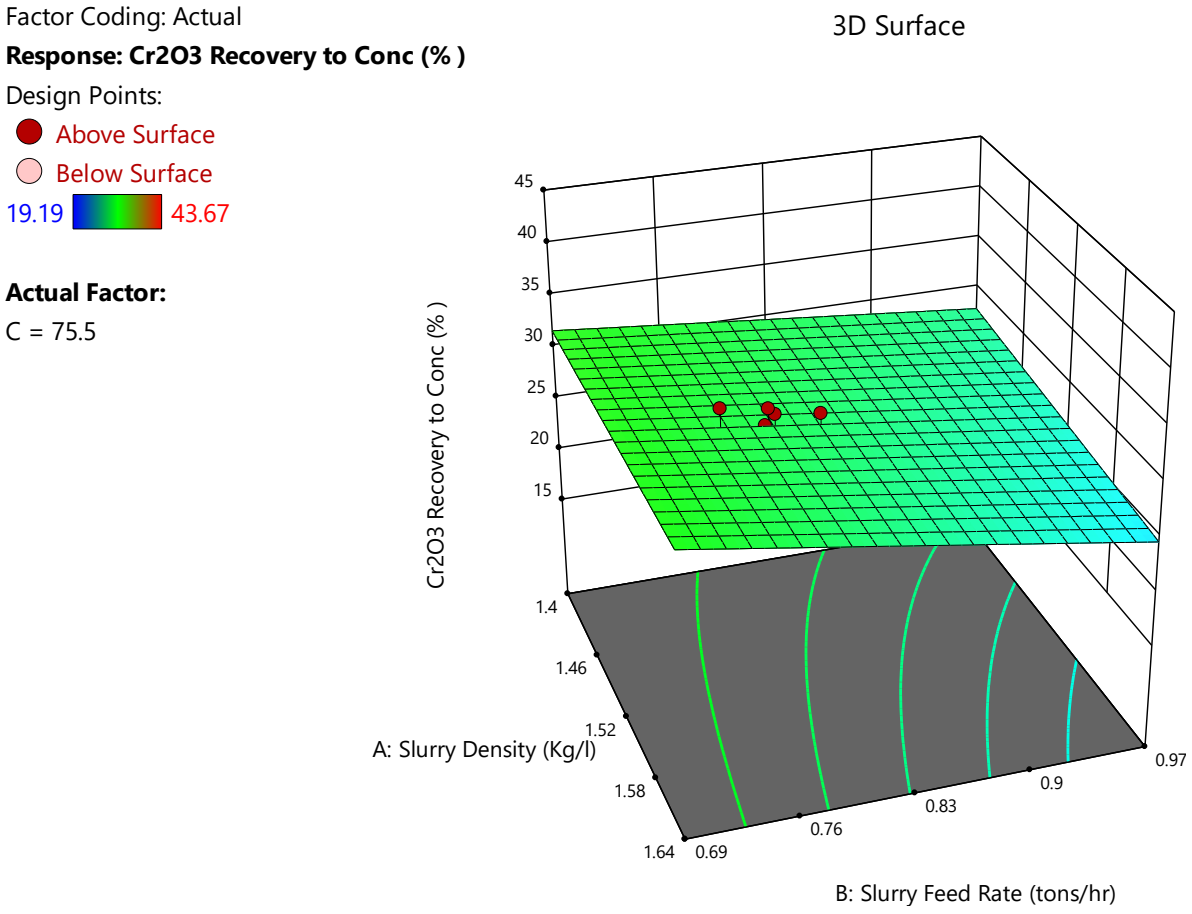

Figure 5.17: Surface plot of Cr_2O_3 Recovery as functions of Slurry feed rate and Slurry density

5.4.2.3 Response Surface Plot for Concentrate Yield as a function of Slurry feed rate and Slurry density

The relationship between yield of mass to concentrate and slurry density and slurry feed rate was also investigated in an analogous way as recovery relationships. From the response surface, higher yield of the concentrate is driven by low feed rate and high slurry density. The relationship of concentrate yield with slurry density and slurry feed rate is like the one for recovery and the two same factors. From Table 5.13, slurry feed rate and concentrate cutter position have a significant correlation with concentrate yield, with both their p-values <0.0001. Slurry density's relationship is not significant at p-value 0.7063 and a small slope in Figure 5.18 proves this point. The other one point to note is that the design points are also above the surface, meaning that there is an optimum point for slurry feed rate and slurry density for a maximum yield.

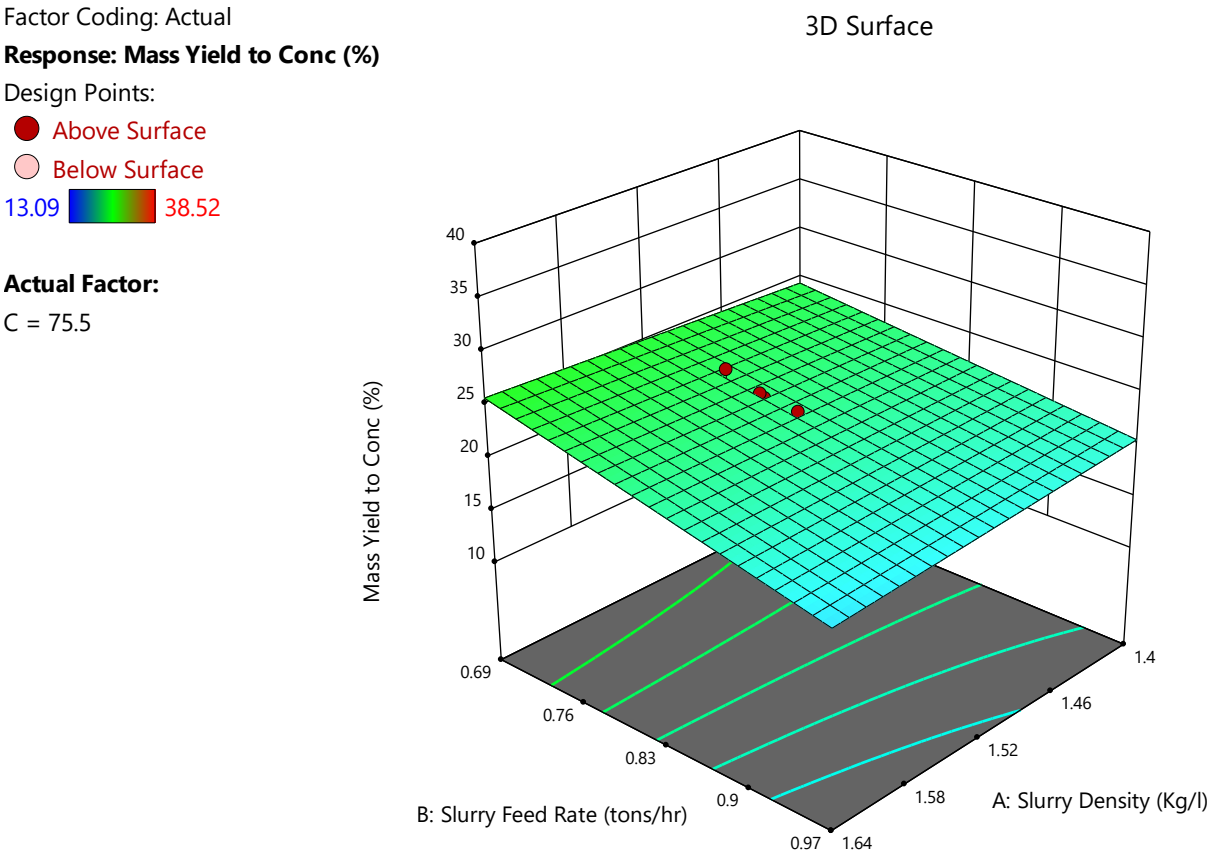

Figure 5.18: Surface plot of Yield as functions of Slurry feed rate and Slurry density

5.4.2.4 Response Surface Plot for Concentrate Grade as a function of Slurry Feed rate and Slurry density

The surface plot for concentrate grade as a function of slurry density and slurry feed rate shows that a higher concentrate grade is favoured by low slurry density and a high slurry feed rate. From the slope gradients and p-values on the ANOVA Table 5.11, the slurry feed rate has a more significant correlation with concentrate grade with a p-value of 0.0444 while the p-value of slurry density is showing no significance at 0.0612. The p-value for the concentrate cutter position for this relationship was <0.0001, showing an extraordinarily strong correlation. There is also an indication that the optimum design points were above the surface by looking at the red pin heads. The low slurry density promotes a higher concentrate grade because free settling is promoted by low density, but the downside to this condition is that the yield will be reduced by a low slurry density.

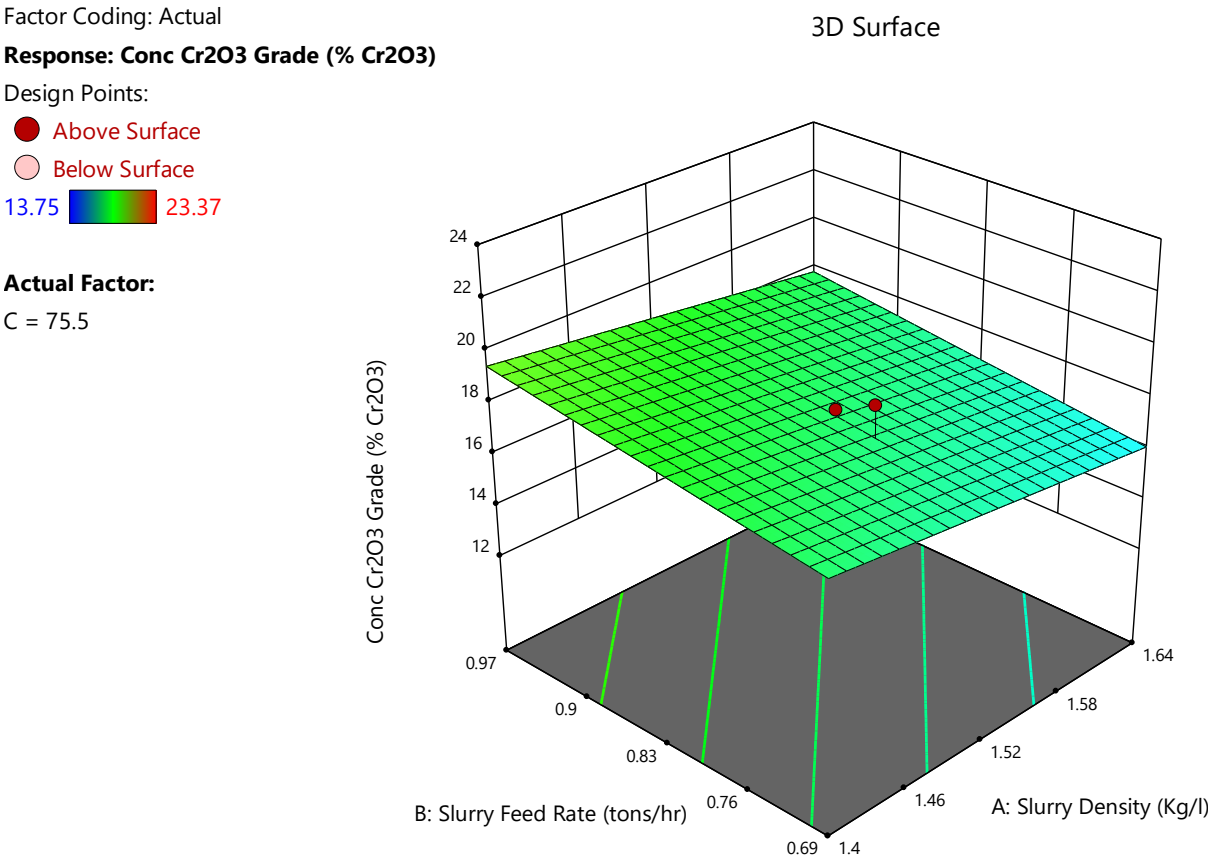

Figure 5.19: Surface plot of Concentrate Grade as functions of Slurry feed rate and Slurry density

5.4.2.5 Response Surface Plot for Enrichment Factor as a function of Slurry Feed rate and Slurry density

The relationship between concentrate Enrichment Factor and slurry density and slurry feed rate is shown in Figure 5.20. Enrichment factor is maximised by low slurry density at high slurry feed rate in an analogous way that grade does. However, at low slurry feed rates the slurry density does not have a significant effect and at high slurry density the slurry feed rate does not have significant effect on enrichment factor. The reason for this pattern is that large particles of low specific gravity (due to poor liberation) are pushed to the outer section of the spiral trough leaving only the high specific gravity high chrome particles in the inside of the trough to collect as clean concentrate.

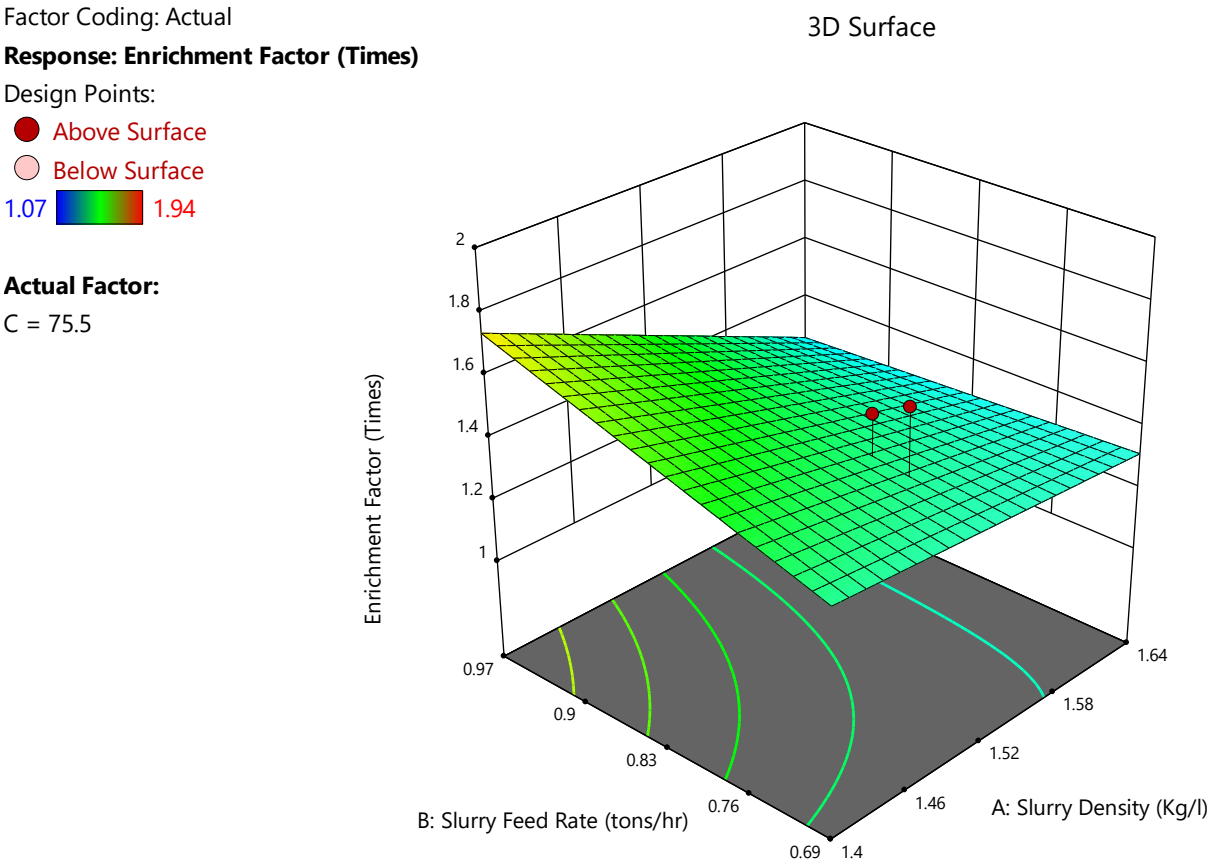

Figure 5.20: Surface plot of Enrichment Factor as functions of Slurry feed rate and Slurry density.

5.4.2.6 Response Surface Plot for Enrichment Factor as a function of Slurry Feed rate and Concentrate Cutter position

When the relationship between enrichment factor and concentrate cutter position and slurry feed rate was plotted on the response surface plane, it was observed that low concentrate cutter position and high slurry feed rate promote high enrichment. It was also observed that slurry feed rate has the bigger influence on enrichment when the cutter position is set at 45mm than when set at 106mm position. At 106mm position, the slurry feed rate slope gradient is almost zero. The p-values for concentrate cutter position and slurry feed rate were <0.0001 and 0.0891, respectively. This means for the two factors, the concentrate cutter position is the major driver of enrichment.

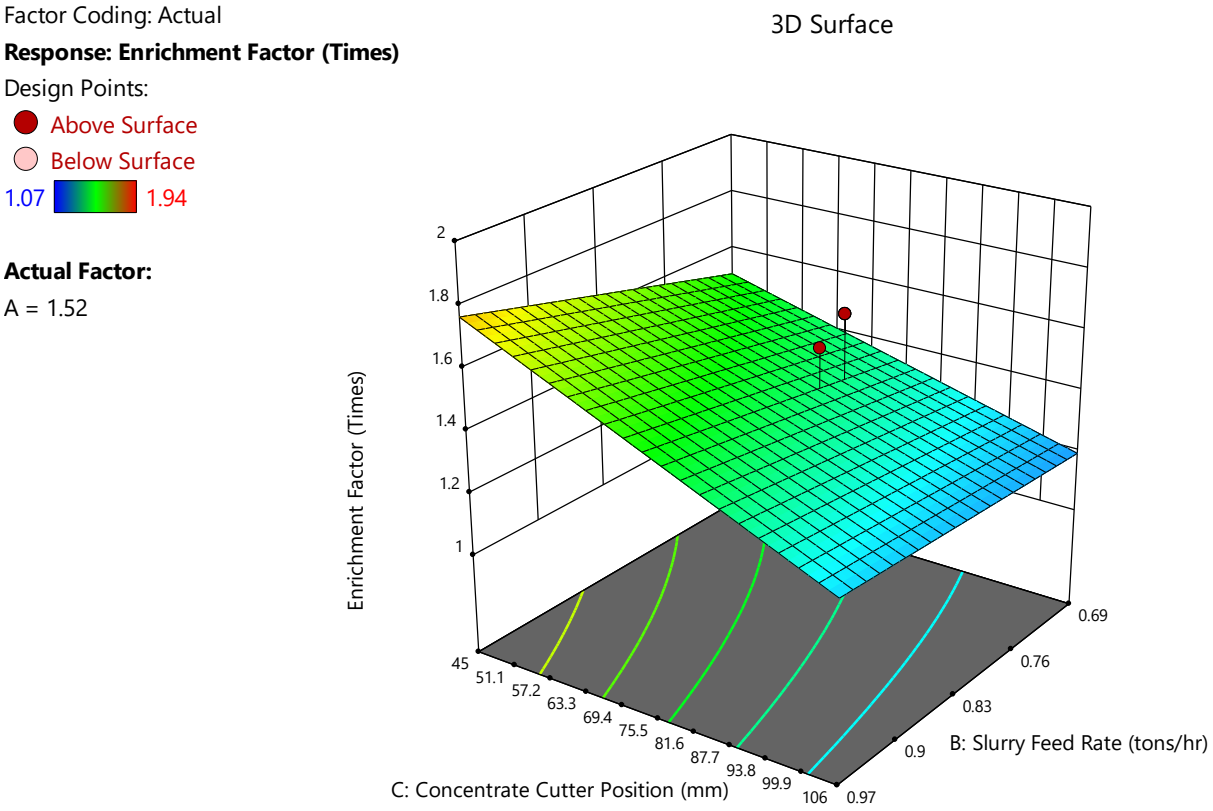

Figure 5.21: Surface plot of Enrichment Factor as functions of Slurry feed rate and Concentrate Cutter position.

5.4.2.7 Response Surface Plot for Enrichment Factor as a function of Concentrate Cutter position and Slurry density

Figure 5.22 shows the response surface for Enrichment Factor as a function of concentrate cutter position and slurry density. The maximum point of Enrichment Factor is located at

minimum concentrate cutter position and minimum slurry density. This is because a narrow concentrate stream contains the highest chrome grade due to profiling of the spiral separation pattern. This separation is enhanced by low slurry density in which settling of high-density chrome particles is promoted. From Table 5.11 the p-values of both factors indicate strong correlation (i.e. less than 0.05) between them and the response parameter. Like the relationship between concentrate cutter position and feed rate, the influence of slurry density is more prominent at low concentrate cutter position. At the highest concentrate cutter position (106mm), the gradient of the slurry density line is not as steep as at 45mm position.

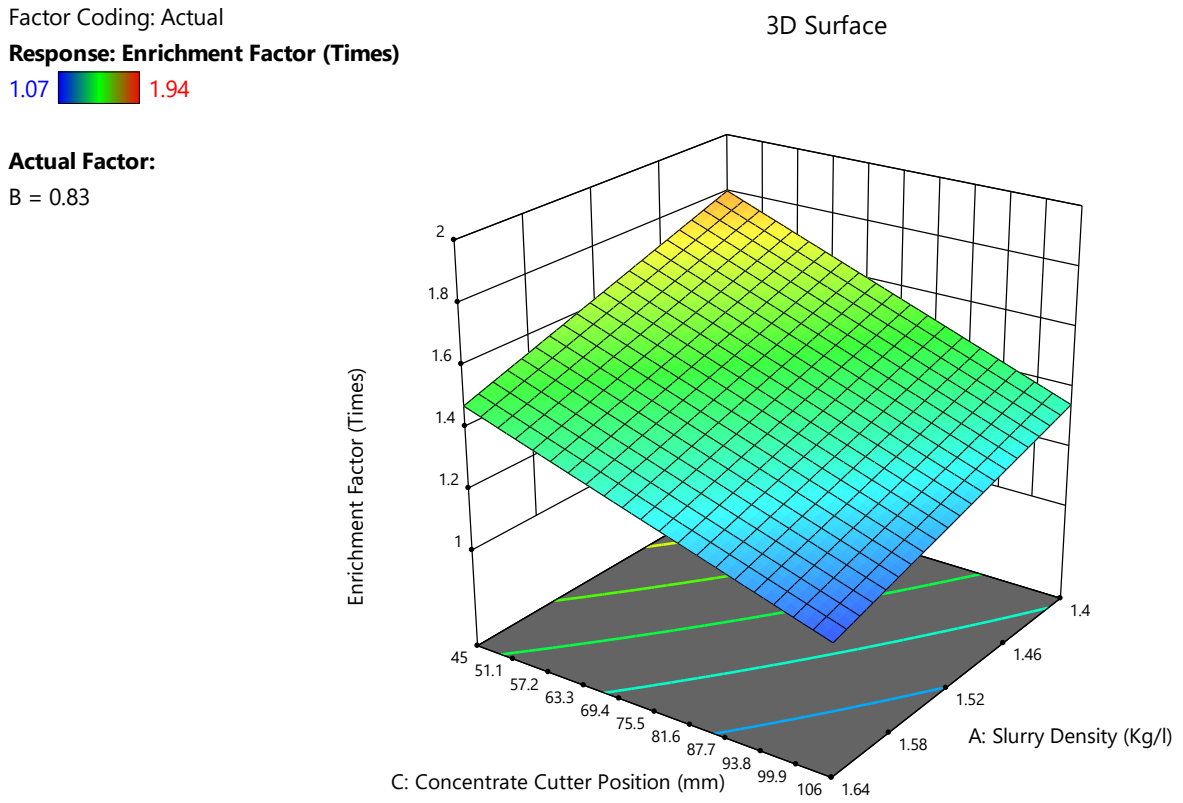

Figure 5.22: Surface plot of Enrichment Factor as functions of Slurry density and Concentrate Cutter position.

5.4.2.8 Response Surface Plot for Tailings Cr_2O_3 Grade factor as a function of Slurry Feed rate and Slurry density

The next section reviews the surface plot for Tailings Cr_2O_3 Grade as a function of slurry feed rate and slurry density. The main goal in the beneficiation of fine to ultrafine chrome is to lower the grade of tailings in terms Cr_2O_3 content because the Cr_2O_3 must be recovered in the

concentrate. From Figure 5.23 below, minimization of the tailings grade is achieved by setting the spirals at high slurry density and high slurry flow rate.

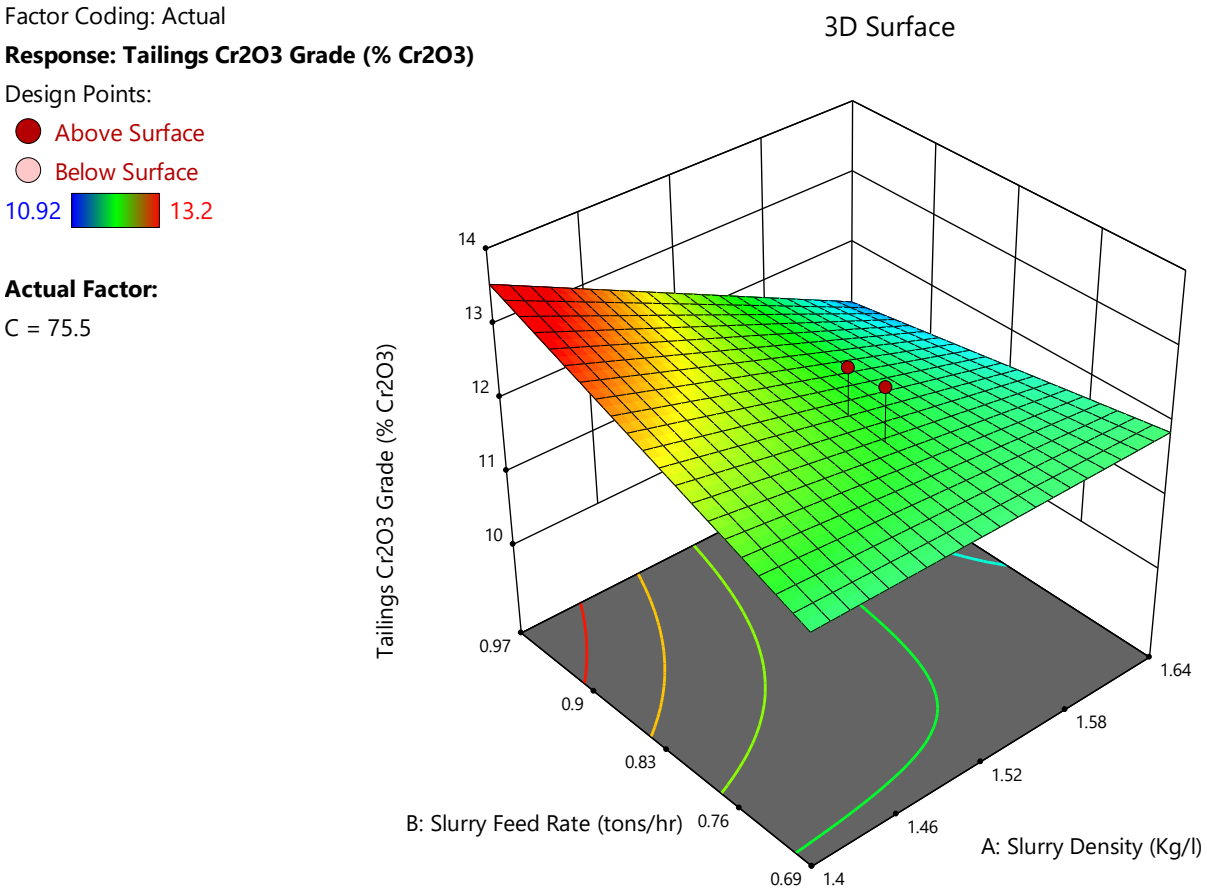

Figure 5.23: Surface plot of Enrichment Factor as functions of Slurry density and Concentrate Cutter position

The p-value for slurry density is given as 0.0443 and the p-value for the interaction factor between slurry density and slurry feed rate is 0.048 indicating that the two factors have a significant interaction effect on tailings grade even though slurry feed rate on its own has no significant effect on tailings grade. The high slurry density ensures that the ultrafine chrome particles do not easily get washed away to the outer portion of the spiral trough, thereby reducing the chrome in the tailings.

5.4.2.9 *Response Surface Plot for Tailings Cr_2O_3 Recovery as a function of Slurry Feed rate and Slurry density*

The surface plot for tailings recovery as a function of slurry density and feed rate has a similar profile as that for tailings grade. Minimization of recovery of Cr_2O_3 into the tailings is driven by high slurry density and low slurry feed rate. The p-values for slurry density and slurry feed rate are both <0.0001 as well as their interaction effect. Between the two factors, slurry density change has the bigger influence on tailings chrome grades at low slurry feed rate.

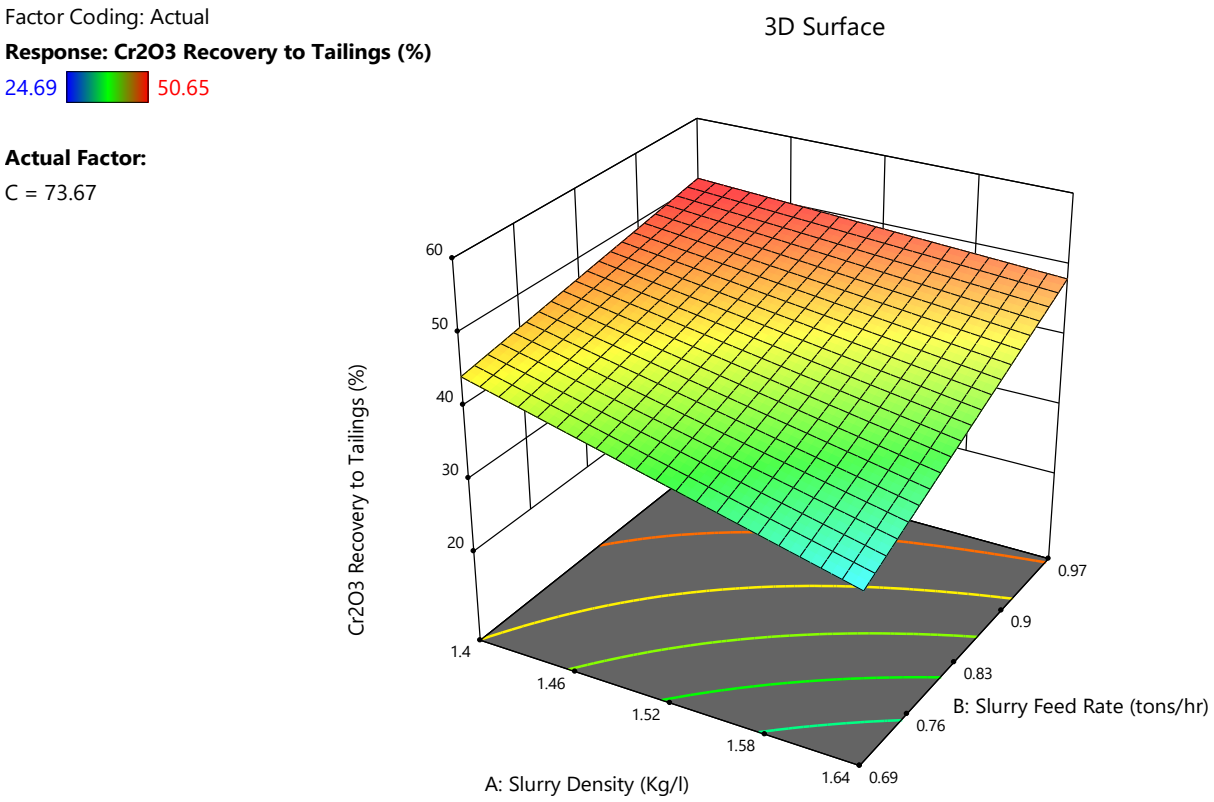

Figure 5.24: Surface plot of Tailings Cr2O3 Recovery as functions of Slurry density and Concentrate Cutter position.

5.4.2.10 *Response surface plot for Tailings Yield factor as a function of Slurry feed rate and Slurry density*

The response surface plot for tailings yield is like the surface plot for tailings recovery. To reduce mass yield to the tailings, the slurry density must be set at high while the slurry feed rate must be low. The p-values for slurry density and slurry feed rate are both <0.0001 and the

interaction factors AB, AC, BC, and ABC are all below 0.05 as per Table 5.11. There is however a condition where the tailings yield may be required to be maximised if the chrome grade in that tailings is low. This talks to high selectivity where high tailings yield at low grade means mass reduction for the next units treating the concentrate streams. The low slurry feed rate and high slurry feed density reduces the mass being pushed to the outer part of the spiral trough.

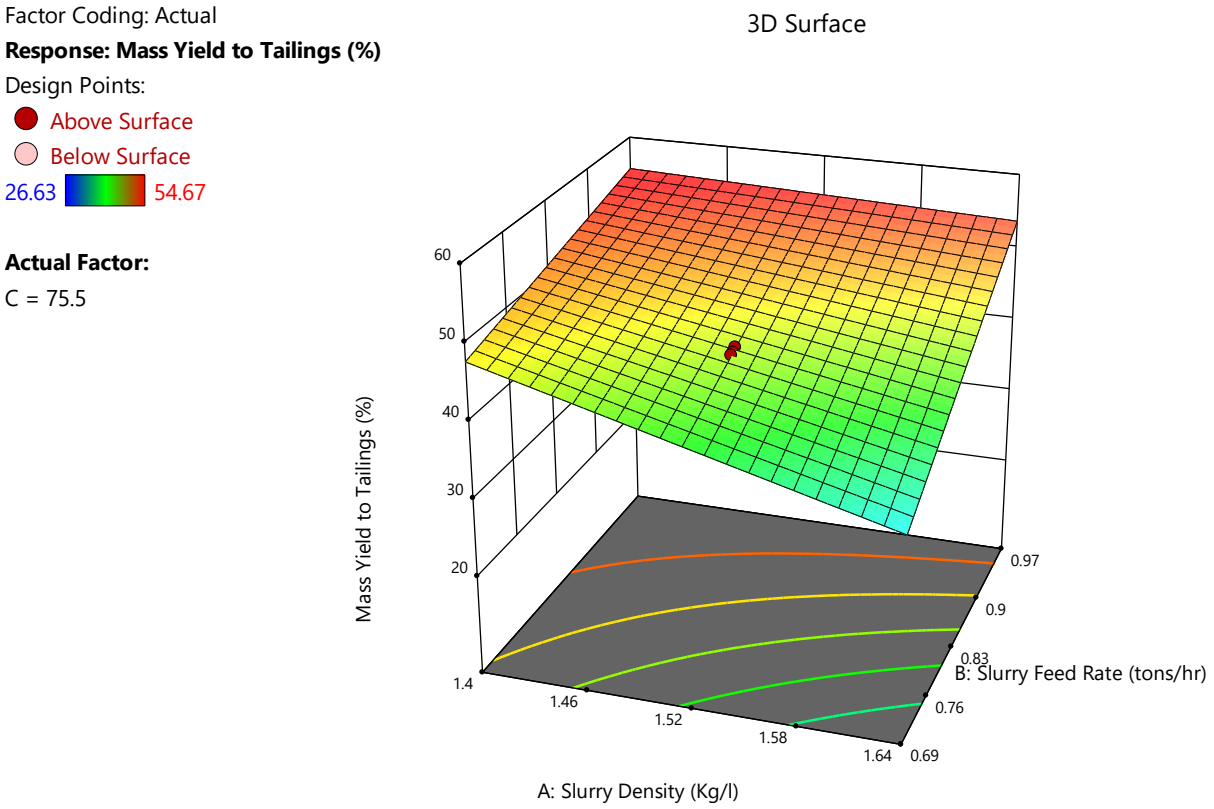

Figure 5.25: Surface plot of Tailings Cr2O3 Recovery as functions of Slurry density and Concentrate Cutter position

The analysis of the above results has shown that from main effect plots as well as response surface methodologies, the spiral main response parameters of chrome grade and recovery are mainly influenced by concentrate cutter position more than slurry density and feed rate. These results are very consistent with the results by Tripathy and Murthy (2012) where they modelled the separation of a 21.95% Cr_2O_3 chrome feed on a spiral. In their work, the sample had 70% of the mass less than 75µm particle size and 30.68% of that mass less than 25µm particle size. Their results were consistent with the relationships between grade and feed rate and grade and concentrate cutter position which showed an inverse relationship. The relationship between grade and slurry density showed an optimum point between 15% and 20% solids.

In terms of relationship between recovery % and the three factors, Tripathy and Murthy's work (2012) showed that concentrate cutter position has the strongest direct correlation with chrome recovery. Slurry density was shown to have an inverse relationship with recovery. There was a disconnect between the results from Tripathy and Murthy and this work on effect of feed rate where for their work the feed rate had a minimum recovery at intermediate level and maximum on lowest and highest level of feed rate whereas this work showed that feed rate has a direct correlation with recovery.

5.4.3 Magnetic Separation Performance tests

The results presented in this section give relationships between input (independent) variables and response parameters which are at play in magnetic separation. The input variables tested are Slurry density (A), dry Feed-rate (B), belt speed (C) and fluidization water (D). These were varied at three levels and their effects were measured on Magnetic fraction Yield, Recovery, Grade, Upgrade ratio and Non-magnetic fraction Yield, Recovery and Grade.

5.4.3.1 Magnetic Separation Fractional Factorial Array and Main effect Plots

The magnetic separation of feed material was tested using the fractional factorial array matrix shown in Table 5.15. The total number of runs was 22 including the centre points. The generation of the main effects plots was done in an equivalent manner to that of spirals in the preceding section.

The three levels at which the slurry relative density was tested are, 1.38, 1.49 and 1.6. Slurry feed rates tested were 1 ton/hr, 1.9ton/hr and 2.8 ton/hr while the magnetic belt speed levels tested were 0.25m/s, 0.375m/s and 0.5m/s. The fluidization water flow rate was tested at the following levels, 21.5 ml/sec, 74.4ml/sec and 127.3ml/sec. Table 5.16 give all the factors and their levels.

Table 5.15: Fractional factorial DOE matrix template for Magnet separation Tests

	Factor 1	**Factor 2**	**Factor 3**	**Factor 4**
Run	**Slurry density (tm^3)**	**Slurry flowrate(t/h)**	**Belt speed (m/sec)**	**Fluidization water flow (ml/sec)**
15	1.38	1.0	0.25	21.5
13	1.38	2.8	0.25	21.5
17	1.38	1.0	0.50	21.5
19	1.38	2.8	0.50	21.5
10	1.38	1.0	0.25	127.3
16	1.38	2.8	0.25	127.3
1	1.38	1.0	0.50	127.3
22	1.38	2.8	0.50	127.3
2	1.49	1.9	0.375	74.4
9	1.49	1.9	0.375	74.4
11	1.49	1.9	0.375	74.4
12	1.49	1.9	0.375	74.4
14	1.49	1.9	0.375	74.4
21	1.49	1.9	0.375	74.4
7	1.6	1.0	0.25	21.5
8	1.6	2.8	0.25	21.5
20	1.6	1.0	0.50	21.5
4	1.6	2.8	0.50	21.5
6	1.6	1.0	0.25	127.3
5	1.6	2.8	0.25	127.3
3	1.6	1.0	0.50	127.3
18	1.6	2.8	0.50	127.3

Table 5.16: Fractional Factorial DOE matrix for Magnetic Separation Preliminary tests

Run	Slurry density(A)	Slurry Feed rate(B)	Belt speed (C)	Fluidization water flow(D)	Feed Cr_2O_3 Grade	Mags Recovery	Mags Yield	Non-Mags Yield	Non-Mags Recovery	Mags Grade	Upgrade ratio
	Kg/L	t/h	m/sec	ml/sec	%	%	%	%	%	%	%
15	1.38	1.0	0.25	21.5	10.99	30.25	20.26	79.74	69.75	16.91	1.54
7	1.6	1.0	0.25	21.5	10.72	30.46	20.89	79.11	69.54	15.24	1.42
13	1.38	2.8	0.25	21.5	11.91	8.28	5.54	94.46	91.72	16.45	1.38
8	1.6	2.8	0.25	21.5	11.13	15.07	11.5	88.5	84.93	13.85	1.24
17	1.38	1.0	0.5	21.5	10.25	41.45	33.4	66.6	58.55	12.72	1.24
20	1.6	1.0	0.5	21.5	11.22	51.6	43.31	56.69	48.4	11.93	1.06
19	1.38	2.8	0.5	21.5	10.23	18.62	13.47	86.53	81.38	14.2	1.39
4	1.6	2.8	0.5	21.5	11.16	7.62	5.45	94.55	92.38	14.75	1.32
10	1.38	1.0	0.25	127.3	10.25	14.94	8.2	91.8	85.06	18.31	1.79
6	1.6	1.0	0.25	127.3	10.88	18.24	10.53	89.47	81.59	18.24	1.68
16	1.38	2.8	0.25	127.3	10.87	6.24	3.76	96.24	93.76	17.74	1.63
5	1.6	2.8	0.25	127.3	10.97	10.91	5.69	94.31	89.09	20.87	1.9
1	1.38	1.0	0.5	127.3	10.56	21.58	12.68	87.32	78.42	17.9	1.7
3	1.6	1.0	0.5	127.3	10.92	23.28	15.85	84.15	76.72	15.8	1.45
22	1.38	2.8	0.5	127.3	10.24	9.15	6.14	93.86	90.85	14.76	1.44
18	1.6	2.8	0.5	127.3	11.46	9.87	7.55	92.45	90.13	15.37	1.34
2	1.49	1.9	0.375	74.4	10.63	13.47	8.81	91.19	86.53	16.14	1.52
9	1.49	1.9	0.375	74.4	11.1	8.16	4.51	95.49	91.84	18.93	1.71
11	1.49	1.9	0.375	74.4	12.38	16.81	11	89	83.19	15.73	1.27
12	1.49	1.9	0.375	74.4	11.39	15.37	8.48	91.52	84.63	11.39	1.12
14	1.49	1.9	0.375	74.4	11.75	10.72	7.89	92.11	89.28	16.38	1.27
21	1.49	1.9	0.375	74.4	10.22	14.91	9.59	90.41	85.09	16.06	1.57

5.4.3.2 *Main effects plots for Magnetic fraction Yield*

Figure 5.26 shows the variation of magnetic yield with slurry density, slurry feed rate, belt speed and fluidization water. From Figure 5.26, the feed rate and wash water have an inverse relationship with magnetic fraction yield. As they move from level 1 to 3 there is a general decrease in the magnetic fraction yield. The same is true for slurry density and belt speed from level 1 to level 2, however both increase markedly with yield from level 2 to 3. In fact, level 2 is a minimum point for magnetic fraction yield against slurry density, belt speed and wash water. The maximization points for the four factors occur at Slurry density L3, Feed rate L1, Belt speed L3 and Wash water L1. The average overall yield for this point is 18.05%.

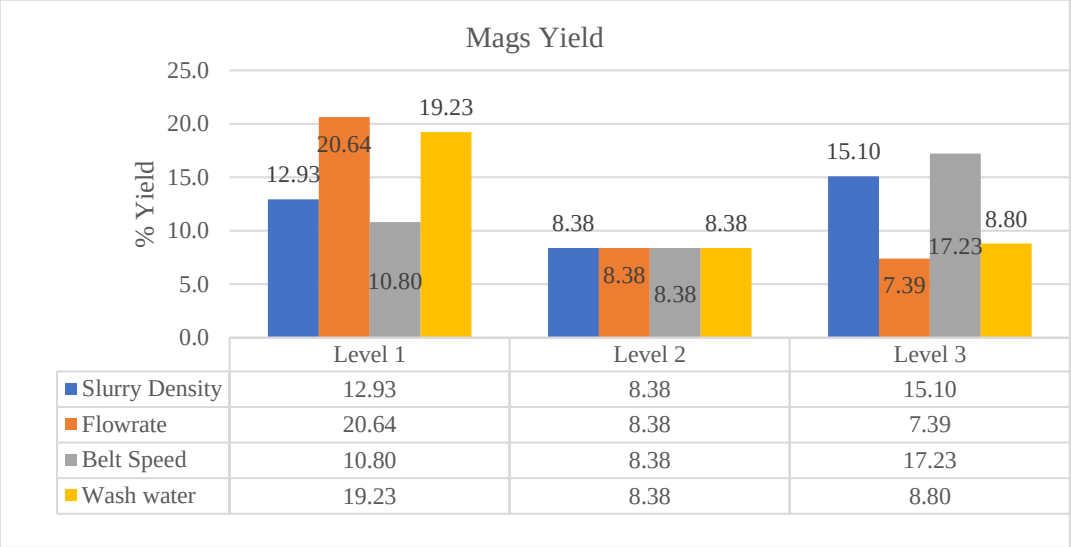

	Level 1	Level 2	Level 3
Slurry Density	12.93	8.38	15.10
Flowrate	20.64	8.38	7.39
Belt Speed	10.80	8.38	17.23
Wash water	19.23	8.38	8.80

Figure 5.26: Main effects plots for Mags Yield means.

5.4.3.3 *Main effects plots for Chrome Recovery to the Magnetic fraction*

Maximization of recovery of chrome to the magnetic fraction requires wash water and feed rate to be set at level 1, belt speed and slurry density at level 3. The factor with the most significant effect is slurry flow rate. This is because at low slurry flow rate, the magnetic field strength effect on the particles is more pronounced than when the flow rate is higher than L1. Wash water has a similar effect on magnetic fraction recovery as slurry flow rate. The average recovery at these levels is 24.54%.

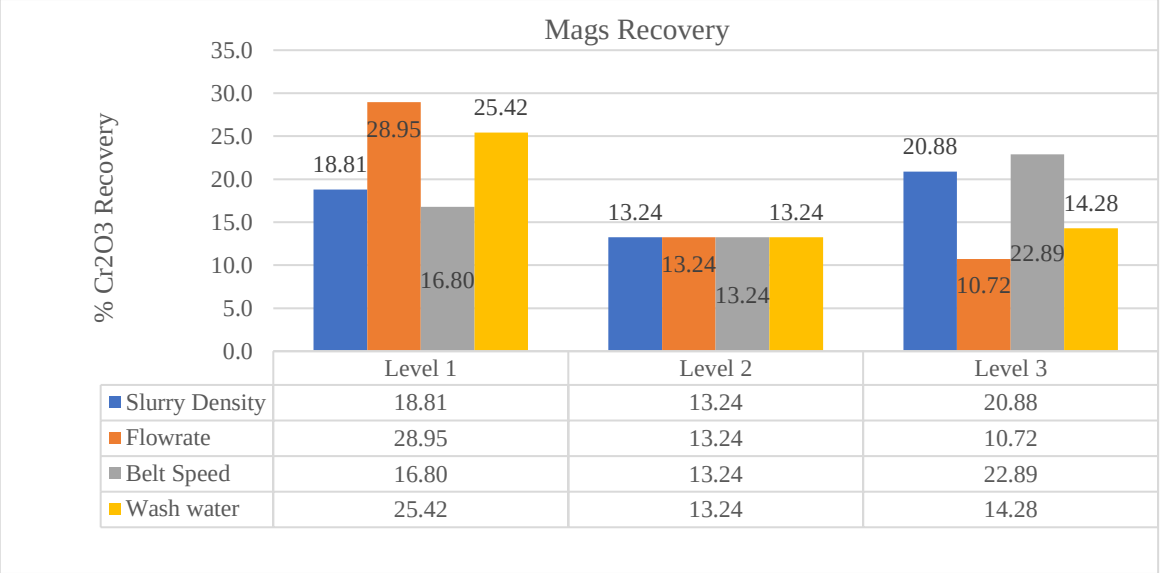

Figure 5.27: Main effects plots for Mags Recovery means

5.4.3.4 Main effects plots for Magnetic fraction Grade

Figure 5.28 shows the response of the grade of the magnetic stream to the variations in the operational factors. The results suggests that the belt speed and wash water have the most significant effect on magnetic fraction grade. An increase in wash water improves mags grade due to wash water effect on washing off the lighter gangue material. On the other hand, when the belt speed increases, there is a more pulling effect on the material including gangue material and this dilutes the grade. Slurry flow rate does not have a considerable influence on grade changes, as the grade remains constant from flowrate level 1 to level 3. Higher slurry density causes a slight reduction in grade but not significantly. To maximise the concentrate grade, the settings for the 4 factors should be, slurry density L1, slurry flow rate L3, belt speed L1 and wash water L3

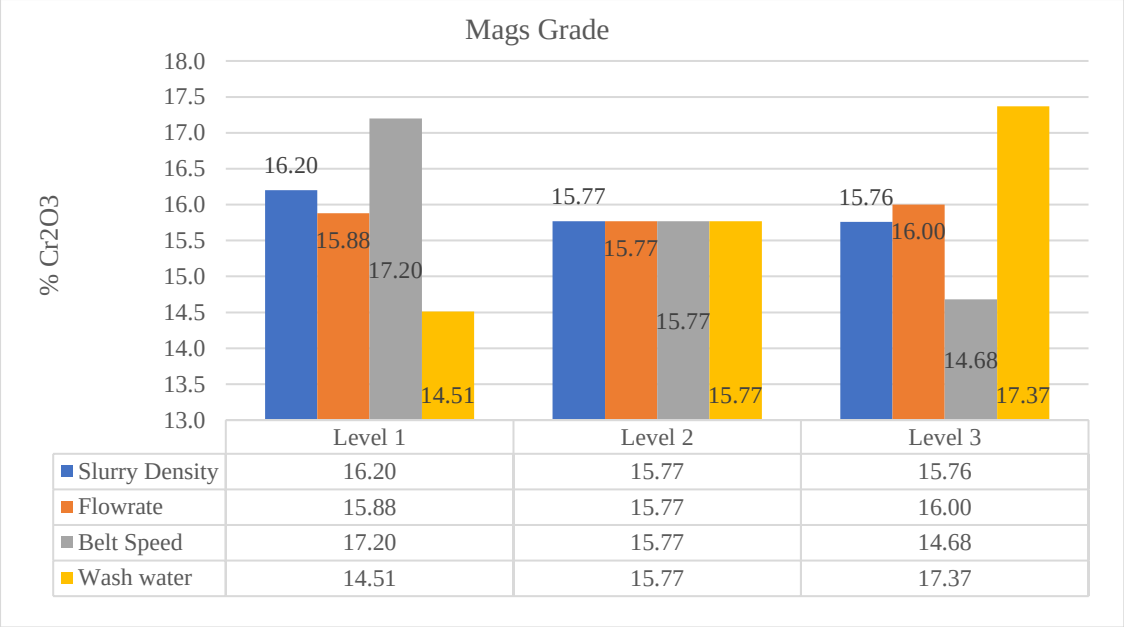

	Level 1	Level 2	Level 3
Slurry Density	16.20	15.77	15.76
Flowrate	15.88	15.77	16.00
Belt Speed	17.20	15.77	14.68
Wash water	14.51	15.77	17.37

Figure 5.28: Main effects plots for Mags Grade

5.4.3.5 Main effects plots for Magnetic fraction Upgrade ratio

Figure 5.29 shows the relationship between magnetic fraction upgrade ratio and the factor effects. The trend for upgrade is like the magnetic fraction grade trends. As the wash water flow increases, the upgrade ratio also increases. Belt speed has an opposite effect to wash water. To maximise this ratio, slurry density, belt speed and feed rate must be set at level 1 while wash water flow must be set at level 3. The average upgrade ratio for these levels is 1.54.

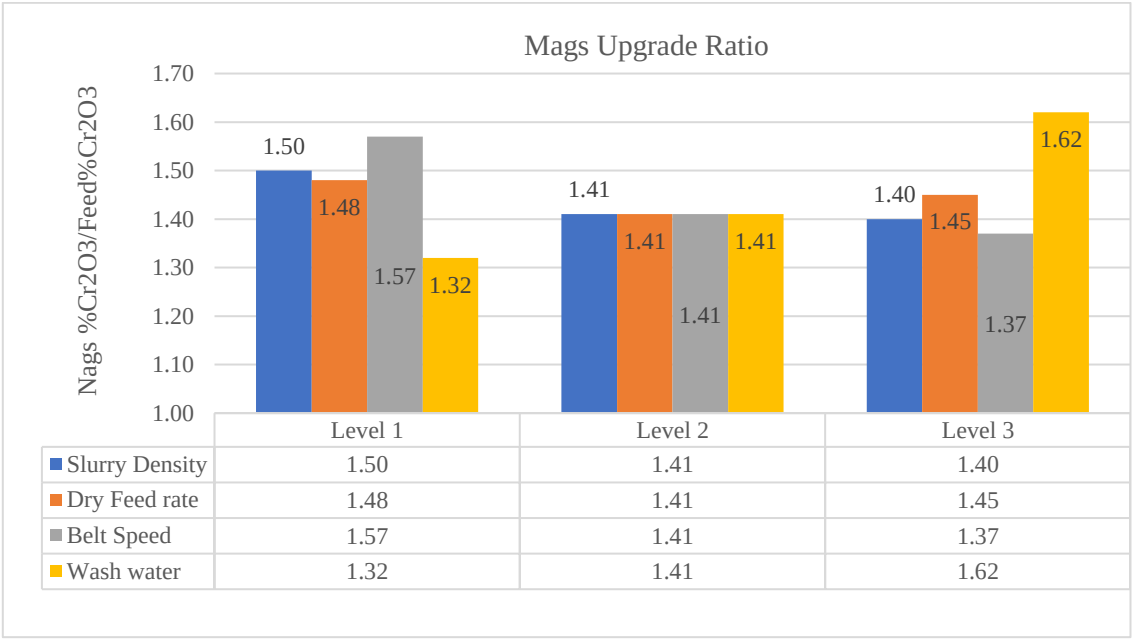

	Level 1	Level 2	Level 3
Slurry Density	1.50	1.41	1.40
Dry Feed rate	1.48	1.41	1.45
Belt Speed	1.57	1.41	1.37
Wash water	1.32	1.41	1.62

Figure 5.29: Main effects plots for Mags Upgrade ratio

5.4.3.6 Main effects plots for Non-magnetic fraction Recovery

Recovery of chrome into the non-magnetic stream must minimised and from Figure 5.30, between level 1 and 2, slurry feed rate and wash water have the biggest effect on loss of chrome to the non-mags. From 2 to 3 there is not much effect since the recovery numbers are constant. To minimise chrome recovery into the non-magnetic stream fluidization water (wash water) and feed rate must be set at level 1 while belt speed and slurry density must be set at level 3.

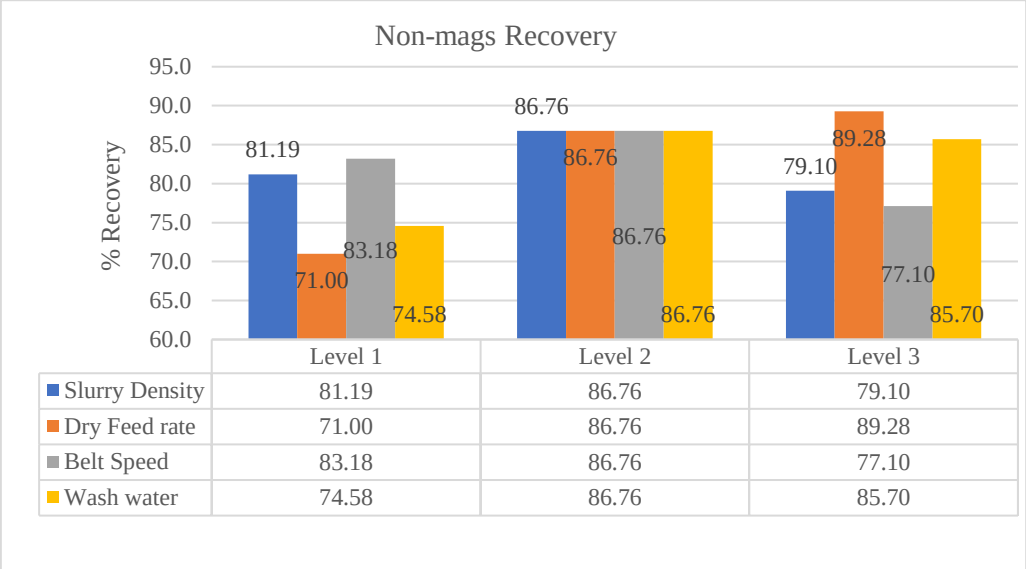

	Level 1	Level 2	Level 3
Slurry Density	81.19	86.76	79.10
Dry Feed rate	71.00	86.76	89.28
Belt Speed	83.18	86.76	77.10
Wash water	74.58	86.76	85.70

Figure 5.30: Main effects plots for Non-mags Recovery

5.4.3.7 Main effects plots for Non-magnetic fraction Yield

The behaviour of the magnetic fraction yield as a function of variation of the factors is like the recovery trends. This is because the recovery and yield are directly proportional to each other. The level settings for the factors to minimise loss of chrome mass into the non-magnetic fraction would be level 1 for wash water and feed rate and level 3 for speed and slurry density. Figure 5.31 show the non-magnetic fraction yield main effect plot.

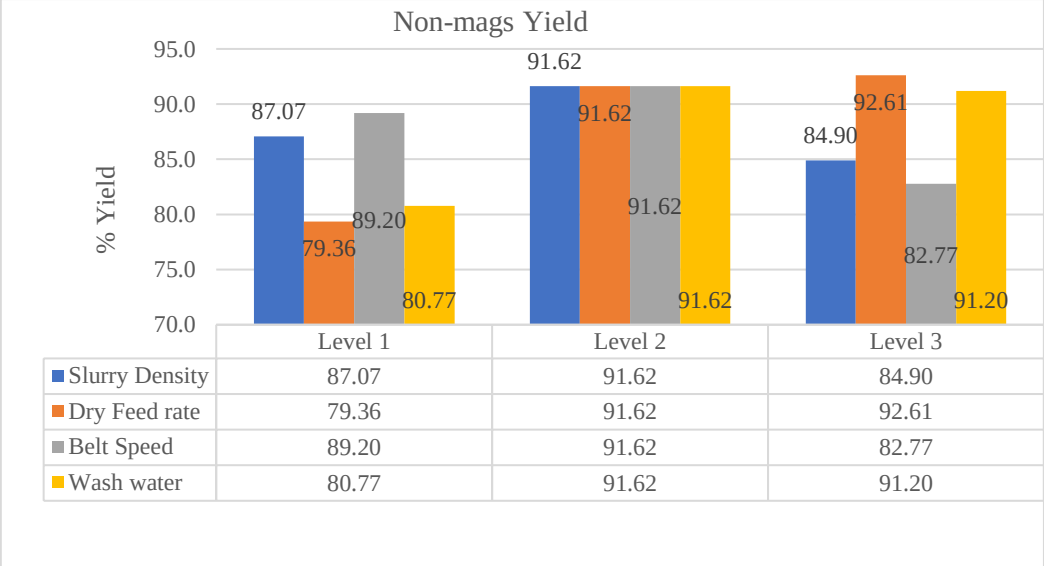

	Level 1	Level 2	Level 3
Slurry Density	87.07	91.62	84.90
Dry Feed rate	79.36	91.62	92.61
Belt Speed	89.20	91.62	82.77
Wash water	80.77	91.62	91.20

Figure 5.31: Main effects plots for Non-mags Yield

5.4.3.8 Main effects plots for Non-mags Grade

The behaviour of the non-magnetic grade is shown in Figure 5.32. The main factor with significant effect on the non-magnetic grade is slurry feed rate. As the slurry feed rate increases from level 1 to 3, there is a corresponding increase in the non-magnetic grade. To minimise the loss of chrome to the non-magnetic fraction, slurry flow rate, slurry density and wash water must be set at level 1 and belt speed at level 3. These factor levels give a non-magnetic grade of 9.58% Cr_2O_3.

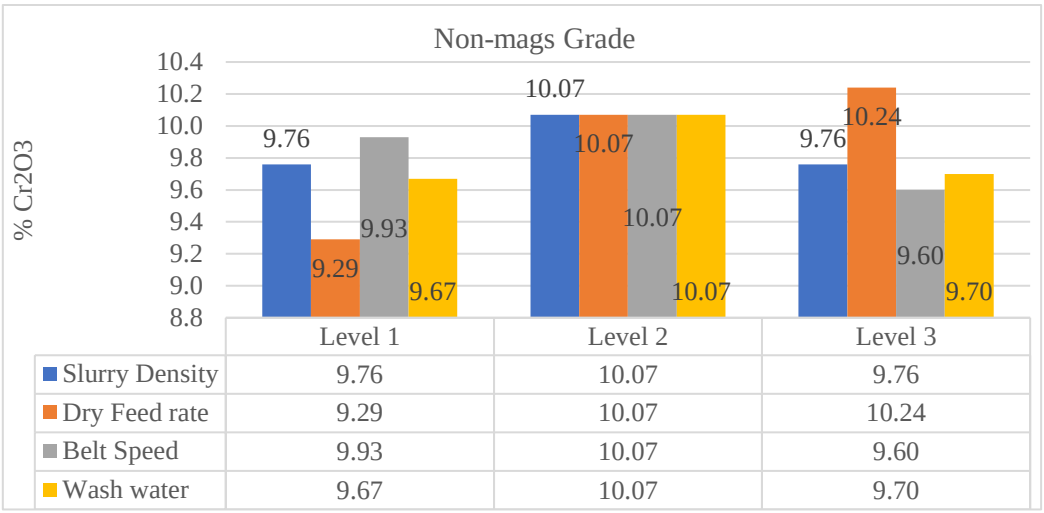

	Level 1	Level 2	Level 3
Slurry Density	9.76	10.07	9.76
Dry Feed rate	9.29	10.07	10.24
Belt Speed	9.93	10.07	9.60
Wash water	9.67	10.07	9.70

Figure 5.32: Main effects plots for Non-mags Grade

5.4.3.9 Factor Statistical Analysis

The design of experiments model that was used for the spirals data analysis was applied for the magnetic separation as well. The results below present the correlation of the factor and response parameters as investigated on the magnetic separator. From Table 5.17 below, the two factors that have significant relationships with all response parameters are feed rate and wash water. Belt speed is correlated with Magnet Grade and Upgrade ratio, but the coefficients are exceedingly small.

Table 5.17: ANOVA Analysis for magnetic separator

	Intercept	**A**	**B**	**C**	**D**
Mags Cr_2O_3 Recovery	15.73		-6.63		-3.94
p-values			< 0.0001		0.0157
Mags Mass Yield	10.63	-0.31	-4.49	1.57	-3.73
p-values		0.81	0.0012	0.23	0.0098
Non-Mags Mass Yield	89.37	0.31	4.49	-1.57	3.73
p-values		0.81	0.0012	0.23	0.0098
Non-Mags Cr_2O_3 Recovery	84.26		6.64		3.93
p-values			< 0.0001		0.0159
Mags Cr_2O_3 Grade	15.96			-1.17	1.34
p-values				0.0152	0.0065
Mags Upgrade ratio	1.46			-0.09	0.14
p-values				0.0437	0.0049

Key:

A Slurry density
B Slurry Feed rate
C Belt speed
D Fluidisation water

In terms of the model, the standard deviations and C.V % are on the high side and the accuracy of the model is not as stable as it could be, especially on the magnetic fraction recovery and yield.

Tables 5.19 and 5.20 give the coded and actual equations for this magnetic separation test results. The predicted points for the whole model are; slurry density-1.49t/m3 slurry flowrate-1.90 t/h, belt speed -0.375 m/sec and wash water 74.4 ml/sec. Coded and actual equations gave magnetic recovery of 28.3% and 26.26% respectively for lower set point (-1) while the upper set point (+1) gave magnetic recovery of 7.16% and 5,60% respectively, showing adequate agreement between coded and actual predicted values.

Table 5.18: Fit Statistics for magnetic separation

	Mags Cr_2O_3 Recovery	Mags Mass Yield	Non-Mags Mass Yield	Non-Mags Cr_2O_3 Recovery	Mags Cr_2O_3 Grade	Mags Upgrade ratio
Std. Dev.	5.71	4.89	4.89	5.71	1.68	0.16
Mean	16.45	11.01	88.99	83.54	16.08	1.47
C.V. %	34.70	44.43	5.50	6.83	10.42	11.06
R^2	0.63	0.60	0.60	0.63	0.46	0.44
Adjusted R^2	0.59	0.51	0.51	0.59	0.40	0.38
Predicted R^2	0.47	0.23	0.23	0.47	0.33	0.29
Adeq. Precision	11.86	9.73	9.73	11.86	7.90	7.37

Table 5.19: Coded Equations

	Mags Recovery	Mags Yield	Non-Mags Yield	Non-Mags Recovery	Mags Grade	Upgrade ratio
Intercept	15.73	10.63	89.37	84.26	15.96	1.46
A		-0.31	0.31			
B	-6.63	-4.50	4.50	6.64		
C		1.57	-1.57		-1.17	-0.09
D	-3.94	-3.73	3.73	3.93	1.34	0.14

Key:

A Slurry density
B Slurry Feed rate
C Belt speed
D Fluidisation water

Table 5.20: Actual Equations

	Mags Recovery	Mags Yield	Non-Mags Yield	Non-Mags Recovery	Mags Grade	Upgrade ratio
Intercept	35.27	24.80	75.20	64.72	17.58	1.55
Slurry density		-2.79	2.79			
Slurry flowrate	-7.36	-4.999	4.999	7.37		
Belt speed		12.60	-12.60		-9.33	-0.73
Fluidization water flow	-0.07	-0.07	0.07	0.07	0.03	0.002

5.4.4 Response Surface Plots for Magnetic Separator

The following section presents the response surface plots for the magnetic separator. From Table 5.17 above only 2 out of the 4 input factors have significant correlations with the response parameters and these will be the ones to be plotted and discussed. From Table 5.17 and the figures to come, letters used to identify each factor are given below for clarity.

A Slurry density
B Slurry Feed rate
C Magnet Belt speed
D Fluidization water

5.4.4.1 Response Surface Plot for Magnetic Recovery as a function of Slurry Feed rate and Fluidization Water

The relationship between magnetic recovery as a function of slurry feed rate and fluidization water is given in Figure 5.33. The purpose of the magnetic separator is to recover chrome to the magnetic fraction. From the design matrix developed and run according to the Design Expert software, slurry feed rate and fluidization water were found to be the only ones with significant correlation with chrome recovery into the magnetic fraction (Magnetic Recovery). The highest recovery was driven by low slurry feed rate and low fluidization water. The explanation for this trend is that when the slurry feed rate is low, it forms almost a monolayer and the flux (mass per unit surface area) of slurry on the belt is low, thereby allowing the bulk of the particles to receive maximum magnetic force. The low fluidization water provides water to dismantle any coagulated particles without washing the chromite particles to the non-magnetic stream. The p-value for the slurry feed rate and fluidization water was <0.0001 and 0.0157 respectively according to Table 6.9. The p-value for BxD interaction is 0.0048.

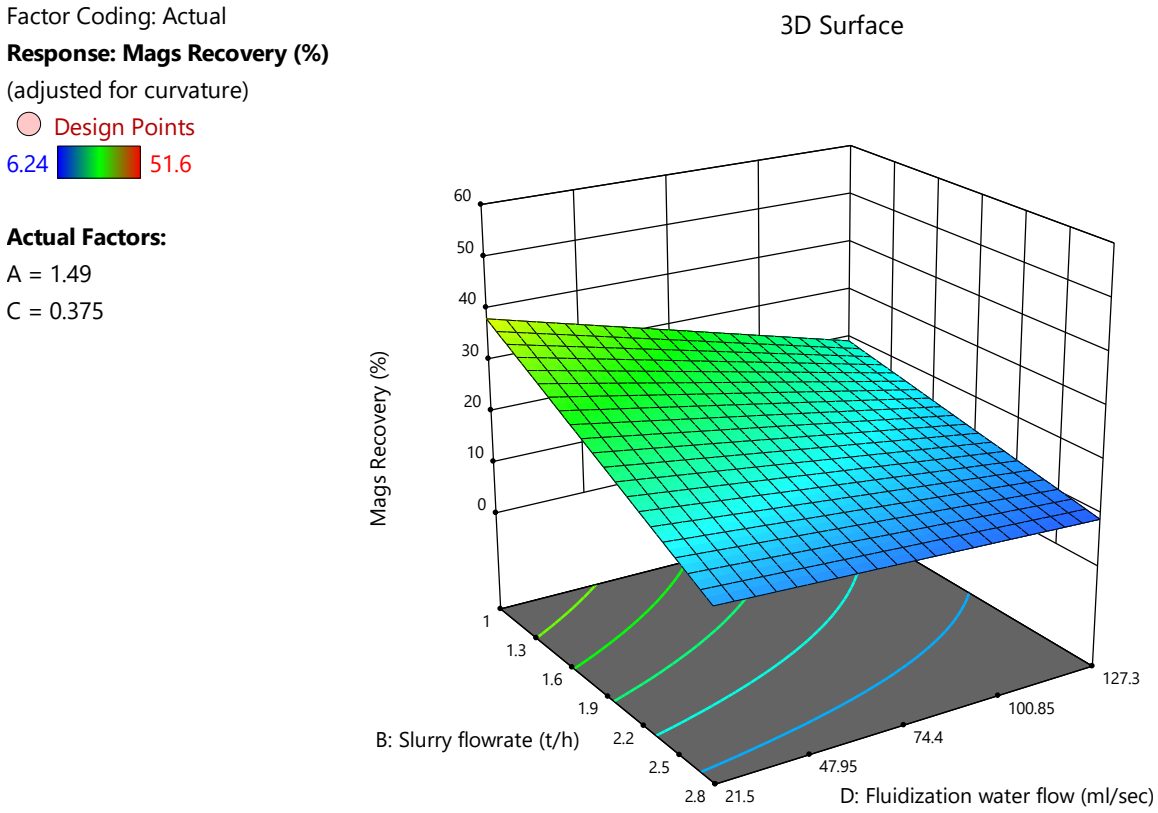

Figure 5.33: Surface plot of Magnetic Cr_2O_3 Recovery as functions of slurry density and fluidization water

5.4.4.2 Response Surface Plot for Magnetic Recovery as a function of Slurry Feed rate and Belt Speed

The other pair of input factors that have significant correlations with Magnet Cr_2O_3 recovery are slurry feed rate and belt speed. The conditions for high recovery to the magnetic fraction are high belt speed and low slurry feed rate. Between the two factors slurry flow rate is more significant since its slope is more than the belt speed slope. The effect of slurry feed rate is more pronounced at high belt speed. The p-value for the BxC interaction effect on recovery is 0.0289.

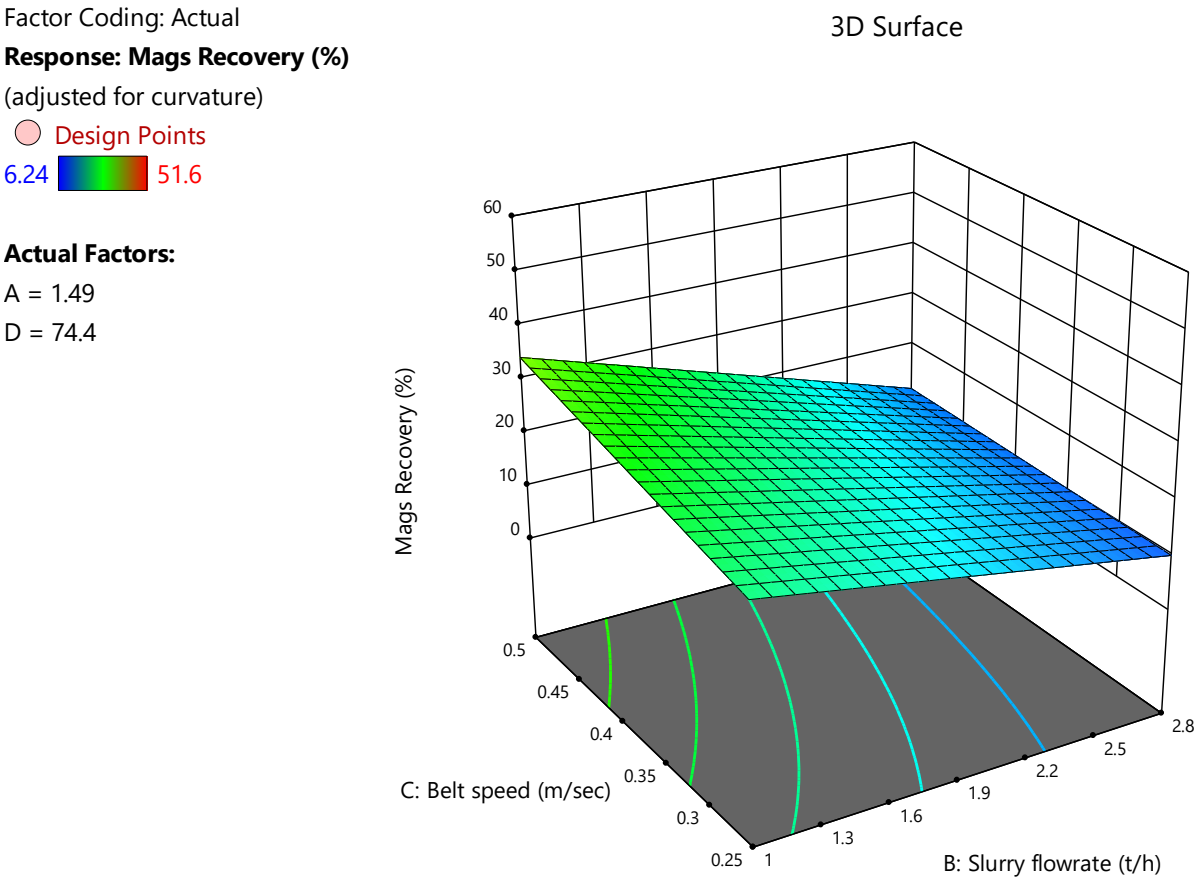

Figure 5.34: Surface plot of Magnetic Cr2O3 Recovery as functions of Slurry Feed rate and Belt speed

5.4.4.3 Response Surface Plot for Magnetic Yield as a function of Slurry Feed rate and belt speed

The response surface plots for Magnetic fraction yield has three sets of significant interaction factors. The first pair is slurry feed rate and belt speed. It must be noted that from Table 5.17 belt speed on its own does have a significant correlation (p-value=0.002) with yield as well as its interaction with slurry feed rate. Slurry feed rate p-value is 0.0012. The interaction factor between belt speed and slurry feed rate has a significant correlation with Magnetic fraction yield with a p-value of 0.0064. The reasons why yield is driven by low slurry feed rate and high belt speed are the same as observed for recovery above.

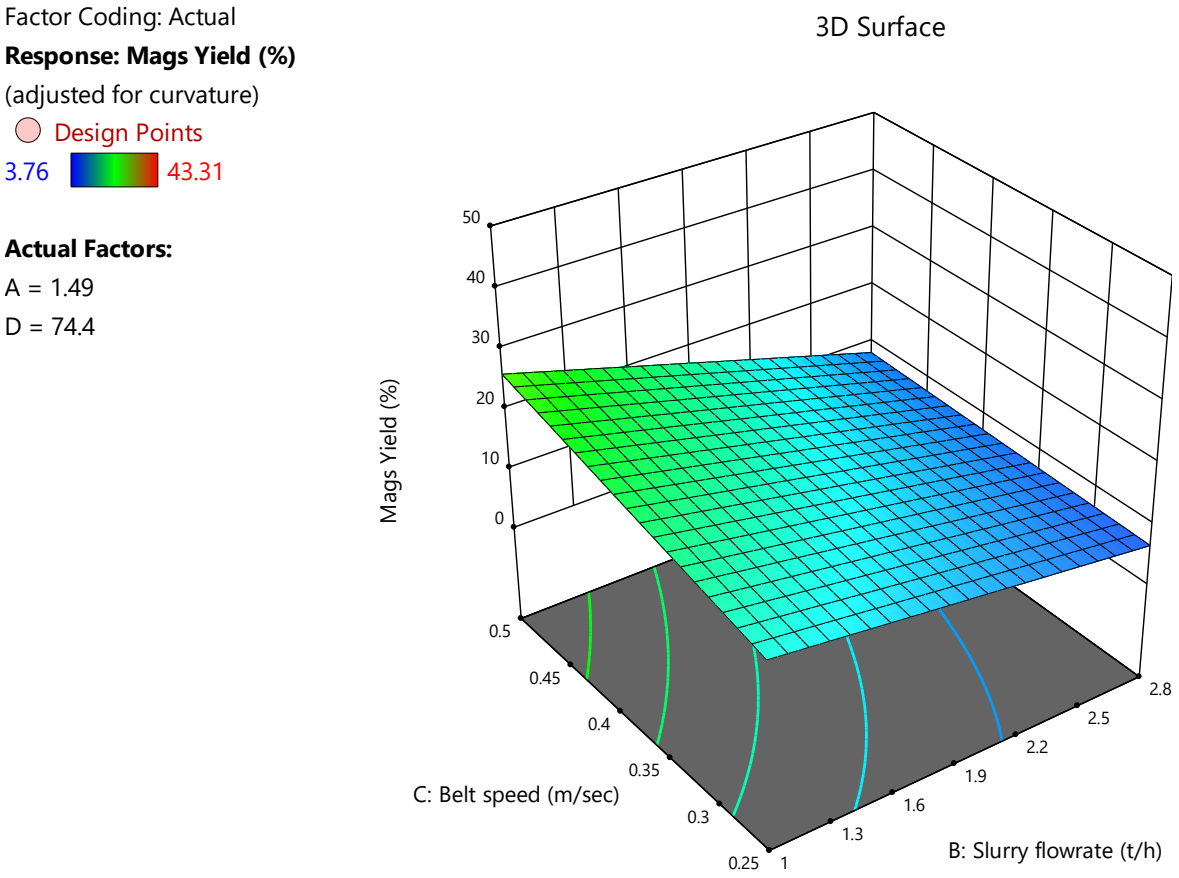

Figure 5.35: Surface plot of Magnetic Yield as functions of Slurry Feed rate and Belt speed

5.4.4.4 Response Surface Plot for Magnetic Yield as a function of Slurry Feed rate and Fluidization water

The results from the DOE matrix carried out on the magnetic separator revealed that Magnetic fraction yield was influenced by slurry feed rate and fluidization water as shown in Figure 5.36 below. Maximization of yield needed low slurry feed rate and low fluidization water. The forces acting on paramagnetic chrome particles are more pronounced when the fluid flow approached a monolayer profile with low fluidization water just enough to dislodge the gangue particles that may have been trapped with the magnetic particles. The p-value for BxD interaction was 0.0012 indicating that the model was significant. The opposite of these conditions lowers the yield due to washing away of mostly fine chromite particles by strong hydrodynamic forces down the slope and, if the slurry feed rate is high the magnet slurry bed ceases to be a monolayer model but a multilayer, which reduces the efficiency of the separation.

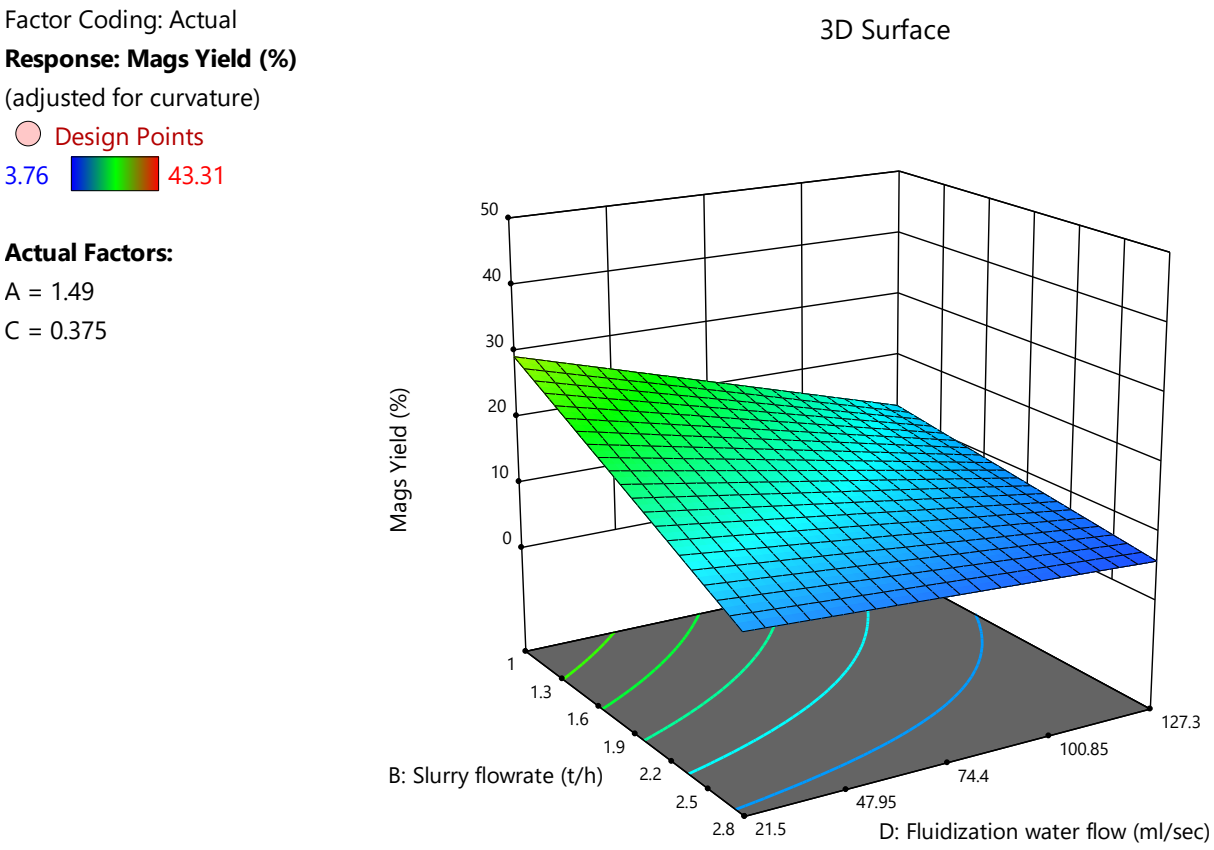

Figure 5.36: Surface plot of Magnetic Yield as functions of Slurry feed rate and Fluidization water

5.4.4.5 Response Surface Plot for Magnetic Yield as a function of Belt Speed and Fluidization water

The relationship between Magnetic fraction yield and belt speed and fluidization water was also a meaningful relationship. Figure 5.37 shows the response surface plot between the two factors acting on Magnetic fraction yield as the response parameter. Between the two factors, getting maximum yield is attained by minimising fluidization water and maximizing belt speed. The correlation of this relationship (CxD interaction) was found to be significant as given by the p-value which was 0.0436. Increasing the belt speed ensures that more particles are exposed to strong magnetic forces as they drop on the magnet belt. The effect is like reducing slurry feed rate.

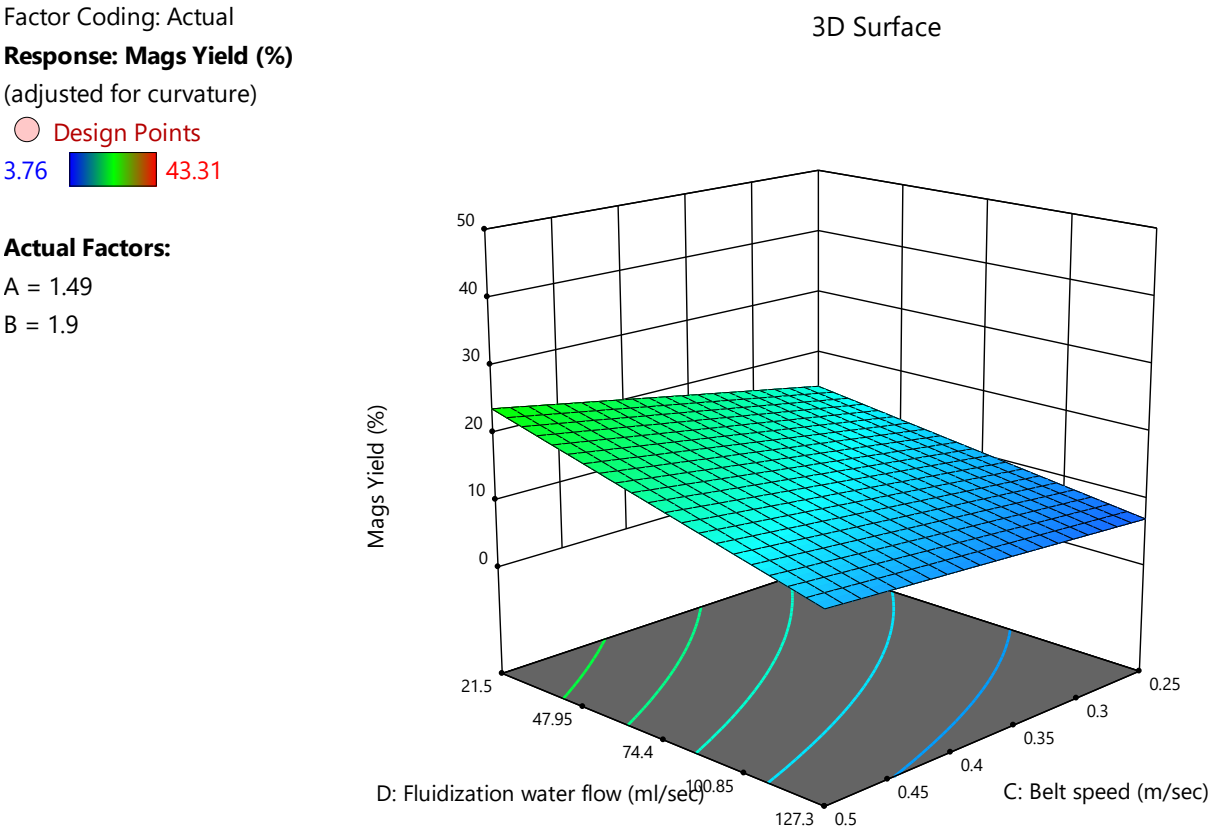

Figure 5.37: Surface plot of Magnetic Yield as functions of Slurry feed rate and Fluidization water

5.4.4.6 Response Surface Plot for Magnetic fraction Grade as a function of Slurry feed rate and Fluidization water flow

The response surface plot for Magnetic fraction Grade as a function of slurry feed rate and fluidization water flow is given in Figure 5.38. Between the two factors, fluidization water flow was the more significant factor with a p-value of 0.0129. Slurry feed rate was not significant with a p-value of 0.9113. It is evident from the gradient of the slurry flow rate that is almost zero. To get an increase in chrome grade of the magnetic fraction, fluidization water needs to be maximised. The reason is that when fluidization water increases, the gangue particles that might have been collected by the magnet through entrapment would be dislodged and washed to the non-magnetic fraction, thereby increasing the grade of the magnetic fraction.

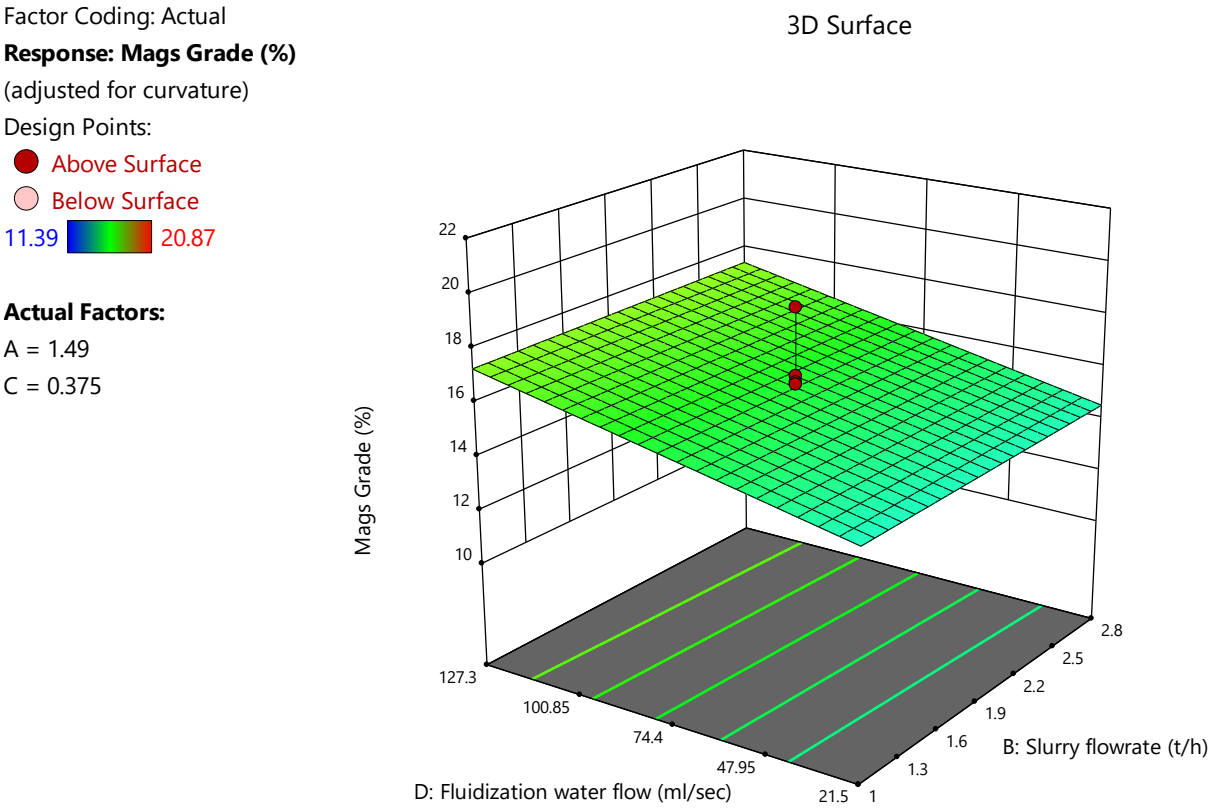

Figure 5.38: Surface plot of Magnetic Cr2O3 Grade as functions of Slurry feed rate and Fluidization water

5.4.4.7 Response Surface Plot for Magnetic fraction Enrichment as a function of Slurry density and Fluidization water flow.

The response surface plot for Magnetic fraction enrichment is shown in Figure 5.39. The only significant factor is fluidization water that has a p-value of 0.0046. To maximise enrichment, the fluidization water needs to be maximised in driving Magnetic fraction enrichment. Slurry density does not have a significant impact on enrichment on this combination.

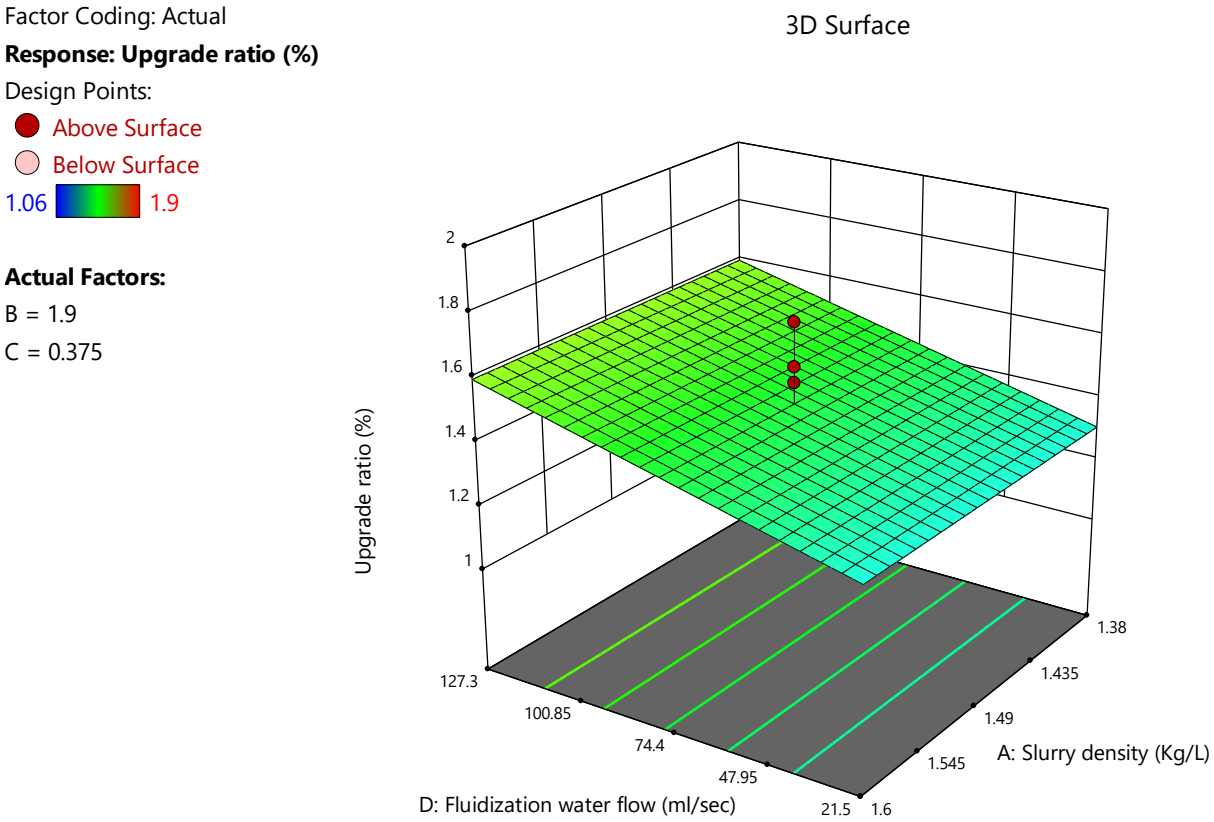

Figure 5.39: Surface plot of Magnetic fraction Enrichment factor as functions of Slurry density and Fluidization water flow

5.4.4.8 Response Surface Plot for Non-Magnetic Cr_2O_3 Recovery as a function of Slurry Feed rate and Fluidization water flow

Figure 5.40 shows the response surface plot for non-magnetic fraction recovery as a function of slurry density and fluidization water flow. From the plot, it is evident that fluidization water has a more significant impact on non-magnetic fraction recovery. To minimise loss of chrome to the no-magnetic fraction, both fluidization water flow and slurry feed rate need to be set at minimum. The p-values for the fluidization water flow and slurry feed rate were 0.0005 and 0.0001 respectively in this model. The model itself was significant with a p-value of <0.0001.

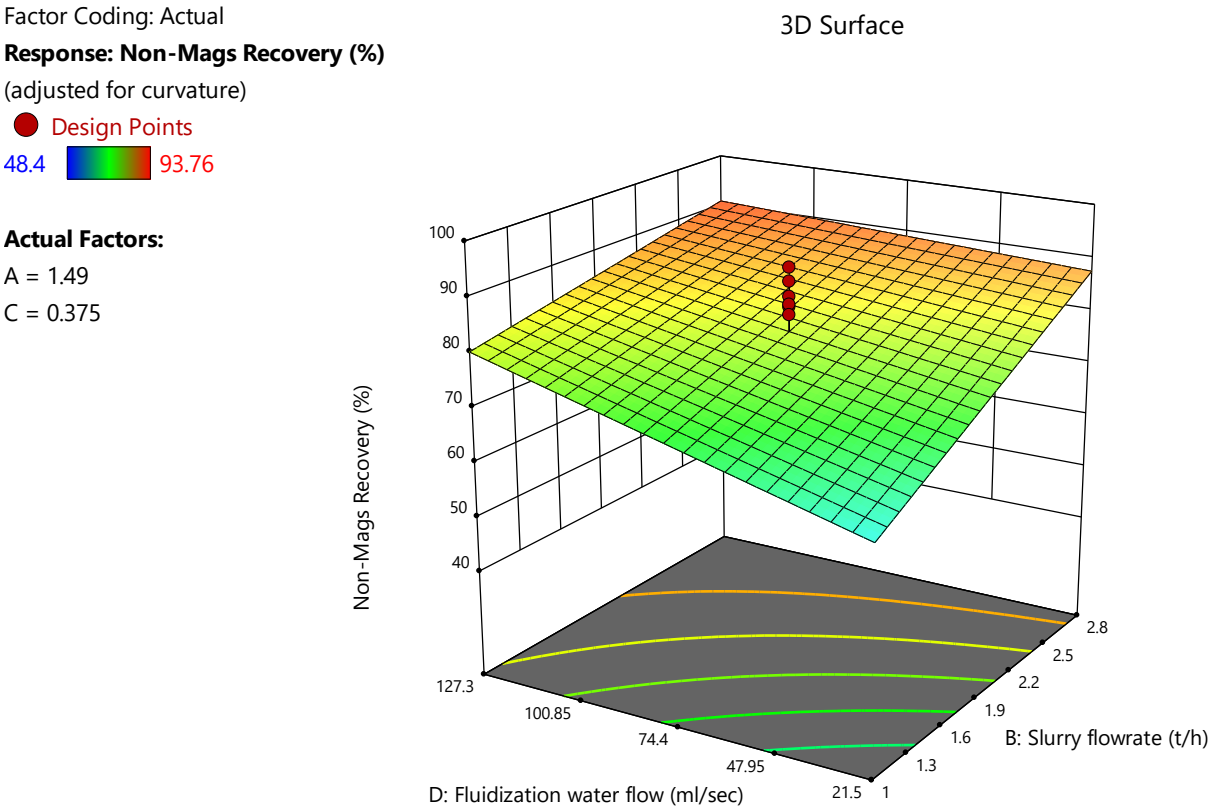

Figure 5.40: Surface plot of Magnetic fraction Enrichment factor as functions of Slurry feed rate and Fluidization water flow

5.4.4.9 Response Surface Plot for Non-Magnetic Yield as a function of Slurry Feed rate and Fluidization water flow.

The following response surface plot relates to the variation of non-magnetic yield when slurry feed rate and fluidization water was changed (Figure 5.41). To minimise non-magnetic yield both factors must be minimised. This condition favours selectivity of the separation process on the magnetic separator. The p-values for slurry feed rate and fluidization water were <0.0001 and 0.0002, showing strong correlation. The non-magnetic fraction yield is directly proportional to non-magnetic fraction chrome recovery in terms of conditions driving their minimisation.

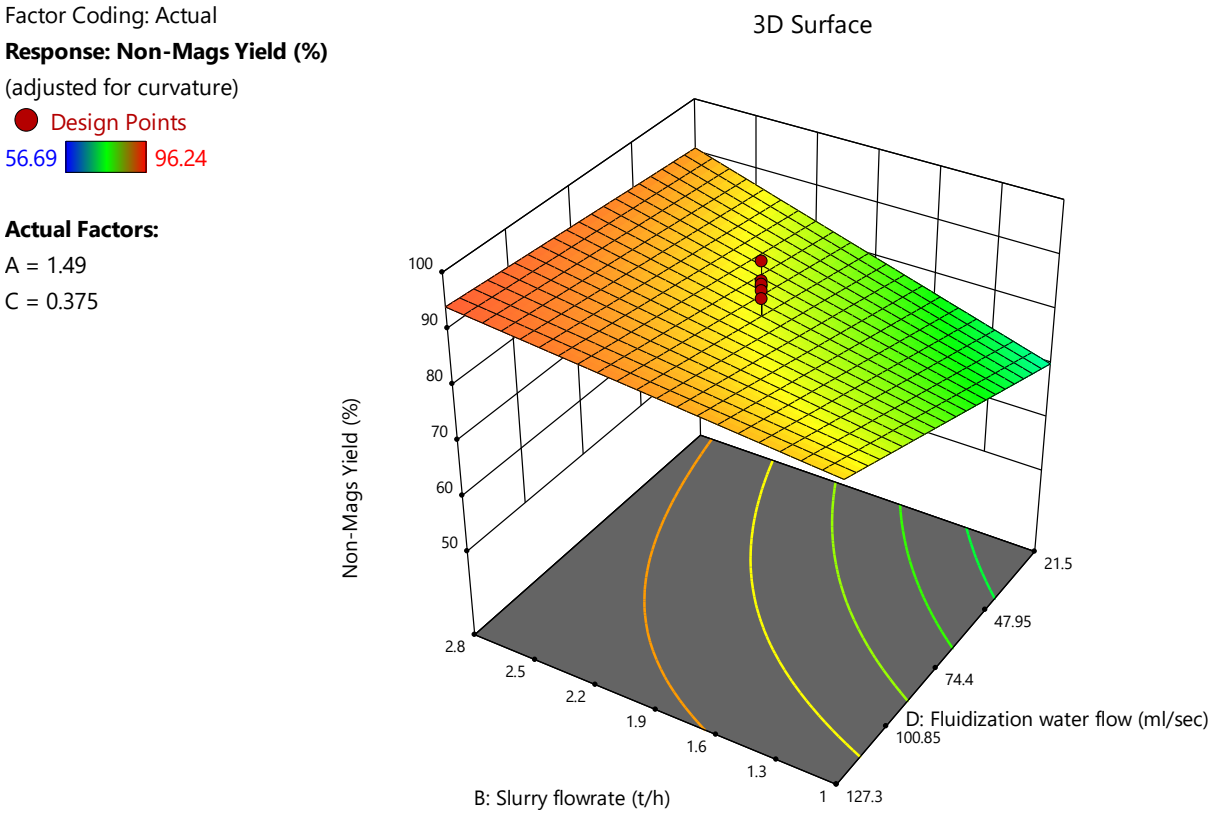

Figure 5.41: Surface plot of Non-magnetic Yield as functions of Slurry feed rate and Fluidization water flow

5.4.4.10 Response Surface Plot for Non-Magnetic Yield as a function of Belt speed and Fluidization water flow

The response surface plot for the effect of the belt speed and fluidization water flow on non-magnetic fraction yield is given in Figure 5.42. In this plot, the fluidization water flow has a more significant impact on non-magnetic fraction yield than belt speed. The p-value for fluidization water flow and belt speed was 0.0002 and 0.002, respectively. To minimise non-magnetic fraction yield, fluidization water must be run at minimum as per design limits and belt speed operated at maximum speed.

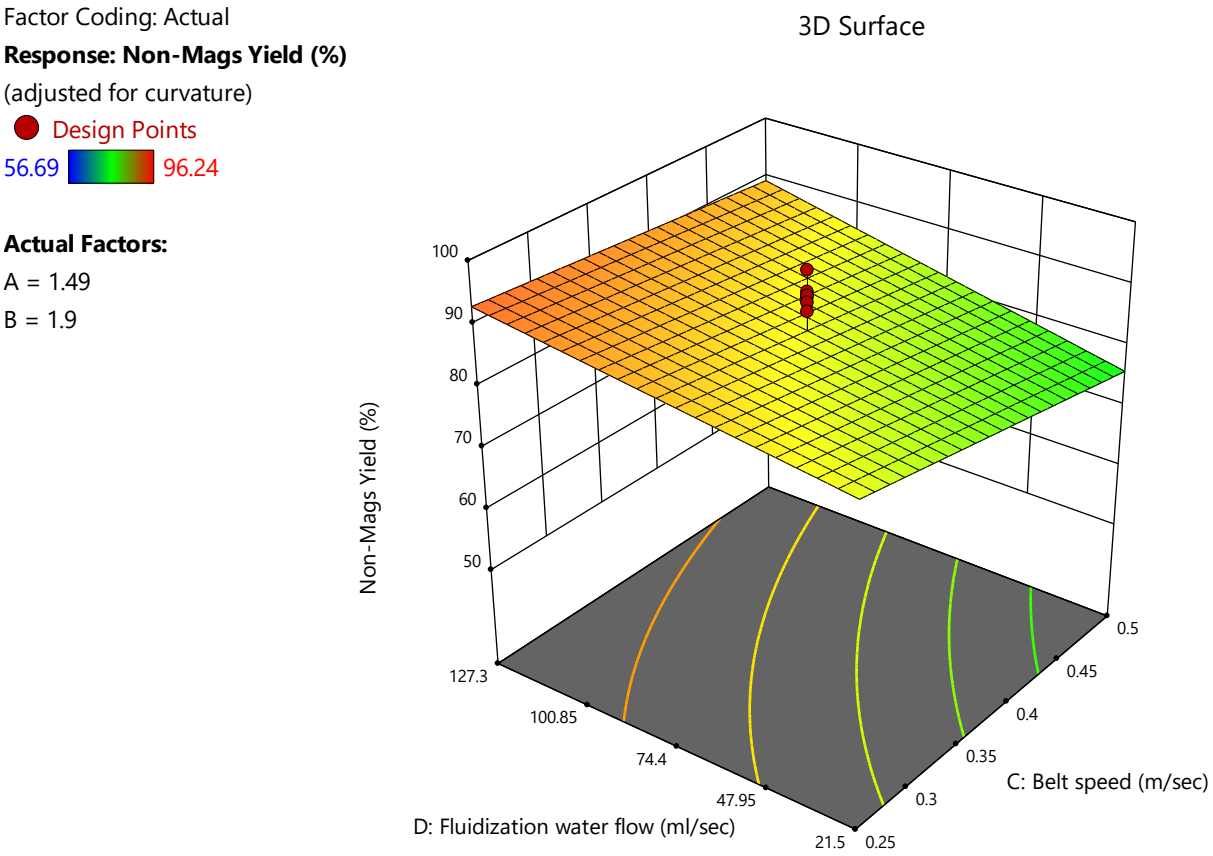

Figure 5.42: Surface plot of Non-Magnetic Yield as functions of Belt speed and Fluidization water flow.

5.4.5 Shaking Table performance tests

Shaking table performance tests were carried out using four independent variables at three levels. The variables tested were slurry density, feed rate, deck angle and wash water. The dependent responses assessed were the concentrate yield, recovery, grade and concentrate upgrade ratio as well as tailing recovery, yield, and grade.

5.4.5.1 Shaking Table Separation DOE Array and Main effect Plots

The following table (5.21) presents the DOE for the shaking table factors and their levels.

Table 5.21: Fractional factorial DOE matrix template for Shaking Table Separation Preliminary Tests

	Factor 1	Factor 2	Factor 3	Factor 4
Run	Slurry Density (t/m^3)	Slurry Flow rate(ml/min)	Wash Water Flow (ml/s)	Table Deck Angle (^{o})
1	1.28	700	180	6
2	1.28	300	180	6
3	1.28	700	100	6
4	1.28	300	100	6
5	1.28	700	180	2
6	1.28	300	180	2
7	1.28	700	100	2
8	1.28	300	100	2
9	1.34	500	140	4
10	1.34	500	140	4
11	1.34	500	140	4
12	1.34	500	140	4
13	1.34	500	140	4
14	1.34	500	140	4
15	1.40	700	180	6
16	1.40	300	180	6
17	1.40	700	100	6
18	1.40	300	100	6
19	1.40	700	180	2
20	1.40	300	180	2
21	1.40	700	100	2
22	1.40	300	100	2

Table 5.22: Fractional Factorial DOE matrix for Shaking table Separation Preliminary tests

	Factor 1	Factor 2	Factor 3	Factor 4		Response 1	Response 2	Response 3	Response 4	Response 5	Response 6	Response 7
Run	Slurry Density	Slurry Flow rate	Wash Water Flow	Table Deck Angle	Feed Cr_2O_3 Grade	Conc Cr_2O_3 Recovery	Conc Yield	Conc Cr_2O_3 Grade	Conc Upgrade Ratio	Tail Grade	Tail Yield	Tail Recovery
	t/m^3	ml/min	ml/sec	°		%	% Mass	% Cr2O3	times	% Cr2O3	Mass %	% Cr2O3
13	1.28	300	100	2	12.09	35.16	19.29	20.38	1.69	10.77	19.52	18.81
2	1.4	300	100	2	12.09	18.94	7.25	32.11	2.66	11.26	35.49	32.50
16	1.28	700	100	2	12.67	41.00	15.26	30.13	2.38	10.55	23.28	21.91
1	1.4	700	100	2	11.98	41.89	18.53	26.00	2.17	10.77	28.65	26.82
22	1.28	300	180	2	11.81	11.22	5.66	23.97	2.03	11.79	54.25	52.32
5	1.4	300	180	2	11.88	25.68	8.72	34.60	2.91	11.61	36.47	36.03
10	1.28	700	180	2	11.98	32.56	10.80	37.73	3.15	9.53	62.42	47.55
14	1.4	700	180	2	12.28	44.77	14.81	36.87	3.00	11.64	36.91	35.21
11	1.28	300	100	6	11.86	30.16	14.22	26.06	2.20	11.79	18.82	18.05
3	1.4	300	100	6	12.09	24.58	8.48	34.27	2.83	11.68	37.72	36.38
8	1.28	700	100	6	11.30	16.25	6.18	33.00	2.92	10.52	50.18	42.03
19	1.4	700	100	6	12.30	21.05	6.36	36.69	2.98	11.18	47.46	47.86
9	1.28	300	180	6	11.62	21.46	9.57	27.64	2.38	12.83	38.76	40.33
6	1.4	300	180	6	12.26	21.19	7.73	32.79	2.67	12.14	55.20	56.00
7	1.28	700	180	6	12.81	17.25	5.46	39.45	3.08	12.09	46.29	44.07
21	1.4	700	180	6	12.43	23.64	9.65	30.26	2.43	12.23	61.68	61.07
4	1.34	500	140	4	11.67	32.36	10.02	37.55	3.22	11.13	44.65	42.78
12	1.34	500	140	4	12.02	30.75	9.71	36.34	3.02	11.03	46.60	44.79
15	1.34	500	140	4	12.13	36.79	11.11	39.00	3.22	11.53	37.88	37.08
17	1.34	500	140	4	12.02	30.92	9.55	37.82	3.15	11.33	45.38	44.03
18	1.34	500	140	4	12.48	15.40	9.92	18.28	1.46	11.27	40.84	39.11
20	1.34	500	140	4	12.67	16.40	9.95	23.37	1.84	13.05	43.55	40.01

5.4.5.2 *Main Effect plots for Concentrate Grade*

Figure 5.43 shows the main effect plots of slurry density, feed rate, deck angle and wash water have on the concentrate grade. Between level 1, 2 and 3, feed rate has the most significant effect on concentrate grade followed by slurry density. Deck angle, slurry density and wash water have significant changes in the transition from level 1 to 2 compared to transition from 2 to 3. To maximise the concentrate grade, all factors must be set at level 3 according to Figure 5.43. The average concentrate grade at these levels is 33.04%.

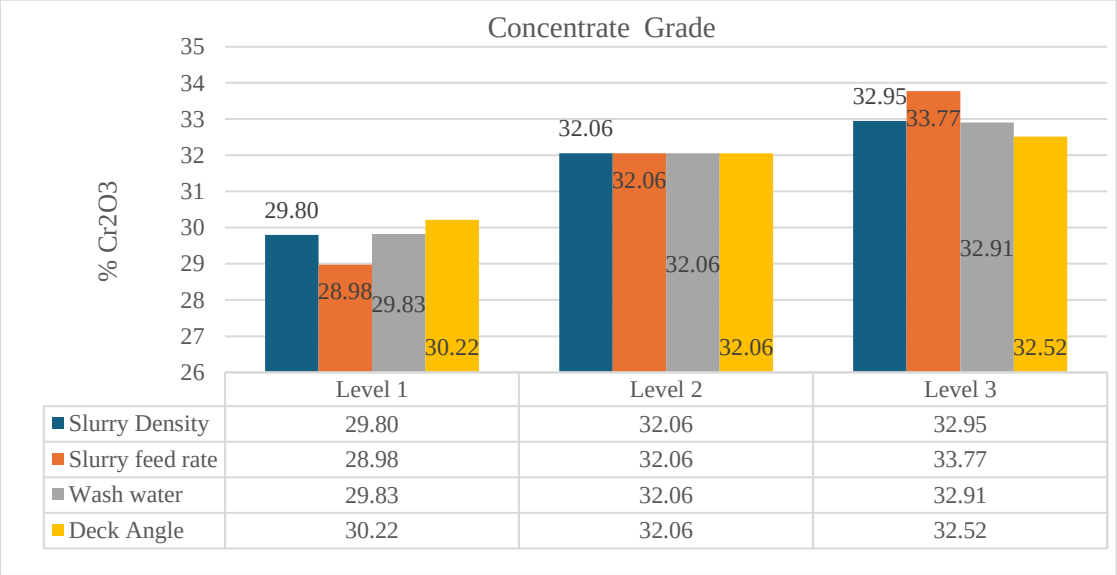

	Level 1	Level 2	Level 3
Slurry Density	29.80	32.06	32.95
Slurry feed rate	28.98	32.06	33.77
Wash water	29.83	32.06	32.91
Deck Angle	30.22	32.06	32.52

Figure 5.43: Main effect plot of concentrate grade at diverse levels of the separation factors.

5.4.5.3 *Main effect for Concentrate Yield*

The effect of shaking table separation factors on concentrate yield is shown in Figure 5.44. Deck angle has the most significant effect on the concentrate yield as demonstrated by the steep inverse gradient from level 1 to 3. As the deck angle increases, the yield decreases. The reason for the inverse relationship is that at shallow deck angle, more material remain trapped on the rifles on the shaking table deck and more mass will move toward the concentrate end, whilst at a steeper deck angle the heavier particles are washed away from the rifles causing concentrate loss to tails. Wash water also shows a decrease in yield as the level increases from 1 to 3. Increase in wash water inadvertently increases the chance to wash off trapped concentrate particles from the riffles. The change in volumetric flow rate of slurry does not

significantly change the yield of the concentrate. Slurry density does not affect the yield of the concentrate significantly even though the level 1 slurry density had the highest yield between the three levels. To maximise concentrate yield, deck angle, wash water and slurry density must be set at level 1 and slurry volume flow at level 3. These factor levels achieve a yield of 11.55%.

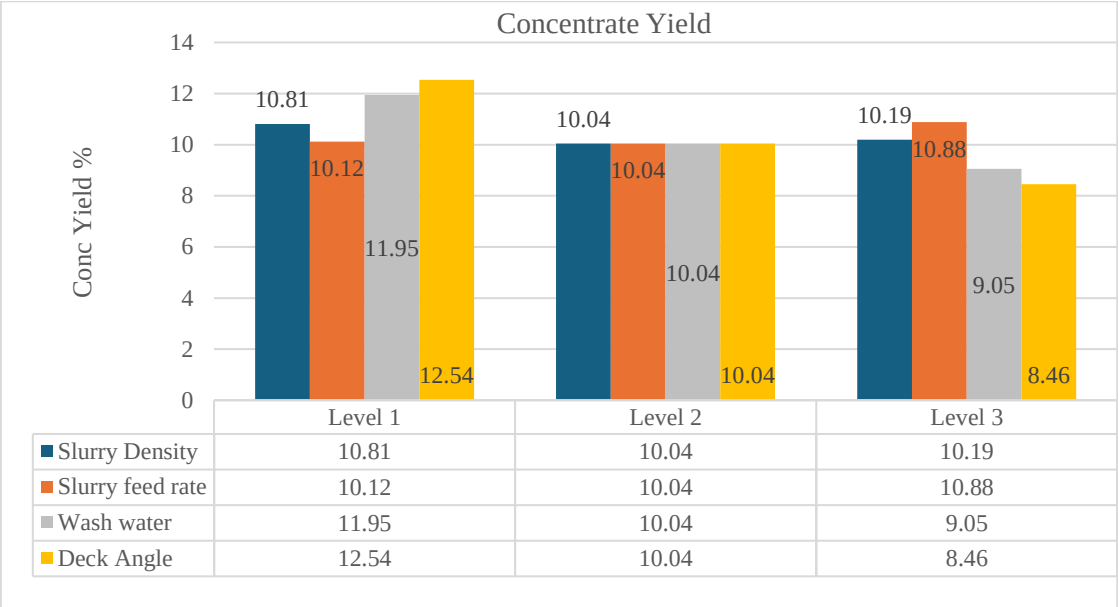

	Level 1	Level 2	Level 3
Slurry Density	10.81	10.04	10.19
Slurry feed rate	10.12	10.04	10.88
Wash water	11.95	10.04	9.05
Deck Angle	12.54	10.04	8.46

Figure 5.44: Main effect trends of Concentrate Yield at diverse levels

5.4.5.4 Main effect plots for Concentrate Recovery

The behaviour of concentrate recovery as independent variables change is shown in Figure 5.45. The trends follow that of the concentrate yield since recovery and yield have a direct correlation. To maximise recovery, the factors must be set at level 1 for wash water and deck angle then level 3 for slurry density and feed rate. The average concentrate recovery at these points is 29.39%.

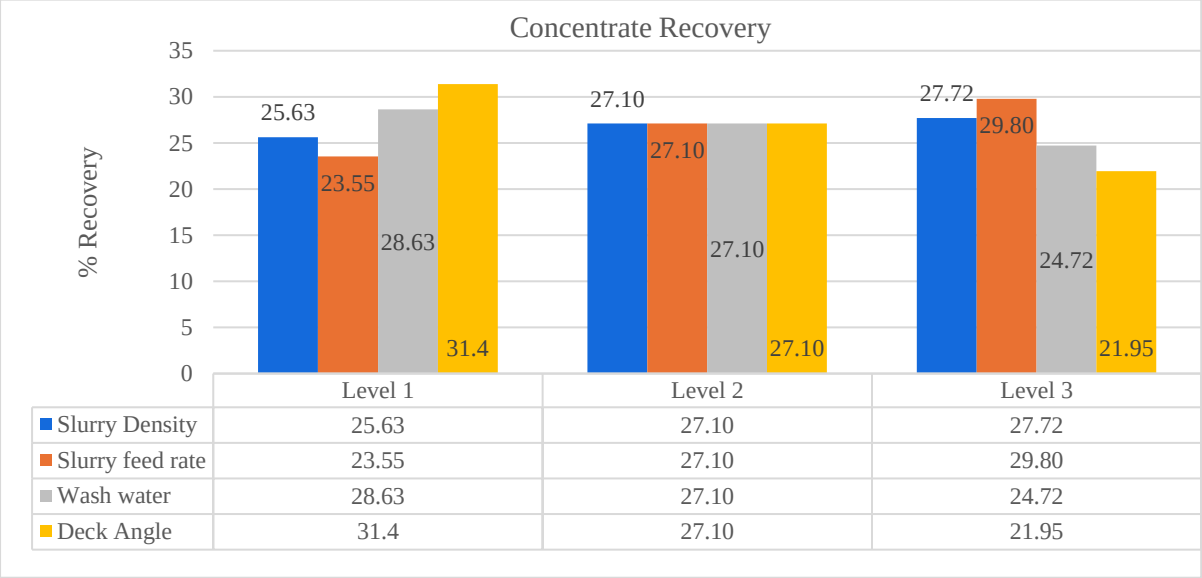

Figure 5.45: Main effect trends of Shaking table Concentrate Recovery

5.4.5.5 Main effect plot for Concentrate Upgrade ratio

The upgrade ratio behaves in a comparable way to concentrate grade. Figure 5.46 shows that feed rate has the most prominent effect on upgrade ratio followed by wash water in terms of impact on the upgrade ratio. Slurry density does not seem to have much influence on upgrade ratio compared to other three factors. Deck angle has the highest influence at the middle point. To maximise the upgrade ratio, the setting of the factors need to be at level 2 for slurry density and deck angle and level 3 for slurry volume flow rate and wash water.

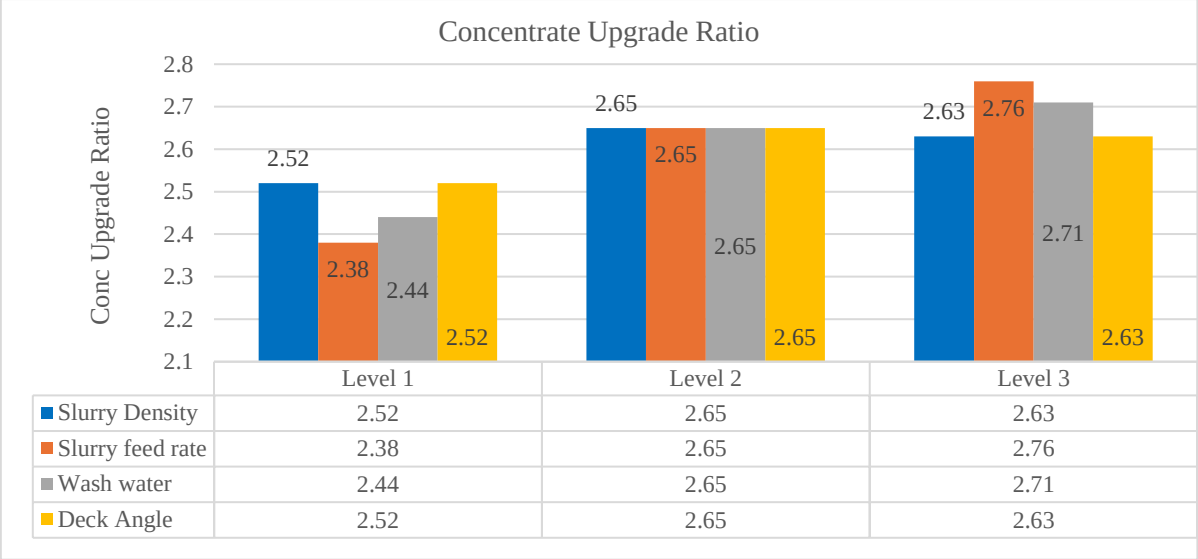

	Level 1	Level 2	Level 3
Slurry Density	2.52	2.65	2.63
Slurry feed rate	2.38	2.65	2.76
Wash water	2.44	2.65	2.71
Deck Angle	2.52	2.65	2.63

Figure 5.46: Main effect trends of Concentrate Upgrade ratio at distinct levels of the separation factors

5.4.5.6 Main effect plots for Tailings Grade

Figure 5.47 below shows the relationship between tailings grade and factors at different levels. Deck angle has the most significant effect on the tailings grade between level 1, 2 and 3. Wash water follows the same relationship on tailings grade as deck angle. Since the goal is to minimise the tail grade, the slurry density must be set at level 1, volumetric slurry flow rate level 3 and deck angle level 1 while wash water must be set at level 1. The average tailings grade at these respective levels is 11.09%.

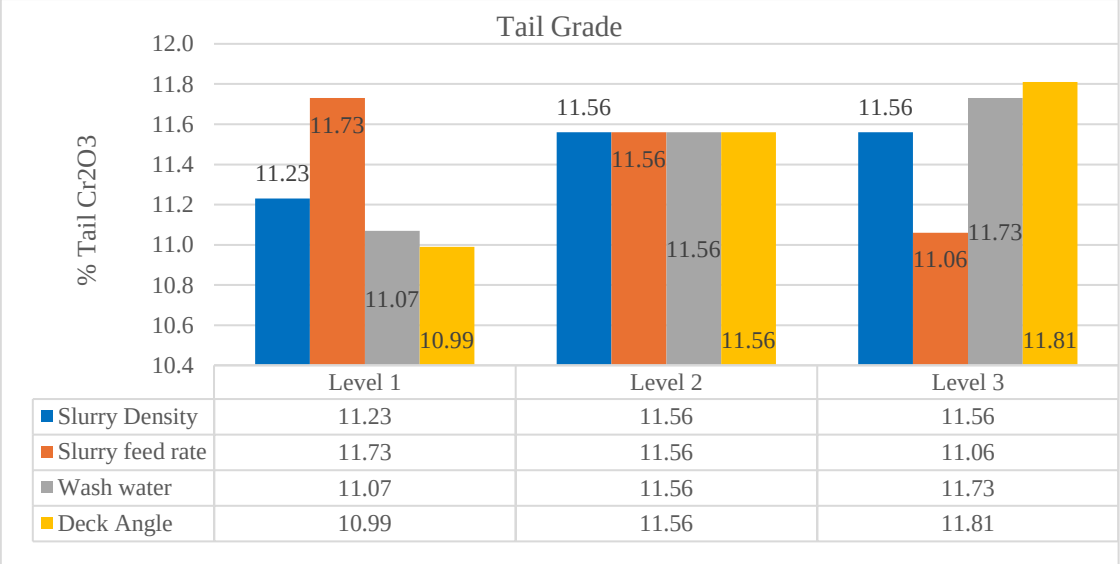

	Level 1	Level 2	Level 3
Slurry Density	11.23	11.56	11.56
Slurry feed rate	11.73	11.56	11.06
Wash water	11.07	11.56	11.73
Deck Angle	10.99	11.56	11.81

Figure 5.47: Main effect trends of Tailings grade at different levels of the separation factors

5.4.5.7 Effect of separation factors on shaking table Tail Recovery.

Figure 5.48 shows the relationship between tailings recovery and the operating factors between levels 1 and 3. Wash water is the most prominent factor of all four from level 1 up to 3. The deck angle follows wash water in terms of its effect on tailings recovery. All the four factors have a positive correlation with tailings recovery. To minimise tailings recovery, all factors must be set at level 1, and the average recovery will be 34.09%.

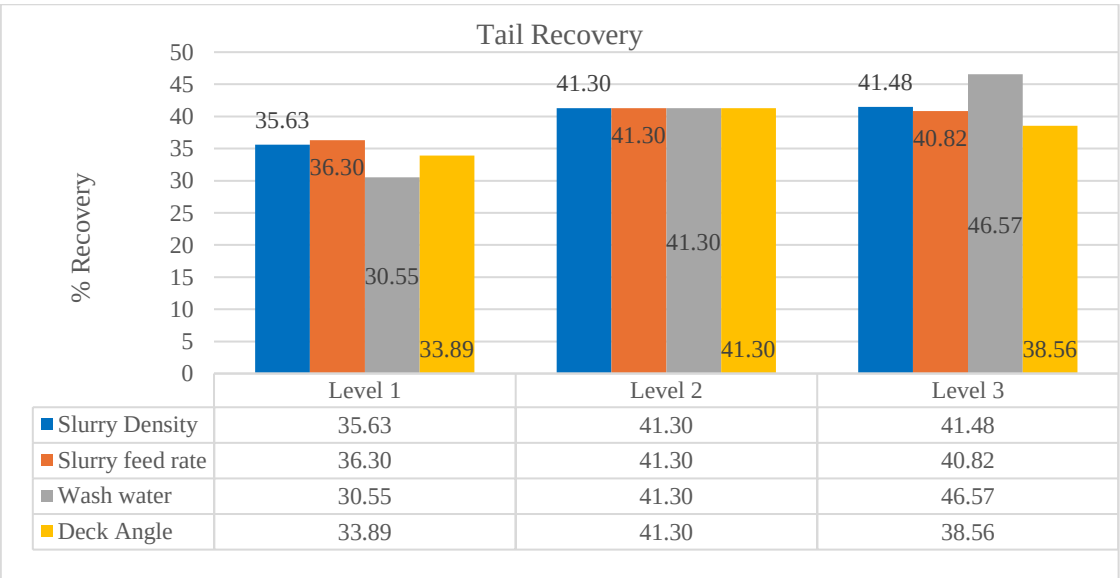

	Level 1	Level 2	Level 3
Slurry Density	35.63	41.30	41.48
Slurry feed rate	36.30	41.30	40.82
Wash water	30.55	41.30	46.57
Deck Angle	33.89	41.30	38.56

Figure 5.48: Main effect trends of tailings recovery at various levels of the separation

5.4.5.8 *Effect of separation factors on shaking table Tailings Yield*

Figure 5.49 shows the relationship between tailings yield and factor changes between levels 1, 2 and 3. This relationship is like that of tailings recovery. To minimise tailings yield, the settings for the separation factors must be at level 1 and the corresponding average tailings yield is 35.75%.

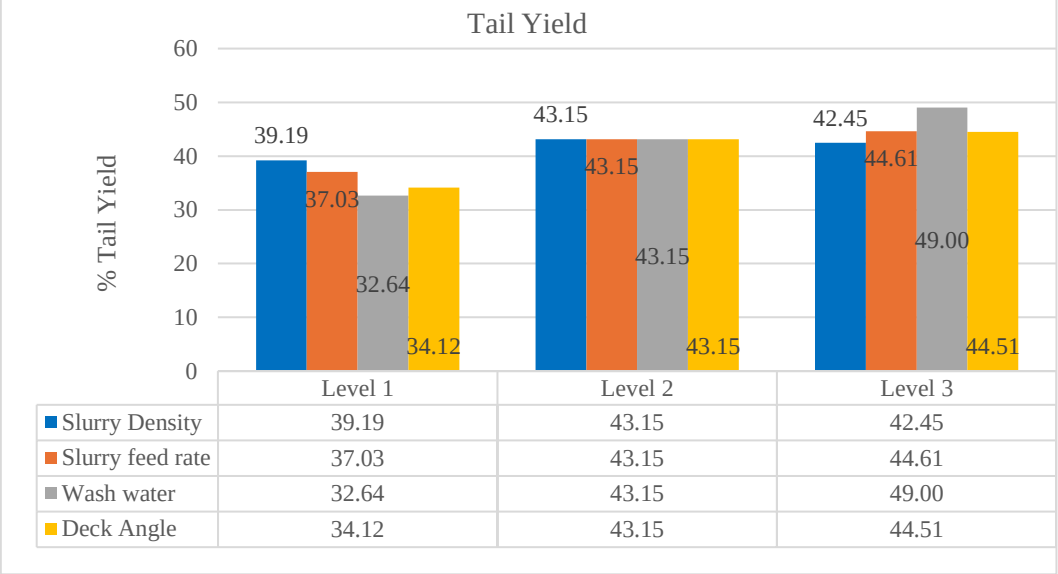

	Level 1	Level 2	Level 3
Slurry Density	39.19	43.15	42.45
Slurry feed rate	37.03	43.15	44.61
Wash water	32.64	43.15	49.00
Deck Angle	34.12	43.15	44.51

Figure 5.49: Main effect trends of tailings yield at different levels of the separation factors

5.4.5.9 *Factor Statistical Analysis for Shaking table separation tests*

The statistical analysis of the design of experiment results for the shaking table tests are presented in the following tables. The results in Table 5.23 show that the only factor with a significant relationship with concentrate recovery and yield parameters is the deck angle. Fluidisation water has significant correlation with shaking table tailings fraction yield and recovery. The other meaningful relationship is the interaction of volumetric flow and deck angle B x D on concentrate recovery. Wash water showed a significant relationship with tailings yield and recovery. The other response parameters like concentrate grade and upgrade ratio did not have a significant correlation with any of the factors within the range of levels tested.

Table 5.23: ANOVA analysis for the Shaking Table preliminary separation tests

	Intercept	A	B	C	D	AB	BD
Concentrate Recovery	26.25		1.01		-4.70		-1.72
p-values			0.1836		0.0258		0.0381
Concentrate Yield	10.37				-2.04		
p-values					0.0300		
Concentrate Grade	31.73	0.25	0.96	3.02	1.32		
p-values		0.9476	0.2030	0.2500	0.4141		
Concentrate Enrichment Ratio	2.71	-0.13	0.09	0.25		-0.14	
p-values		0.6632	0.1217	0.2351		0.2352	
Tail Grade	11.48	0.33		0.53	0.41		
p-values		0.3393		0.0626	0.0257		
Tail Yield	43.70			13.09			
p-values				0.0033			
Tail Recovery	41.51			12.82			
p-values				0.0016			

From Table 5.24, C.V % values are on the high side on Concentrate Recovery and Yield as well as Tail Yield and Recovery. This could have been due to an experimental setup where the highest concentrate grade of the shaking table was targeted by cutting rich on the table cutter. However, the most significant factor that was observed to consistently affect grade and recovery is Deck angle, and this is consistent with the two analysis methods. Al-Tangani *et al.* (2020) also found a significant effect of deck angel on recovery compared with wash water and feed rate. On grade and feed rate, they found that grade is more sensitive to feed rate compared wo wash water. This result was not consistent in this work as wash water and feed rate were not having significant impact on grade. Looking at the signal to noise ratio as indicated by Adeq Precision, only 2 out of 7 response parameters have their S/N ratios below 4% for Concentrate Yield and Upgrade ratio. This shows that the model is robust. One notable phenomenon on the shaking table process was that slurry density and feed rate did not have significant correlations with Concentrate response parameters. This is because for a process that depends on heavy washing to get the final grade, the initial slurry density and feed rate are made insignificant by the impact of Wash water and Deck angle.

The two equations; coded and actual, (Table 5.25 and 5.26) have shown some consistency across response parameters and they could be used as a general tool to focus on the fewer factors whose impact could then be optimized through an iterative process. The Coded equation recovery for -1 and +1 points are 31.66% and 20.8%, respectively. These numbers are

consistent with the main effect plots presented in the earlier section where it was shown that Deck angle has an inverse correlation with recovery.

Table 5.24: Fit Statistics for the Shaking table preliminary separation tests

	Concentrate Recovery	Concentrate Yield	Concentrate Grade	Concentrate Upgrade Ratio	Tail Grade	Tail Yield	Tail Recovery
Std. Dev.	7.72	3.50	6.26	0.49	0.67	9.81	8.80
Mean	26.79	10.37	31.56	2.60	11.44	41.45	39.31
C.V. %	28.83	33.69	19.85	19.20	5.88	23.67	22.39
R^2	0.43	0.21	0.20	0.21	0.38	0.36	0.39
Adjusted R^2	0.34	0.18	0.01	0.03	0.27	0.33	0.37
Predicted R^2	0.10	0.014	-0.17	-0.06	0.07	0.20	0.25
Adeq Precision	7.27	3.88	4.27	3.34	6.33	5.53	6.04

Table 5.25: Coded Equation

	Concentrate Recovery	Concentrate Yield	Concentrate Grade	Concentrate Enrichment Ratio	Tail Grade	Tail Yield	Tail Recovery
Intercept	26.25	10.37	31.73	2.71	11.48	43.70	41.51
A			0.25	-0.13	0.33		
B	1.01		0.96	0.09			
C			3.03	0.25	0.53	13.09	12.82
D	-4.70	-2.04	1.32		0.41		
AB				-0.14			
BD	-1.72						

Table 5.26: Actual Equation

	Concentrate Cr_2O_3 Recovery	Concentrate Mass Yield	Concentrate Cr_2O_3 Grade	Concentrate upgrade Ratio	Tail Cr_2O_3 Grade	Tail Yield	Tail Cr_2O_3 Recovery
Intercept	8.95	14.46	13.37	-6.27	5.78	12.83	11.26
Slurry Density			2.12	5.91	2.75		
Slurry Feed rate	2226.14		482.27	823.02			
Wash Water Flow			0.05	0.004	0.008	0.20	0.20
Table Deck Angle	2.81	-1.02	0.66		0.20		
Slurry Density X Slurry Feed rate				-585.99			
Slurry Feed rate X Table Deck Angle	-429.90						

5.4.5.10 Response Surface Plot for Shaking Table Concentrate Cr_2O_3 Recovery as a function of Slurry feed rate and Deck Angle

The investigation of factors affecting shaking table concentrate Cr_2O_3 recovery involved four factors. These factors were slurry density (A), slurry feed rate (B), wash water flow rate (C) and deck angle (D). The response surface shown in Figure 5.50 shows the variation of chrome recovery into the concentrate as a function of slurry feed rate and deck angle. To maximise recovery, the model shows that deck angle must be lowered to 2°, and slurry feed rate increased to 0.014t/hr. Deck angle is more significant than Slurry feed rate. The p-values for deck angle (D) and interaction factor BxD are 0.0258 and 0.0381, respectively.

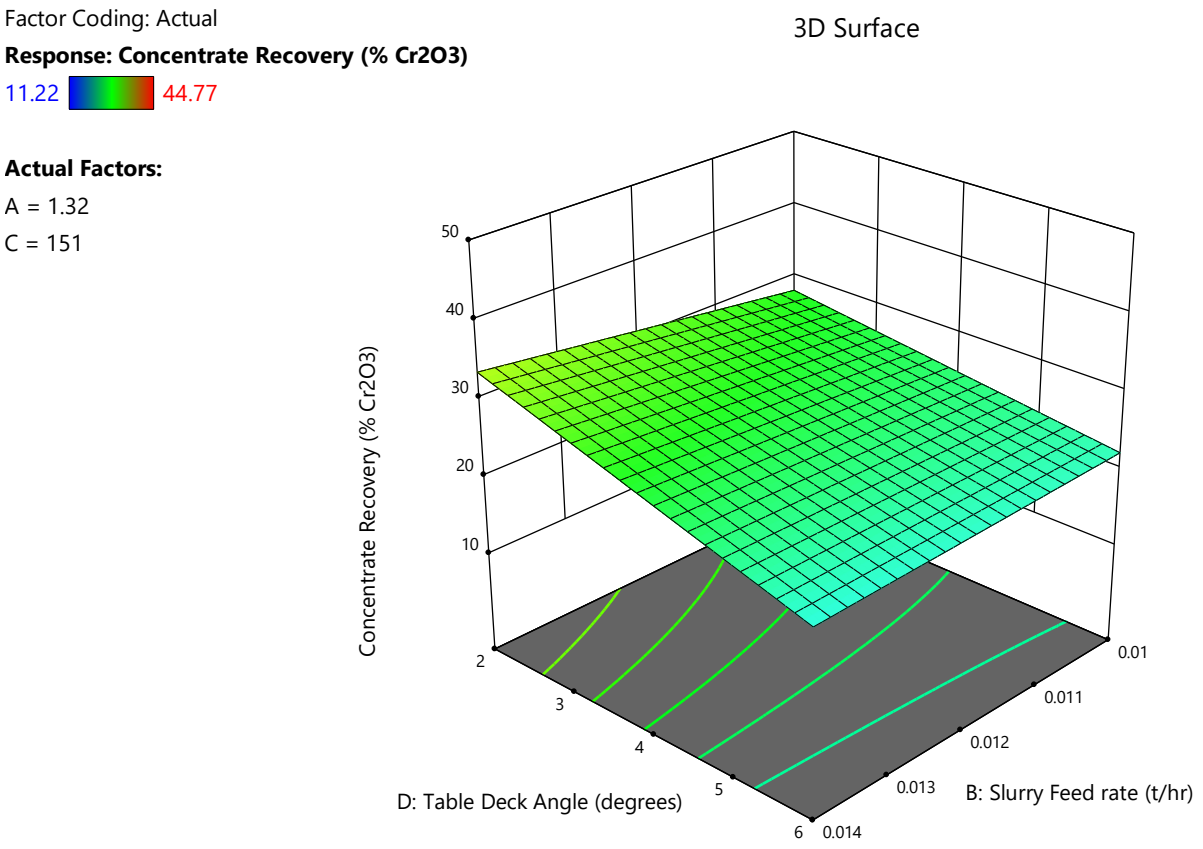

Figure 5.50: Surface plot of Shaking Table Concentrate Cr2O3 Recovery as functions of Deck Angle and Slurry feed rate

The deck angle of 2° means that the deck is almost flat, and this has an effect of moving most of the concentrate towards the discharge end of the shacking table. This way the material has

more residence time on the deck. This promotes Cr_2O_3 recovery into the concentrate. Slurry feed rate has a positive correlation with recovery at low angle more than at steep angles.

5.4.5.11 Response Surface Plot for Shaking Table Concentrate Yield as a function of Slurry density and Deck Angle

The concentrate yield profile is almost similar in shape to recovery response plot. To maximise yield on the shaking table, the deck angle must be shallow (2°). The slurry density does not have any significant impact on yield as shown in Figure 5.51 below. This is because the wash water quantity administered onto the shaking table is large enough to make sure that even high- or low-density feed ends up well spread on the shaking table surface to form almost a monolayer. The deck angle p-value for the model was 0.03.

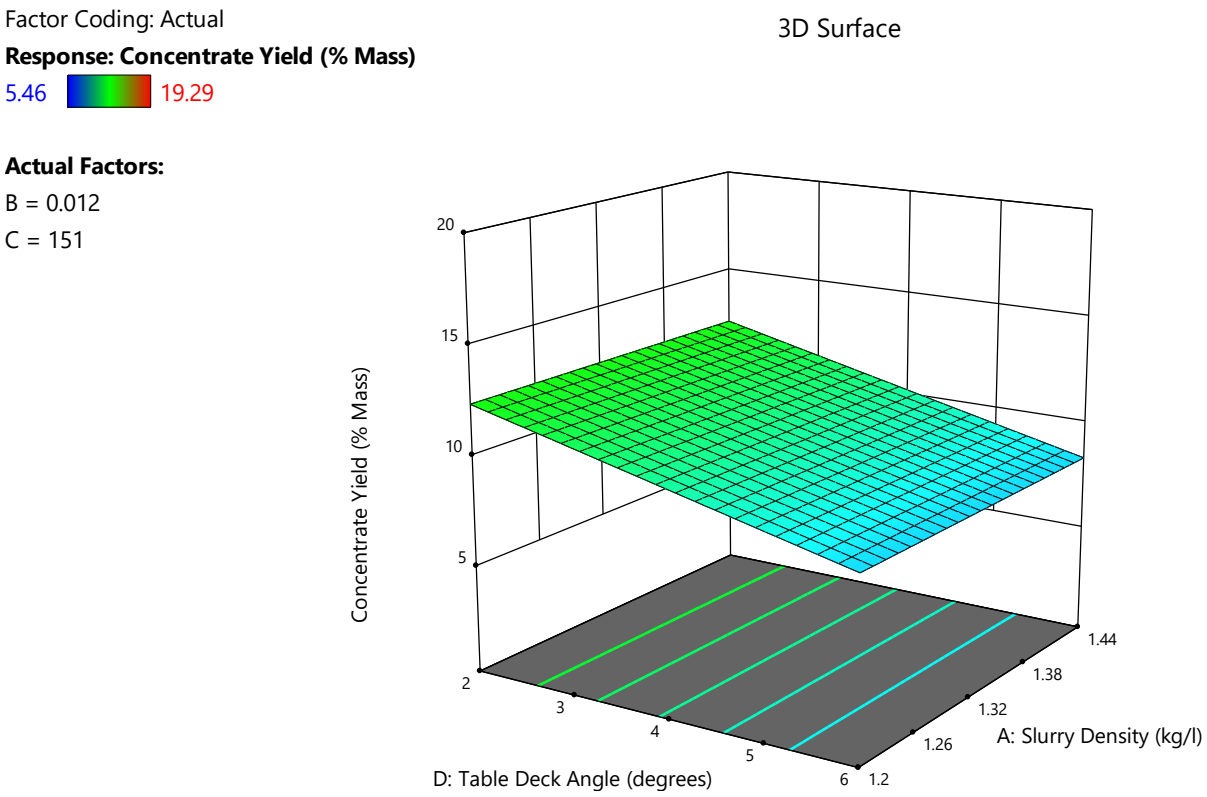

Figure 5.51: Surface plot of Shaking Table Concentrate Yield as functions of Slurry density and Deck angle

5.4.5.12 Response Surface Plot for Shaking Table Tailings Grade as a function of Slurry density and Deck Angle

The Response surface for Shaking table Tailings grade as a function of Deck Angle and Slurry density is shown in Figure 5.52 below. To minimise tailings grade on the shaking table requires that Deck angle and Slurry density be minimised. A shallower angle promotes more residence time for particles, and this will result in more cleaning of the feed before it exits the table as tailings. The p-value for Deck angle for this model was 0.0257 while that for slurry density was not significant at p-value of 0.3393.

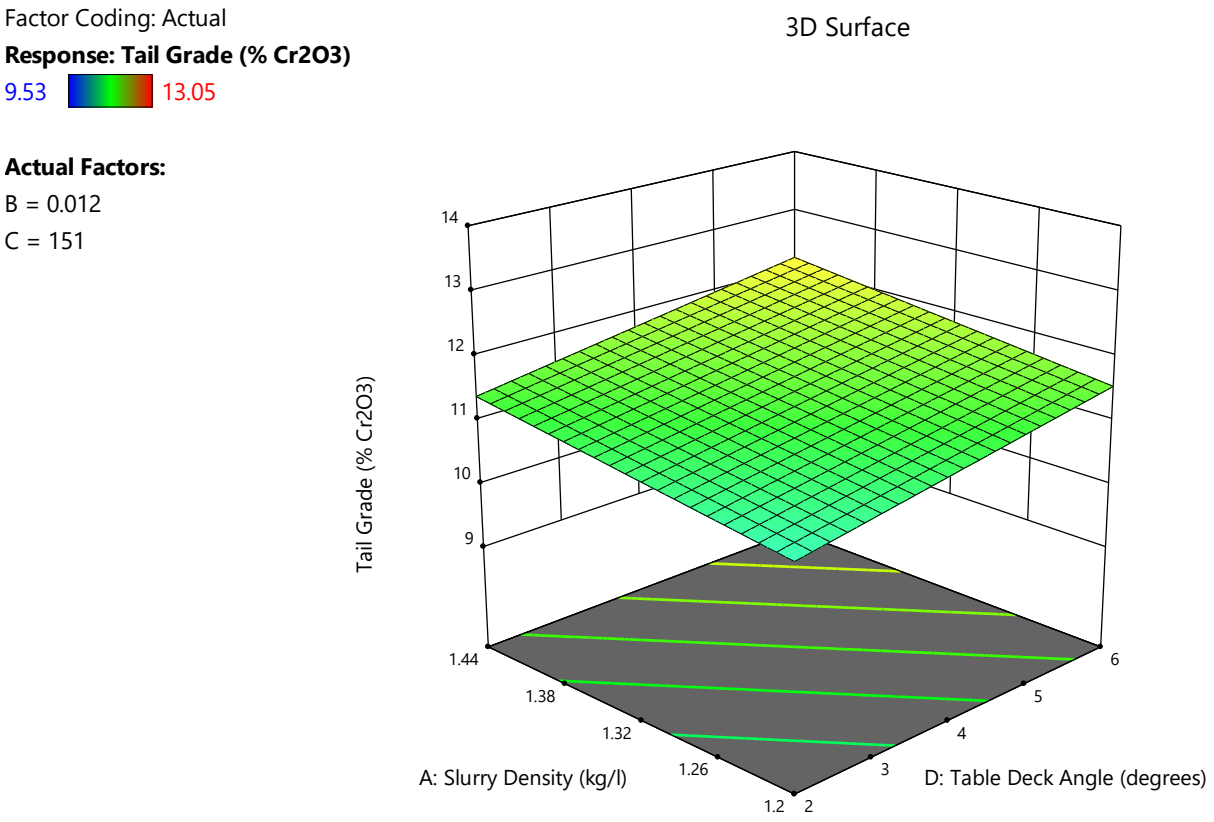

Figure 5.52: Surface plot of Shaking table Tailings Grade as functions of Slurry density and Deck angle

It must be noted that the surface response plot models for concentrate grade and enrichment factor were not significant because the grade was forced to reach a minimum value by changing the concentrate cutter position during the test-work. This reduced the number of variables to manage but the result was that there were no response surfaces for these response parameters.

5.4.6 Separation equipment performance summary

The evaluation of separation equipment takes into consideration the impact of input parameters on the response parameters as an average of the combined effect. The unit tests were performed mainly to determine the most critical input factors on response parameters for the 3 units of separation as well as determining the most appropriate application of each separation unit in a circuit used to recover ultrafine chrome. As such there must a ranking method to determine the distinct roles of spirals, magnets and shaking tables in a beneficiation circuit of the ultrafine chrome feed material under investigation.

To subject all the three-separator equipment to the same evaluation criteria, minimum acceptable recovery and enrichment ratio were set at 20% and 1.4, respectively. This means that the comparison of the performance of the three separators was based on a minimum recovery of 20% and a minimum enrichment ratio of 1.4. A unit that gave best results on the two criteria would be considered more suitable for the function than the others. The rationale of choosing recovery and enrichment ratio was that recovery covers yield and enrichment ratio covers grade. The choice of 1.4 is based on the Tharisa chrome operations practice where an upgrade of 1.4 is normally targeted as a minimum. The 20 % recovery was chosen based on internal technical feasibility evaluation for the chrome operation at Tharisa.

The sections below present summarised effect of input parameters and their levels on the response parameters. Most important in these results is the determination of what is the most important response parameter i.e. yield, recovery, grade, or Upgrade/Enrichment ratio used to evaluate the performance of a separation unit for a particular function.

The overarching goal of this research is to establish a separation system that can recover ore material that is predominantly made up of particles that are not currently recoverable via the conventional process of spiral concentration. The separation unit that shows better recovery than others become the first choice for a unit to perform the duty of recovery in the circuit. Once the unit has shown better recovery characteristics, the next performance key characteristic is enrichment ratio and concentrate grade. The ranking which was used to produce selection criteria of the response parameters was the following:

Rank # 1:	Concentrate Cr_2O_3 recovery.
Rank # 2:	Concentrate upgrade ratio.
Rank # 3:	Concentrate Cr_2O_3 grade.

After consideration of these three criteria then the performance of the unit in terms of rejecting mass at exceptionally low grades would be considered. This means that recovery of the chrome into the tailings fraction is considered after the first three have been maximised or optimized. The combination of factor levels that maximises the three response parameters becomes the priority combination and will be used as the starting point for confirmatory experimental runs or tests. The following sections evaluate the most critical factors and their combinations that were used to produce full circuit.

5.4.6.1 Spiral Separation - summary of results

Table 5.27 shows the best mean values of the investigated response parameters against the operational factors at the preferred levels as discussed in section 5.4.1 (Spirals Main effects plots). Table 5.27 is a summary result of the spirals heat map of recovery and enrichment ratio equal to or above 20% and 1.4, respectively.

Table 5.27: Fractional Factorial summary matrix for Spiral Response-Factor combinations

Spirals	Factor 1	Factor 2	Factor 3		Response 1	Response 2	Response 3	Response 4	Response 5	Response 6	Response 7	
Run	Slurry Density (Kg/L)	Slurry Feed Rate (t/hr)	Conc. Cutter Position (mm)	Feed Grade (% Cr_2O_3)	Conc Cr_2O_3 Recovery (%)	Conc Cr_2O_3 Grade (%)	Conc Mass Yield (%)	Upgrade Factor	Tailings Cr_2O_3 Grade	Tailings Cr_2O_3 Recovery	Tailings Mass Yield (%)	Efficiency (%)
22	1.42	0.88	45	12.67	23.41	23.37	14.66	1.84	13.05	45.62	51.19	10.0%
4	1.42	0.74	45	12.24	22.52	20.69	15.00	1.69	13.00	45.26	47.99	8.6%
1	1.62	0.60	45	11.62	23.97	18.84	17.80	1.62	12.97	24.69	26.63	7.0%
6	1.52	0.76	75.5	12.29	32.15	16.46	24.80	1.61	11.74	40.37	43.64	8.4%
9	1.52	0.79	75.5	12.22	31.48	18.77	23.71	1.54	12.77	41.15	45.58	8.9%
11	1.42	0.70	45	12.48	23.58	18.28	15.77	1.46	11.27	43.43	47.12	8.9%
10	1.62	0.60	45	12.65	23.06	18.05	17.46	1.43	12.59	25.42	27.59	6.4%
21	1.42	0.92	106	12.15	36.04	17.34	29.49	1.43	13.20	50.49	54.3	7.5%
				Mean	**27.03**	**18.98**	**19.84**	**1.58**	**12.57**	**39.55**	**43.01**	**8.20%**
				Min	**22.52**	**16.46**	**14.66**	**1.43**	**11.27**	**24.69**	**26.63**	**6.41%**
				Max	**36.04**	**23.37**	**29.49**	**1.84**	**13.20**	**50.49**	**54.30**	**10.02%**

The mean, minimum and maximum of these responses are shown in the three bottom rows of the table. These numbers represent the performance of the spirals within the selection criteria of 20% recovery and 1.4 enrichment ratio. To maximise recovery on the spirals requires

operating at a density of 1.42, feed rate of 0.92 t/h and a concentrate cutter position of 106mm. This combination is depicted by run 21 in Table 5.27. Run 4 in the Table 5.27 represents the minimum recovery combination. Figure 5.53 below shows the operating field of the spirals that was determined from the screening tests summarised for performance above 20% Recovery and 1.4 Enrichment ratio.

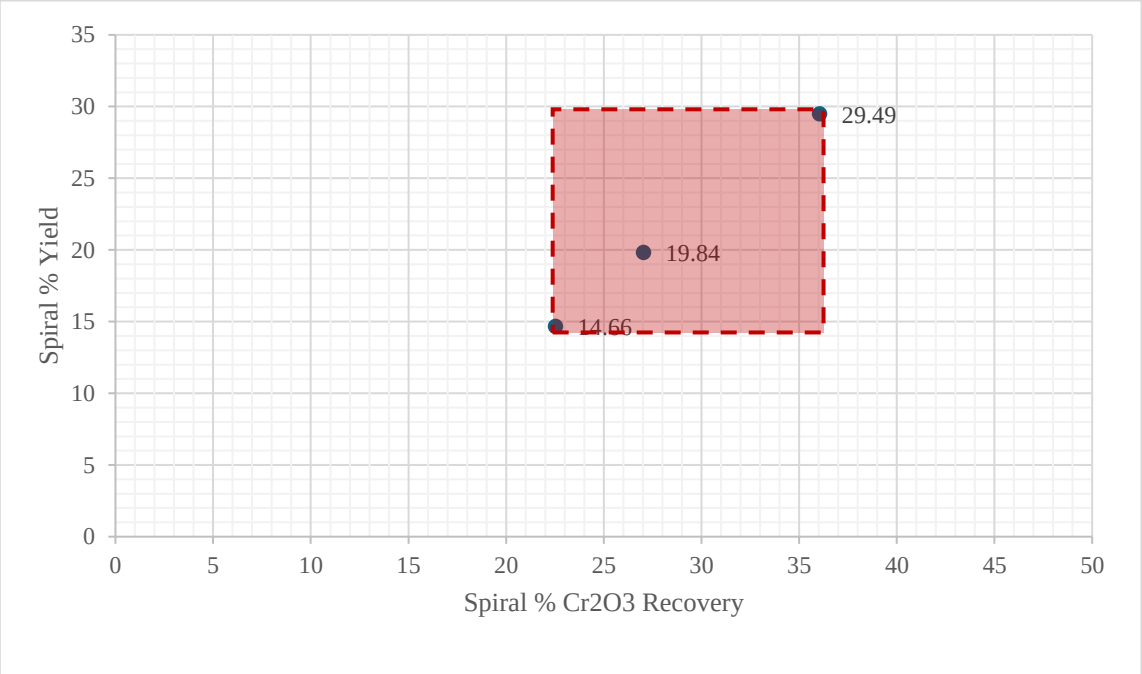

Figure 5.53: Spiral Recovery-Yield plot for operating field of ≥20% Recovery and ≥1.4 Enrichment ratio

The figure shows that the maximum recovery attained was 36.04% at a mass Yield of 29.49%. The minimum Yield at minimum recovery was 14.66%. Figure 5.54 shows the Recovery-Enrichment ratio relationship operation field for a spiral. It shows that at a minimum recovery of 22.52 % the minimum enrichment factor was 1.84 while at maximum recovery of 36% it was 1.43.

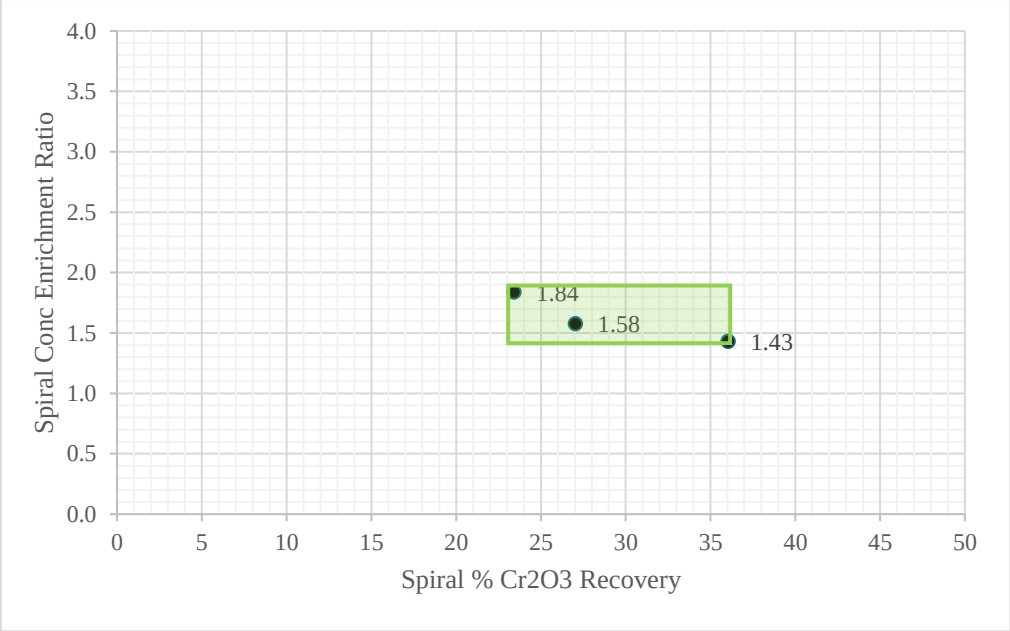

Figure 5.54: Spiral Recovery-Enrichment factor plot for operating field of ≥20% Recovery and ≥1.4 Enrichment ratio

The relationship between input factors and response parameters for the spiral concentration is given in Table 5.28 below. This table is a summary of the Taguchi based Main Effect plot method (discussed in section 5.4.1) to evaluate the factors which have the main effect on the response parameter. To maximise concentrate recovery, all three factors must be run at level 3 (highest) while enrichment ratio maximization requires setting all the input parameters at level 1. These two conditions conflict with each other and the best out of this conflict is to seek an optimum that is average of the levels. That means running at level 2 in at least two factors and see the results. Intermediate performance is found in level 2 where there is a balance of recovery, upgrade, and grade. That's means the spiral must operate at a slurry density of 1.52 t/m^3, feed rate of 0.78-0.83 t/h and concentrate cutter position of 75mm. Results from the ANOVA analysis also gave a predicted position as; slurry density 1.50t/m^3, dry feed rate 0.83 t/h and concentrate cutter position as 50.49 mm. It must be noted that enrichment ratio and concentrate grade have a positive correlation in these results hence for grade maximization the input factors must be set at level 1.

Table 5.28: Response and Input parameter Levels correlation for Spirals. (Main Effects)

Spiral Response Parameter	Best Response Mean Value	Corresponding Factor Level		
		Slurry Density Level	Feed Rate Level	Conc Cutter Position Level
SP Concentrate Recovery	33.98	3	3	3
SP Concentrate Yield	28.19	3	3	3
SP Concentrate Grade	18.87	1	1	1
SP Concentrate Enrichment ratio	1.54	1	1	1
SP Tailings Recovery	35.7	3	3	1
SP Tailings Yield	38.99	3	3	1
SP Tailings Grade	11.94	3	2	3

5.4.6.2 Magnet separation - summary of results

Table 5.29 shows the magnet separation performance for a modified heat map with minimum recovery of 20% and Enrichment ratio of 1.4. These minimum conditions have been similarly applied to the magnet as was applied to spiral separation for ease of comparison. From the table, the conditions for maximum recovery (30.46%) are supported by setting the magnet at highest slurry density (L3) and lowest Slurry feed rate, belt speed and fluidization water (L1) which is given by experimental run 5. The optimum conditions though are given by run 4 that maximises both recovery and enrichment ratio.

Table 5.29: Fractional Factorial summary matrix for Magnet Response-Factor combinations

	Factor 1	Factor 2	Factor 3	Factor 4		Response 1	Response 2	Response 3	Response 4	Response 5	Response 6	Response 7	
Run	Slurry Density (Kg/L)	Slurry Feed Rate (t/hr)	Belt speed (m/s)	Fluidization water flow (ml/sec)	Feed Cr_2O_3 Grade (%)	Mags Recovery (%)	Mags Yield %)	Non-Mags Yield (%)	Non-Mags Recovery (%)	Mags Cr_2O_3 Grade (%)	Upgrade ratio	Non-Mags Cr2O3 Grade (%)	Efficiency (%)
8	1.38	1.0	0.5	127.3	10.56	21.58	12.68	87.32	78.42	17.9	1.7	9.45	9.95%
4	1.38	1.0	0.25	21.5	10.99	30.25	20.26	79.74	69.75	16.91	1.54	9.91	11.22%
6	1.6	1.0	0.5	127.3	10.92	23.28	15.85	84.15	76.72	15.8	1.45	9.36	8.34%
5	1.6	1.0	0.25	21.5	10.72	30.46	20.89	79.11	69.54	15.24	1.42	9.19	10.72%
					Mean	26.39	17.42	82.58	73.61	16.46	1.53	9.48	10.06%
					Min	21.58	12.68	79.11	69.54	15.24	1.42	9.19	8.34%
					Max	30.46	20.89	87.32	78.42	17.90	1.70	9.91	11.22%

The mean, maximum and minimum of the recovery and yield for the chosen operating window are shown in Figure 5.55 below. For this window, the yield varies between 12.68% and 20.89% while recovery varies between 21.5% and 30.46%. as shown in Table 5.29. The operating window for the recovery and enrichment ratio is given in Figure 5.56. From this operating window, the enrichment ratio varies between 1.42 and 1.70.

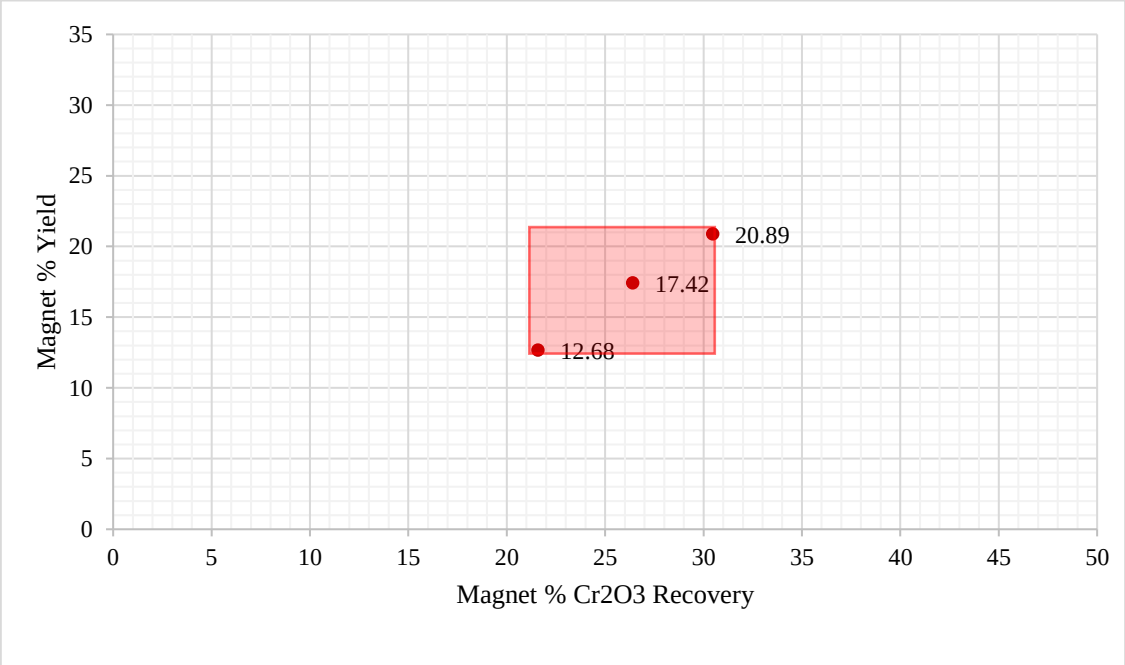

Figure 5.55: Magnet Recovery-Yield plot for operating field of ≥20% Recovery and ≥1.4 Enrichment ratio

Looking at the field of operation in terms of yield (Figure 5.55) at specified recoveries, the magnet has significantly lower yield compared to the spirals. This means that the magnet has a narrower operating window for mass yield purposes hence is poor at mass recovery. Considering Recovery vs Enrichment ratio of magnet at these limits (≥20% recovery and ≥1.4 enrichment ratio), the magnet has a narrow operating window compared to Spirals with enrichment ratio between 1.42 and 1.70 compared to 1.43 and 1.84 for spirals above. The results also show that magnets can achieve a much higher upgrade ratio that spirals.

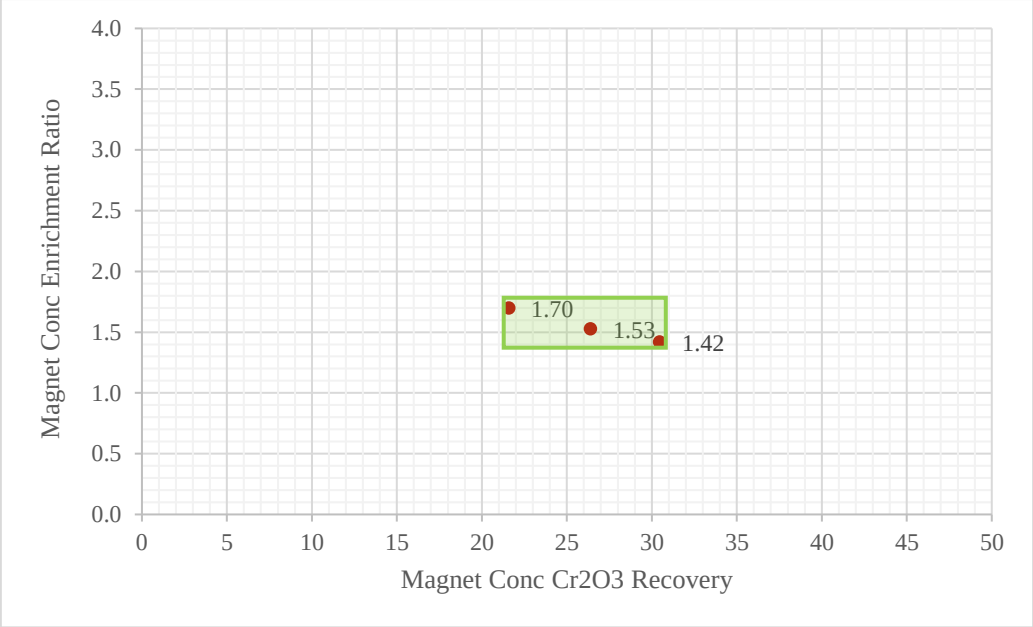

Figure 5.56: Magnet Recovery-Enrichment ratio plot for operating field of ≥20% Recovery and ≥1.4 Enrichment ratio

Table 5.30, derived from the main effect plots analysis show that the recovery is maximised by tests conducted at low fluidization water flowrate and low slurry flow rate whereas upgrade and grade are maximised by high fluidization water and low belt speed. The two tests which balance these two positions are experimental run 4 and 8 from Table 5.30. The compromise settings chosen for the magnet run was slurry density 1.38t/m3, slurry feed rate 0.81t/h, belt speed 0.5m/s and 74.4 ml/s fluidization water. From the ANOVA analysis presented earlier the predicted settings for the four factors are slurry density-1.49t/m^3, slurry flowrate-1.90 t/h, belt speed -0.375 m/sec and wash water 74.4 ml/sec.

Table 5.30: Response and Input parameter levels correlation for Magnet separation

Magnet Response Parameter	Mean Value	Corresponding Factor Level			
		Slurry Density Level	Feed Rate Level	Belt Speed Level	Fluidization water Level
Magnetic Conc Recovery	**24.54**	**3**	**1**	**3**	**1**
Magnetic Conc Yield	18.05	3	1	3	1
Magnetic Conc Grade	16.69	1	3	1	3
Magnetic Conc Enrichment ratio.	**1.54**	**1**	**1**	**1**	**1**
Non-Mags Recovery	84.84	1	3	1	3
Non-mags Yield	90.02	1	3	1	3
Non-mags Grade	9.58	1	1	3	1

5.4.6.3 Shaking Table Separation - summary of results

The shaking table summary test results (at ≥20% recovery and ≥1.4 enrichment ratio) for the performance test-work are shown in Table 5.31. The difference between the shaking table performance and that of spirals and magnet is that besides higher levels of recovery obtained, the upgrade ratio and grade of the concentrate is almost double that of the two units. The shaking table has shown exceptional performance in terms of upgrading exceptionally low feed grades to target grades but still having high mass yield to the concentrate. The purpose of shaking table is to provide grade sharpening. In view of this, the shaking table's performance was reviewed on the basis that it is a grade/upgrade unit rather than a recovery unit. Table 5.31 shows the modified heat map for the separator performance test results in which the minimum recovery and enrichment ratio have been set at 20% and 1.4, respectively. In terms of recovery and yield, the minimum values are 21.05% and 6.36%, respectively. The maximum values are 44.77% and 19.29%, respectively. The maximum and minimum enrichment ratios are 2.03 and 3.22, respectively. To indicate the operating window performance in comparison to the spirals and magnet performance, Figures 5.57 and 5.58 show much wider window than the spirals and magnets.

The only downside to this performance of the shaking table is the capacity or throughput. Per ton of throughput the shaking table is a more expensive unit than both the magnet and spirals. For this reason, the positioning of the shaking table would be best for small streams which are at higher grades to capitalise on its enriching capabilities.

Table 5.31: Fractional Factorial summary matrix for Shaking table Response-Factor combinations

	Slurry Density (Kg/L)	Slurry Feed Rate (t/h)	Wash Water Flow (ml/sec)	Table Deck Angle (°)	Feed Cr_2O_3 Grade (%)	Conc Cr_2O_3 Recovery (%)	Conc Mass Yield (%)	Conc Cr_2O_3 Grade (%)	Conc. Enrichment Ratio	Tailings Cr_2O_3 Grade (%)	Tailings Mass Yield %)	Tailings Cr_2O_3 Recovery (%)	Efficiency (%)
13	1.34	500	140	4	11.67	32.36	10.02	37.55	3.22	11.13	44.65	42.78	25.3%
2	1.34	500	140	4	12.13	36.79	11.11	39.00	3.22	11.53	37.88	37.08	29.2%
16	1.28	700	180	2	11.98	32.56	10.80	37.73	3.15	9.53	62.42	47.55	24.7%
1	1.34	500	140	4	12.02	30.92	9.55	37.82	3.15	11.33	45.38	44.03	24.3%
5	1.34	500	140	4	12.02	30.75	9.71	36.34	3.02	11.03	46.60	44.79	23.9%
10	1.4	700	180	2	12.28	44.77	14.81	36.87	3.00	11.64	36.91	35.21	34.2%
14	1.4	700	100	6	12.3	21.05	6.36	36.69	2.98	11.18	47.46	47.86	16.8%
3	1.4	300	180	2	11.88	25.68	8.72	34.60	2.91	11.61	36.47	36.03	19.2%
8	1.4	300	180	6	12.26	21.19	7.73	32.79	2.67	12.14	55.20	56.00	15.3%
9	1.4	700	180	6	12.43	23.64	9.65	30.26	2.43	12.23	61.68	61.07	16.0%
6	1.4	300	100	6	14.26	24.58	8.48	34.27	2.40	11.68	37.72	36.38	18.8%
7	1.28	700	100	2	12.67	41.00	15.26	30.13	2.38	10.55	23.28	21.91	29.5%
21	1.28	300	180	6	11.62	21.46	9.57	27.64	2.38	12.83	38.76	40.33	13.5%
4	1.28	300	100	6	11.86	30.16	14.22	26.06	2.20	11.79	18.82	18.05	18.1%
12	1.4	700	100	2	11.98	41.89	18.53	26.00	2.17	10.77	28.65	26.82	26.5%
15	1.28	300	100	2	10.04	35.16	19.29	20.38	2.03	10.77	19.52	18.81	17.6%
					Mean	30.87	11.49	32.76	2.71	11.36	40.09	38.42	22.06%
					Min	21.05	6.36	20.38	2.03	9.53	18.82	18.05	13.45%
					Max	44.77	19.29	39.00	3.22	12.83	62.42	61.07	34.15%

The trend of the recovery versus yield shown on Figure 5.57 shows a correlation between Yield and Recovery for the shaking table. This relationship is also true for the spiral and the magnet. This means that for a specific grade the recovery and yield have a direct relationship.

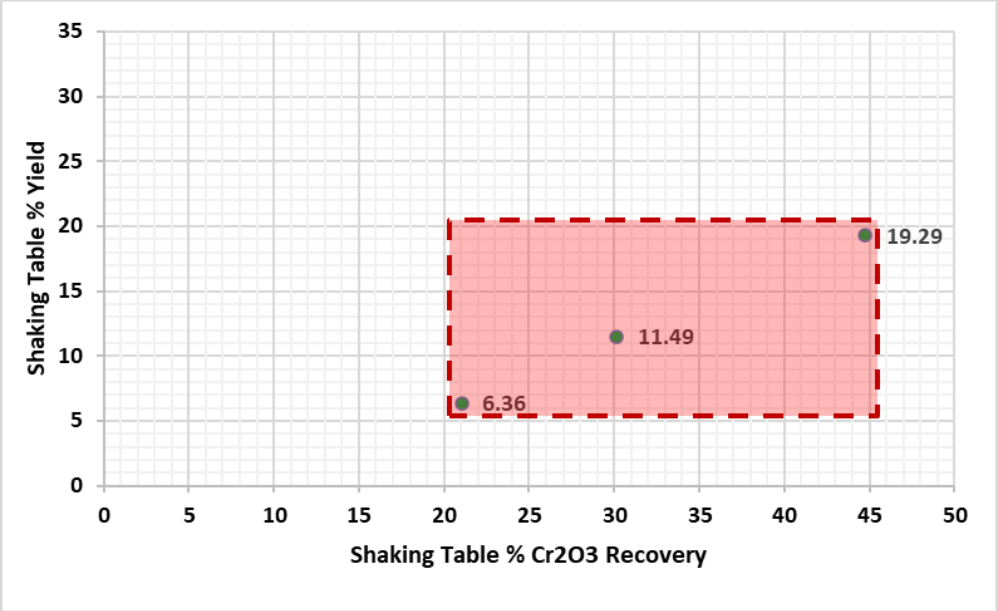

Figure 5.57: Shaking table Recovery-Yield plot for operating field of ≥20% Recovery and ≥1.4 Enrichment ratio

The enrichment ratio and recovery trend in Figure 5.57 shows an inverse relationship.

As the recovery increases, the enrichment ratio decreases, which is a similar trend for grade - recovery curve.

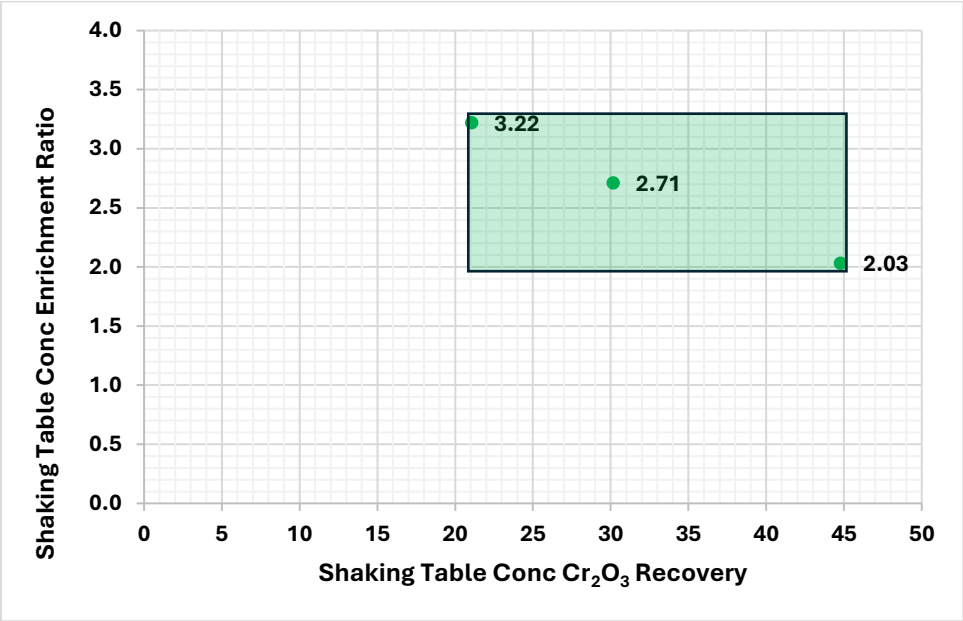

Figure 5.58: Shaking table Recovery-Yield plot for operating field of ≥20% Recovery and ≥1.4 Enrichment ratio

Table 5.32: Response and Input parameter Levels correlation for Shaking table

Shaking Table Response Parameter	Mean Value	Corresponding Factor Level			
		Slurry Density	Feed Rate	Wash water	Deck Angle
ST Concentrate Recovery	29.39	3	3	1	1
ST Concentrate Yield	11.55	1	3	1	1
ST Concentrate Grade	33.04	3	3	3	3
ST Concentrate Upgrade	2.69	2	3	3	2
ST Tailings Recovery	34.09	1	1	1	1
ST Tailings Yield	35.75	1	1	1	1
ST Tailings Grade	11.71	2	3	3	2

To maximise on the Concentrate upgrade and grade Table 5.31 has given the conditions as; slurry density 1.34, feed rate 700ml/min, wash water 180 ml/s and deck angle between level 2 and 3. i.e. between 4º and 6º. Table 5.32 shows a few possible combinations to give the high grade and upgrade while also maintaining high recoveries. These combinations are those for test runs 14, 15, 10, and 17. Given these conditions, the shaking table's settings were set at 1.34 density, 500 ml/min (0.01428t/h) slurry flow rate, 140ml/sec wash water and 4º deck angle.

The summary of results of Single Units separations performance tests shown in Figure (5.59) reveal the key capabilities of the three separation units selected in this study for the beneficiation of ultrafine chrome.

The key imperative in minerals beneficiation is to maximise the recovery of mineral values and prepare them in form of a concentrate that attains a target grade or a grade that meets the minimum requirements of the next process whilst minimizing the loss of the mineral value to the final discarded tails. Figure (5.59) shows that the shaking table achieved the highest Concentrate grade and upgrade ratio in comparison to the spiral and magnet concentrates, making the shaking table a suitable candidate for effective upgrade and grade control than spirals and magnets. It can also be observed that the shaking table has the least recovery of chrome to the tailings while the magnet has the highest recovery to the tailings. This further favours the shaking table as the most suited separator to be placed as the final unit in a circuit as it minimizes loss of the chrome minerals to the final tails. The results show that the most suitable separator for roughing is the spiral as it has the highest concentrate recovery and yield compared to the magnets and the shaking table. The magnets perform poorly in terms of both concentrate yield and grade in comparison to the spirals and shaking table though its concentrate grade is comparable to that of the spiral. The main attraction of the magnet is the

low tails grade. Considering that in the setup of the current study the magnet has only two products i.e. the magnetic and non-magnetic fractions, it can be effectively deployed as a scavenger for the richer tails from the other two units.

Therefore, the proposed multi-unit circuit should include the spiral as the first (rougher) unit of the circuit and the magnet be used to scavenge from the middling and/or tailings of the spirals. The intermediate concentrates produced from the spirals and magnet would then be fed to the shaking table for grade sharpening and production of final product.

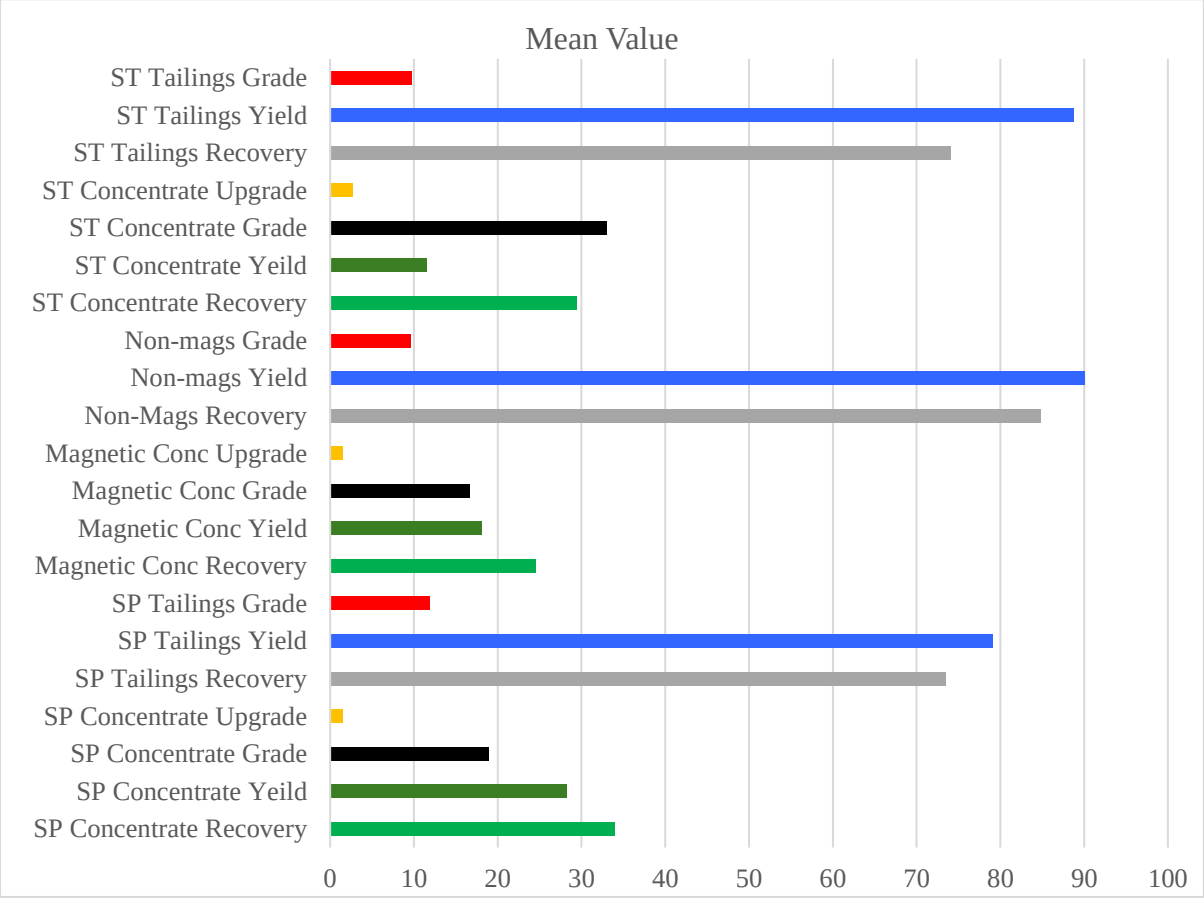

Figure 5.59: Graphical representation of the comparison of three separation unit performances

5.4.6.4 Summary of the Equipment Separation results

The critical analysis of the three units' performance has led to the proposal of where and how each of the three pieces of the separation units would be utilised in a full circuit. The spiral was chosen as the first unit of the circuit, and the reason is its flexibility in terms of changing the mass yield and recovery by simply changing the cutters' positions. The other reason is that from a commercial perspective, the spiral has higher throughput per unit compared to the magnet and shaking table. The magnet was chosen to play a scavenger role by recovering

chrome from either middlings and or tailings. The attraction of the magnet is that it can recover particles which the spiral may not be able to recover easily due to the particles being outside of the gravity separation envelop and that it also produces the lowest tails grade. The shaking table was chosen as the last unit to upgrade the intermediate concentrates to the final product grade due to its capability to achieve the highest grades and upgrade ratios.

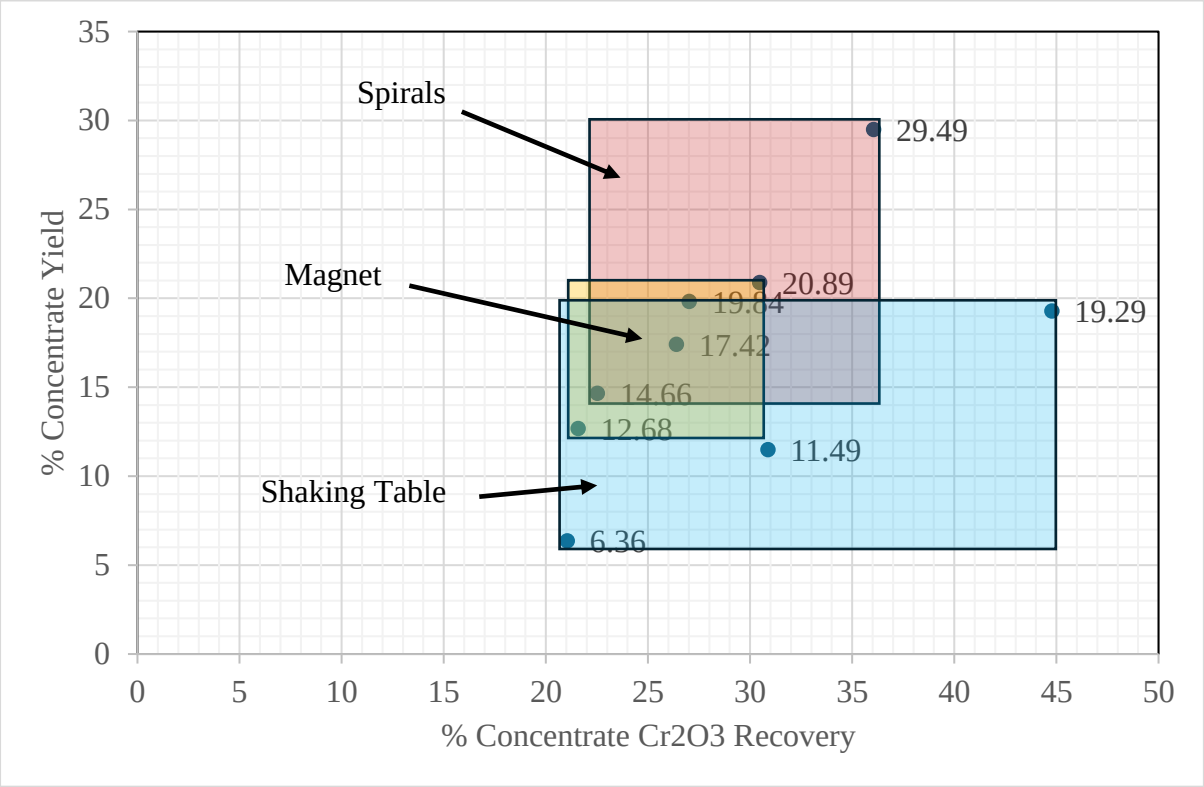

Figure 5.60: Spiral, magnet and shaking table Mass Yield – Cr2O3 Recovery operating fields for determination of unit position in the circuit

The next chapter discusses the results of the full circuit test-work which were performed using the units connected to make a complete circuit.

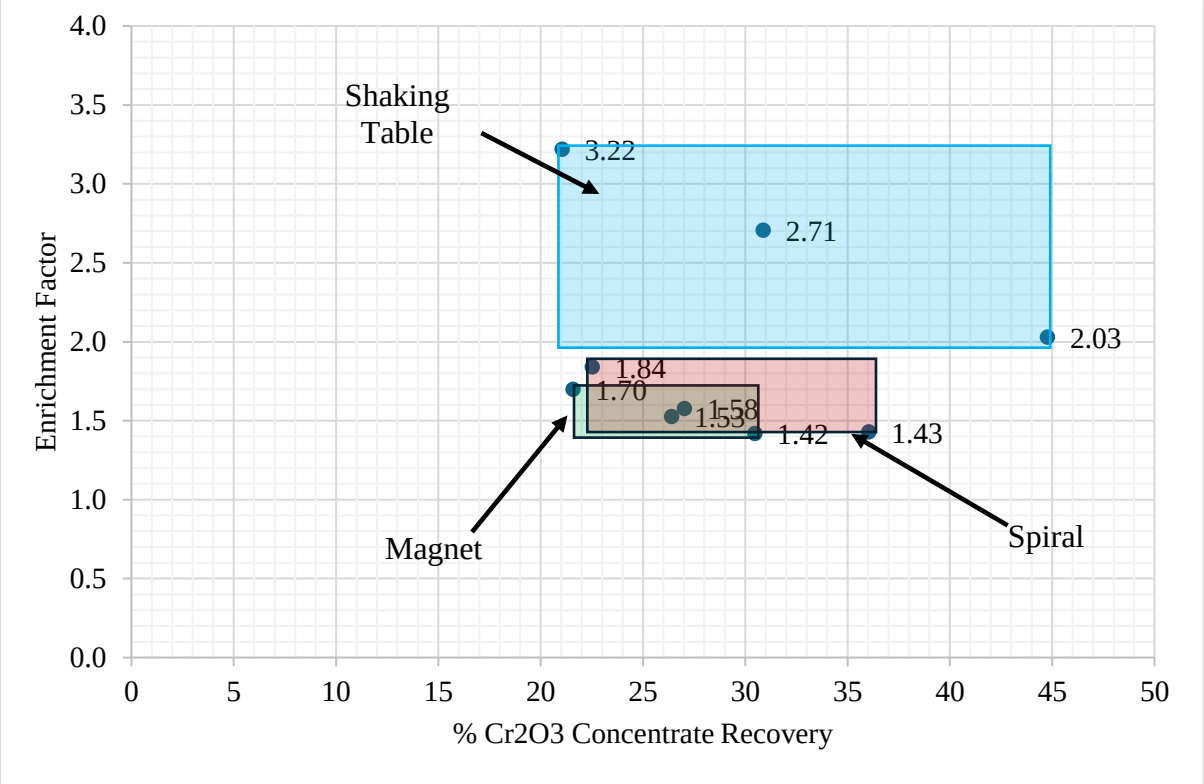

Figure 5.61: Spiral, magnet and shaking table Enrichment – Cr2O3 Recovery operating fields for determination of unit position in the circuit

.

CHAPTER 6: CIRCUIT DEVELOPMENT HEURISTICS

The development of a full separation circuit for the recovery of ultrafine chrome was advised by the results of single unit separation tests presented in chapter 5. Results from single unit separation tests revealed performance of each unit in terms of yield of the value streams, recovery of the chrome to the value streams, grade of the value stream and the upgrade of the chrome assay from feed to the value product stream. The positioning of each of the separation units in the circuit was based on the most suitable function in the circuit to produce a target product grade of about 40% ±1.5% Cr_2O_3.

6.1 Separation Units Combination

The units that were utilized for the development of the full circuit were the same units that were used during the single unit separation performance tests in the previous chapter. These included the triple start-five turn M1T53 shallow angle spiral, mainly deployed for ultrafine material. This spiral was designed and supplied by Met-Q, a mineral processing equipment manufacturer. The magnetic separation equipment used is a pilot scale Wet High Intensity Magnetic Separator (WHIMS) belt magnet designed and manufactured by Malvern Engineering. The screen used for the classification of test streams is a Rhologan screen supplied by Rhologan Engineering and it was used at two particle size panels -25µm and 106µm panels. A laboratory scale Holman-Wilfley shaking table was used for the shaking table tests the specifications of all these units were given in Chapter 3. The choice and layout of these pieces of equipment was based on the goal of producing a chrome product at a target grade of 40±1.5% Cr_2O_3.

6.2 Full Circuit Set-up

Based on the results of the single unit tests in Chapters 5, two different separation circuit configurations were proposed and tested using the fresh feed. In preparation for these two full circuit test-work, the feed was collected as current arising from the operating plant, homogenised and stored in $1m^3$ floor bins. Particle size distribution and chemical composition of the homogeneous feed was measured. The following sections describe in detail the two full circuit configurations that were evaluated.

6.2.1 Spiral-Magnet-Screen-Shaking table Circuit – Config1

The first circuit of the multi-unit design was made up of a spiral as the starter separator in the circuit. This is because a spiral was deemed as the most appropriate roughing unit, and it has easily changeable cutter settings that allow for quick adjustment of the recovery to the downstream units. In the spiral, it is easy to visually determine high-grade streams of chromite as the spiral separates the chromite from the gangue, and this flexibility is the reason the spiral occupies that first position. Particle size distribution analysis was done on the spiral feed and products to determine the size by assay distribution of the chrome mineral in the three products streams. The concentrate from the spiral was sent to the screen separately to screen off and remove +106µm particle size fraction, which has been shown from mineralogical studies in Chapter 4 to contain exceptionally low levels of chromite. The middlings and the tailings of the spiral were sent for magnetic separation for tailings grade minimisation. The magnetic fraction of the middlings magnetic separation process was sent to a 106µm screen to remove the course particles that contain low chromite. The undersize streams from the screening process were sent to separate shaking tables for final concentrate production. The spiral tailings magnetic fraction was also sent to a separate shaking table.

The pulp density adjustment of the feed to the shaking table was done by either addition of water to high-density streams or decantation of the settled water in the low-density products to lower and increase pulp density, respectively. The slurry flow rates used in each unit were the flowrates determined at the single unit separation tests stage, and minor adjustments were made to the streams when conditions needed to be changed. Similarly, the equipment settings were set to the levels determined from the single unit equipment test-work.

6.2.1.1 Spiral separation stage

The spiral unit separation stage was initiated with the density adjustment of the feed to the spiral. The "as is" density of the feed stock for the spiral was higher than the desired density, and water addition and agitation was done to homogenise the feed and adjust the density to the set point before pumping the slurry to a distributor above the spiral. Figure 6.1 shows the basic equipment utilised in the spiral separation stage. The agitated tank was fed with high density feed slurry and water was added to get the density to 1.52 t/m^3. Once the correct density was attained, a spiral feed valve on a circulating pump was opened to start feeding the spiral. The concentrate cutter position was set at 80 mm, and the tail cutter position was set at 166mm. Feed and product samples for volumetric and dry flow rates were taken simultaneously using

stopwatch and measuring jugs. Density measurements were done on each of the streams. Once the required number of repeat samples were reached, bulk samples for downstream units feed material were collected into 1m^3 floor bins.

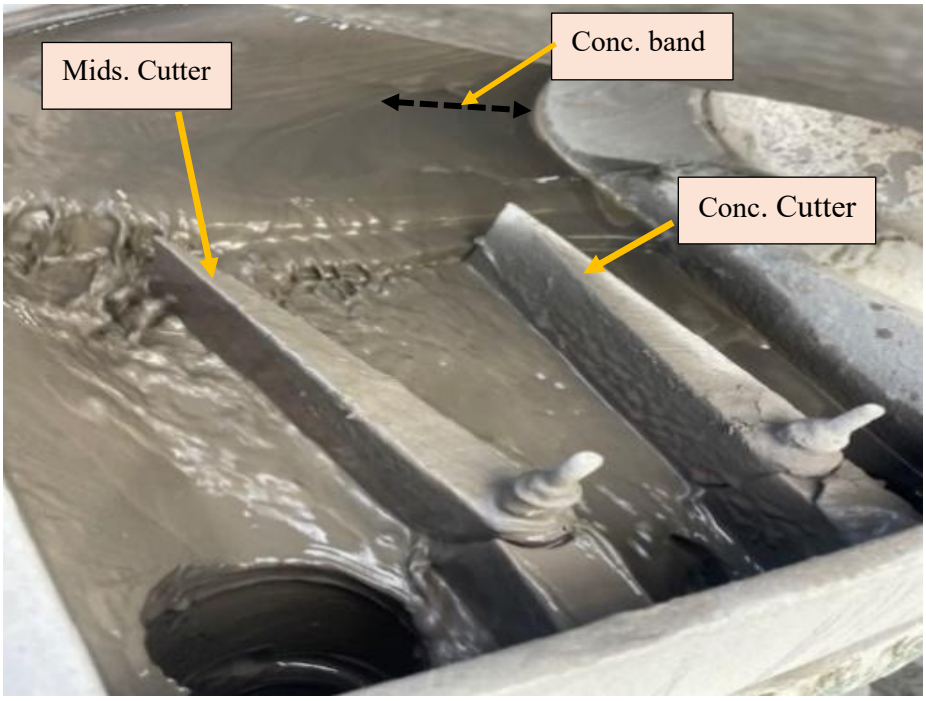

Figure 6.1: Spiral separation and cutter positions

The spiral unit separation feed and products streams were sampled for particle size distribution. This test was done to determine how to treat the material in the next unit of the combined circuit. The spiral bulk concentrate sample was dewatered through a filter press and then dried in an oven set at 110^{o}C in preparation for shaking table processing.

6.2.1.2 Magnetic separation stage

The products from the spiral test-work were collected into flow bins. The middlings and tailings were directed to the magnetic separation process. This decision was made because from the unit equipment tests, it was observed that the middlings and the tailings chrome grades were different from that of the feed, meaning that there was still an opportunity to scavenge chrome from these streams. The magnet was used to scavenge the chrome in the middlings and tailings streams for further concentration on the shaking table.

The spiral middlings stream was fed into a feed preparation tank to adjust the density to a density determined on the magnet screening test, the density which was 1.38t/m^3. Once the desired density was attained and the feed rate setting on the variable speed drive pump set at

0.81t/h and the fluidization water flow at 0.2682m^3/ton (74.5 ml/sec), the magnet feed valve was opened to start feeding the magnetic separator. Timed samples were collected using the same method that was used for the spiral sampling, for mass balance calculations. The non-magnetic fraction of this separation process was reprocessed on the magnet to give the chrome another recovery chance.

The spiral tailings were also treated separately on the magnetic separator to determine the extent of recovery of the chrome in the spiral tailings stream. The magnetic fraction stream was collected for further processing on the shaking table. Figure 6.2 shows the magnetic separation equipment used and the material being processed.

Slurry distribution on the magnet bed.

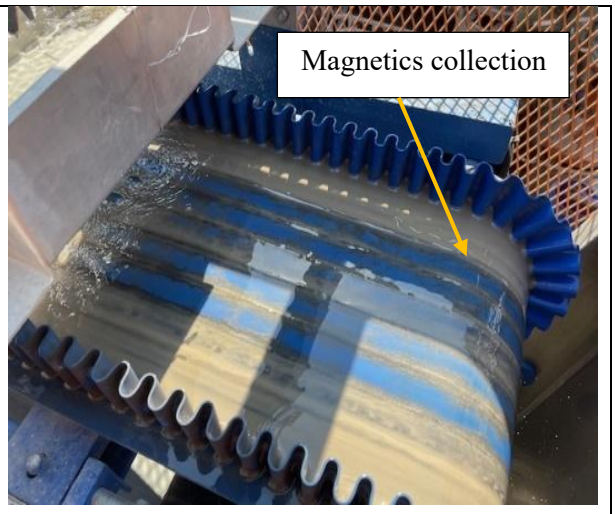

Magnetic discharge end showing partially cleaned magnetic fraction.

Figure 6.2: Magnetic separation equipment and the material distribution on the bed

The independent variables that were optimized in the magnetic separation system were the belt speed, fluidization water flow, slurry density and slurry flow rate. The magnet angle could not be easily changed and was considered a 'hard-to-change' factor. It was not changed for the duration of test-work.

6.2.1.3 Shaking table separation stage

The shaking table test-work were conducted on material preconcentrated from spirals and magnetic separators. All material (spiral concentrate and magnetic fractions) tested on the shaking table were first dewatered and then filtered to prepare for drying in an oven. The bulk concentrates were left to dry in an oven for minimum of 12 hours at 110ºC. Once dried and cooled, the agglomerated lumps were broken using hand-pressured steel rollers. The purpose of the rollers was to break the particle agglomerates so that each particle would be exposed to the shaking table forces as an individual to ensure unhindered separation and concentration. The prepared dry powder samples were homogenised using sample splitter to take a representative sample and weigh it to make a slurry with a measured volume of water. In the shaking table test runs, the target slurry density was set at 1.34t/m^3. The measured dry sample and water were mixed in a 20-litre plastic bucket fitted with an agitator as shown in Figure 6.3, to mix and adjust the slurry to the required density. The slurry was agitated for 30 minutes before feeding to the shaking table. Pumping of the slurry to the shaking table deck was done through a Wattson Marlow Ddos30 peristaltic pump, with a maximum volume flow of 500ml/min. The wash water supply valve was set at 140 ml/sec and the deck angle set at 4º.

The determination of the product streams grades in the operation of the shaking table is mainly a visual process as the choice of the cutter position is determined visually. The interface of the concentrate and middlings is a diffuse one, such that it is easy to cut too clean or too dirty with totally different outcomes for a table whose conditions are ideal for an on-spec product. Timed samples of products were also collected for mass balance determination. The test-work on the shaking table was a batch process. Due to the significantly high chrome in the middlings of the rougher shaking table run, the middlings were reprocessed on the shaking table to scavenge the chrome.

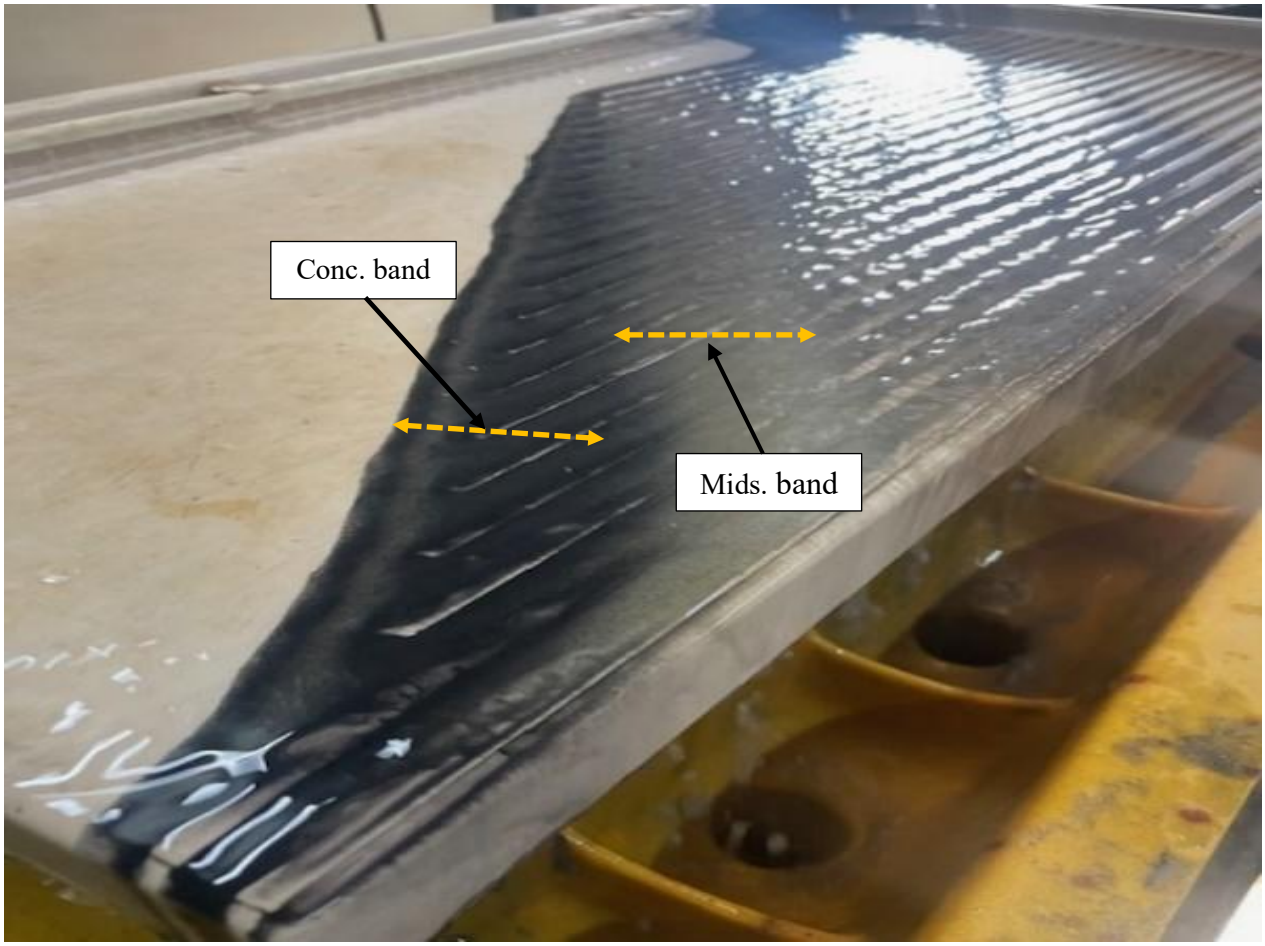

Figure 6.3: Shaking table separation profile.

The full circuit combination described in this section is shown in Figure 6.4. It shows the multi-separator units that were used in configuration 1 to beneficiate the chrome tailings feed to produce a final target grade of 40±1.5% Cr_2O_3.

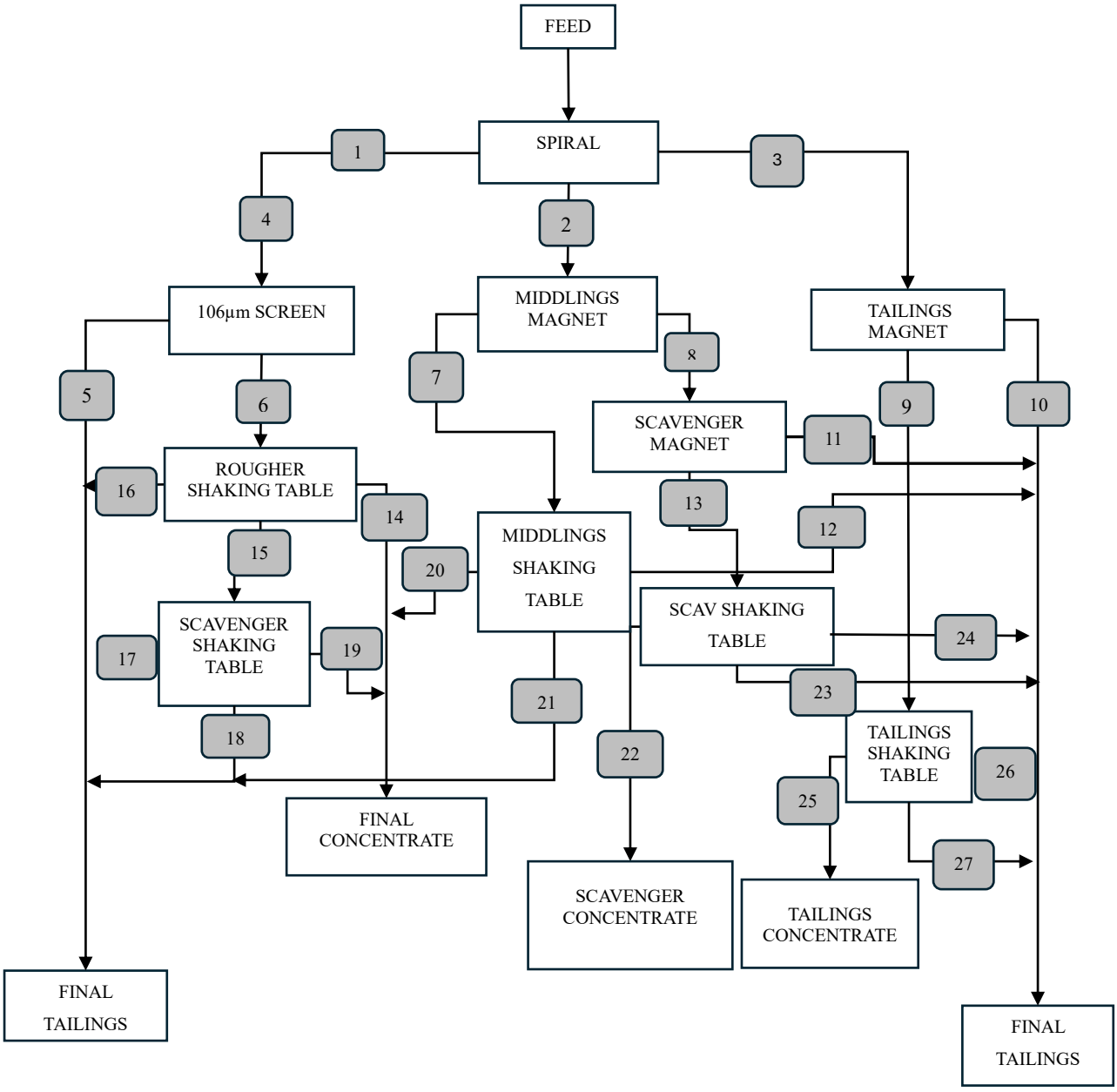

Figure 6.4: Multi-separator unit circuit set-up to produce target grade chrome products – Configuration 1

Stream Key

Stream 1	Spiral concentrate
Stream 2	Spiral middlings
Stream 3	Spiral tailings
Stream 4	106µm Screen feed
Stream 5	Screen O/S
Stream 6	Screen U/S
Stream 7	Spiral middlings magnet concentrate
Stream 8	Spiral middlings magnet tailings

Stream 9	Spiral tailings magnet concentrate
Stream 10	Spiral tailings magnet tailings
Stream 11	Spiral middling scavenger magnet tailings
Stream 12	Middlings concentrate shaking table tailings
Stream 13	Middling scavenger magnet concentrate
Stream 14	Spiral concentrate rougher shaking table concentrate
Stream 15	Spiral concentrate rougher shaking table middlings
Stream 16	Spiral concentrate rougher shaking table tailings
Stream 17	Spiral concentrate middlings scavenger shaking table tailings
Stream 18	Spiral concentrate middlings scavenger shaking table middlings
Stream 19	Spiral concentrate middlings scavenger shaking table concentrate
Stream 20	Spiral middlings shaking table concentrate
Stream 21	Spiral middlings shaking table middlings
Stream 22	Spiral middlings magnet shaking table concentrate
Stream 23	Spiral middlings magnet shaking table middlings
Stream 24	Spiral middlings magnet shaking table tailings
Stream 25	Spiral tailings magnet shaking table concentrate
Stream 26	Spiral tailings magnet shaking table middlings
Stream 27	Spiral tailings magnet shaking table tailings

6.2.2 Screen-Spiral-Screen-Shaking table Circuit – Configuration 2

The second circuit configuration that was proposed and tested as an alternative to the spiral-magnet-screen-shaking table configuration was the screen-spiral-screen-shaking table configuration. This circuit was tested to investigate the effect of splitting the feed stream into streams of -25µm and +25µm particles. This was triggered by the feed material characterisation studies which indicated that the feed material is made up of almost 50% by mass of +25µm and -25µm particles sizes. The analysis of these two size fractions also showed that the -25µm fraction has a much higher chrome content than the +25µm. Hence the splitting of the streams which narrows the particle size range will have positive influence on separation efficiency. The coarser stream was made up of particles +25µm while the finer stream was made up of 100% -25µm particles. The following sections describe the experimental procedure that was followed in testing this circuit.

6.2.2.1 + 25 µm separation: Spiral to Shaking table

A feed stock collected from the spiral tails of the same operating plant was wet screened using the Rhologan screen until 1 m^3 slurry of +25µm was generated. This +25µm fraction was densified by decanting water until a density of 1.52 t/m^3 was attained. The concentrate cutter position was set at 60mm and the tailings cutter position set at 136mm. The feed rate to the spiral was set at 0.83t/h, using a variable speed drive pump. Timed samples were collected for

stream assay as well as mass balance. Bulk concentrate samples were collected for further separation on the shaking table.

The collected spiral concentrate was dewatered, dried, and homogenised using a sample splitter before mixing it with premeasured water volume to adjust the slurry density to 1.34 t/m^3, which is the slurry density required for shaking table separation. The shaking table test runs were performed at a deck angle of 4^o, wash water flow of 36 m^3/ton of slurry (140 ml/s) and dry feed flowrate of 0.014 t/h. Samples from the shaking table were also collected for stream assay analysis as well as for mass balance around the shaking table.

6.2.2.2 -25 µm separation: Spiral to Shaking table

The -25-micron particle size stream from the screening of the original feed was decanted to remove excess water and homogenised to a density of 1.52 t/m^3. When the pump was set to give the target slurry flow rate of 0.83 t/h to the spiral, it was observed that there was virtually no separation of the chromite happening to the inner concentrate stream as normally observed. To improve separation, the slurry density was lowered progressively while checking for visible streaks of dark chromite line on the inner part of the trough. This was done while the feed rate was also lowered to a level where there was lamellar flow across the width of the trough. Timed samples for stream assays and mass balance were taken. Bulk spiral product samples from the –25 µm micron feed test-work were collected for eventual separation on the shaking table.

It can be seen from Figure 6.5 that the difference between the flowsheet arms of the circuit for +25µm and -25µm is that the -25µm arm does not have screening of the spiral concentrate at 106µm microns for the obvious reason that the material is already below 25µm.

The results of the full circuit experimental test-work are presented in the next chapter. Full circuit yield and recoveries are discussed, indicating the overall performance of the proposed circuits to beneficiate the ultrafine chrome.

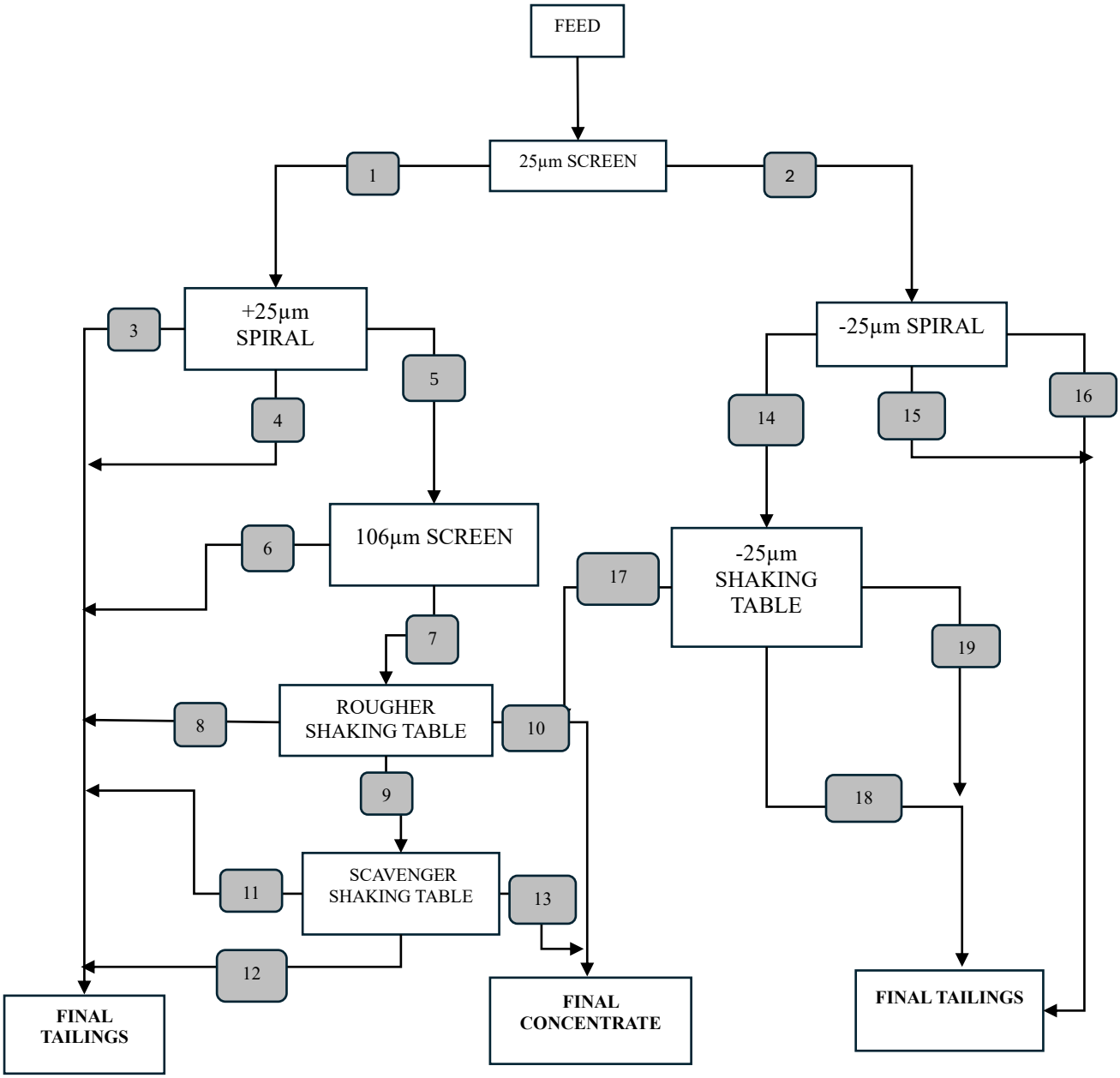

Figure 6.5: Gravity-only circuit set-up to produce high-grade chrome products – Configuration 2

The following is a stream numbering key showing the identity of the streams.

Stream Key

Stream 1	25µm screen oversize
Stream 2	25µm screen undersize
Stream 3	+25µm screen spiral tailings
Stream 4	+25µm screen spiral middlings
Stream 5	+25µm spiral concentrate
Stream 6	106µm screen oversize
Stream 7	106µm screen undersize

Stream 8	Rougher shaking table tailings
Stream 9	Rougher shaking table middlings
Stream 10	Rougher shaking table concentrate
Stream 11	Scavenger shaking table tailings
Stream 12	Scavenger shaking table middlings
Stream 13	Scavenger shaking table concentrate
Stream 14	-25µm spiral concentrate
Stream 15	-25µm spiral middlings
Stream 16	-25µm spiral tailings
Stream 17	-25µm shaking table concentrate
Stream 18	-25µm shaking table middlings
Stream 19	-25µm shaking table tailings

.

CHAPTER 7: CIRCUIT ANALYSIS – RESULTS AND DISCUSSION

7.1 Introduction

The development of a full separation circuit for the recovery of ultrafine chrome was guided by the results of Single Units Separation performance tests. Results from single unit separation tests revealed the performance of each unit in terms of yield of the value streams, recovery of the chrome to the value streams, grade of the value stream and the upgrade of the chrome assay from feed to the value product stream. The positioning of each of the separation units was based on the most suitable function in the circuit to produce a product of the target grade of about 40% ±1.5% Cr_2O_3. The next section presents and analyses the deportment of the different oxides in the size fractions of the concentrate, middlings, and tailings streams during processing of the feed material on the spiral separator. To have adequate insight into the separation process, it is prudent to understand how the particles behave from the spiral feed point to the products and across the size fractions.

7.1.1 Spiral feed and products fractional analysis.

The particle size distribution of the spiral feed and products is given in Table 7.1 and shown in Figure 7.1. The screen sizes used in the sieve tests to determine the PSD were 25µm, 38µm, 53µm, 75µm, and 106µm, respectively. The intermediate sizes (12.5µm, 31.5µm, 45.5µm, 64µm and 90.5µm) were determined by calculation to smoothen the graphs in Figure 7.1.

From Table 7.1, for the feed the mass generally increases as the particle size decreases except for the +25µm size fraction which shows a lower mass than all the other fractions, a phenomenon that was observed consistently in this material. The concentrate stream has higher mass percentages than the feed in all the size fractions except the -25µm size fraction. The middlings stream has a mass distribution by size class that is comparable to that of the feed. The tailings stream has much less coarse fractions and much more finer particles. This shows that the ultra-fines are largely lost with the tailings in spiral separators One outstanding pattern is the amount of material reporting to the -25µm in all the streams. This shows that the bulk of the material is below 25µm. From recovery of Cr_2O_3 perspective, the chrome report predominantly to the ultrafine fractions of -25µm. The results also show that most of the coarse chrome reports to the concentrate compared to the middlings and tailings for spiral separation.

Table 7.1: Particle size distribution and chrome recovery into size fractions

	% Mass				% Cr_2O_3 recovery			
Size Fraction	**Feed**	**Concentrate**	**Middlings**	**Tailings**	**Feed**	**Concentrate**	**Middlings**	**Tailings**
+106µm	8.84	20.97	8.44	1.63	1.46	3.57	0.92	0.93
+75 µm	8.00	10.81	8.44	3.06	2.62	7.09	1.43	0.27
+53 µm	9.89	10.59	11.93	5.51	6.67	13.93	5.67	1.34
+38 µm	12.00	15.25	11.73	9.59	12.08	22.85	11.32	4.06
+25 µm	7.37	14.62	8.85	13.06	9.81	21.96	10.80	11.32
-25 µm	53.89	27.75	50.62	67.14	67.36	30.60	69.85	82.07
Total	100	100	100	100	100	100	100	100

Table 7.2 shows the recovery of mass and chrome from each of the respective size fractions into the corresponding size class in the different product streams. For example, the feed stream has 8.84% of the total mass in the 106µm size fraction. Of this 8.84%, 25.43% reports to the concentrate, 59.11% to the middlings and 15.46% to the tailings upon screening. In terms of the chrome (Cr_2O_3) distribution, only 1.46% of Cr_2O_3 in the feed is in the +106 µm size fraction. Of this 1.46%, 26.17% Cr_2O_3 reports to concentrate, 39.17% to the middlings and 34.66% to the tailings. Table 7.2 shows that recovery of chrome into the concentrate averages 24.37% between +25µm and +106µm with higher recoveries as the size fraction increases. One incredibly significant observation is that for the -25µm the recovery of chrome into the concentrate is only 4.87%. Significantly higher recoveries of chrome are reported in the middlings and tailings. It was evident that under the conditions in which the spirals were run, the -25µm size chrome particles were difficult to recover into the concentrate. To increase the recovery of chrome into the concentrate, the concentrate cutter position can be opened towards the middlings stream which has an effect of reducing the concentrate grade and increasing the mass yield.

Table 7.2: Chromite recovery per size fraction

	% Mass				Total	% Cr_2O_3 Recovery				Total
Size Fraction	**Feed**	**Concentrate**	**Middlings**	**Tailings**		**Feed**	**Concentrate**	**Middlings**	**Tailings**	
+106µm	8.84	25.43	59.11	15.46	100	1.46	26.17	39.17	34.66	100
+75 µm	8.00	14.48	65.33	20.19	100	2.62	28.98	33.86	37.16	100
+53 µm	9.89	11.48	74.72	13.80	100	6.67	22.41	52.69	24.91	100
+38 µm	12.00	13.63	60.55	25.8	100	12.08	20.28	58.09	21.62	100
+25 µm	7.37	21.27	74.39	4.34	100	9.81	23.99	68.20	7.81	100
-25 µm	53.89	5.52	58.18	36.30	100	67.36	4.87	64.23	30.90	100
Total	100					100				

The PSD results in Figure 7.1 show that the spiral concentrate contains the coarsest particles, and the tailings stream has the finest particles whilst the feed and middlings have intermediary particle size and share remarkably similar PSDs. From the PSD graph, it is seen that for the tailings stream, 80% mass is smaller than approximately 37µm while for feed and middling fractions 80% is smaller than 68µm and for Concentrate stream 80% of the mass is smaller than 106µm.

These results are in alignment with the liberation results in chapter 4, which reported that the feed sample has 87% of the chromite particles at ≥90% liberation. Of this 87% volume, in the 106µm size fraction the ≥90% liberation is only 41.9%. The balance of 41.9% is distributed between 10% and 90% liberation. All the other size fractions less than 106µm down to less 25µm have more than 90% of the chromite volume having more than 90% liberation.

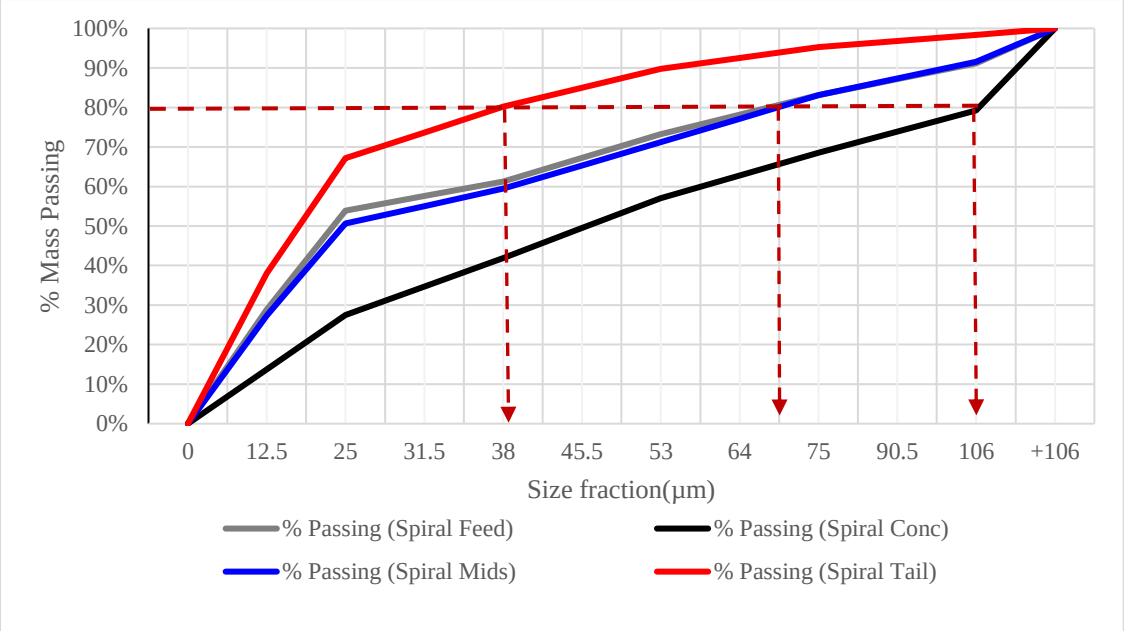

Figure 7.1: Particle size distribution of spiral Feed, Concentrate, Middlings and Tailings

Table 7.3 below shows the chemical assays of the spiral streams whose particle distribution is given in Figure 7.1 of the 6 main oxides making up the spiral stream's mineral composition Cr_2O_3, FeO and MgO (Figure 7.2), show an upgrade from feed to the concentrate. SiO_2, CaO and Al_2O_3 show a downgrade from feed to concentrate. Mineralogically, Cr_2O_3 and FeO exist as chromite $FeCr_2O_4$ while MgO exists as Enstatite-Ferrosilite $(Mg,Fe)SiO_3$, Diopside $(CaMgSi_2O_6)$, Amphibole $(Mg_7Si_8O_{22}(OH))$ and Talc $(Mg,Fe)_3(Si,Al)_4O$. Table 7.4 below gives the relative abundance and the densities of each of the minerals.

Table 7.3: Chemical assays of the Feed, Concentrate, Middlings and Tailings of the spiral separation process

Fraction	Cr_2O_3 %	FeO %	SiO_2 %	CaO %	Al_2O_3 %	MgO %
Spiral Feed Sample	8.76	9.29	41.09	9.02	20.13	14.45
Spiral Concentrate Sample	17.19	15.55	35.53	7.17	18.74	17.95
Spiral Middlings Sample	7.69	8.98	43.09	9.98	20.72	14.63
Spiral Tailings Sample	8.27	9.13	41.85	9.97	21.31	14.18

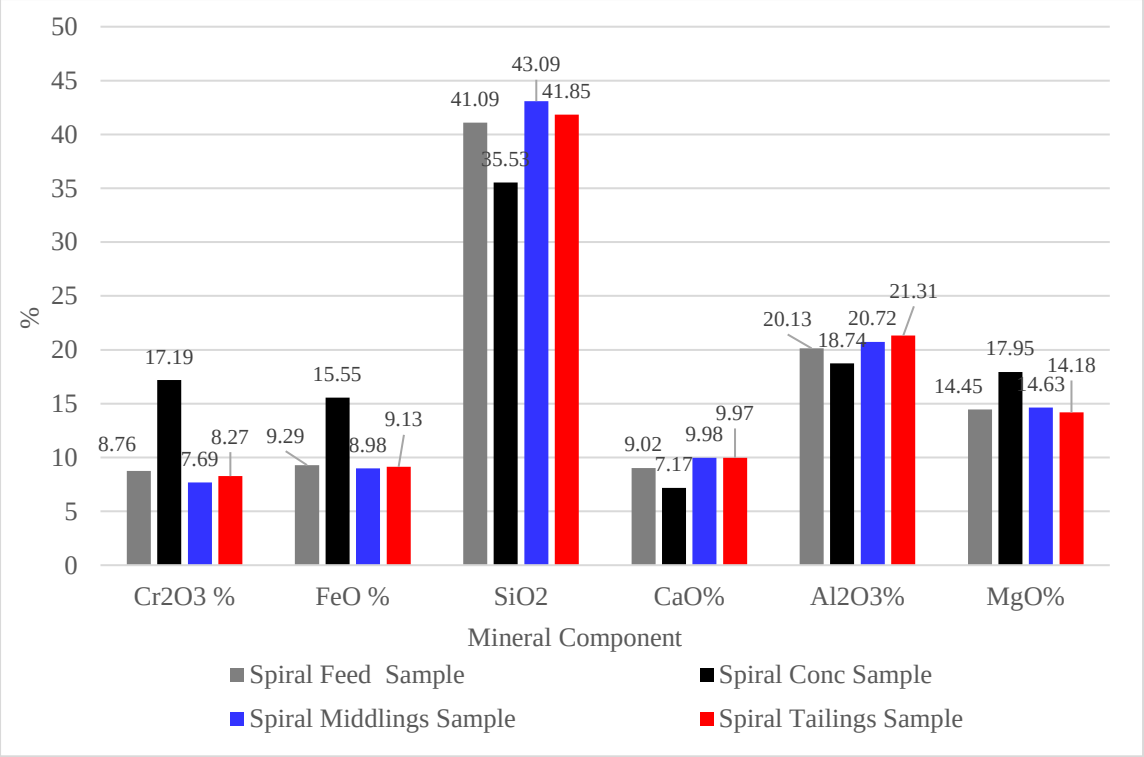

Figure 7.2: Main Oxide content in Spiral feed, concentrate, middlings and tailings

The two main drivers for gravity separation, especially in the spirals, are density and particle size. For chromite (Cr_2O_3 and FeO) there is an upgrade from feed to concentrate due to density difference between the two oxides and the other lower density oxides in the feed sample. The mineral which contains MgO and is in substantial proportions is Enstatite-Ferrosilite with a density of 3.3 kg/l. The other main oxides are the alumino-silicates, and their density is around 2.6 kg/l hence these oxides will downgrade from a feed into the concentrate. The reason MgO upgrades in the concentrate is because the density of the MgO containing mineral is 3.3 kg/l which is closer to the density of chromite ($FeCr_2O_4$) than the feldspar which has a density of 2.6 kg/l. The behaviour of MgO in the spiral separation means that the selectivity of chrome separation is compromised since MgO containing mineral which is a gangue mineral reports to the spiral concentrate. The distribution of the oxides into the distinct size fractions would help give some insight into how particle size effect can affect the concentration process using spirals.

Table 7.4: Relative abundance of the main mineral oxides in the spiral feed sample

Mineral	Relative Mass (%)	Mineral Density (kg/l)
Feldspar ($KAlSi_3O_8$)	41.7	2.6
Enstatite-Ferrosilite (Mg, Fe)SiO_3	29.2	3.3
Chromite ($FeCr_2O_4$)	18.0	4.4
Diopside ($CaMgSi_2O_6$)	2.7	3.4
Amphibole ($Mg_7Si_8O_{22}(OH_2)$	2.1	3.0
Chlorite $(Mg,Fe)_3(Si,Al)_4O$	1.7	2.8
Talc ($Mg_3Si_4O_{10}(OH)_2$	1.4	2.7

7.1.2 Spiral feed and products main oxides fractional analysis.

The spiral concentrate was screened into size fractions from 25µm to 106µm to determine how the oxides are distributed in these fractions. The enrichment factors for the Cr_2O_3, FeO and MgO from feed to concentrate are 1.96, 1.67 and 1.24, respectively. Figure 7.3 shows that Cr_2O_3 has the highest grade in the -75µm to +25µm size fractions. A similar trend was observed with FeO. In the case of MgO, it was observed that the highest grades were found between +53µm and +106µm fractions.

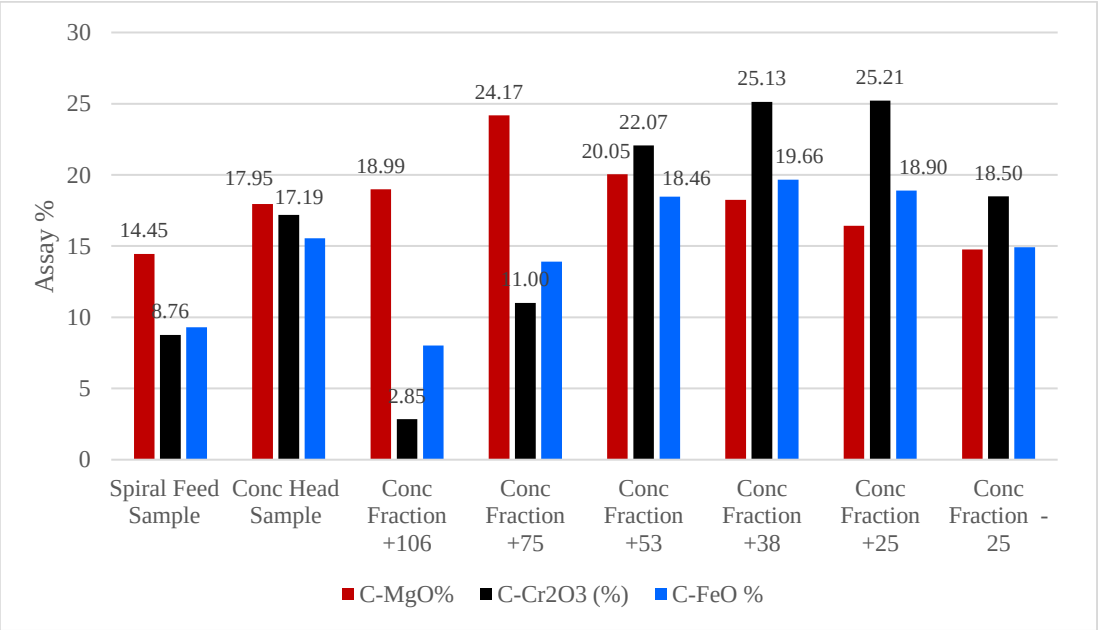

Figure 7.3: Fractional analysis for the three upgrading oxides

It can therefore be inferred that the liberation of chromite is highest in the size fractions between -75µm and +25µm. Also, screening the concentrate on a 106µm screen removes 20% of the mass at 2.85% Cr_2O_3, 8.02% FeO and 18.99% MgO. This action potentially helps to upgrade the Cr_2O_3 % and reduce the MgO% in the -106µm fraction remaining for further processing.

Figure 7.4 shows the fractional analysis of the CaO, Al_2O_3 and SiO_2 in the spiral concentrate. SiO_2 downgrades from feed to concentrate indicating that the spirals reject SiO_2 to the middlings and tailings. Analysis of the SiO_2 in the size fractions show that it is mainly concentrated in the +75µm fraction. Al_2O_3 has a slightly different trend of distribution in the fractions. It has minimum concentration in the -106+75µm size fraction and then increases as the particle size decreases. CaO is more concentrated in the +106µm size fraction where it concentrates to above 10% with the rest of the fraction almost uniform around 5%. Screening the concentrate on a 106µm screen removes SiO_2 and Al_2O_3 thereby assisting in the upgrading of the value components i.e., Cr_2O_3 and FeO.

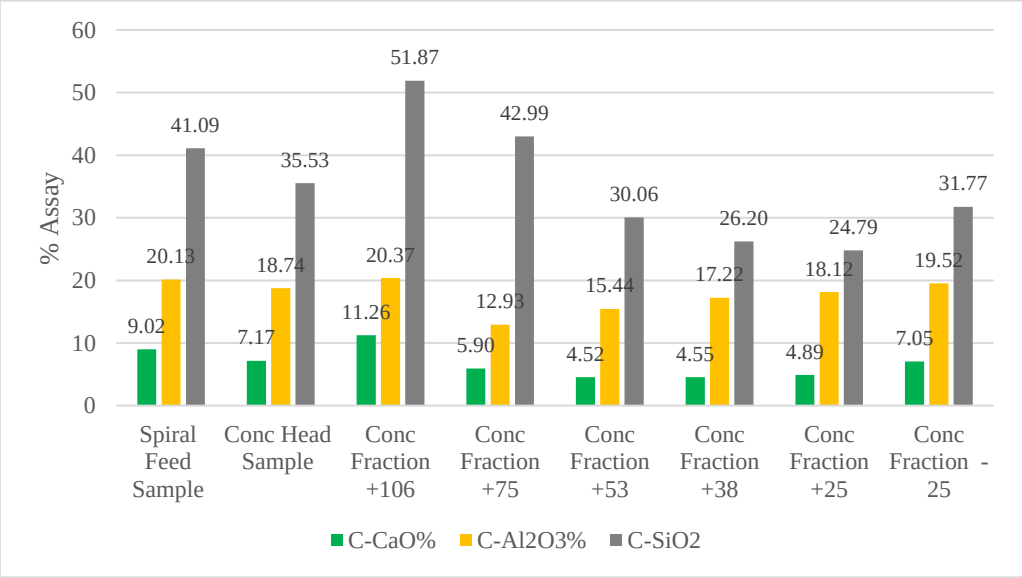

Figure 7.4: Fractional analysis for three downgrading oxides in the spiral Concentrate stream

7.1.3 Spiral middlings fractional analysis

The distribution of the three high density oxides in the middlings size fraction is presented in Figure 7.5. Cr_2O_3 and FeO have higher concentrations in the finer size fractions. On the other hand, the MgO has the highest concentration in the +38µm to -75µm size fractions. An interesting observation on the MgO and Cr_2O_3 between 58µm and 106µm is that there a wide gape of assays such that screening the +53µm fraction will leave a higher concentration of

Cr_2O_3 since its assay in the coarser size fraction above 53µm is less than 4% but that of MgO is above 10%.

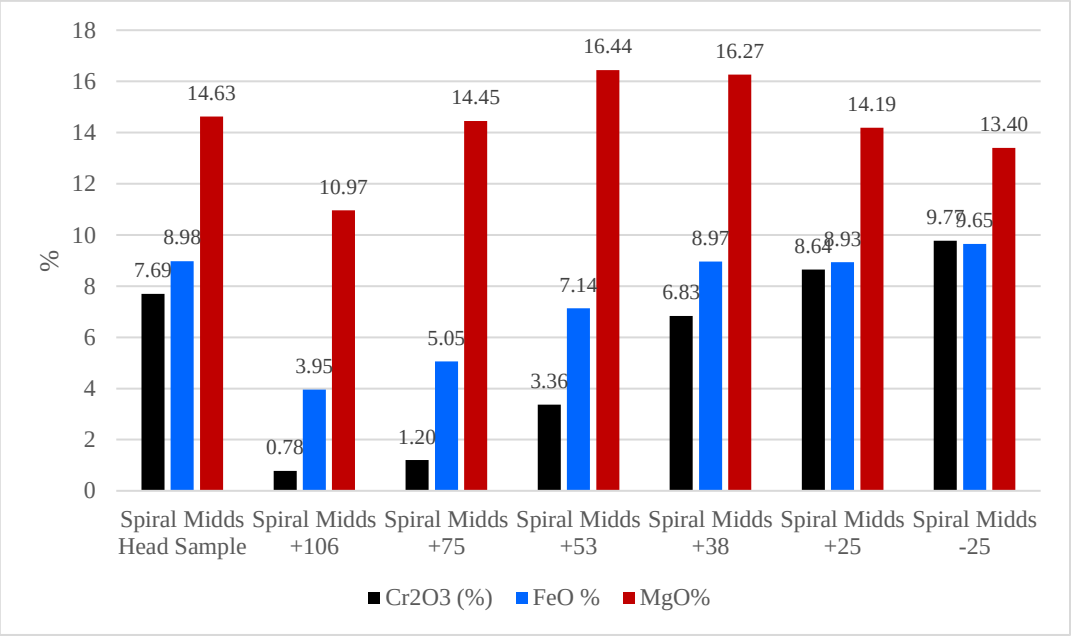

Figure 7.5: Fractional analysis for Cr_2O_3, FeO and MgO in the spiral middlings stream

The other three oxides (SiO_2, CaO and Al_2O_3) do not show significant changes across the size fractions except for a slight dip on all three between -38µm and +25µm as shown in Figure 7.6. For these oxides, the concentration is uniform in the distinct size fractions meaning the associations that give the assays levels is consistent across the size fraction.

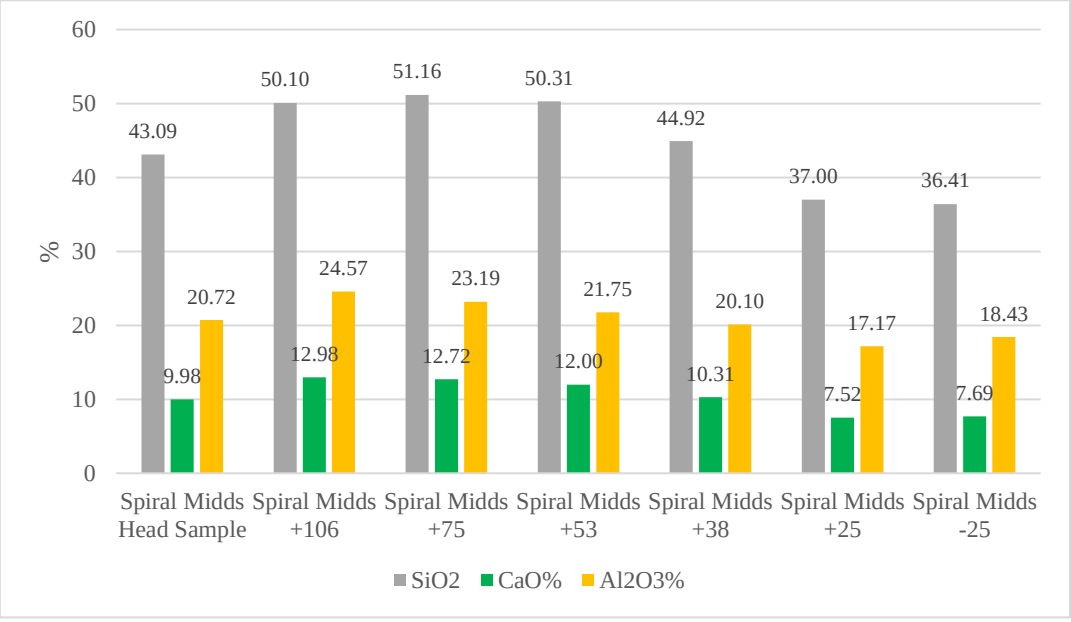

Figure 7.6: Fractional analysis for SiO_2, CaO and Al_2O_3 in the spiral middlings stream

7.1.4 Spiral tailings fractional analysis.

The tailings profile for the Cr_2O_3, FeO and MgO is given in Figure 7.7. It shows that for all three oxides; the concentration is relatively high in the 106µm fraction and drastically drops in the -106+75µm fraction and then increases uniformly as the particle size decreases from -75 µm to -25µm. The difference in concentration between MgO and Cr_2O_3 is also significant and most in the +38µm and -75µm. The concentration of Cr_2O_3 and FeO is highest in the -25µm size fraction.

The other oxides (SiO_2, CaO and Al_2O_3) are evenly distributed across all the size fractions as shown in Figure 7.8. What can be seen is that even though there is not much difference of concentration between the size fractions, there is higher concentration of all three oxides in the 75µm and 38 µm.

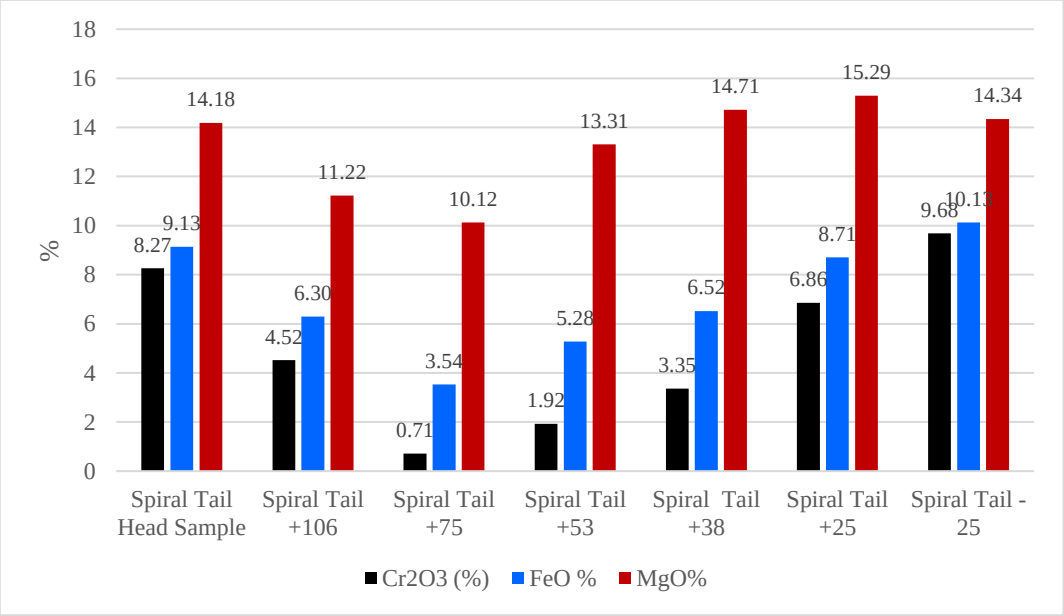

Figure 7.7: Factional analysis for Cr_2O_3, FeO and MgO in the spiral tailings stream

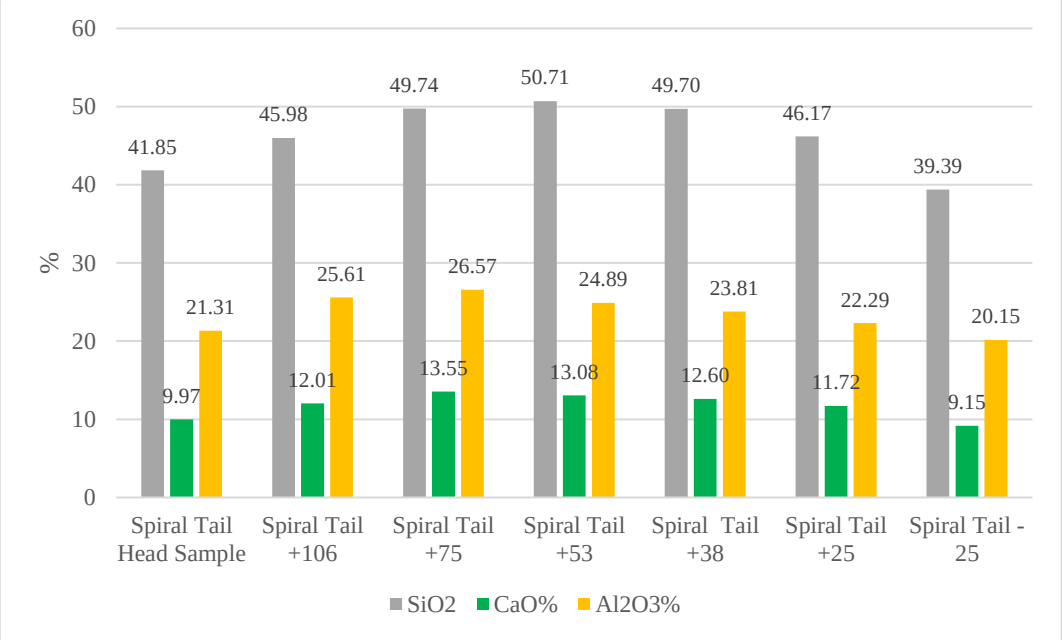

Figure 7.8: Fractional analysis for SiO_2, CaO and Al_2O_3 in the spiral tailings steam.

7.2 Full circuit Configuration 1 – Spiral-Magnet-Screen-Shaking table

This section discusses the results of a full circuit separation using spirals, magnet, screen and shaking table circuit as per experimental methodology presented in Chapter 7 and depicted in Figure 7.9. Based on the equipment performance test results presented in Chapter 7, the spiral separator was chosen to be the first unit of the full circuit configuration 1. The reason for selecting spiral separator as the first unit was that it has a good balance of recovery capacity and upgrade in terms of chromite.

7.2.1 Spiral Separation analysis.

The spiral separation stage of the full circuit was conducted under conditions that were determined from the equipment selection stage. The set of conditions at which the spiral separation tests were performed were determined by the Taguchi Main Effect plots as well as the Design Expert model predicted values. Table 7.5 shows the two sets of conditions predicted from two evaluation methods and the final set of conditions the experiment was conducted at.

Table 7.5: Spiral conditions as determined by Taguchi Main Effects plots and Design Expert Model

Spiral Input Factor	Taguchi Model	Design Expert Model	Final Condition Set Chosen
Slurry Density (t/m^3)	1.52	1.50	1.52
Slurry Flowrate (t/h)	0.83	0.83	0.83
Concentrate Cutter Position (mm)	75.00	50.49	80.00

Table 7.6 and Figure 7.9 below show that the results of the spiral separation results.

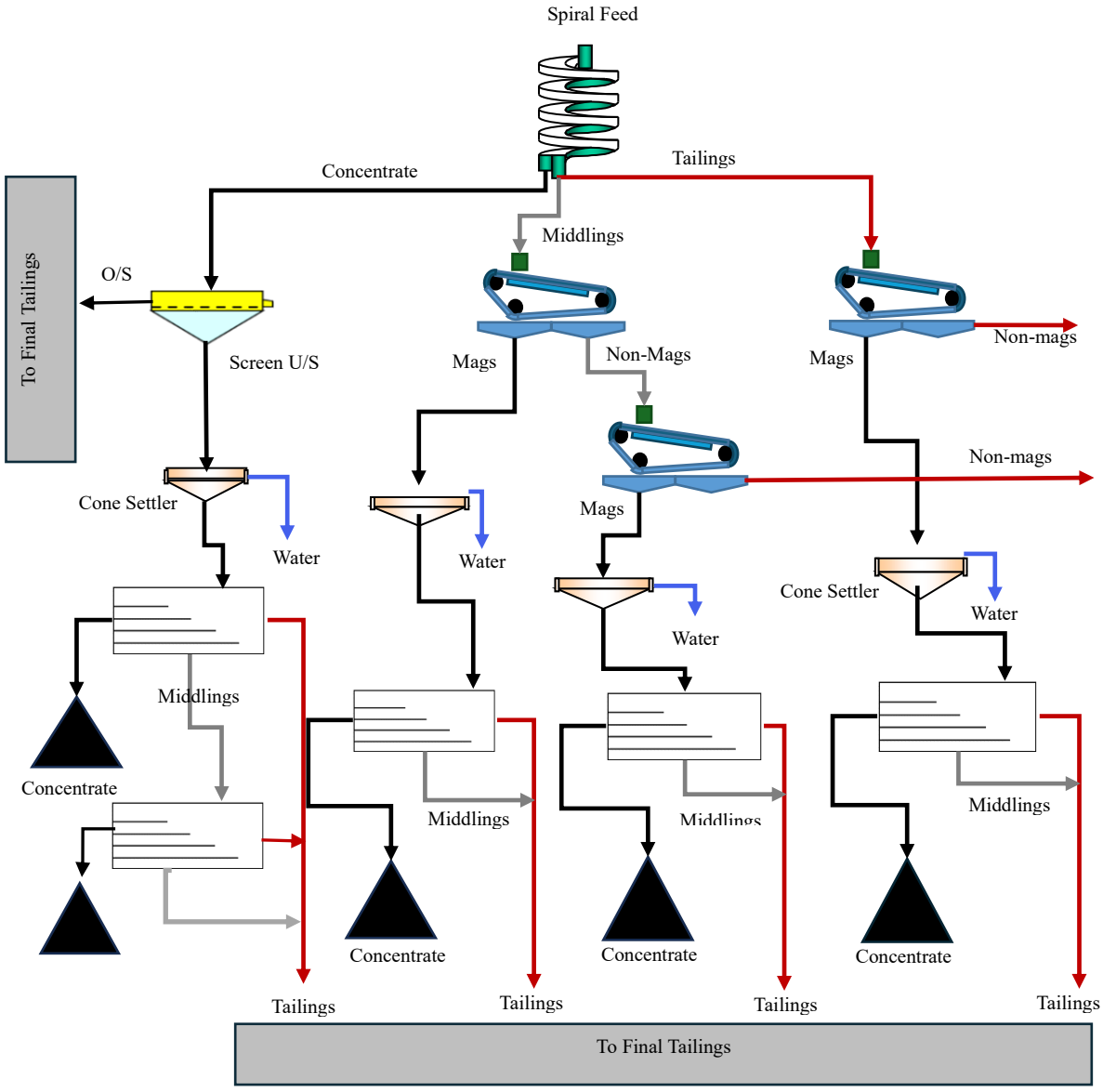

Figure 7.9: Full circuit testing (Spiral, Magnets, Screens and Shaking tables)

The spiral feed stream containing 10.68% Cr_2O_3 was fed into the spiral, and there was separation that resulted in Cr_2O_3 enrichment of 1.22 times in the concentrate stream with a grade of 13.35%. Equally, FeO and MgO also had an enrichment into the concentrate stream. The other three oxides did not upgrade but rather downgraded slightly into the concentrate stream as shown in Figure 7.10.

Table 7.6: Spirals separation results of mass yield, recovery, and grades of the main oxides in each spiral stream

Stream Name	Mass Yield %	Cr_2O_3 Rec %	Cr_2O_3 %	FeO%	SiO_2 %	CaO %	Al_2O_3 %	MgO %
Ave Spiral Feed			10.68	10.52	37.65	8.409	18.80	14.07
Ave Spiral Concentrate	23.1	30.6	13.35	12.46	35.12	7.136	16.63	15.64
Ave Spiral Middlings	48.7	43.4	9.11	9.40	38.93	9.095	19.60	13.55
Ave Spiral Tailings	28.2	26.1	9.31	9.54	38.47	8.977	19.61	13.32

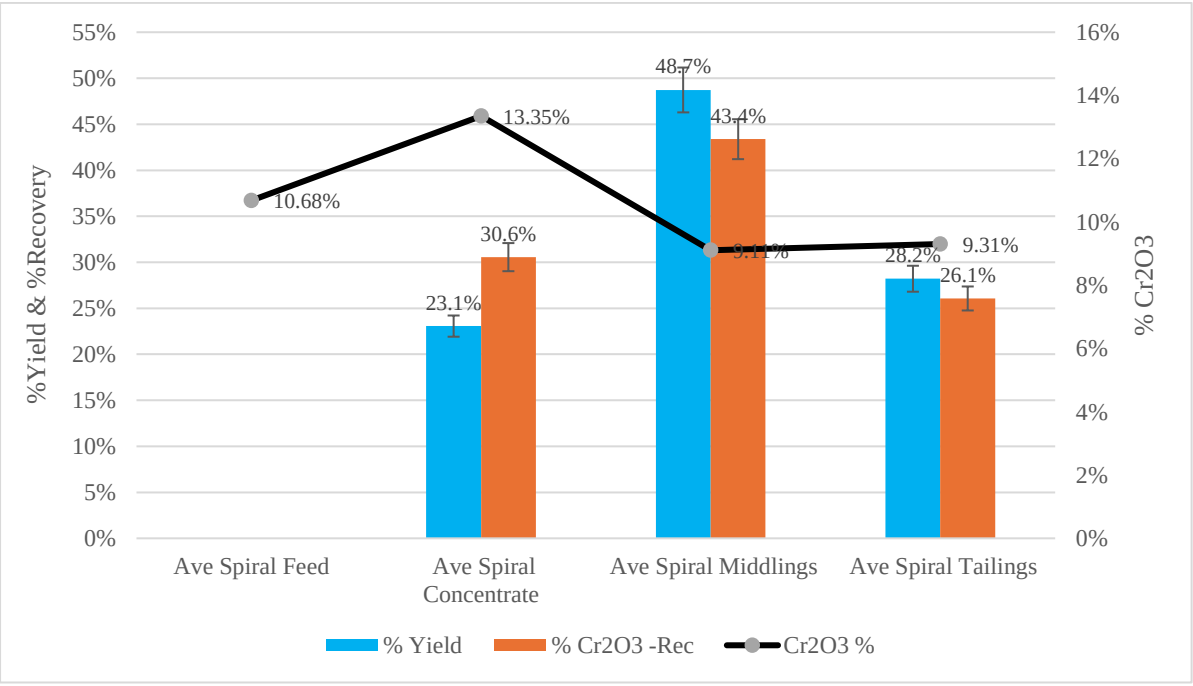

Figure 7.10: Spiral Yield, Recovery and Cr grades of product streams

Assessment of the middlings and tailings concentration of the oxides shows that the middlings stream does not necessarily have an intermediate grade between the concentrate and tailings streams. The reason is that the liberated chrome in the feed distributes itself almost equally between middlings and tailings due to the size effect. The ultrafine chrome gets washed to the edges of the spiral trough due to buoyancy forces and reports to tailings. The middlings streams will have slightly coarser particles (than the tailings) but finer than the concentrate particles. As a result, the middlings and tailings assays for all oxides are almost equal as seen in Figures 7.11 and 7.12.

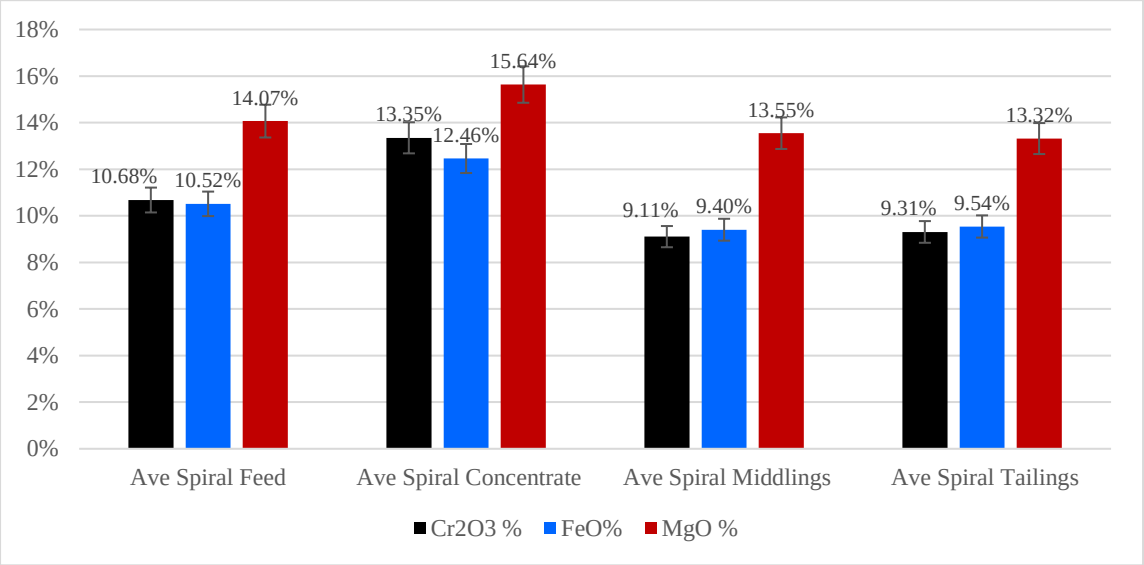

Figure 7.11: Concentration of Cr_2O_3, FeO and MgO in the Spiral streams

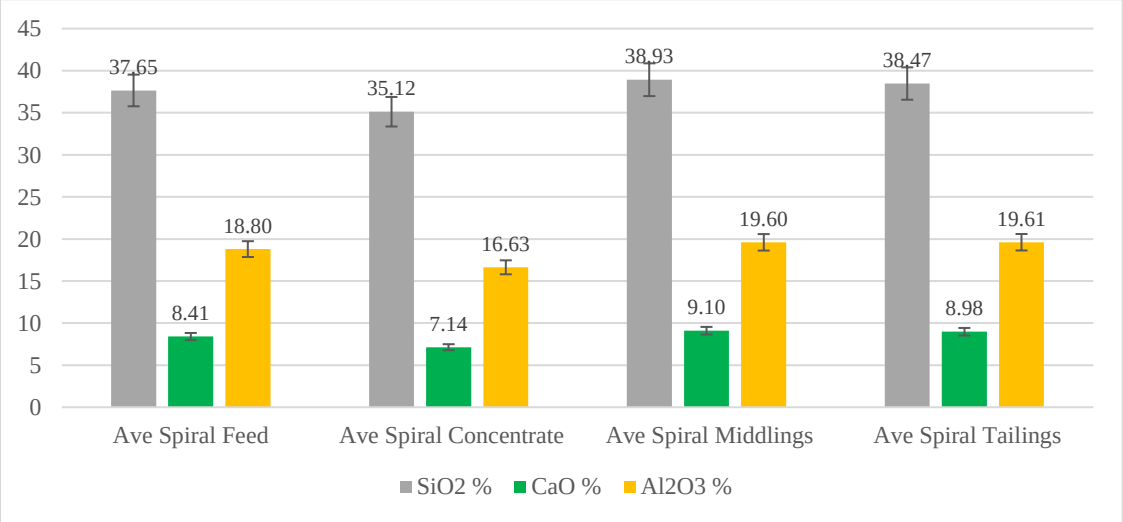

Figure 7.12: Concentration of SiO_2, CaO, and Al_2O_3, in the Spiral streams

7.2.2 Spiral middlings magnetic separation analysis.

The middlings stream from the spirals was processed on a magnet with the conditions determined from the Taguchi Main Effect plots in conjunction with the Design Expert model predicted conditions. Table 7.7 below gives the predicted conditions and the final conditions that were used for the spiral middlings magnet rougher experimental run.

Table 7.7: Magnet rougher run for the spiral middling stream

Magnet Input Factor	Taguchi Model	Design Expert Model	Final Condition Set Chosen
Slurry Density (t/m^3)	1.38	1.49	1.38
Slurry Flowrate (t/h)	0.768	1.90	0.81
Belt Speed (m/s)	0.5	0.375	0.375
Fluidization water (ml/sec)	21.5	74.4	74.5

The final set of conditions for the magnet were chosen after observing experimental runs performed using predicted conditions. These conditions were fine-tuned while observing the magnet product results. The magnet was used to generate material for the next processing stage (shaking table).

Figures 7.13, 7.14 and Table 7.8 show that the three oxides associated with higher density minerals (Cr_2O_3, FeO and MgO) all upgraded in the magnetic fraction stream of the magnet. The other three oxides (Al_2O_3, SiO_2 and CaO) were downgraded into the magnetic fraction. The magnetic separation phenomenon takes advantage of the magnetic properties of the component subjected to the magnetic force separation. Enstatite-Ferrosilite $(Mg,Fe)SiO_3$ is a chain composed of $MgSiO_3$ and $FeSiO_3$ with various levels of substitution. Enstatite-Ferrosilite is paramagnetic and is collected with $FeCr_2O_4$ into the concentrate and this explains why MgO upgrades into the magnetic fraction during magnetic separation.

Table 7.8: Yield, Recovery and Assays for major oxides for Spiral middlings magnetic separation

Stream Name	% Yield	$\%Cr_2O_3$ Recovery	Cr_2O_3 %	FeO%	SiO_2 %	CaO %	Al_2O_3 %	MgO %
Average Magnet Feed			9.13	9.65	44.529	9.78	20.06	14.14
Average Magnetic Fraction	8.2	18.4	20.24	18.66	32.674	4.64	13.80	18.04
Average Non-Magnetic Fraction	91.8	81.6	8.05	8.66	45.681	10.33	20.94	13.62

The Al_2O_3, CaO and SiO_2 were shown to be recovered into the non-magnet stream of the magnet. This is because these oxides do not contain significant paramagnetic minerals in them. The oxides still found in the magnetic fraction are due to the inefficiency of separation driven by low fluidization water, as well as lesser amounts still attached to the chrome particles due to incomplete liberation especially in the +106µm size fraction.

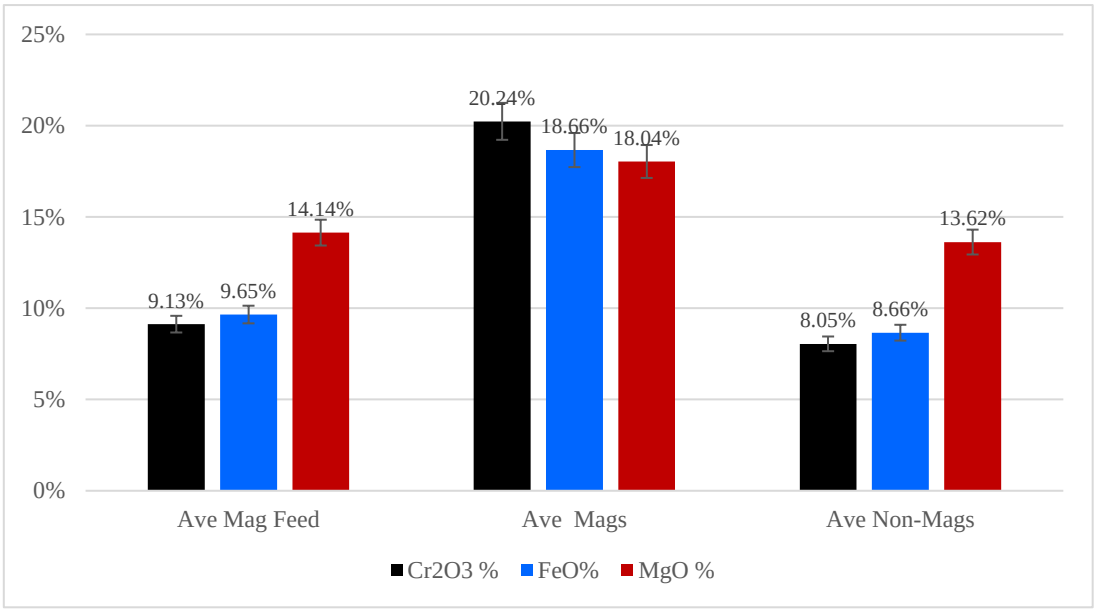

Figure 7.13: Concentration of Cr_2O_3, FeO and MgO in the magnet streams

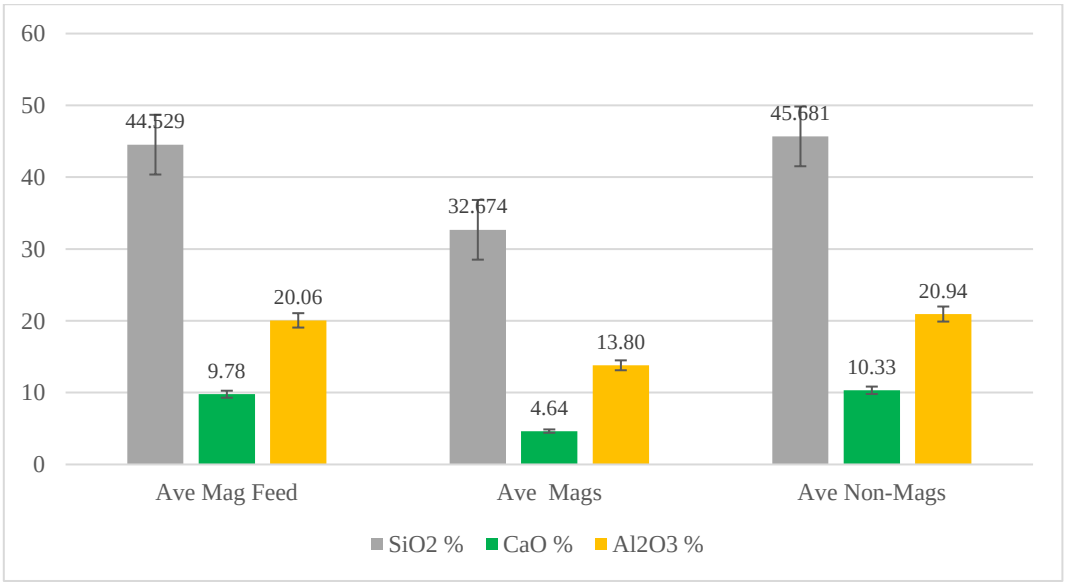

Figure 7.14: Concentration of SiO_2, CaO, and Al_2O_3, in the magnet streams

7.2.3 Spiral Tailings magnetic separation analysis.

The tailings stream from the spiral separation was sent to a magnet for scavenging of the chromite remaining in the stream. The one adjustment on the magnet that was done during the tailings magnetic separation run was the belt speed. After realizing that for the rougher magnetic separation the chrome upgrade was extremely high and the recovery was too low, the belt speed was adjusted from 0.375m/s to 0.5m/s. This was done to improve on the recovery of the chrome to the downstream units. With this adjustment, the magnetic fraction Yield for the tailings run increased to 17.2% while the Recovery increased to 22.70 from 8.21% and 18.40%, respectively.

Table 7.9: Yield, Recovery and Assays for major oxides for Spiral Tailings magnetic separation.

Stream name	% Mass Yield	% Cr_2O_3 Recovery	Cr_2O_3 %	FeO%	SiO_2 %	CaO %	Al_2O_3 %	MgO %
Ave Spiral Tail Magnet Feed			8.41	8.87	41.55	9.46	20.03	13.10
Ave Spiral Tail Magnet Mags	17.12	22.70	10.94	10.92	37.90	7.81	17.96	14.09
Ave Spiral Tail Magnet Non-Mags	82.88	77.30	7.70	8.04	41.63	9.64	20.11	12.86

The trends of upgrades and downgrades on specific oxides (Figure 7.15) in the magnetic and non-magnetic fractions are like what was observed in the rougher magnet runs and behavior of the mineral components under the magnetic forces is like the rougher magnetic separation behaviour.

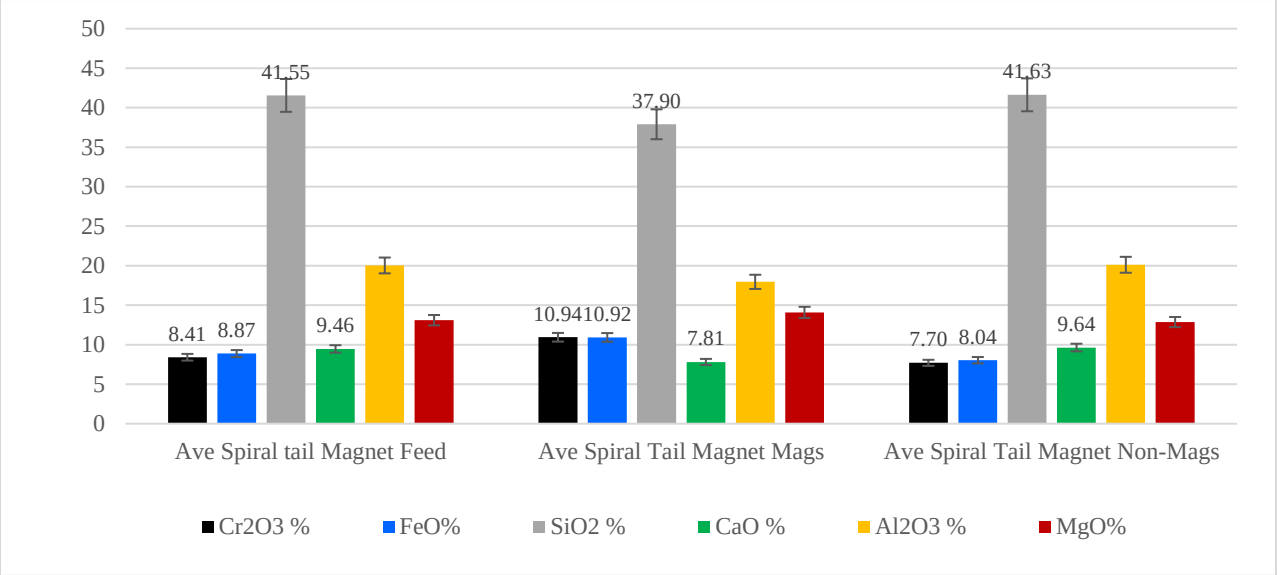

Figure 7.15: Concentration of major oxides in the Spiral Tailings magnet streams

7.2.4 Spiral Middlings Scavenger magnetic separation analysis.

The scavenger magnetic separation run was performed to determine the potential to recover more chrome from the non-magnetic fraction of the rougher magnetic run. The conditions under which this run was performed are like the tailings magnet run. (Slurry density-1.38t/m3, Slurry feed rate -0.81t/h, Belt speed-0.5m/s and Fluidization water-74.5ml/s).

Table 7.10 and Figure 7.16 show the separation achievement of the scavenger magnet. The chrome was reduced from 7.55% in the feed down to 6.97% in the non-magnetic fraction with the magnetic fraction upgrading to 11.03%. FeO and MgO also show the same trends while SiO_2, CaO and Al_2O_3 all show downgrade in the magnetic fraction.

Table 7.10: Yield, Recovery and Assays for major oxides for Spiral Tailings magnetic separation

Stream name	% Mass Yield	% Cr_2O_3 Recovery	Cr_2O_3 %	FeO%	SiO_2 %	CaO %	Al_2O_3 %	MgO %
Ave Scavenger Magnet Feed			7.55	8.12	42.215	9.52	20.04	12.63
Ave Scavenger Magnet Mags	18.14	25.96	11.03	10.49	38.130	7.95	18.20	13.94
Ave Scavenger Magnet Non-Mags	81.86	74.04	6.97	7.54	42.727	9.96	20.56	12.32

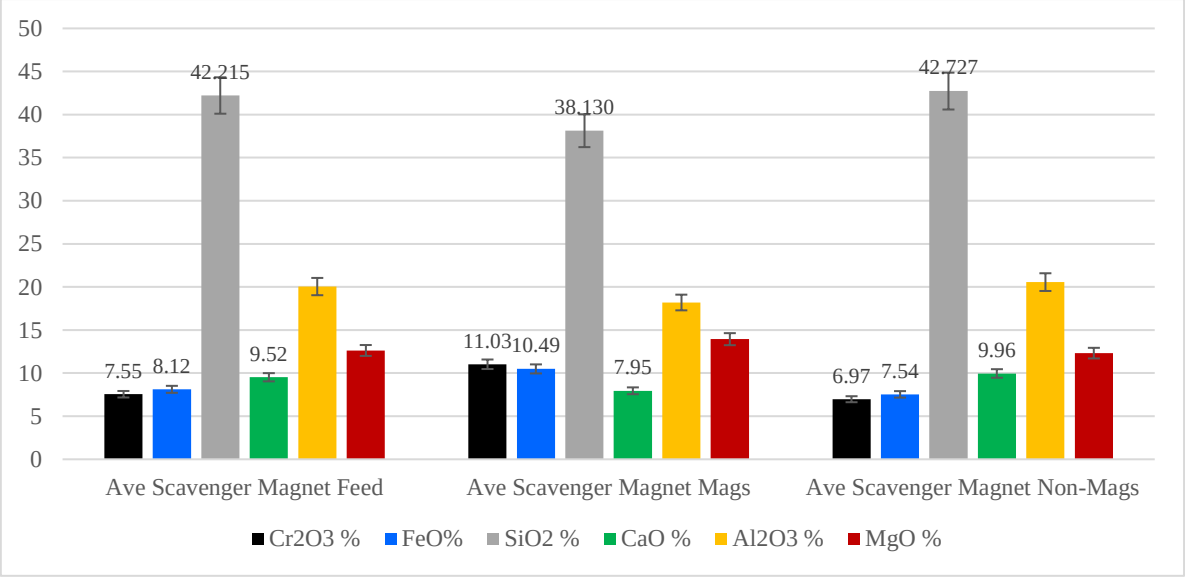

Figure 7.16: Concentration of main oxides, in the Scavenger magnet streams

7.2.5 Spiral Concentrate Shaking table separation analysis.

The following section presents the Spiral concentrate shaking table experimental runs. The conditions on the shaking table were determined from the Taguchi and the Design Expert model data. The table (7.11) gives the shaking table conditions predicted and chosen for the final shaking table runs. The final settings on the shaking table were determined after a few iterations with slight changes in the "easy-to-change" cutter positions for concentrate and middlings. The slurry density and feed rate, wash water and angle were not changed during the iterations. The final set-points were, slurry density-1.34 t/m^3, slurry feed rate- 0.014 t/h (500ml/min), wash water – 140ml/sec and deck angle -4^o.

Table 7.11: Shaking table conditions for running the Spiral concentrates

Shaking Table Input Factors	Taguchi Model	Design Expert Model	Final Condition Set Chosen
Slurry Density (t/m^3)	1.34	1.34	1.34
Slurry Flowrate (t/h)	0.0135	0.014	0.014
Deck Angle (^{o})	4	2	4
Wash water (ml/sec)	140	140	140

The results of shaking table experimental runs under the conditions presented in Table 7.11 are presented in Table 7.12 below. The variables that were adjusted are the concentrate and tailings

cutter positions changed to attain desired grade while at the same time focusing on maximizing concentrate yield. The concentrate grade was determined by visually checking the colour of the concentrate stream and adjusting accordingly for ultrafine chrome recovery. The colour difference between a concentrate on specification and that off-specification is an exceptionally fine line making it difficult to cut on grade.

Table 7.12: Shaking table runs Yield and Recovery performance

Stream Name	% Mass Yield	% Cr_2O_3-Recovery	Cr_2O_3 %	FeO%	SiO_2 %	CaO %	Al_2O_3 %	MgO%
Shaking table Feed			17.11	15.86	34.69	6.00	16.01	15.88
Shaking table Conc	22.28	52.92	41.24	27.62	7.51	1.27	16.11	12.88
Shaking Table Middlings	42.16	28.46	11.79	12.08	38.78	8.41	18.3	13.9
Shaking Table Tails	35.56	18.62	9.11	9.96	40.82	8.58	17	14.01

Figure 7.17 shows the relationship between yield, recovery, and grade of the concentrate of the shaking table experimental run on the spiral concentrate. From Figure 7.17and Table 7.12 it is seen that there is 52.92% recovery of chrome into 22.28% mass of the concentrate at a grade of 41.15% Cr_2O_3. The middlings mass yield was 42.16% with a chrome recovery of 28.46% while the tailings stream mass yield was 35.56% with a chrome recovery of 18.62%. It is critical that close attention be paid to the concentrate-middling interface to avoid taking high grade chrome to the middlings resulting in low yield to the concentrate. Equally, the interface between the middlings and tailings needs to be accurately determined to avoid losing chrome to the tailings.

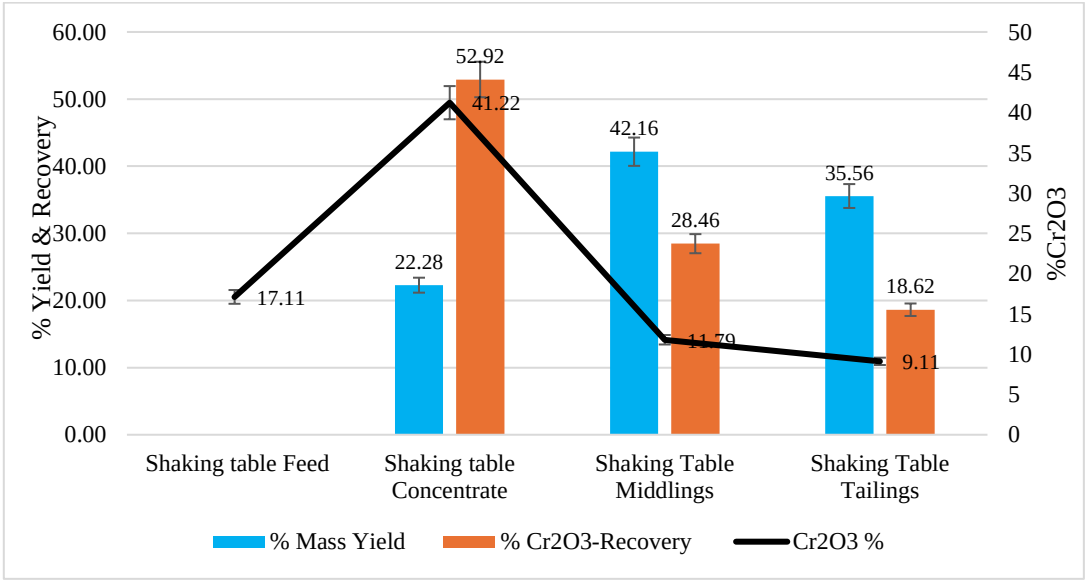

Figure 7.17: Shaking Table streams mass yield & recovery with concentrate grade

The behaviour of the high-density oxides (Cr_2O_3, FeO and MgO) on the shaking table is different from how they behaved on the spiral separator. On the spiral, the Cr_2O_3, FeO and MgO upgraded into the concentrate while CaO, Al_2O_3 and SiO_2 downgraded. The shaking table results show a different behaviour of the MgO oxide in that only Cr_2O_3 and FeO were upgrading into the concentrate while the rest of the oxides were downgrading into the concentrate. Figure 7.18 shows the trends of high-density oxides (Cr_2O_3, FeO and MgO) during separation on the shaking table. Of these three oxides, MgO downgraded from feed to concentrate showing that the shaking table had a more effective separation effect than the spirals and magnetic separators. The explanation to this different behaviour on spirals and shaking could be the difference between vertical and horizontal stratification phenomenon during separation. On the shaking table the vertical stratification is more pronounced than the horizontal whereas on the spiral it is the opposite. Due to the difference in density between MgO host minerals and the Cr_2O_3 & FeO host mineral, the MgO host mineral rises to the top of the strata where it is exposed to flowing film of wash-water and then gets washed immediately resulting in more effective separation. In the spiral and magnetic separators, the horizontal stratification does not fully develop as the flowing film mixes the stream as it moves from the inner part of spiral to the outside and this process partly destroy separation profile as the chrome stream flows down the spital helix.

Figure 7.19 shows the changes in low density oxides (Al_2O_3 SiO_2 and CaO) as the spiral concentrate is processed on the shaking table, CaO and SiO_2 showed a significant downgrade compared to Al_2O_3. This means that MgO and Al_2O_3 were not rejected from the concentrate as much as SiO_2 and CaO were. This shows that the shaking table selectively cleaned out SiO_2 and CaO from the shaking table feed producing concentrate low in SiO_2 and Cao. The marginal downgrade of Al_2O_3 from feed to concentrate shows that the mineral component (Chlorite) that hosts Al_2O_3 has higher density (2.8t/m^3) than that of Feldspar (2.6t/m^3) which hosts SiO_2 limiting the chances of Al_2O_3 being separated easily to the top layer of strata. This scenario makes the downgrade of Al_2O_3 difficult on the shaking table.

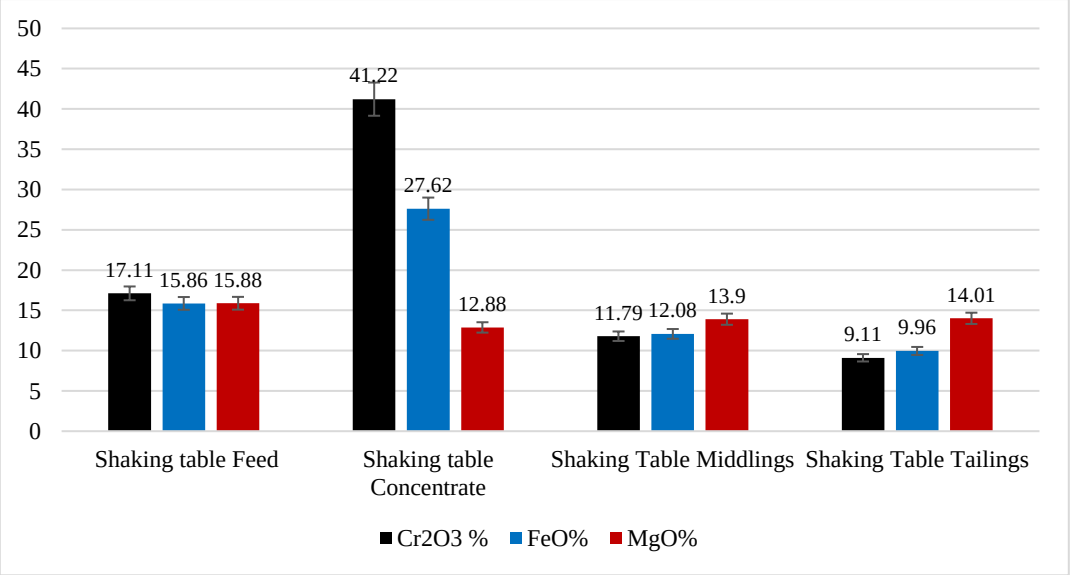

Figure 7.18: Cr_2O_3, FeO and MgO changes between Shaking table feed and products

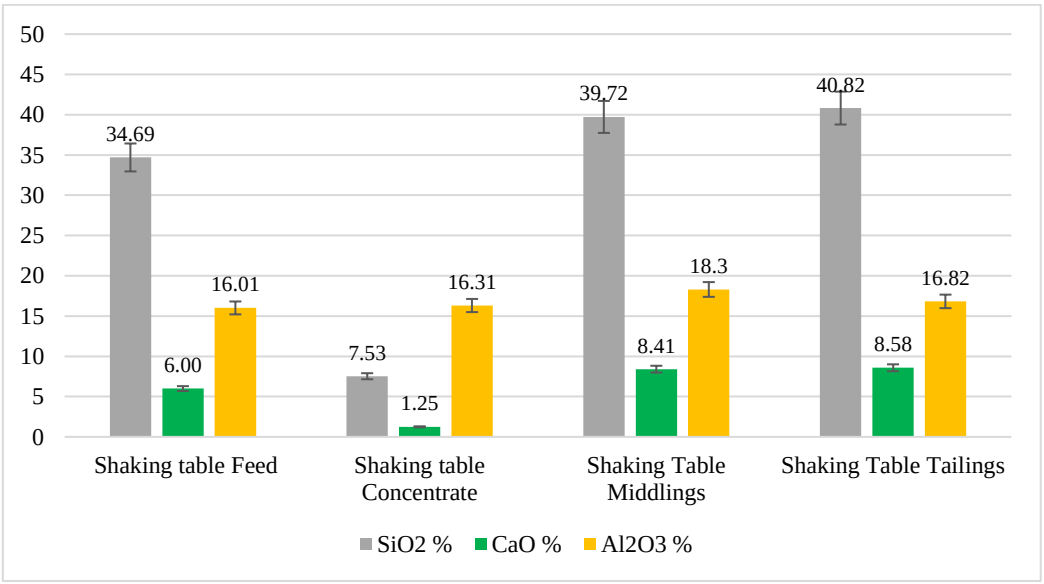

Figure 7.19: SiO_2, Al_2O_3 and CaO changes between Shaking table feed and products

7.2.6 Rougher Magnet concentrate Shaking table separation analysis.

The magnetic fraction from the rougher magnet separation was sent to the shaking table for upgrading to the final product. The slurry density was adjusted to 1.34t/m3 and the slurry feed

rate was set at 0.014t/h (500ml/min wet slurry). The angle and wash water were set at 4° and 140ml/sec respectively as shown in the table below.

Table 7.13: Shaking table input factors for concentrating Rougher Magnet concentrate

Shaking Table Input Factors	Taguchi Model	Design Expert Model	Final Condition Set Chosen
Slurry Density (t/m^3)	1.34	1.34	1.34
Slurry Flowrate (t/h)	0.0135	0.014	0.014
Deck Angle (°)	4	2	4
Wash water (ml/sec)	140	140	140

The feed to the shaking table was 20.24% Cr_2O_3 and it was upgraded to 41.95% in the shaking table concentrate. The downgrade of the SiO_2 and CaO in the concentrate is worth mentioning here. SiO2 changes from 30.72% in the feed to 2.55% in the concentrate while CaO also changes from 4.60% in the feed to 0.57% in the concentrate as shown in Table 7.14 and Figure 7.21 below. This behaviour is like that of a spiral concentrate concentrated on the shaking table.

The Al_2O_3 upgrades from 13.13% in the feed to 16.90% in the concentrate and MgO downgrades from 16.28% in the feed to 10.00% in the concentrate. From this trend it shows that for shaking table concentration, Cr_2O_3, FeO and Al_2O_3 increase in the concentration in the concentrate while SiO_2, CaO and MgO decrease.

Table 7.14: Shaking table Yield and Recovery for Rougher Magnet concentrate

Stream name	% Mass Yield	% Cr_2O_3 Recovery	Cr_2O_3 (%)	FeO%	SiO_2 %	CaO %	Al_2O_3 %	MgO %
Ave Shaking Table Feed			20.24	16.56	30.72	4.60	13.13	16.28
Ave Shaking Table Concentrate	10.20	24.31	41.95	27.43	2.55	0.57	16.90	10.00
Ave Shaking Table Middlings	68.89	58.26	14.92	15.73	34.48	4.72	12.24	17.65
Ave Shaking Table Tailings	20.91	17.42	14.83	15.23	35.03	7.70	17.09	15.31

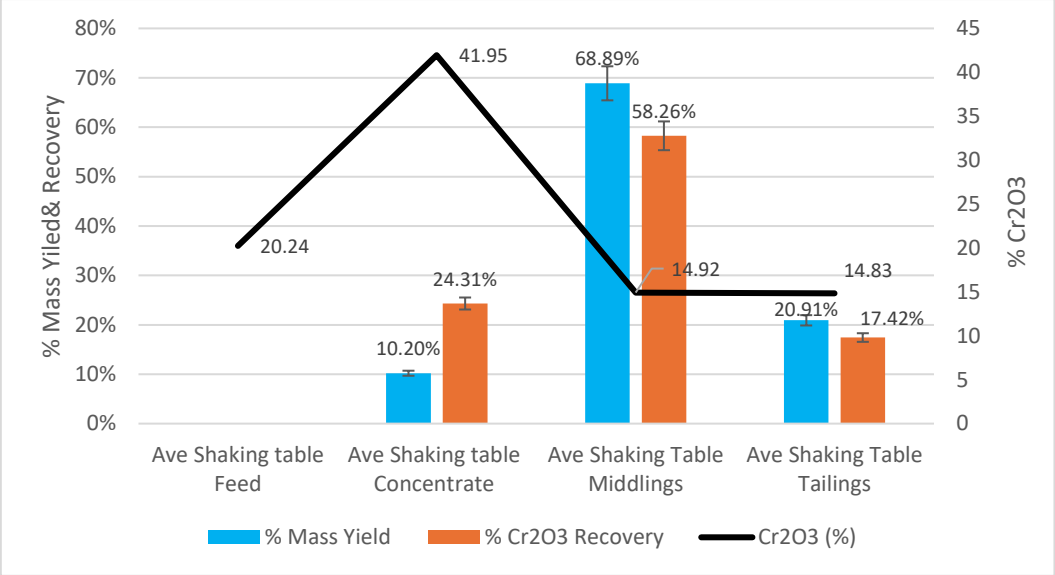

Figure 7.20: Spiral Yield, Recovery and Cr grades of Rougher magnet concentrate shaking table product streams

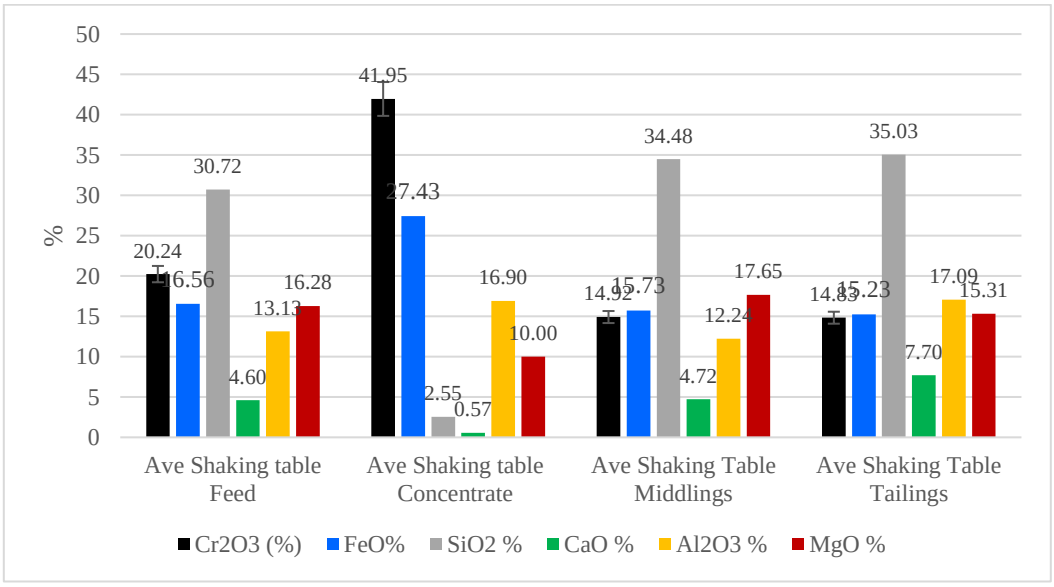

Figure 7.21: Concentration of main oxides, in the rougher magnet concentrate shaking table streams

7.2.7 Scavenger magnet concentrate shaking table separation analysis.

The scavenger magnet concentrate was also treated on the shaking table under the same settings to get the highest possible final product. The yield and recovery on the shaking table is given

in Figure 7.22 and Table 7.15 below. One very prominent trend on the mass distribution across the shaking table products is that about 30% of the mass goes to middlings while 63% goes to tailings. In terms of recovery of the Cr_2O_3, only 15% is recovered into the concentrate while 26% and 58% is distributed into middlings and tailings, respectively. The reason for this trend is that the Scavenger magnet concentrate is mainly constituted of ultrafine particles that were rejected in the rougher magnet non-magnetic stream. The final concentrate for this scavenger shaking table run did not reach the target grade of 40%±1.50% as shown in Table 7.15 and Figure 7.23 below. It only could get to 25.27% Cr_2O_3. Also, the silica downgrade was exceptionally low (41.83% to 26.28%) as compared to that observed in other shaking runs involving coarse particles. CaO is the only oxide that had a significant downgrade from 24.39% to 2.64% in the concentrate.

Table 7.15: Shaking table Yield and Recovery for Scavenger Magnet concentrate

Stream Name	% Mass Yield	% Cr_2O_3 Rec	Cr_2O_3 (%)	FeO%	SiO_2 %	CaO %	Al_2O_3 %	MgO %
Ave Shaking table Feed			11.30	10.38	41.83	12.34	24.39	16.20
Ave Shaking table Concentrate	7.81	15.36	25.27	20.26	26.28	2.64	12.20	19.51
Ave Shaking Table Middlings	29.06	26.52	11.73	11.26	40.78	12.28	23.09	17.09
Ave Shaking Table Tailings	63.13	58.28	11.86	11.23	39.60	10.79	21.86	15.04

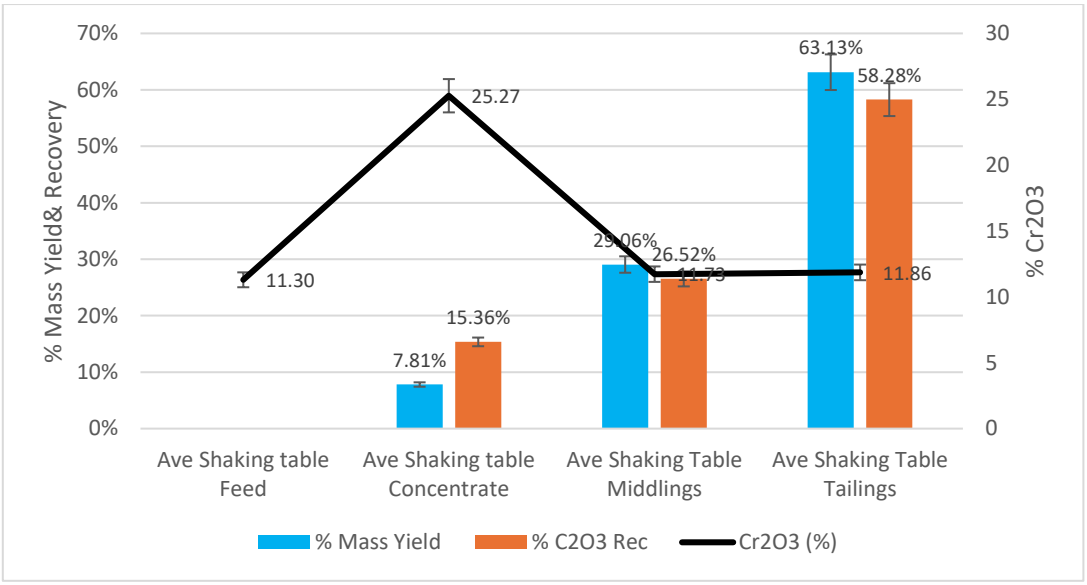

Figure 7.22: Spiral Yield, Recovery and Cr grades of Scavenger magnet concentrate shaking table product streams

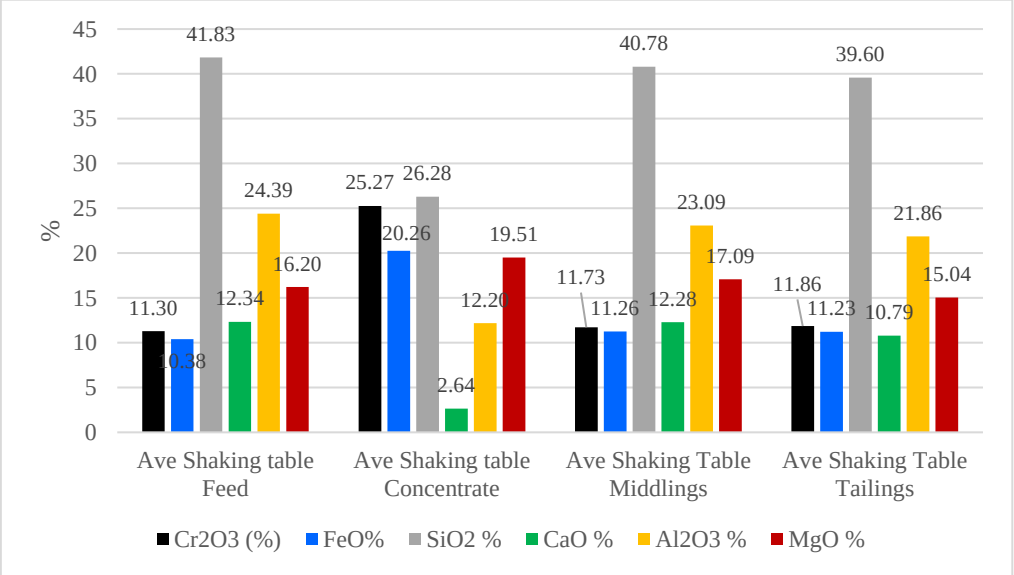

Figure 7.23: Concentration of main oxides, in the Scavenger magnet concentrate shaking table streams

7.2.8 Spiral Tailings magnet concentrate shaking table separation analysis.

The spiral tailings stream that was subjected to magnetic separation produced a magnetic concentrate of chrome grade 10.77%. This concentrate was run on the shaking table and the

products are given in Table 7.16 below. From the particle size distribution done on spiral streams, the spiral tailings it was determined that 80% of the particles are below 38µm. This material was run on the magnet and the concentrate from magnetic separation then processed on the shaking table to produce these results. Only 8.30% of mass was collected into the concentrate at a chrome grade of 35.09%. The bulk of the mass reported to tailings (58.83%) and the balance to middling. In terms of recovery, 24.45% recovered to concentrate with 53.86% recovered to tailings as depicted in figures 7.24 and 7.25.

The SiO_2 did decrease from 41.54% to 15.59% but was not enough to boost the concentrate grade. This is the reason the shaking table concentrate grade did not reach the target grade. Only CaO decreased significantly from 11.00% to 1.90% in the concentrate. Al_2O_3 in this run did decrease significantly from 23.30% to 14.90%. MgO remained fairly stable in the streams meaning that it did not significantly downgrade to assist with pushing the concentrate grade up.

Table 7.16: Shaking table Yield and Recovery for Spiral Tailings magnet concentrate

Stream Name	% Mass Yield	% Cr_2O_3 Recovery	Cr_2O_3 %	FeO%	SiO_2 %	CaO %	Al_2O_3 %	MgO%
Ave Shaking Table Feed			10.77	10.53	41.54	11.00	23.30	15.97
Ave Shaking Table Concentrate	8.30	24.45	35.09	22.55	15.59	1.90	14.90	16.75
Ave Shaking Table Middlings	32.87	21.68	7.85	9.59	44.72	8.98	18.23	16.43
Ave Shaking Table Tailings	58.83	53.86	10.92	10.67	41.30	10.08	21.96	14.75

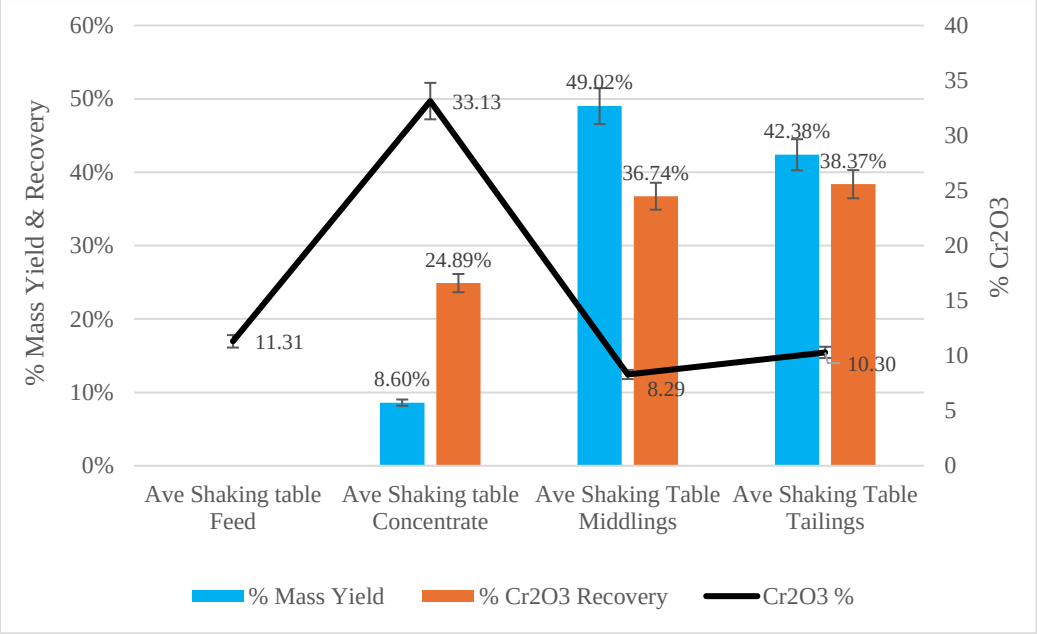

Figure 7.24: Spiral Yield, Recovery and Cr grades of Spital Tailings magnet concentrate shaking table product streams

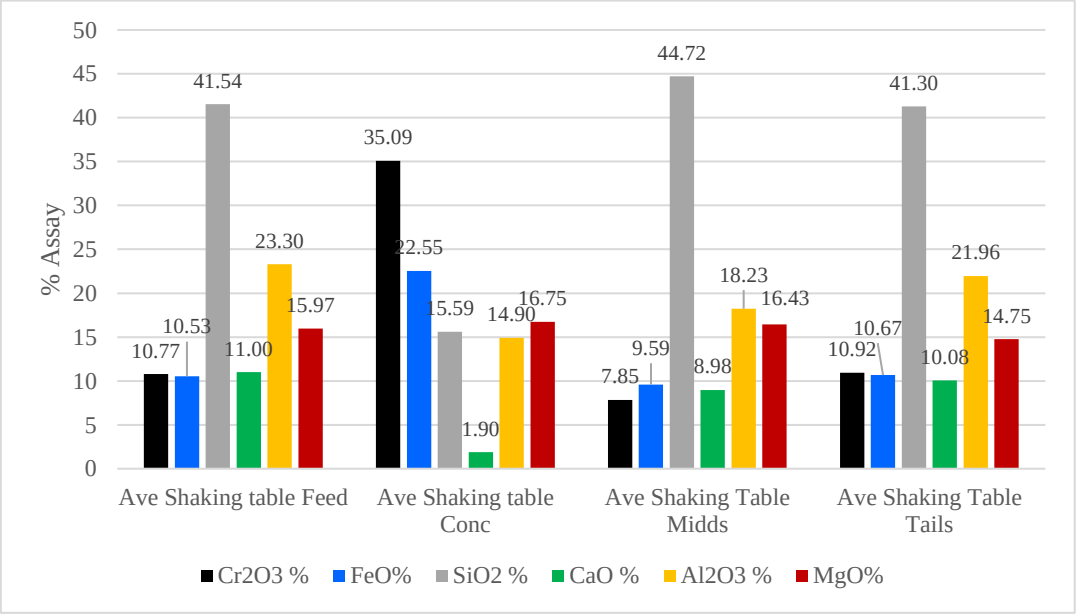

Figure 7.25: Concentration of main oxides, in the Spiral Tailings magnet concentrate shaking table streams

7.2.9 Shaking table middlings Re-cleaner separation analysis

During the running of the Spiral concentrate shaking table tests, the middlings were collected for trial re-cleaning tests on the shaking table. Table 7.17 below gives feed, products and yield

and recovery numbers for the re-cleaning tests. The grade of the concentrate attained was 38% Cr_2O_3. Al_2O_3 and MgO did not change between the streams, but SiO_2 and CaO downgraded significantly, and this pushed the concentrate grade to 38%. From the graph in Figure 7.26 below, the bulk of the chromite is in the concentrate at 54.49% recovery and mass yield of 15.88%. The bulk of the mass is in the middling totaling 71.67% yield at 33.86% recovery of chrome.

Table 7.17: Shaking table Yield and Recovery for Shaking table middling Re-cleaning

Stream name	% Mass Yield	% Cr_2O_3 Recovery	Cr_2O_3 %	FeO%	SiO_2 %	CaO %	Al_2O_3 %	MgO%
Shaking Table Feed			11.81	14.61	34.25	5.77	15.48	14.93
Shaking table Concentrate	15.88	54.49	37.99	26.54	8.59	0.64	15.19	13.18
Shaking Table Middlings	71.67	33.86	5.23	24.70	12.46	1.88	15.65	12.31
Shaking Table Tailings	12.45	11.65	10.36	10.64	41.08	8.43	18.97	13.17

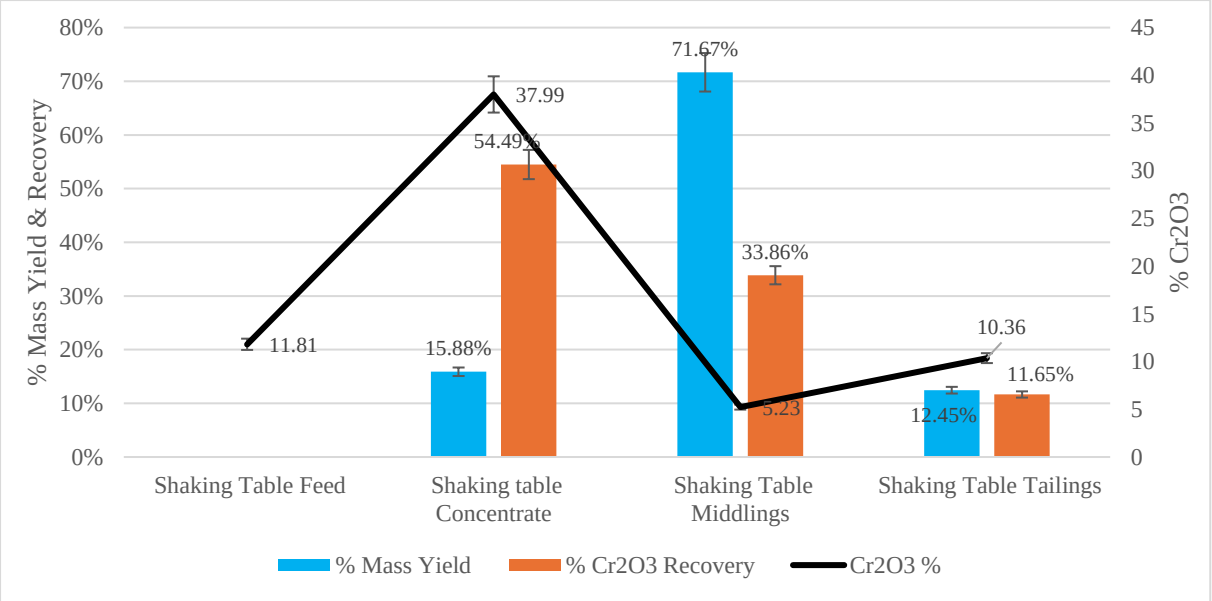

Figure 7.26: Spiral Yield, Recovery and Cr grades of Shaking table Re-cleaning shaking table product streams

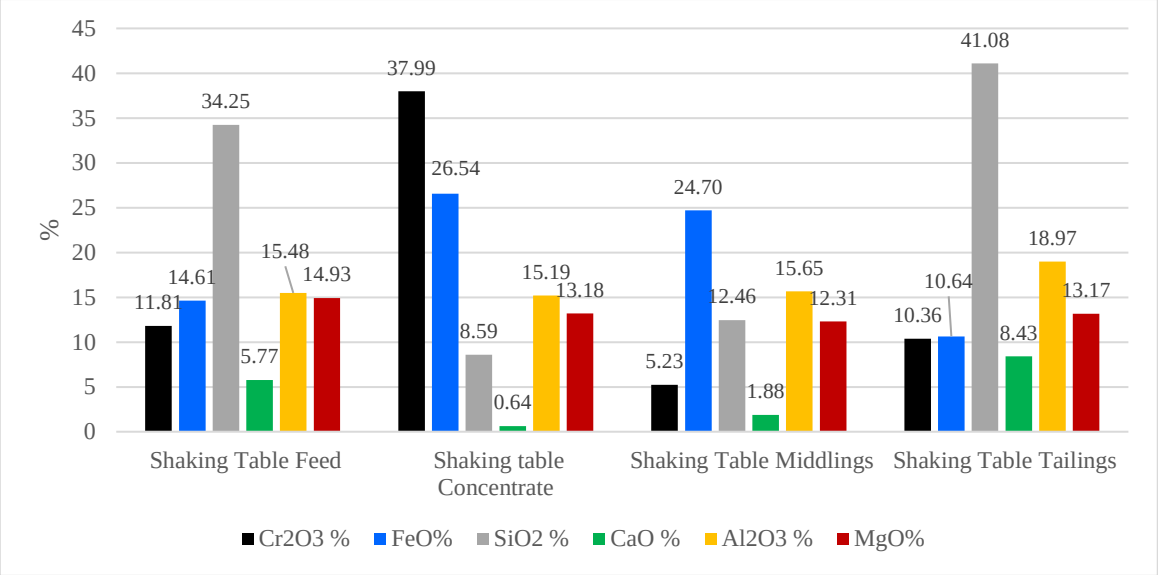

Figure 7.27: Concentration of main oxides, in the Shaking table middling Re-cleaner product streams

7.2.10 Full circuit mass balance

The full circuit mass balance for the spiral, magnet, screen and shaking table is presented in Table 7.18. The key outcomes of the test-work for this circuit are;

The final chromite product on target grade is from spiral concentrate and rougher magnet concentrate.

The chromite concentrates from spiral tailing magnetic fraction and scavenger magnetic fraction both did not reach the target chrome grade of 40% hence those streams are sent to tailings.

The Overall Recovery achieved of the circuit was 19.01%.

The achieved Overall Mass Yield of the circuit was 5.81%.

The combined final grade of the concentrate was 40.59% Cr_2O_3.

The tailings grade for the circuit was 8.52% Cr_2O_3.

Table 7.18: Full circuit mass balance for Spiral, Magnet, Screen and Shaking table units

	Spiral				Screen						Spiral Conc Shaking Table				Mids Re-cleaner Shaking Table			
Stream	Feed	Conc	Mids	Tails	Feed	O/S	U/S				Feed	Conc	Mids	tails	Feed	Conc	Middlings	Tailings
Grade	10.68	14.41	8.97	9.31	14.41	3.08	17.07				17.11	41.24	11.79	9.11	11.79	37.99	5.23	10.36
Section Yield		23.06	48.72	28.22		19	81					22.22	42.2	35.58		15.88	71.67	12.45
Overall Yield		23.06	48.72	28.22		4.38	18.68					4.15	7.88	6.65		1.25	5.65	0.98
Section Recovery		30.56	43.38	26.06		6.88	93.12					53.07	28.35	18.58		24.31	58.26	17.43
Overall Recovery		30.56	43.38	26.06		2.10	28.46					15.10	8.07	5.29		1.96	4.70	1.41
Cr Units		3.32	4.37	2.63		0.13	3.19					1.71	0.93	0.61		0.48	0.30	0.10
					Middlings Magnet						Middling Mag Shaking Table							
Stream					Feed	Mags	N/Mags				Feed	Conc	Mids	tails				
Grade					8.97	20.26	7.89				20.26	41.95	14.92	15.83				
Section Yield						8.24	91.76					10.2	68.89	20.91				
Overall Yield						4.01	44.71					0.41	2.77	0.84				
Section Recovery						18.44	81.56					24.31	58.26	17.43				
Overall Recovery						8.00	35.38					1.94	4.66	1.39				
Cr Units						0.81	3.53					0.17	0.41	0.13				
								Scavenger Magnet			Scavenger Shaking Table							
Stream								Feed	Mags	N/Mags	Feed	Conc	Mids	tails				
Grade								7.89	11.03	6.97	11.03	28.41	9.51	9.98				
Section Yield									18.14	81.86		7.28	61.81	30.91				
Overall Yield									8.11	36.60		0.59	5.01	2.51				
Section Recovery									25.93	74.07		12.51	35.55	51.94				
Overall Recovery									9.17	26.21		1.15	3.26	4.77				
Cr Units									0.89	2.55		0.17	0.48	0.25				
					Tailings Magnet						Tailings Mags Shaking Table							
Stream					Feed	Mags	N/Mags				Feed	Conc	Mids	tails	Feed Grade			10.68
Grade					9.31	10.94	7.7				10.94	31.17	8.73	9.67	Conc Yield			5.81
Section Yield						17.11	82.89					8.89	65.17	25.94	Conc Recovery			19.01%
Overall Yield						4.83	23.39					0.43	3.15	1.25	Conc Grade			40.59%
Section Recovery						22.68	77.32					25.36	51.77	22.87	Tails Grade			8.52%
Overall Recovery						5.91	20.15					1.50	3.06	1.35				
Cr Units						0.53	1.80					0.13	0.27	0.12				

7.3 Full circuit Configuration 2 analysis – Screen - Spiral-Magnet-Screen-Shaking Table.

The second circuit configuration proposed is depicted in Figure 7.28. In this configuration, the feed material was first screened on a 25µm screen to produce two size fractions, the +25µm and -25µm. These two size fractions were fed separately to the spiral separator to produce three products each and the stream with highest grade was then treated on the shaking table to produce a final product.

The purpose of the first screen was to separate the feed into fine (+25µm) and ultra fine particles (-25µm) to reduce the particle size-density effect during the gravity separation of the spiral and shaking table. The second screen was used on the spiral concentrate stream to remove the +106µm particles before feeding onto the shaking table. From the mineralogical analysis of the feed material, it was observed that particles larger than 106µm do not contain significant amount of chrome due to poor liberation at this particle size. Removing the +106µm size fraction has two benefits for the separation process. The first benefit is that removing coarse particles ensures better separation efficiency due to near-size effect. The second benefit is that removing about 20% of the mass means that there is extra capacity created for the downstream unit and this will improve efficiency.

7.3.1 Feed Screening on 25 µm Screen.

The screening of the feed stream on the 25 µm screen produced two fractions and the mass yield and recovery of each stream is given in Table 7.19 below.

Table 7.19: Fractional analysis of the 25 µm screen products

Stream Name	% Mass Yield	% Cr_2O_3 Recovery	Cr_2O_3 %
Feed stream			8.26
-25 µm Fraction	41.18	46.71	9.38
+25 µm Fraction	58.82	53.29	7.49

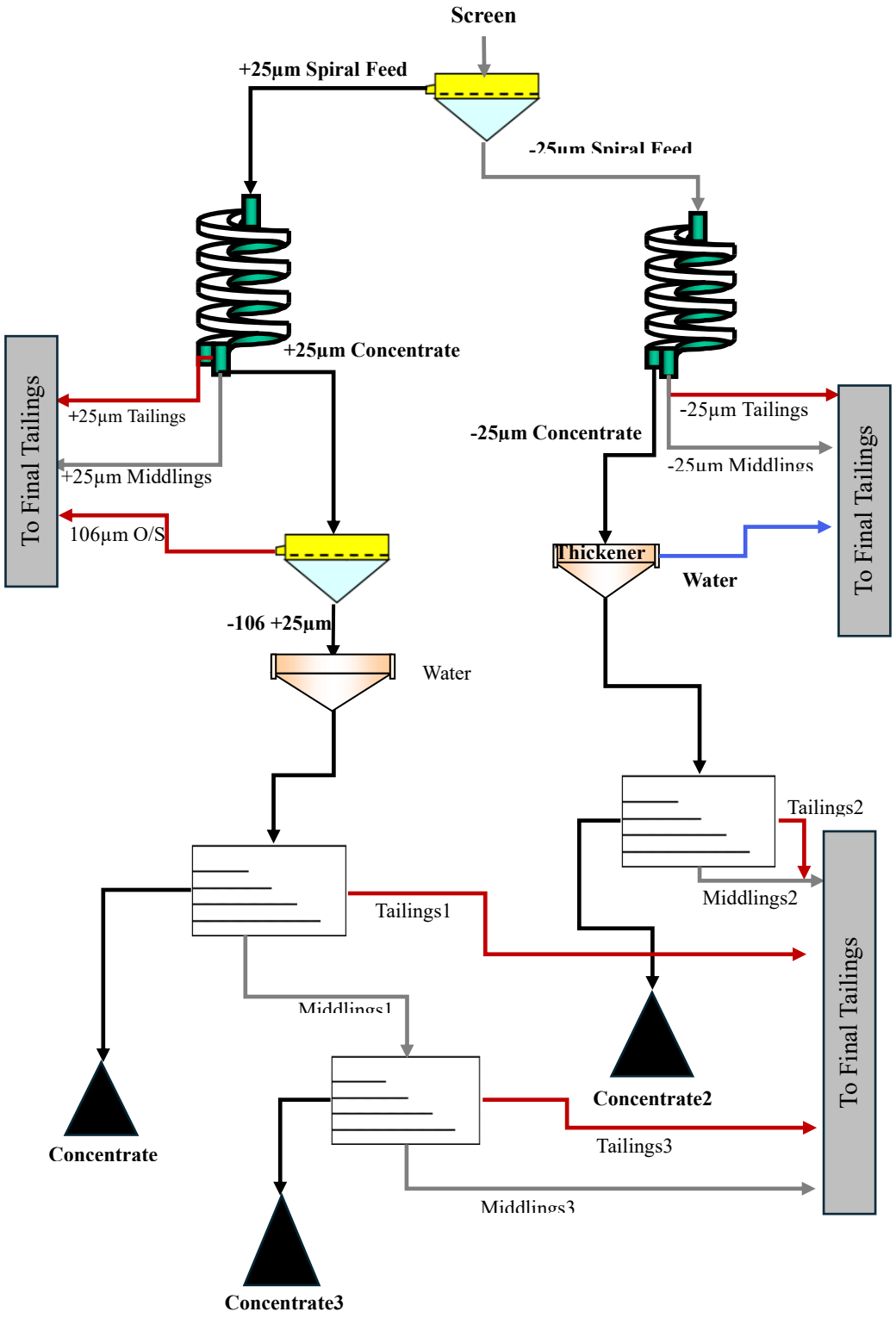

Figure 7.28: Circuit configuration of Screen, Spiral, Screen and Shaking table

From the Table 7.20, the +25µm size fraction contains more mass and chrome units than the -25 µm size fraction but the grade of the -25 µm fraction is higher than the +25 µm size fraction.

7.3.2 Spiral Separation -+25µm fraction.

The spiral separation of the +25µm fraction produced a concentrate grade that was not remarkably high because the recovery of the chromite in the concentrate stream was exceedingly high compared to other spiral runs conducted before. Looking at the partitioning of the main oxides between the three product streams, Cr_2O_3, FeO and MgO upgraded into the concentrate while the other three oxides downgraded (Figure 7.30). This is expected due to the density effects on gravity separation.

The mass yield and recovery into the concentrate showed that 50.42% of the feed reported to the concentrate at a grade of 12.49% giving a recovery of 76.27%. An interesting observation is that the middlings and tailings chrome grades are both below 4%. This shows significant selectivity in terms of chrome separation.

Table 7.20: Spiral Yield, Recovery and Cr grades of spiral separation product streams

Stream Name	% Mass Yield	% Cr_2O_3 Recovery	Cr_2O_3 %	FeO%	SiO_2 %	CaO %	Al_2O_3 %	MgO %
Spiral Feed			7.49	9.47	46.3	9.38	19.74	15.56
Spiral Concentrate	50.42	76.27	12.49	12.93	40.5	6.68	15.92	17.65
Spiral Middlings	31.42	15.12	3.56	7.34	50.1	10.97	21.46	13.96
Spiral Tailings	23.36	8.62	2.71	5.65	51.3	12.00	23.80	12.38

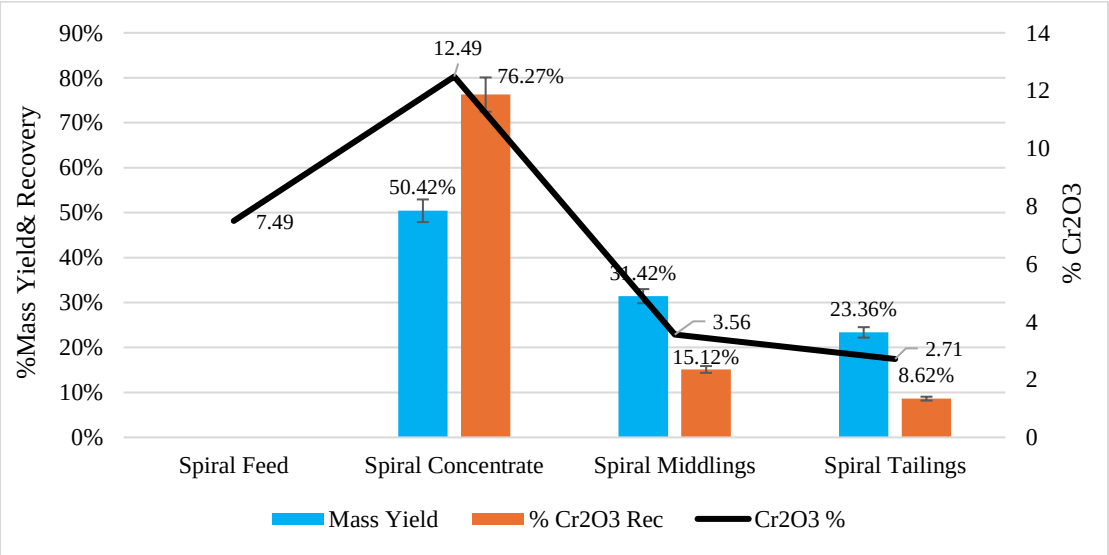

Figure 7.29: Spiral Yield, Recovery and Cr grades of product streams

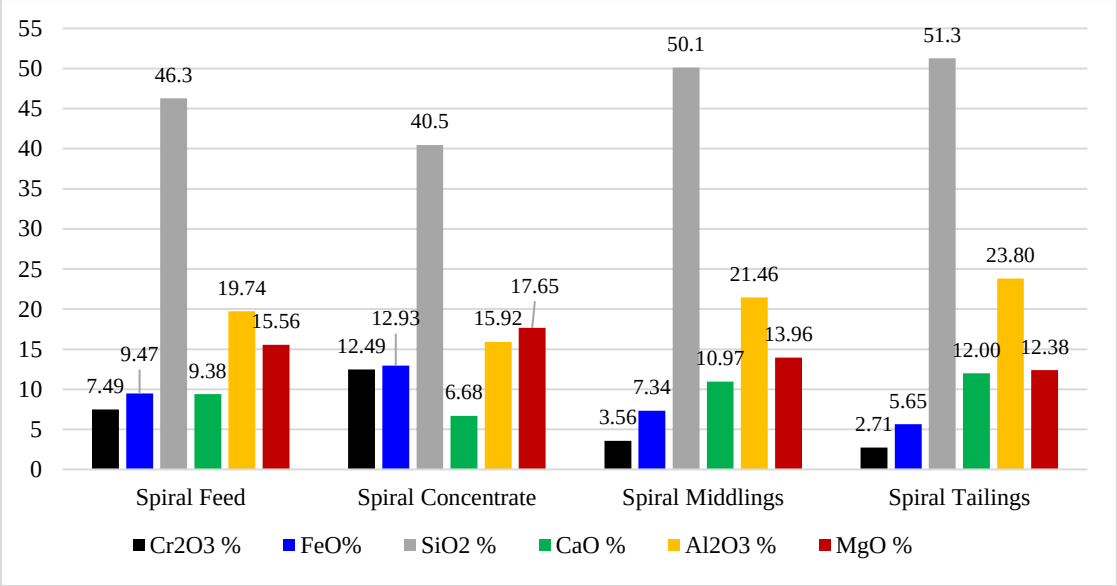

Figure 7.30: Concentration of main oxides, in the Spiral product streams

7.3.3 Spiral Concentrate Shaking table separation.

The screening of the spirals concentrate stream only resulted in a marginal increase in grade from 12.49% to 13.41% Cr_2O_3 as shown in Table 7.21. In terms of mass reduction, 19.20 % was removed from the concentrate before feeding to the shaking table. This mass reduction also resulted in chrome losses of 13.25% in the oversize with a grade of 8.60% Cr_2O_3. The CaO and SiO_2 are oxides which were preferentially removed from the concentrate while Al_2O_3 did not show meaningful change. MgO downgraded a bit from 16.86% to 11.52% in the concentrate as shown in Figures 7.31 and 7.32. Compared to the other shaking table runs before, this shaking table feed did not have slimes because of the elimination of the -25µm particles. The final concentrate reached the target grade of 40% and the recovery was also significantly high. With the middlings at 33.79% recovery, the selectivity of the shaking table on the feed was not as sharp as the spiral separation process.

Table 7.21: Recovery and Mass Yield on 106µm screen

Stream Name	**% Mass Yield**	**% Cr_2O_3 Recovery**	**Cr_2O_3 %**
106 µm Screen Feed.			12.49
-106µm fraction.	80.80	86.75	13.41
+106µm fraction.	19.20	13.25	8.60

Table 7.22: Shaking table Yield, Recovery and Cr grades of spiral concentrate separation

Stream Name	% Mass Yield	% Cr_2O_3 Rec	Cr_2O_3%	FeO%	SiO_2%	CaO%	Al_2O_3%	MgO%
+25 Shaking Table Feed			13.41	12.83	37.40	13.07	17.18	16.86
+25 Shaking Table Concentrate	17.03	55.37	41.52	26.69	2.28	0.91	17.68	11.52
+25 Shaking Table Middlings	50.67	33.79	8.52	11.23	43.98	14.53	14.62	20.58
+25 Shaking Table Tailings	32.30	10.84	4.29	6.73	47.23	18.04	21.91	13.59

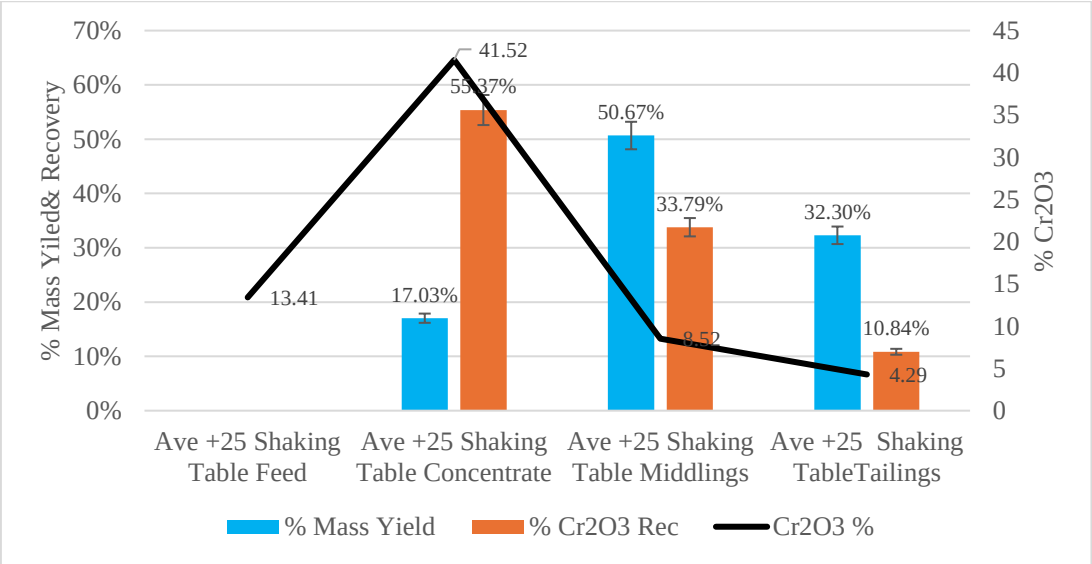

Figure 7.31: Shaking table Yield, Recovery and Cr grades of product streams

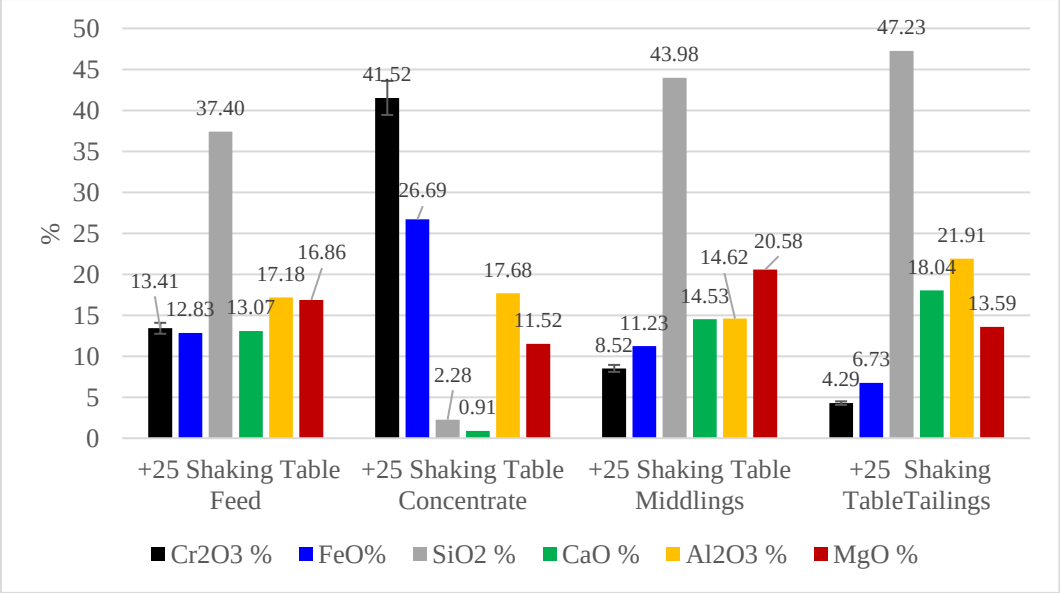

Figure 7.32: Concentration of main oxides, in the Shaking table product streams

7.3.4 Shaking Table Middling Re-cleaning.

When the shaking table runs were made, a middling sample was collected for further processing on the shaking table to determine the amenability of this fraction to separation on the shaking table. The conditions were maintained the same as those for the rougher shaking table separation. One striking feature of this experiment was that the shaking table feed-grade was exceptionally low in comparison to the spiral concentrate or magnet concentrate streams normally fed to the shaking table. However, the upgrade experienced on this run was exceptionally high at 4.49. The tailings grade was also exceptionally low (3.65% Cr_2O_3) meaning that the losses to the tailings were low. Table 7.23 and Figures 7.33 and 7.34 show the mass yield and recovery numbers for this test. Even though the final grade was remarkably close to 40%, the recovery to both concentrate and middlings was equal. This showed that the separation efficiency was low but the recovery of the Cr_2O_3 to the concentrate was almost 50%. The levels of CaO and SiO_2 were almost reduced to zero, but Al_2O_3 and MgO did not change significantly.

Table 7.23: Shaking table Yield, Recovery and Cr grades for Middlings Re-cleaner separation

Stream Name	% Mass Yield	% Cr Rec	Cr_2O_3 %	FeO %	SiO_2 %	CaO %	Al_2O_3 %	MgO %
+25µm Recleaner Feed			8.86	12.14	35.09	5.96	14.75	14.77
+25µm Recleaner Concentrate	15.34%	46.60%	39.75	24.93	0.15	0.37	15.20	9.85
+25µm Recleaner Middlings	61.35%	46.90%	10.00	9.46	43.86	6.84	13.44	17.76
+25µm Recleaner Tailings	23.31%	6.15%	3.65	4.90	47.85	11.20	20.51	11.78

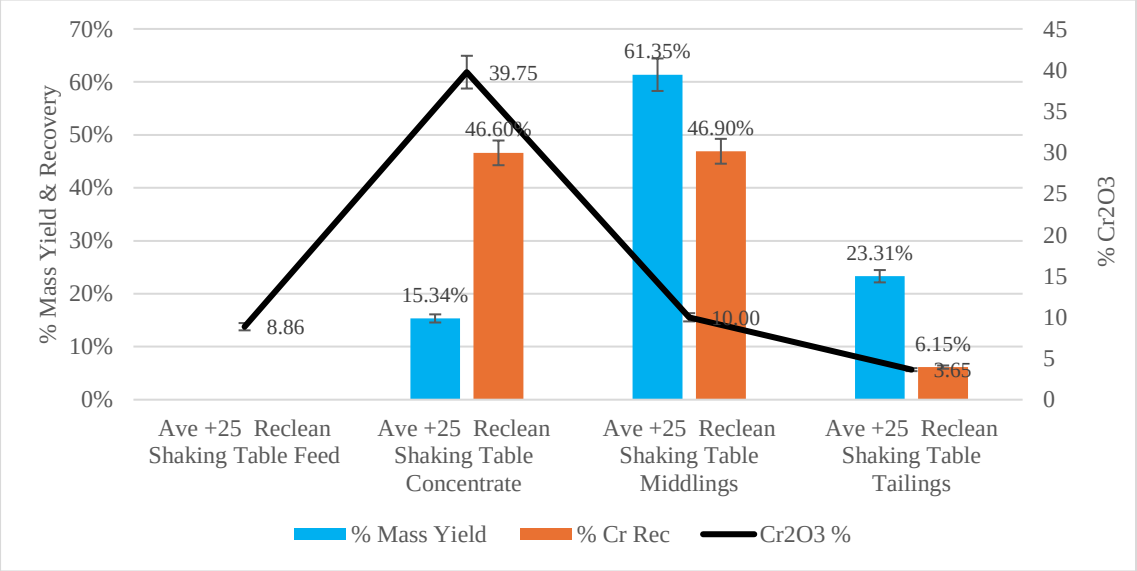

Figure 7.33: Re-cleaner Shaking table Yield, Recovery and Cr grades of product streams

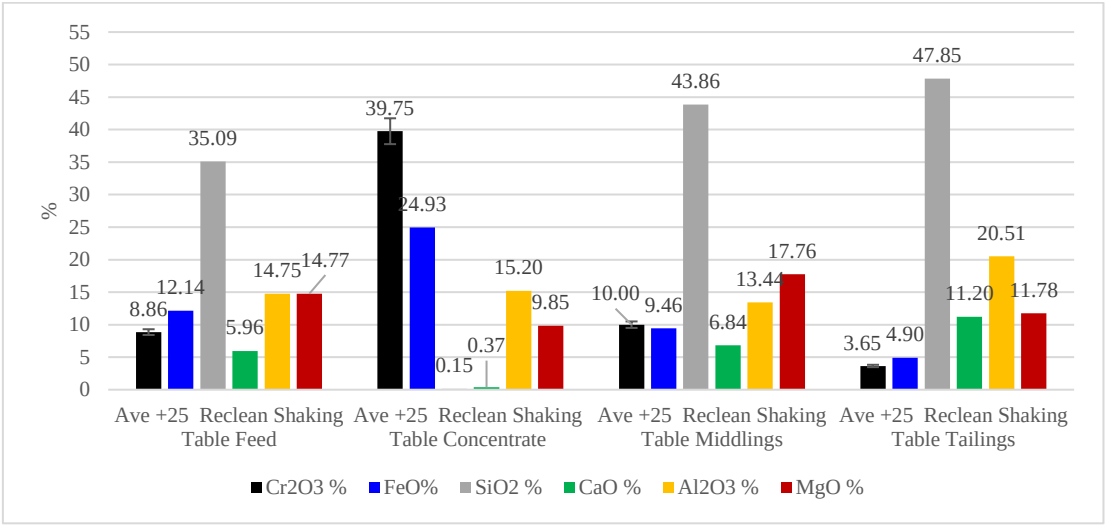

Figure 7.34: Concentration of main oxides, in the Shaking table Re-cleaner product streams

7.3.5 Spiral Separation - 25µm Fraction.

The undersize of the 25µm screen product was prepared for spiral separation by adjusting the slurry density to 1.34kg/L. This was the density observed to get optimum separation on the spiral trough. Because of the particle size of the stream, the flow rate was reduced from the 0.76t/h that was used for coarse fraction to 0.150t/h. These conditions were chosen to reduce the effect of hydrodynamic forces on the particles so that gravity forces become more prominent. From Table 7.24, the recovery of chrome into the concentrate stream was 42% while middlings and tailings were 22 and 35%, respectively. In terms of mass yield, the bulk of the feed went to tailings at a grade of only 6.86%. The recovery of chrome into concentrate and tailings shows that separation is difficult as the particle size decrease especially below 25µm.

Table 7.24: Spiral Yield, Recovery and Cr grades for -25µm separation

Stream Name	% Mass Yield	% Cr_2O_3 Rec	Cr_2O_3 %	FeO%	SiO_2 %	CaO %	Al_2O_3 %	MgO %
-25 µm Spiral Feed			9.38	9.20	41.75	8.31	17.94	13.91
-25 µm Spiral Concentrate	26.59	42.17	14.37	11.78	36.38	6.11	14.96	15.19
-25 µm Spiral Middlings	26.90	22.48	7.55	7.49	44.21	9.51	19.12	12.58
-25 µm Spiral Tailing	46.51	35.34	6.86	6.05	44.46	9.98	20.42	11.19

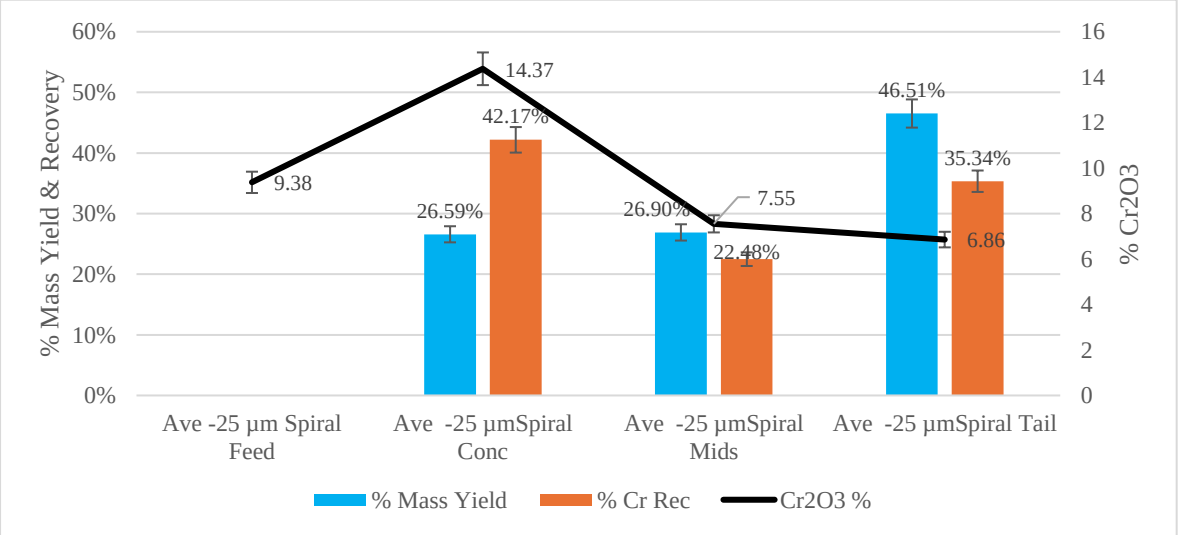

Figure 7.35: -25µm Spiral Yield, Recovery and Cr grades of product streams

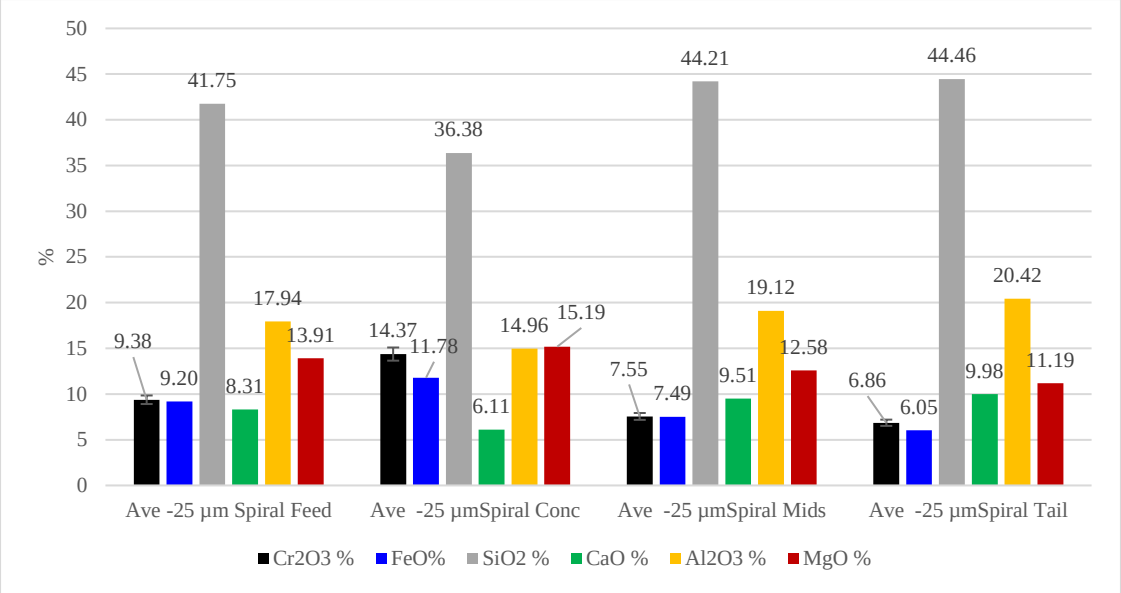

Figure 7.36: Concentration of main oxides, in the -25µm Spiral product streams

7.3.6 Shaking Table separation - 25µm Spiral Concentrate.

The concentrate from the spiral separation run of the -25µm fraction was fed to the shaking table. The shaking table settings were slurry density – 1.34kg/L, feed rate -0.014t/h. washwater-140ml/sec and deck angle – 4º. Table 7.25 gives the mass yield and recovery of the shaking table run. The recovery of the chrome into the concentrate was 13.85% while the mass yield was 13.85%. The middlings had a 60.39% yield and a 72.86% recovery. This showed that the separation of ultrafine particles became difficult, and this resulted in a concentrate grade of 36.55% Cr_2O_3. The SiO_2 separation which has been achieved easily in the coarser fraction was not as easy. It decreased from 35% to 10.53 %. Only CaO achieved significant downgrade from 7.92% to 1.11% as depicted in Figure 8.37 and 8.38.

Figure 7.37 shows that only 13.85% chrome was recovered into the concentrate while the rest went to the middlings. Only 13.30% was recovered into the tailings. The main oxides graph (Figure 7.38) shows that SiO_2, Al_2O_3 and MgO did not separate much compared to the Cr_2O_3 and FeO. This marginal separation at -25µm is due the indifferent behavior of particles in a fluid at ultrafine sizes. That is why gravity separation at ultrafine sizes is very difficult, hence the use of other methods like flotation and leaching or even smelting.

Table 7.25: Yield, Recovery and Cr grades for -25µm Shaking Table separation

Stream Name	% Mass Yield	% Cr_2O_3 Rec	Cr_2O_3 %	FeO%	SiO_2 %	CaO %	Al_2O_3 %	MgO %
-25 µm Feed			14.37	12.74	35.02	7.92	18.93	14.42
-25 µm Concentrate	7.83	13.85	36.55	24.90	10.53	1.11	14.85	13.39
-25 µm Middlings	60.39	72.86	14.64	12.80	34.62	7.63	18.54	14.45
-25 µm Tailings	31.78	13.30	10.87	10.63	37.93	8.49	19.07	13.49

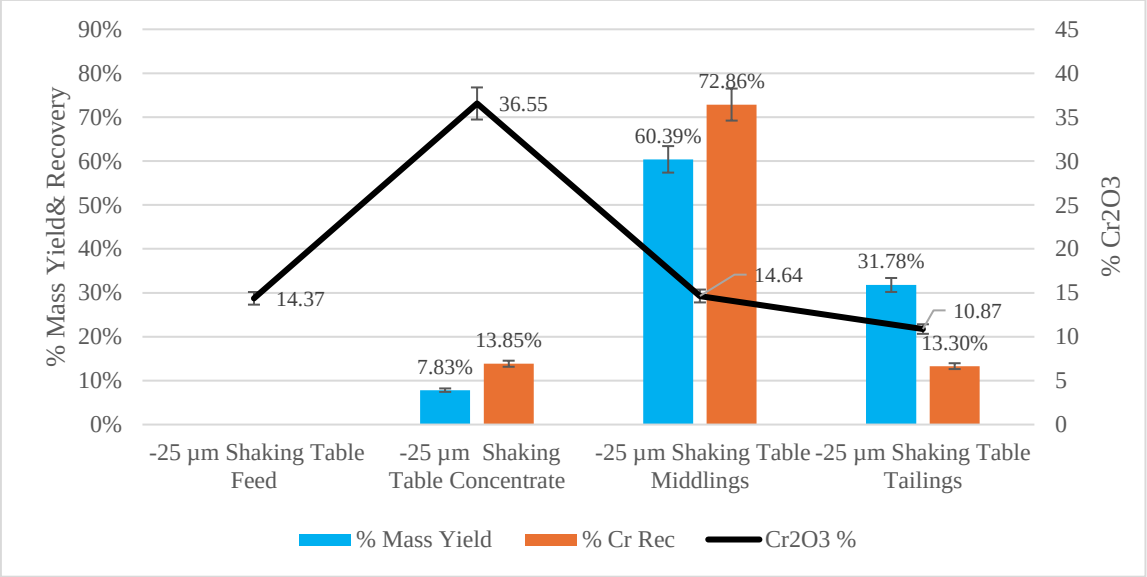

Figure 7.37: -25µm Shaking Table Yield, Recovery and Cr grades of product streams

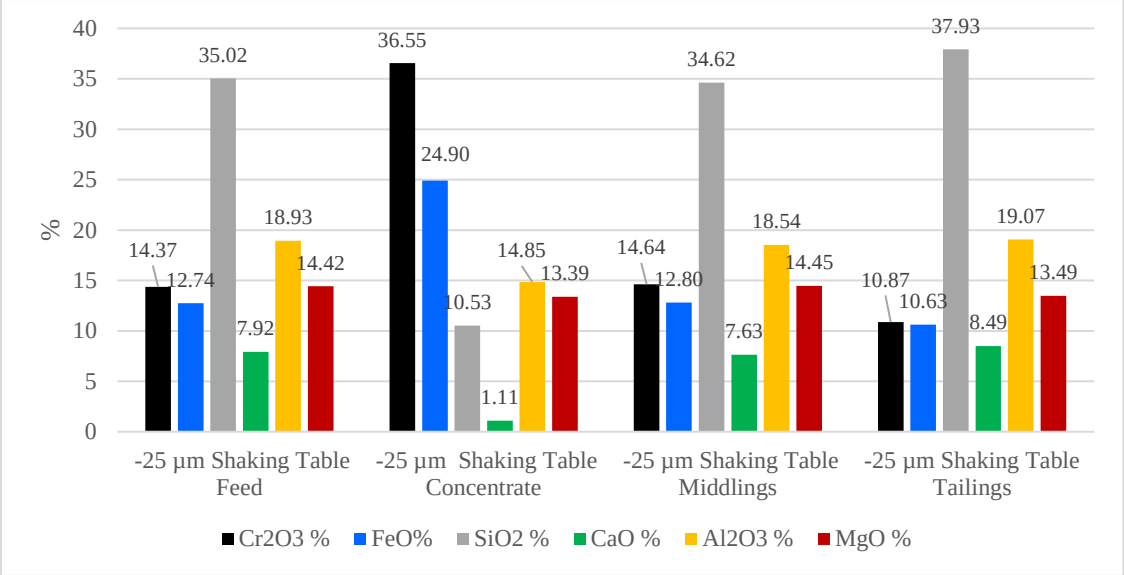

Figure 7.38: Concentration of main oxides, in the -25µm Shaking Table product streams

7.3.7 -25µm Screen - Spiral - Screen - Shaking Table separation Mass Balance.

The separation of chromite by utilizing narrow particle size range is presented in Table 7.26 in the form of a mass balance. From the table, the top rows represent the +25µm stream treated first on the spiral and then the concentrate screened on a 106µm screen to remove the coarse unliberated particles. The key outcomes of the circuit are:

The coarse size fraction (+25µm) contributed 5.94% mass yield to the final concentrate.

The ultrafine size fraction (-25µm) produced 1.06% mass yield to the final concentrate.

The overall recovery achieved in the circuit was 29.28%.

The overall yield of the circuit was 7.00%.

The combined final concentrate grade was 40.07% Cr_2O_3.

The final tailings grade of the circuit was 7.12% Cr_2O_3.

Table 7.26: -25µm Screen - Spiral - Shaking Table separation

	25µm Screen			+25µm Spiral Separation				106µm Screen			+25µm Spiral Conc Shaking Table				Middling Re-cleaner Shaking Table			
Stream	**Feed**	**O/S**	**U/S**	**Feed**	**Conc**	**Mids**	**Tail**	**Feed**	**O/S**	**U/S**	**Feed**	**Conc**	**Mids**	**Tail**	**Feed**	**Conc**	**Mids**	**Tail**
Grade	8.26	7.49	9.38	7.49	12.49	3.56	2.71	12.49	8.62	13.41	13.41	**41.51**	8.52	4.29	8.52	**39.75**	10	3.65
Section Yield		58.82	41.18		50.42	31.42	18.16		19.2	80.8		17.03	50.67	32.3		15.34	61.35	23.31
Overall Yield		58.82	41.18		29.66	18.48	10.68		5.69	23.96		4.08	12.14	7.74		1.86	7.45	2.83
Section Recovery		53.3	46.7		77.29	14.46	8.25		13.25	86.75		55.35	33.37	11.28		46.6	46.9	6.5
Overall Recovery		53.3	46.7		41.20	7.71	4.40		5.46	35.74		19.78	11.93	4.03		5.56	5.59	0.78
Cr Units		4.406	3.86		3.70	0.66	0.29		0.49	3.21		1.69	1.03	0.33		0.74	0.74	0.10
				-25µm Spiral Separation							-25µm Spiral Conc Shaking Table					Performance		
Stream				**Feed**	**Conc**	**Mids**	**Tail**				**Feed**	**Conc**	**Mids**	**Tail**	*Feed Grade*			*8.26*
Grade				9.38	14.37	7.55	8.83				14.37	**35.05**	16.27	13.55	*Overall Conc Yield*			*7.00*
Section Yield					26.59	26.9	46.51					9.66	46.73	43.61	*Overall Conc Recovery*			*29.28*
Overall Yield					10.95	11.08	19.15					1.06	5.12	4.78	*Overall Conc Grade*			*40.07*
Section Recovery					42.17	22.48	35.35					20.03	45.02	34.95	*Cr Units In*			*8.27*
Overall Recovery					19.69	10.50	16.51					3.94	8.87	6.88	*Cr units Out*			*2.81*
Cr Units					1.57	0.84	1.69					0.37	0.83	0.65	*Overall Tails Grade*			*7.12%*

7.3.8 Final Circuit Configuration.

The two circuit configurations which were proposed and tested produced results which were compared to make the final decision on the most profitable circuit. The table below provides a clear comparison of decision-making purposes.

Table 7.27: Circuit Configuration comparison

CONFIGURATION 1						
	Spiral	**Magnet**	**Shaking table 1**	**Shaking table 2**	**Shaking table 3**	**Overall**
Feed (%Cr_2O_3)	10.68	8.97	17.11	11.79	2026	**10.68**
Conc. Recovery (%)	30.56	18.44	53.07	24.31	24.31	**19.01**
Conc. Yield (%)	23.06	8.24	22.22	15.88	10.20	**5.81**
Conc. Grade (%Cr_2O_3)	14.41	20.26	41.24	37.99	41.95	**40.59**
Tailings Grade (%Cr_2O_3)	9.31	7.89	9.11	10.36	15.83	**8.52**
CONFIGURATION 2						
	Spiral (+25µm)	**Spiral (-25µm)**	**Shaking table (+25µm)**	**Shaking table (+25 µm)**	**Shaking table (-25µm)**	**Overall**
Feed (%Cr_2O_3)	7.49	9.38	13.41	8.52	14.37	8.26
Conc. Recovery (%)	77.29	42.17	55.35	46.60	20.03	29.28
Conc. Yield (%)	50.42	26.59	17.03	15.34	9.66	7.00
Conc. Grade (%Cr_2O_3)	12.49	14.37	41.51	39.75	35.05	40.07
Tailings Grade (%Cr_2O_3)	2.71	8.83	4.29	3.65	13.55	7.12

Configuration 2 gave better results than 1 in terms of recovery, yield, and tailings grade while the concentrate grade was similar for both configurations. The configuration 2 had streams of narrow particle size which promote efficient gravity separation as can be seen in Table 7.27 above. The selectivity is also better for configuration 2 for the same reasons. The other factor on the MgO selective rejection of shaking table could be the shape that makes it easy to float above the stream and get washed easily compared to spiral and magnetic separation.

Using the technical performance indicators, the viable option is configuration 2. However, for the complete business viability assessment, an economic evaluation considering the Capital (CAPEX) and Operational (OPEX) expenditure needs to be conducted. A combination of technical viability and an economic evaluation will produce a business model upon which investment decisions will be based. The next chapter discusses a high-level economic model for the chosen circuit configuration.

CHAPTER 8: TECHNO-ECONOMIC MODEL OF PROPOSED PLANT CIRCUIT

8.1 Introduction

The project cost of any study is especially important as it is the main determinant of feasibility of a project in practical terms. For process plants feasibility studies, technical feasibility is normally followed by an evaluation of cost feasibility. Both studies normally require a lot of time and effort hence there is a cost to a feasibility study. The level of accuracy of an estimated cost of a project is proportional to the cost incurred in generating the components of the costs. In this study, the author followed a sequential flow (Figure 8.1) of metallurgical test-work and equipment sizing data to arrive at a Total Capital Cost required to build a plant designed from the results presented and discussed in Chapter 7. The process flow followed is shown in Figure 8.1 below.

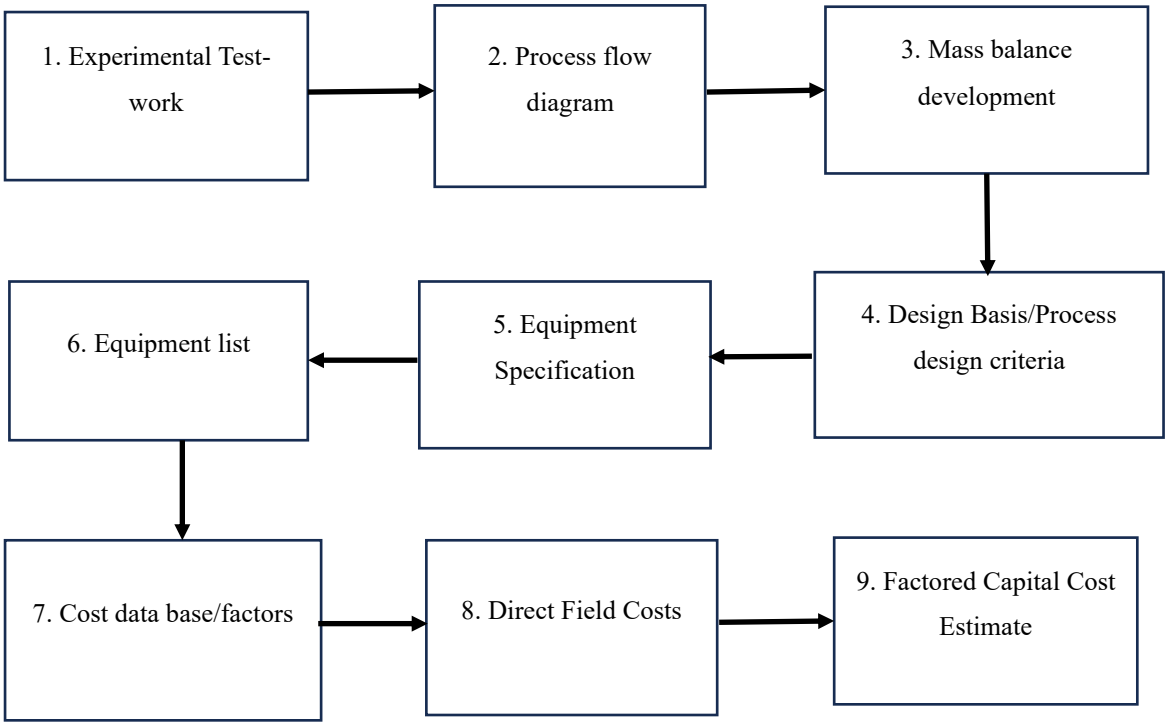

Figure 8.1: Capital estimation process flow for chosen circuit

8.1.1 Background to Cost Estimation

The development of capital budgets is key to any cost engineer since the decision to either go or not go ahead with a detailed feasibility study rests in the initial cost estimates presented to the executives. According to Rodl, Prinzing and Aichert (1985), a project may be divided into three main phases namely, (i) Conception, (ii) Definition and (iii) Execution. After phases (i) and (ii) management decisions need to be made after preparation of Capital Expenditure estimates documents. The Capex estimates are developed through different routes and each of the routes is unique in the level of effort or cost and corresponding accuracy. There is always a trade-off between preparation effort and expected accuracy. The balance between these two imperatives hinges on the attraction of the qualitative benefits from the concept originator. However, there are processes to be followed if a Capex estimate is required. Amasterdam (2018) in his M.Sc. thesis gave an outline (Table 8.1) of five capital cost estimate classes and the characteristics as defined by AACE International. The same table was presented by Dysert (2003) in his article on Cost estimating skills in the Chemical Engineering journal. For the purposes of this study, the cost estimate class is assumed to be at Class 4 where the purpose is concept or feasibility study

Table 8.1: Cost Estimate Classification Matrix

ESTIMATE CLASS	**MATURITY LEVEL OF PROJECT DEFINITION** Expressed as % of complete definition.	**END USAGE** Typical purpose of Estimate	**METHODOLOGY** Typical estimating method	**EXPECTED ACCURACY** Typical ± range relative to index of 1.	**PREPARATION EFFORT** Typical degree of effort relative to lease cost index of 1
Class 5	0% to 2%	Screening/feasibility	Stochastic (factors and/models) or judgement	4 to 20	1
Class 4	1% to 15%	Concept study or feasibility	Primarily stochastic	3 to 12	2 to 4
Class 3	10% to 40%	Budget authorization or control	Mixed but primarily stochastic	2 to 6	3 to 10
Class 2	30% to 75%	Control or bid/tender	Primarily deterministic	1 to 3	5 to 20
Class 1	65% to 100%	Check estimate or bid/tender	Deterministic	1	10 to 100

8.1.2 Estimation methods

There are several cost estimation methods available to the cost practitioners. Amsterdam (2018) presented five generally applied methods, and each has its own strengths and weaknesses.

(i) **Turnover Ratio Method**: This method uses a ratio of Turnover to the Capital Invested. The limitation of this method is that for a project where there is no history of sales performance, it is difficult to get the accurate ratio.

(ii) **The Exponent method:** This is also called the six-tenth rule of William. It relates the known costs and capacity of plant A to estimate the costs of plant B at an intended capacity, according to the equation below.

Equation 8.1 $$\text{Cost B} = \text{Cost A x (Capacity B/Capacity A)n}$$

where Cost B is the unknown cost of item B, Cost A is the known cost of item A, Capacity B is the known capacity of item B, Capacity A is the known capacity of item A, and n is the exponent related to the product. This exponent's value is between 0.1 and 1.0 but is normally 0.6 hence the name six-tenth rule.

(iii) **Parametric Method**: in this method the capital cost C is governed by the equation,

Equation 8.2 $$C = K \times N \times F$$

where C is the Capital cost, N is the number of functional units, F represents the variety of parameters such as temperature, pressure or capacity and K is the proportional constant. The difficulty with this method is that it does not indicate the major costs in a project hence difficult to produce alternatives. The other disadvantage is that it assumes that a simple pump may have the same cost as furnace for example and this is not always true or realistic.

(iv) **Factorial or Factored Method**: this method requires a basic flowsheet to be prepared, equipment sized and cost or price of pieces of equipment determined. After this information is available, special factors are used to account for the rest of the costs associated with construction. There is a little more effort in this method

since the estimator must get budget costs either from vendors or using historical cost records from previous projects.

(v) **Detailed Estimates**: in this method every detail is costed separately based on flowsheet, plot plans, and labour hours involved. This is the most accurate method but also costs the most and is used for cost control during construction.

8.1.3 Costs Indices

The process of cost estimation as indicated above most of the time uses past cost number of the pieces of equipment. To accurately give the current cost estimation, the estimator must give an estimate of current cost based on the past cost. To do this one needs to use cost indices. This is based on the equation below.

Equation 8.3 $$(Cost_{t=1}/Cost_{t=2}) = (Index_{t=1}/Index_{t=2})$$

where $Cost_{t=1}$ is the past cost of item, $Cost_{t=2}$ is the required current cost of same item, $Index_{t=1}$ is the cost past Index at time t=1 and $Index_{t=2}$ is the cost index now (Mular,1982).

8.1.4 Factorial Method

In this work, the author chose the factorial method for cost estimation of the circuit proposed. The factorial method lends itself to the work done by H.J Lang (1948) who is regarded as the founding father of cost estimation. In his method, Lang put more effort into determining the actual cost of major equipment necessary to perform the conversion task in the process part i.e. pumps and processors. Lang produced a factor to be used when determining the cost of equipment Ek to derive an estimated total cost. The following equation was developed by Lang and has been used extensively to do project cost estimates.

Equation 8.4 $$C_{TDC} = F_L \times \sum E_k$$

Where C_{TDC} is the total depreciated cost, E_k is the total delivered cost of mechanical equipment and F_L is the Lang factor (Wain, 2014). Below is a table showing values of Lang factors applied in three different scenarios.

Table 8.2: Value of the Lang factors as originally published by H.J Lang (1948)

Type of process	F_L value
Solids	3.10
Solids/Fluids	3.63
Fluids	4.74

From Table 8.2, the total depreciated cost is either3.10, 3.63 or 4.74 times the delivered cost of main processing equipment. The difference between solids, fluids or mixed processes is the amount of piping associated with main processing equipment leading to increased costs where there is more fluid involved. There have been other variants of Lang's method, but the main principle remains the same. With more data coming through because of numbers coming from practical projects, the FL values have been reviewed and developed but the relationship between solids, mixed and fluids still holds. Table 8.3 shows the method of Peters and Timmerhaus in tabular form, with its origins in Lang's method.

Table 8.3: Peters and Timmerhaus cost estimation method (1991)

Cost item	**Process type**		
	Solids	*Solids/Fluids*	*Fluids*
Delivered equipment	**1.00**	**1.00**	**1.00**
Equipment installation labour	0.45	0.39	0.47
Instrumentation and control	0.09	0.13	0.18
Piping	0.16	0.31	0.66
Electrical installations	0.10	0.10	0.11
Buildings	0.25	0.29	0.18
Yard improvements	0.13	0.10	0.10
Services facilities	0.40	0.55	0.70
Land	0.06	0.06	0.06
Direct Plant Costs (DPC)	**2.64**	**2.39**	**3.46**
Engineering and supervision	0.33	0.32	0.32
Construction expenses	0.39	0.34	0.41
Direct and Indirect costs (DIC)	**3.36**	**3.59**	**4.20**
Contractor's fee	0.17	0.18	0.21
Contingency	0.34	0.36	0.42
Total depreciable costs (TDC)	**3.87**	**4.13**	**4.83**
Working capital	0.68	0.74	0.86
Total Capital investment (TIC)	**4.55**	**4.87**	**5.69**

For this work, the author chose the mixed system (Solids/Fluids) factor for the TDC (4.13) because there is a mix of fluids and solids handling in the process. The solids part mainly relates to the stacker section where the stacked product is moved in dump and side tipper trucks. In the pipes the material is slurry and as such the Solid/Fluid system was chosen.

The presentation of the whole chapter will follow the flow in Figure 8.1 for ease of linking the rationale used to produce the final capital costs for the circuit chosen in this work.

8.2 Experimental Test-work

The experimental test-work that resulted in the choice of a circuit was carried out using three main processing pieces of equipment, namely spirals, vibrating screens and shaking tables. The processing sequence followed was screening, spiral separation, screening and shaking table separation. The first screening was done to separate the feed into +25µm and -25µm size fraction streams. The +25µm stream spiral concentrate was screened on a 106µm screen to

remove coarse particles that were low in chrome and the -106µm concentrate fraction fed onto a shaking table for final chrome production. The -25µm stream was processed through a separate spiral separator and the concentrate was then cleaned using a shaking table. Two shaking table concentrates were produced from the two streams (-25µm and +25µm). Tables 8.4 and 8.5 show the circuit performance indicators in terms of sectional and overall yield and recovery.

Table 8.4: Experimental Test-work results

Unit Sectional Performance	***%***	***Overall Circuit Performance***	***%***
Feed Grade	8.26		
Coarse Spiral Concentrate Mass Yield	50.42	Coarse Spiral Overall Concentrate Mass Yield	29.66
Coarse Spiral Concentrate Cr_2O_3 Recovery	77.29	Coarse Spiral Overall Concentrate Cr_2O_3 Recovery	41.20
Fines Spiral Concentrate Mass Yield	26.59	Fines Spiral Overall Concentrate Mass Yield	10.95
Fines Spiral Concentrate Cr_2O_3 Recovery	42.17	Fines Spiral Overall Concentrate Cr_2O_3 Recovery	19.69
106µm Screen U/S Mass Yield	80.8	106µm Screen U/S Overall Mass Yield	23.96
106 µm Screen U/S Cr_2O_3 Recovery	86.75	106 µm Screen U/S Overall Cr_2O_3Recovery	35.74
Coarse Shaking Table Rougher Concentrate Mass Yield	17.00	Shaking Table Rougher Overall Concentrate Mass Yield	4.08
Coarse Shaking Table Rougher Concentrate Cr_2O_3 Recovery	55.35	Shaking Table Rougher Overall Concentrate Cr_2O_3 Recovery	19.78
Coarse Shaking Table Scavenger Concentrate Mass Yield	15.34	Coarse Shaking Table Scavenger Overall Concentrate Mass Yield	1.86
Coarse Shaking Table Scavenger Cr_2O_3 Recovery	46.46	Coarse Shaking Table Scavenger Overall Cr_2O_3 Recovery	5.56
Fines Shaking Table Rougher Concentrate Mass Yield	9.66	Fine Shaking Table Rougher Overall Concentrate Mass Yield	1.06
Fine Shaking Table Rougher Cr_2O_3 Recovery	20.03	Fine Shaking Table Rougher Overall Cr_2O_3Recovery	3.94
Overall Concentrate Yield	***7.00***		
Overall Concentrate Cr_2O_3 Recovery	***29.28***		
Overall Concentrate Grade	***40.07***		
Overall Tailings Grade	***7.12***		

8.3 Process Flow Diagram

This section presents the process flow diagram of the circuit discussed in Chapter 7 as the final beneficiation circuit for ultrafine chrome feed. Some of the equipment used in the test-work has been scaled up from laboratory to plant scale to address the tonnage requirements. These pieces of equipment are screens and shaking tables. The spiral used in the test-work was a plant size spiral so there was no requirement for scaling up. The other change from the laboratory scale to the plant size process is the dewatering process that was attained by decanting water from settled slurries to reach the desired density. In the proposed large-scale plant, the density adjustment will be performed by use of hydro cyclones. The following subsections present the equipment in each sub-section and its purpose.

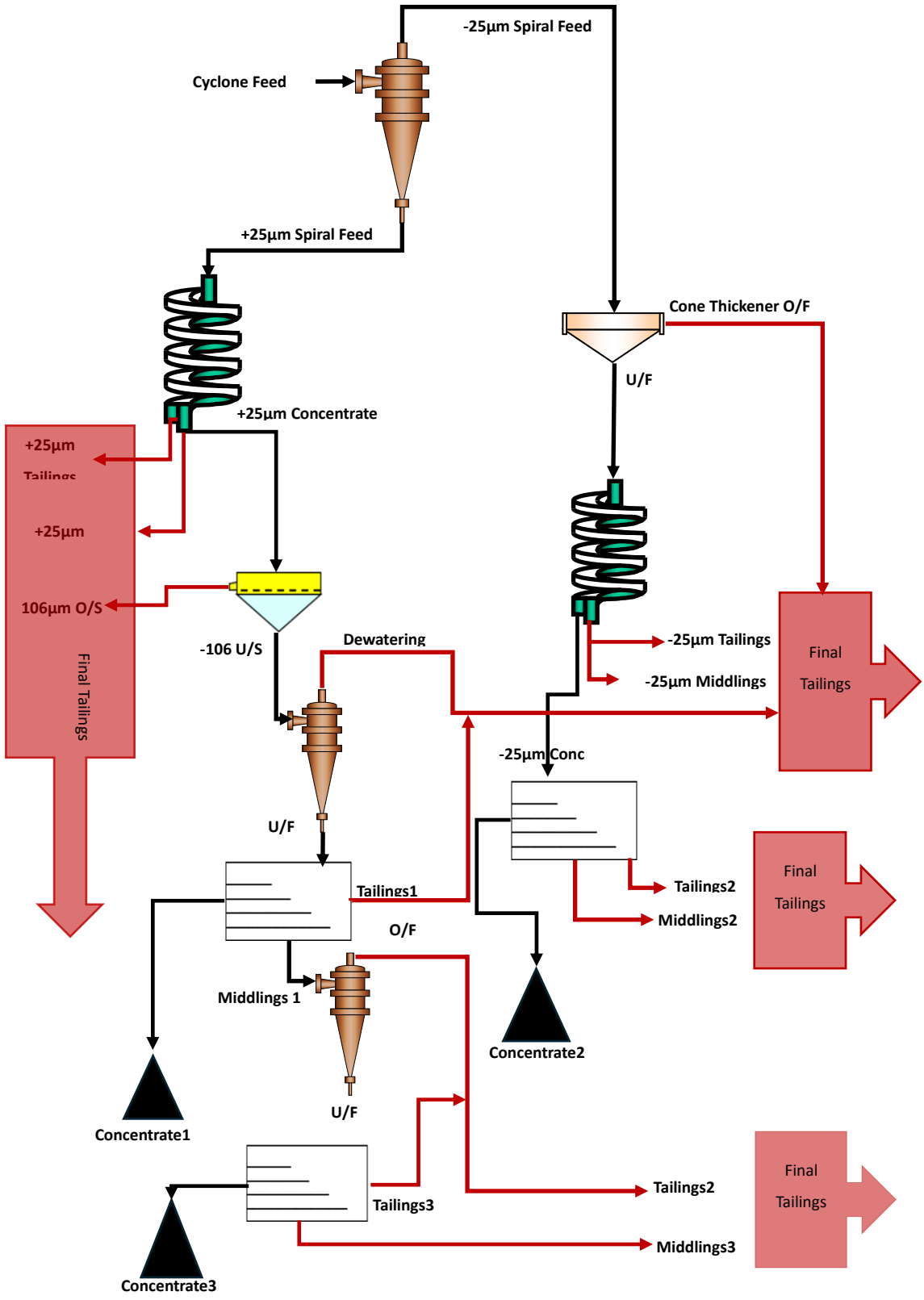

Figure 8.2: Process Flow Diagram for the final circuit

8.4 Mass Balance

The mass balance of the circuit is given in Table 8.6. In the table, the two sections of the circuit are given with the coarse section at the top while the fine section is given at the bottom. From the mass balance streams, all the streams indicated in red are tailings streams, and the those indicated in black are still within the circuit, going to the next processing unit or to the final product.

Table 8.5: Mass Balance for the chosen circuit for ultrafine chrome beneficiation

COARSE	**Classifying Cyclone**			**+25µm Spiral Separation**				**106µm Screen**			**+25µm Spiral Conc Shaking Table**				**Middling Re-cleaner Shaking Table**			
Stream	**Feed**	**U/F**		**Feed**	**Conc**	**Mids.**	**Tail**	**Feed**	**O/S**	**U/S**	**Feed**	**Conc**	**Mids.**	**Tail**	**Feed**	**Conc**	**Mids.**	**Tail**
Grade (Cr_2O_3)	**8.26**	**7.49**		**7.49**	**12.49**	3.56	2.71	**12.49**	8.62	**13.41**	**13.41**	**41.51**	**8.52**	4.29	**8.52**	**39.75**	10	3.65
Section Yield		**58.82**			**50.42**	31.42	18.16		19.2	**80.8**		**17.03**	**50.67**	32.3		**15.34**	61.35	23.31
Overall Yield		**58.82**			**29.66**	18.48	10.68		5.69	**23.96**		**4.08**	**12.14**	7.74		**1.86**	7.45	2.83
Section Recovery		**53.3**			**77.29**	14.46	8.25		13.25	**86.75**		**55.35**	**33.37**	11.28		**46.6**	46.9	6.5
Overall Recovery		**53.3**			**41.20**	7.71	4.40		5.46	**35.74**		**19.78**	**11.93**	4.03		**5.56**	5.59	0.78
Cr Units		**4.406**			**3.70**	0.66	0.29		0.49	**3.21**		**1.69**	**1.03**	0.33		**0.74**	0.74	0.10
FINE				**-25µm Spiral Separation**							**-25µm Spiral Conc Shaking Table**					**Performance**		
Stream			**O/F**	**Feed**	**Conc**	**Mids.**	**Tail**				**Feed**	**Conc**	**Mids.**	**Tail**	***Feed Grade***			***8.26%***
Grade (Cr_2O_3)			**9.38**	**9.38**	**14.37**	7.55	8.83				**14.37**	**35.05**	16.27	13.55	***Overall Conc Yield***			***7.00%***
Section Yield			**41.18**		**26.59**	26.9	46.51					**9.66**	46.73	43.61	***Overall Conc Recovery***			***29.28%***
Overall Yield			**41.18**		**10.95**	11.08	19.15					**1.06**	5.12	4.78	***Overall Conc Grade***			***40.07%***
Section Recovery			**46.7**		**42.17**	22.48	35.35					**20.03**	45.02	34.95	***Cr Units In***			***8.27%***
Overall Recovery			**46.7**		**19.69**	10.50	16.51					**3.94**	8.87	6.88	***Cr units Out***			***2.81%***
Cr Units			**3.86**		**1.57**	0.84	1.69					**0.37**	0.83	0.65	***Overall Tails Grade***			***7.12%***

8.5 Design Basis

The design basis for this plant is given in Figure 8.3 and Table 8.6 below. Figure 8.3 shows the Daily tonnage of the tailings produced by the plant whose material was used in this test-work. Jan 2024 was chosen because it had the most stable feed rate throughout the month. The average daily feed rate was 10838 t/d and when arranged in descending order (as shown in Figure 8.3) the 80-percentile tonnage per day was 12163 t/d marked in red colour. The 80-percentile tonnage was calculated to be 506 t/h while the average throughput was 451 t/h. For design purposes, 500 t/h was used to calculate capacities of different pieces of equipment.

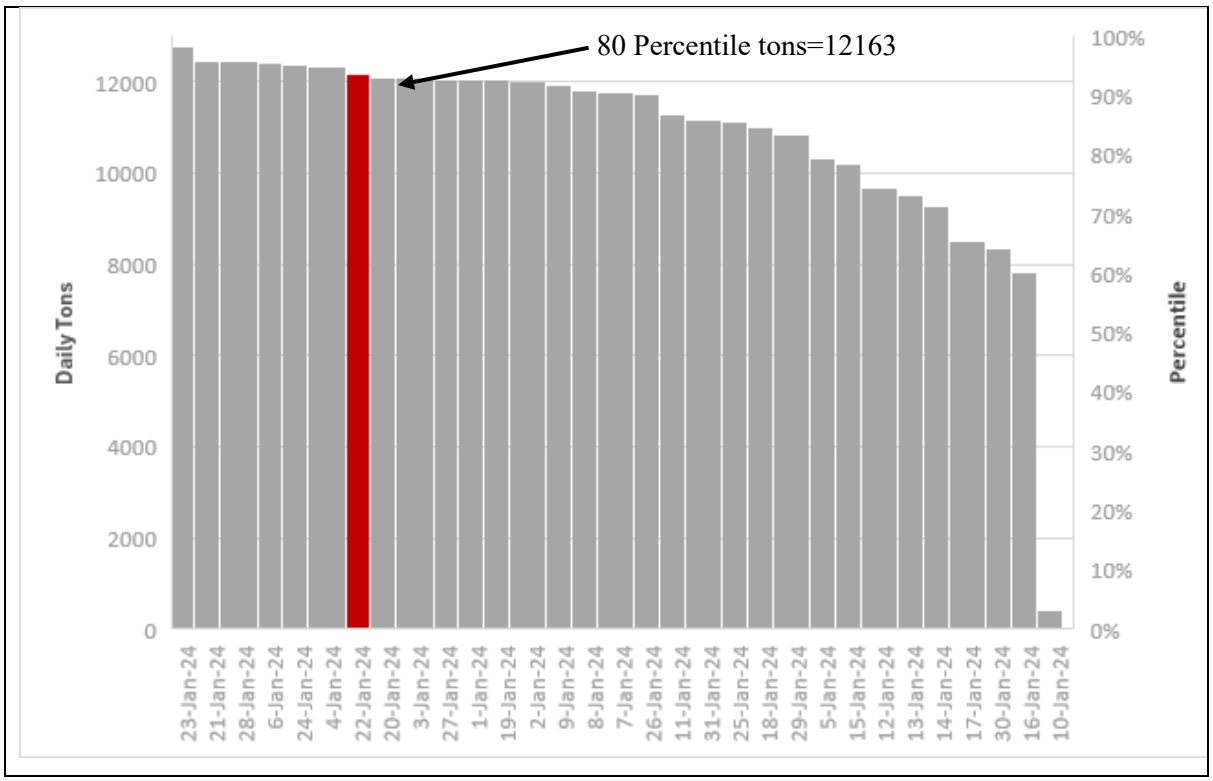

Figure 8.3: January 2024 feed trend used to calculate the design throughput

Table 8.6 gives a summary of the design basis used to calculate the throughput. The plant will be running for 365 days and 24 hours per day. The planned shutdown follows a pattern of 24 hours plus 16 hours making an average of 10 hours per week. The average feed grade is set at 9.5% Cr_2O_3 achieving a yield of 7% at an average product grade of 40 % Cr_2O_3 translating to 288350 tons per annum.

Table 8.6: Design basis table for the beneficiation of ultrafine chrome

Item Description	Units	Value	Comments
Days per annum	d/a	365	
Operating hours	h/d	24	
Total annual hours	h/a	8760	
Statutory holidays	d/a	0	Plant does not stop for holiday
Planned Maintenance	h/w	10	24 hours and 16 hours per month
	h/a	521	
Plant annual operating hours	h/a	8239	
Plant overall utilization	%	94	
Plant feed rate-design	t/a	4 119 286	
	t/h	500	Based on 80 percentiles of daily tonnage
Design feed grade (% Cr_2O_3)	%	9.50	
Chrome concentrate yield	%	7.00	Based on the mass balance performance
Concentrate production	t/a	288 350	
	t/m	24 029	
	t/h	35.00	
Concentrate grade	%Cr_2O_3	40	Target grade
Chromite (Cr_2O_3) recovery	%	29.47	Based on mass balance performance

8.6 Equipment Specification

The equipment specification section discusses the key pieces of equipment in each section of the circuit. These specifications are derived from the requirements to produce the results as per experimental test-work. The assumption is that these pieces of equipment will be run on a continuous basis as opposed to batch tests carried out during pilot and laboratory testing. Table 8.7 gives a list of equipment used in the test-work that were replaced by continuous units in this proposed circuit.

Table 8.7: Equipment replacement from laboratory scale to industrial scale

Laboratory	Industrial	Purpose
Rhologan (25µm) MK5 Screen.	CY180/8 cyclone	Classification of feed into +25µm and -25µm
Rhologan (106µm) MK5 Screen.	5-Deck Vibrating Screen	Screening out 106µm particles from spiral tailings before running on shaking table.
1 m^3 Floor bins (water decant)	600m^3 High Rate Settling Thickener	Density adjustment of the -25µm spiral feed.
1 m^3 Floor bins (water decant)	20-Way CY125 dewatering cyclone.	+25 µm Shaking table feed density adjustment.
Holman-Wilfley Model 800 Table	999 Triple Deck Shaking Tables	Production of chrome concentrate final product.
N/A	20-Way CY125 dewatering cyclone.	Dewatering final concentrate stream for staking.
N/A	20-Way CY350 dewatering cyclone.	Dewatering cyclone for thickener feed stream.

8.6.1 Feed Preparation Section

The feed preparation section is made up of classifying hydro-cyclones arranged in a cluster format to classify the feed stream into +25µm and -25µm size streams. There are two classifying cyclone clusters, each with 20 CY180/8 cyclones. At any one point 15 cyclones will be running and 5 on standby. The diameter of the cyclone is 180mm, Vortex finder 60mm, Spigot 25mm.

The operating pressure will be 95kPa and the flow per cluster of 572m^3/hr. The purpose of the classifying cyclone is to separate the feed stream into -25µm particles and +25µm particles so that the two streams are fed to the spirals separately. The cyclone overflow at a slurry density of 1.13 t/m^3 will be fed into the settling cone thickener for the purpose of dewatering the stream until the slurry density has reached a density of 1.34 t/m^3 suitable for feeding the spiral separator. The cyclone underflow stream will be diluted from 1.88 t/m^3 to a density of 1.52 t/m3 suitable for feeding coarse stream spirals. Once the slurry density has been adjusted to the suitable level, the streams are fed to the next circuit section for spiral separation as shown in Figure 8.2.

8.6.2 Spiral Separation Section

The spiral separation section consists of two sections treating classified streams of -25µm and +25µm particle sizes. The spirals specifications are given below in Table 8.8.

Table 8.8: M1T53 Spiral specification

Parameter	Value/measurement	Units
Pitch, U	360	mm
Height, H (Centre Column height)	2600	mm
Slope, S (α)	7	degrees
Trough Slope (θ)	9	degrees
Diameter	880	mm
Inner Radius (Centre column diameter)	160	mm
Tonnage per start (max)	1	t/hr

The coarse cyclone underflow stream of +25µm particle size is fed into the coarse spirals section comprising of 120 spirals arranged in 12 banks of 10 spirals each. The fine cyclone overflow that is a -25µm stream is first fed into a settling cone for densification of the feed to the spirals by means of settling the solid particles while the water overflows at the top of the settling cone. The underflow of the settling cone with a density of 1.34 t/m^3 is fed into another section of spirals comprising of 20 banks of 10 spirals. The spiral middlings and tailings from both sections are discarded as tailings via a cyclone classifier next to the final tailings thickener.

The concentrate of the coarse spirals is fed into the 106µm screens for the removal of ±106µm particles which are low in chrome. The screen oversize is sent to the tailings cyclone next to the final tailings thickener while the screen undersize is sent to the shaking tables feed cyclones to adjust the density before feeding onto the coarse shaking tables. The spiral concentrate of the fines spirals is sent directly to the fines shaking tables.

8.6.3 Shaking Table Separation Section

The shaking tables section comprises of vibrating screens for screening the coarse spirals concentrate, the cyclone cluster section for densifying the shaking tables feed as it comes from the screen underflow at low density of 1.18 t/m^3. The screen section comprises six 5-deck vibrating screens. Each deck has a capacity of 4 t/h with a panel aperture size of 106 µm.

The Rougher shaking tables are fed by two 20-way 125mm cyclone clusters and the scavenger tables are fed by one 20-way 125mm cluster cyclone with specifications given in Table 8.9 below.

Table 8.9: 125mm Cyclone Specifications

Parameter	Value
Diameter	125mm
Vortex Finder	30mm
Spigot	18mm
Pressure	110kPa
Mass Yield	97%
Cr_2O_3 Recovery	99%

The shaking table sub-section has a total of 52 triple-deck shaking tables (model 999-Deister), with 26 of the 40 shaking tables regarded as the primary shaking tables treating screen undersize fraction. The middlings streams from the 26 primary tables are sent for densification on 20-way cluster 125mm cyclones before feeding the 14 scavenger shaking tables.

The fines spiral concentrate is first diluted with water to get the density down from 1.58t/m^3 to 1.34t/m^3 before sending it to 12 shaking tables. The Deister 999 Shaking Tables specifications are given in Table 8.11.

Table 8.10: Deister 999 Shaking Tables Specifications

Parameter	Value
Feed rate	0.4 – 2.3 t/h per deck
Wash water	0.7 – 3.6 m3/h per deck
Stroke length	13 – 19 mm
Stroke frequency	265 – 280 strokes/mina
End Elevation	5 – 20 mm/m
Side Tilt	10 – 25 mm/m

8.6.4 Chrome Concentrate Handling Section

The chrome concentrate section consists of a 20-way 125mm cyclone cluster. The specifications of the cluster are the same as those of the shaking table feed cyclones discussed above in Table 8.10. The slurry density of the concentrate to the cyclone will be 1.08t/m^3 and the cyclone underflow density will be 2.89t/m^3 with the overflow density of 1.00t/m^3. This cyclone overflow will be returned to the thickener for recovery of clean water.

8.6.5 Tailings Handling Section

The tailings handling section is responsible for the recovery of the bulk of the water in the tailings streams of the circuit. All tailings streams from the different sections of the plant first combine into tailings cyclone feed tank. The cyclone cluster at the tailings section is a 20-way 350mm diameter cyclone, the specifications of which are given in Table 8.12. The tailings cyclone removes water and fine particles into the cyclone overflow at a density of 1.13 t/m^3 and the cyclone underflow density increased to 2.7 t/m^3. The cyclone overflow feed the thickener where a flocculant is added to assist with particles coalescence to speed up settling. The densified slurry (2.4-2.7 t/m^3) discharged at the bottom of the thickener gets pumped to the disposal tank that is also fed with cyclone underflow stream and then gets pumped to the tailings storage facility (TSF).

Table 8.11: 350mm Cyclone Specifications

Parameter	Value
Diameter	350mm
Vortex Finder	120mm
Spigot	55-60mm
Pressure	85kPa
Underflow Mass Yield	80%
Cr_2O_3 Recovery	97%

8.7 Equipment List

This section provides a list of key pieces of equipment whose specifications were determined either by the mass or water balance given in Tables 8.13 – 8.15. The equipment making the list (Table 10.16) is process equipment as well as pumps. The sizing of the equipment is based on the volumes that will be processed or handled in each of the sections. The volumes of slurry to be treated in each of the sections and in each specific piece was determined by the mass and water balances given in Tables 8.13 and 8.15 below. The negative sign on the numbers in the mass and water balance indicate dewatering or densification is required. The numbers in blue background indicate that water will be required to reduce the density.

.

Table 8.12: Mass and Water balance – Feed preparation and Concentrate screening

Coarse Section	**Units**	**Stock**	**180mm Cluster Cyclone**							**106µm Screen**		
Stream			**Feed**	**U/F**	**O/F**					**Feed**	**O/S**	**U/S**
Stream #		**1**	**2**	**3**	**4**					**9**	**10**	**11**
Grade	% Cr_2O_3	8.26	8.26	7.49	9.38					12.49	8.62	13.41
Section Yield	%	100	100	58.82	41.18						19.2	80.8
Slurry density	t/m3	1.58	1.25	1.88	1.13					1.4	1.8	1.18
Solids SG	-	2.75	2.75	2.68	2.73					2.93	2.74	2.97
Solids by Mass	% w/w	57.7	31.43	74.7	18.15					43.4	70.0	23.0
Solids by Volume	% v/v	33.14	14.29	52.38	7.51					20.73	45.98	9.14
Dry Solids	t/h	**500**	500	294.10	205.90					148.29	28.47	119.81
Water	t/h	366.8	1090.9	99.8	928.3					193.6	12.2	401.2
Total Pulp	t/h	866.8	1590.9	393.9	1134.2					341.9	40.7	521.0
Pulp Flow	m3/h	548.59	1272.7	209.5	1003.7					244.2	22.6	441.5
Process Water	m3/h		724.1							144.5	12.36	22.07
Wash water	m3/h											
Overall Yield				58.82	41.18						5.69	23.96
Section Recovery				53.3	46.7						13.25	86.75
Overall Recovery				53.3	46.7						5.46	35.74
Cr Units				4.40	3.86						0.49	3.21

Table 8.13: Mass and Water balance - Coarse shaking tables section

Coarse Section	Units	Stock	+25µm Spiral Conc Shaking Table				Middling Re-cleaner Shaking Table			
Stream			**Feed**	**Concentrate**	**Middlings**	**Tailings**	**Feed**	**Concentrate**	**Middlings**	**Tailings**
Stream #		**1**	**12**	**13**	**14**	**15**	**16**	**17**	**18**	**19**
Grade	% Cr_2O_3	8.26	13.41	41.51	8.52	4.29	8.52	39.75	10	3.65
Section Yield	%	100		17.03	50.67	32.3		15.34	61.35	23.31
Slurry density	t/m3	1.58	1.34	1.08	1.13	1.08	1.34	1.08	1.35	1.08
Solids SG	-	2.75	2.97	4.3	2.77	2.52	2.77	4.28	2.8	2.48
Solids by Mass	% w/w	57.7	38.3	9.7	18.0	12.0	39.7	9.7	40.5	12.2
Solids by Volume	% v/v	33.14	17.26	2.42	7.34	5.15	19.21	2.44	19.54	5.29
Dry Solids	t/h	**500**	119.81	**20.40**	60.71	38.7	60.71	**9.31**	37.25	14.15
Water	t/h	366.8	193.4	191.0	276.5	282.6	92.2	87.0	54.8	102.1
Total Pulp	t/h	866.8	313.2	211.4	337.2	321.3	152.9	96.3	92.0	116.3
Pulp Flow	m3/h	548.59	233.7	195.7	298.4	298.0	114.1	89.2	68.1	107.8
Process Water	m3/h		-207.8				-184.3	5.7049		
Overall Yield				**4.08**	12.14	7.74		**1.86**	7.45	2.83
Section Recovery				55.35	33.37	11.28		46.6	46.9	6.5
Overall Recovery				**19.78**	11.93	4.03		**5.56**	5.59	0.78
Cr Units				1.69	1.03	0.33		0.74	0.74	0.10

Table 8.14: Mass and Water balance – Fines Spirals and Shaking Tables

Fine Section		Stock	-25µm Spiral Separation				-25µm Spiral Conc Shaking Table			
Stream			**Feed**	**Concentrate**	**Middlings**	**Tailings**	**Feed**	**Concentrate**	**Middlings**	**Tailings**
Stream #		**20**	**21**	**22**	**23**	**24**	**25**	**26**	**27**	**28**
Grade		9.38	9.38	14.37	7.55	8.83	14.37	35.05	16.27	13.55
Section Yield			100	26.59	26.9	46.51		9.66	46.73	43.61
Slurry density	t/m3	1.13	1.34	1.58	1.36	1.30	1.34	1.08	1.35	1.08
Solids SG	-	2.73	2.77	3.03	2.68	2.74	3.03	4.05	3.12	2.97
Solids by Mass	% w/w	18.15	39.71	54.79	42.23	36.34	37.87	9.84	38.29	10.95
Solids by Volume	% v/v	7.51	19.21	28.57	21.43	17.24	16.75	2.62	16.59	3.98
Dry Solids	t/h	205.90	205.90	54.75	55.39	95.76	55.39	**5.35**	25.88	24.15
Water	t/h	928.26	312.63	45.17	75.78	167.76	90.86	49.05	41.71	196.40
Total Pulp	t/h	1134.16	518.53	99.92	131.2	263.53	146.25	**54.396**	67.6	220.55
Pulp Flow	m3/h	1003.68	386.96	63.24	96.45	202.71	109.14	50.366	50.01	204.53
Process Water	m3/h		-615.63				45.69			
Overall Yield				10.95	11.08	19.15		**1.06**	5.12	4.78
Section Recovery				42.17	22.48	35.35		20.03	45.02	34.95
Overall Recovery				19.69	10.50	16.51		**3.94**	8.87	6.88
Cr Units				1.57	0.84	1.69		0.37	0.83	0.65

Table 8.15: Equipment list for ultrafine chrome beneficiation

Equipment/Description	Code/#	Quantity
Trash Removal Linear Screen	MIPLSc	1
Coarse Primary Spiral Distributor	16-Way	1
Fine Primary Spiral Distributor	24-Way	1
Secondary Spiral Distributor	32-Way	32
Coarse Spirals	M1T53	120
Fine Spirals	M1T53	200
Feed Classifying Cyclone	20wCY 180/8	2
Scavenger Tables Distributor	16-Way	1
Scavenger Shaking Tables Feed Dewatering Cyclone	20wCY125	1
Rougher Shaking Tables Distributor	16-Way	2
Rougher Shaking Table Feed Dewatering Cyclone	20wCY125	2
Fines Shaking Tables Distributor	16-Way	1
Final Product Dewatering Cyclone	20wCY125	2
Guard Dewatering Cyclone	20wCY350	1
Dewatering Cone Thickener	RBHOL-600	2
Feed Preparation Pumps	HM200	4
Coarse Spirals Feed Pumps	HM200	2
Coarse Spirals Concentrate Pumps	HM100	4
Coarse Spirals Middlings & Tailings pumps	HM150-55kw	2
Fine Spiral Concentrate Pumps	HM75	4
Fine Spirals Middlings and Tailings pumps	HM75-30kw	4
Screen Undersize pumps	HM150-30kw	4
Screen Oversize pumps	HM75	2
Rougher Shaking Tables Concentrate Pumps	HM150-30kw	4
Rougher Shaking Tables Middlings Pumps	HM200	2
Rougher Shaking Tables Tailings	HM200	2
Scavenger Shaking Tables Concentrate Pumps	HM150-30kw	2
Scavenger Shaking Tables Middlings & Tailings Pumps	HM150-30kw	2
Fines Shaking Tables Concentrate Pumps HM100	HM100	2
Fines Shaking Tables Middlings & Tailings Pumps	HM250	2
Final Tailings Cyclone Feed Pumps 400MCR	400MCR	2
Thickener Underflow Pumps HM250	HM250	2
Tailings Disposal Pumps HM250	HM250	6
Coarse Concentrate Screens	D5Z102100	6
Shaking Tables	DST999	52
Tailings Thickener	THKØ38	1
Cross-Cut Samplers	Feed, Conc & Tails	3

8.8 Equipment Cost Data

The equipment cost for this project is given in Table 8.16. In the table, there are two sections where some equipment has 2021 and 2024 costs while the other only has 2024 costs. The list of equipment with 2024 costs (current costs) was supplied by subsidiary of the holding company where it was easy to get current prices of those pieces of equipment. The other section with 2021 and 2024 has prices supplied from external vendors. The author used the 2021 cost figures and applied escalation factors based on the South African Inflation Adjustment calculator. From July 2021 when the prices were given to March 2024, there is an increase of 16.48 %. This represents an inflation rate of 8.2% per annum. This inflation rate was applied to the 2021 prices and projected to the 2024 prices. The 2024 column of costs consists of actual prices and 2021 inflation adjusted costs for the pieces of equipment where prices were not readily available. The total cost of the main equipment is R173,940,937.

When this cost is plugged into the Peter and Timmerhaus table, the results are presented in Table 8.17. To get the Total Depreciable Costs (TDC), the main equipment costs E_k was multiplied by the Lang factor of 4.13. The TDC for this project is R718,376,073 with a working capital cost (OpEx) of R128,716,294 per annum. From the table, the other components of plant direct costs are calculated using the given factors as per Peters and Timmerhaus method. These direct plant costs amount to R335,706,010 and the main drivers of this number are service facilities, equipment installation labour, piping, and buildings. The next big component is the indirect cost under engineering and construction costs. These costs are R114,801,019 and the two components are almost equal. One other critical component is the contingency amount, which is the money for covering any unforeseen emergencies that may arise as the project progresses. This contingency amount was R62,618,738, which is about 8.7% of the Total Depreciable Costs. The working capital component for the project is R128,716,294 and is 17.9% of the TDC for this project. To get the monthly Operating Expenditure (OpEx), the working capital is divided by 12 months, and this amount is R10,726,358.

Table 8.16: Main equipment cost for the ultrafine beneficiation

Equipment/Description	Code/#	2021 Cost	2024 Cost (Adjusted)	Total Costs
Coarse Primary Spiral Distributor	16-Way		R37,589	R37,589
Fine Primary Spiral Distributor	24-Way		R48,000	R48,000
Secondary Spiral Distributor	32-Way		R57,478	R1,839,296
Coarse Spirals	M1T53		R71,862	R8,623,440
Fine Spirals	M1T53		R71,862	R14,372,400
Feed Classifying Cyclone	20wCY 180/8		R1,223,840	R2,447,680
Scavenger Tables Distributor	16-Way		R37,589	R37,589
Scavenger Shaking Tables Feed Dewatering Cyclone	20wCY125		R750,642	R750,642
Rougher Shaking Tables Distributor	16-Way		R37,589	R75,178
Rougher Shaking Table Feed Dewatering Cyclone	20wCY125		R750,642	R1,501,284
Fines Shaking Tables Distributor	16-Way		R37,589	R37,589
Final Product Dewatering Cyclone	20wCY125		R750,642	R1,501,284
Guard Dewatering Cyclone	20wCY350		R3,564,223	R3,564,223
Trash Removal Linear Screen	MIPLSc	R877,955.00	R1,034,230.99	R1,034,230.99
Dewatering Cone Thickener	RBHOL-600	R5,680,692.03	R6,691,855.21	R13,383,710.42
Feed Preparation Pumps	HM200	R206,167.00	R242,864.73	R971,458.90
Coarse Spirals Feed Pumps	HM200	R50,275.00	R59,223.95	R118,447.90
Coarse Spirals Concentrate Pumps	HM100	R10,744.00	R12,656.43	R50,625.73
Coarse Spirals Middlings & Tailings pumps	HM150-55kw	R50,275.00	R59,223.95	R118,447.90
Fine Spiral Concentrate Pumps	HM75	R7,873.00	R9,274.39	R37,097.58
Fine Spirals Middlings and Tailings pumps	HM75-30kw	R10,744.00	R12,656.43	R50,625.73
Screen Undersize pumps	HM150-30kw	R10,744.00	R12,656.43	R50,625.73
Screen Oversize pumps	HM75	R7,873.00	R9,274.39	R18,548.79
Rougher Shaking Tables Concentrate Pumps	HM150-30kw	R10,744.00	R12,656.43	R50,625.73
Rougher Shaking Tables Middlings Pumps	HM200	R50,275.00	R59,223.95	R118,447.90
Rougher Shaking Tables Tailings	HM200	R50,275.00	R59,223.95	R118,447.90

Scavenger Shaking Tables Concentrate Pumps	HM150-30kw	R10,744.00	R12,656.43	R25,312.86
Scavenger Shaking Tables Middlings & Tailings Pumps	HM150-30kw	R10,744.00	R12,656.43	R25,312.86
Fines Shaking Tables Concentrate Pumps HM100	HM100	R10,744.00	R12,656.43	R25,312.86
Fines Shaking Tables Middlings & Tailings Pumps	HM250	R50,275.00	R59,223.95	R118,447.90
Final Tailings Cyclone Feed Pumps 400MCR	400MCR	R352,864.00	R415,673.79	R831,347.58
Thickener Underflow Pumps HM250	HM250	R69,898.00	R82,339.84	R164,679.69
Tailings Disposal Pumps HM250	HM250	R34,240.00	R40,334.72	R242,008.32
Coarse Concentrate Screens	D5Z102100	R1,811,980.00	R2,134,512.44	R12,807,074.64
Shaking Tables	DST999	R1,434,208.00	R1,689,497.02	R87,853,845.25
Tailings Thickener	THKØ38	R17,119,100.00	R20,166,299.80	R20,166,299.80
Cross-Cut Samplers -Feed, Conc and Tails	F, C&T	R497,451.00	R585,997.28	R1,757,991.83
Total				**R173,940,937.81**

Table 8.17: Cost estimates based on Peters and Timmerhaus

Item	Solids/Fluids Factor	Solid/Fluids Costs
Delivered equipment	**1**	**R173,940,938**
Equipment installation labour	0.39	R67,836,966
Instrumentation and control	0.13	R22,612,322
Piping	0.31	R53,921,691
Electrical installations	0.1	R17,394,094
Buildings	0.29	R50,442,872
Yard improvements	0.1	R17,394,094
Services facilities	0.55	R95,667,516
Land	0.06	R10,436,456
Direct Plant Costs (DPC)	***2.39***	***R415,718,841***
Engineering and supervision	0.32	R55,661,100
Construction expenses	0.34	R59,139,919
Direct and Indirect costs (DIC)	***3.59***	***R624,447,967***
Contractor's fee	0.18	R31,309,369
Contingency	0.36	R62,618,738
Total depreciable costs (TDC)	***4.13***	***R718,376,073***
Working capital	0.74	R128,716,294
Total Capital investment (TCI)	***4.87***	***R847,092,367***

8.9 Economic Evaluation

To evaluate the economic viability of this project, key financial numbers relating to the cashflows of this project are presented below and used in the financial calculation. The following numbers are assumed for the plant capacities and the prevailing conditions in the commodities sector.

Monthly Nominal metallurgical chrome production	*21626 tons*
Transport cost per ton of metallurgical chrome	*R1400.00*
US Dollar price per ton of metallurgical chrome	*290.00*
Monthly Operational Cost of the plant	*R10,726,358*
Current US$/Rand exchange rate	*18.51*
Discount rate	*11.75%*

Table 8.18 shows the cashflow for a period of 5 years to determine the Net Present value of the project.

Table 8.18: Cashflow performance of the project over five years

	Present Value	**Year 0**	**Year 1**	**Year 2**	**Year 3**	**Year 4**	**Year 5**
Capital Investment (Rmil.)	718.4	718.4					
Chrome Tons			259,512	259,512	259,512	259,512	259,512
Revenue (Rmil.)			1,393.0	1,393.0	1,393.0	1,393.0	1,393.0
OpEx (Rmil.)			-128.7	-128.7	-128.7	-128.7	-128.7
Transport Costs (Rmil.)			-363.3	-363.3	-363.3	-363.3	-363.3
Net Revenue (Rmil.)			901	901	901	901	901

From Table 8.19, upon completion of the project and having incurred costs of R718.4 million, the plant produced 259,512 tons per year. At the current price of $290/ton the gross revenue is R1 393 million. The operational expenses including transportation costs amount to R492 million. The net revenue per annum is R901 million. When the future annual revenue is discounted to the current value, the results are shown in Table 8.19.

Table 8.19: Net Present Value table for the 5-year operating period of the project

			Revenue (Rmil.)					
	Present Value (Rmil.)	**Discount factor**	**Year 0**	**Year 1**	**Year 2**	**Year 3**	**Year 4**	**Year 5**
Year 0	-718.4	1.000	-R 718.4					
Year 1	806.4	0.895		901				
Year 2	721.7	0.801			901			
Year 3	646.0	0.717				901		
Year 4	577.5	0.641					901	
Year 5	517.2	0.574						901
NPV	**2,550.5**							

From the table above, the NPV for the project is R2,550.5 million at a discount rate of 11.75% per year. The payback period is 10.6 month (11 months). This results that the project's NPV is positive with the first year and this indicates a very profitable project. The decision recommended to the executive of the company is to go ahead with Front End Engineering Design work to get actual design costs for the execution of the project.

CHAPTER 9: CONCLUSIONS AND RECOMMENDATIONS

9.1 Conclusions

9.1.1 Introduction

The main objective of the research was to design a viable circuit for beneficiating ultrafine chrome tailings from a PGM and chrome processing plant. The research pathway involved investigation of key material properties of the feedstock, of the plant tailings, equipment options for ultrafine beneficiation and process variables to optimise separation. In this work, the plant tailings used for the test work was found to be 80% passing 75µm of which about 50% was passing 25 µm and was considered ultrafine. The chromite content of the material ranged between 7% and 12% Cr_2O_3. Pursuant to developing a viable circuit for beneficiating ultrafine chrome and PGM tailings to recover chromite the following objectives were set out:

a) To characterise the ultrafine tailings arising from a chrome and PGM beneficiation operation at Tharisa Minerals (Pty) Ltd in terms of mineralogical, physical properties and assay by size.
b) To investigate the influence of feed preparation units such as screens and densifiers on upgrading the ultrafine feed material.
c) To investigate the recovery, grade and yield response of the ultrafine chromite and associated gangue components in the ultrafine products of spirals, magnets and shaking tables individually and in permuted combinations using two/three levels of variables like (i) feed rate, (ii) solids concentration, (iii) spitter or cutter position and (iv) dressing water.
d) To investigate the impact of mineralogical and physical properties of the ultrafine chrome feed material on the processing response parameters such as yield, recovery, and product grade.
e) To establish correlations of processing response parameters such as yield, recovery, and product grade to the process variables for singular separation and combinations of separation units.
f) To develop a high-level economic evaluation of the optimum flow sheet.

The following sections will present conclusions derived from results of the study.

9.1.2 Feed characterisation

The characterization of the feed material was done to determine (a) the chemical composition, (b) particle size distribution, (c) mineral phase identification and abundance, (d) mineral liberation and association and (e) grain size distribution of the investigated chrome processing tailings. The following results on the analysis of the tailings is given in the sections below.

9.1.2.1 Chemical Assay

The main components of the feed material were found to be SiO_2–42.49%, Al_2O_3-17.18%, MgO-11.66%, Fe_2O_3-11.21%, Cr_2O_3-9.01% and CaO-7.32% with minor oxides making the balance. The level of Cr_2O_3 indicates that this is a lean source (tailings) of chromite due to prior recovery operations, silica, alumina, and magnesia being the main diluent materials in the gangue.

9.1.2.2 Particle size distribution and Fractional Analysis

Results from cumulative particle size distribution showed that almost half the mass (49.6%) was less than 25µm and about 80% was below 75µm. Of the 50.4% mass above 25µm, 9.4% was above 106µm while 19.8% was in the -75+53µm. As the particle size decreases from 106 to 25 µm the Cr_2O_3 concentration increases from 1.56% to 11.04% with Fe_2O_3 showing a similar trend, increasing from 6.07% in 106µm to 12.54% in the -25µm particles. The other main oxides, SiO_2, and CaO showed opposite trend from that of Cr_2O_3 and Fe_2O_3. This result indicated that chromite is mainly concentrated in the ultrafine size fractions.

9.1.2.3 Mineralogical characteristics

X-Ray diffraction analysis of the sample showed that the most predominant mineral was feldspar with 41.7% mass contribution, dropping linearly from 58.1% in the +106µm fraction to 37.7% in the -25µm fraction. This trend shows that feldspar is predominant in the coarser fractions than finer. The mineral second in abundance was enstatite-ferrosilite (pyroxene member) that had 29.2% mass contribution. The peak concentration for enstatite-ferrosilite was in the -106+75 µm at 35.8% and then linearly dropping to 26.9% in the -25µm fraction. This trend followed the feldspar trend except for the +106µm fraction. Chromite was the third mineral in terms of abundance at 18% in the feed sample, increasing from 2.90% in the +106 up to 24.6% in the -53+25 µm fraction before dipping slightly to 20.6% in the -25 µm. This trend was opposite to those of the feldspar and enstatite-ferrosilite, meaning that at finer particle sizes more chromite was prevalent than the gangue components of feldspar and enstatite-

ferrosilite. The other minor minerals in the feed sample were diopside and amphibole at 2.7% and 2.1%, respectively.

9.1.2.4 Chrome and Iron deportment

Chrome and Iron deportment in the particles showed that Cr % was 36.38%, Fe 24.90%, Al 7.60%, Mg 4.60%, and O 26.37%, respectively. This gave a Cr/Fe ratio of 1.45 and compared to 1.8 of a pure chromite grain, showing that this chromite mineral was less pure than the pure Cr_2O_3 and FeO matrix. The ratio was reduced by the presence of Al and Mg in the chromite. The absence of Si in the EDS results shows that Si does not substitute with Fe or Cr in this chromite mineral spinel. The deportment analysis showed that all the Cr in the chromite sample came from the chromite mineral while Fe was contributed from chromite, enstatite-ferrosilite, chlorite amphibole and magnetite.

9.1.2.5 Mineral Associations

Mineral associations data on chromite grains showed that on average, from +106µm particle size down to -25µm about 97.71% of the perimeter was free meaning that there was no mineral associated with chromite. Only 2.29% of the surface was associated with feldspar and enstatite-ferrosilite. At +106µm the free surface of the chromite grains was found to be 71.90% and the associated surface was with feldspar at 13.18% and enstatite-ferrosilite at 6.01% with balance of 3.07% being pores. The association data showed that the particles below 106µm are almost fully liberated and any separation processes that depend on free surface to separate chrome from other gangue particles the selectivity would be improved in finer size range in comparison to +106µm size which has 13% of surface associated with gangue components.

9.1.2.6 Chrome Liberation

Three main classes of liberation were used to classify the liberation volume % of the particles. These classes are;

- Liberated-≥70 liberation of particles,
- Middling - ≥30%, <70% liberation of particles
- Locked-<30% liberation.

It was shown that 90.9% of the chrome particles were in the liberated class, 6% in the "Middling" class, and 3.2% in the "Locked" class. In terms of the distinct size fractions, the "Liberated" class increased from 50.3% in the +106 µm size to 95.6% in the -25µm size

fraction. The pattern observed was that as the particle size decreased, the degree of liberation increased. Given that this material was tailings from another chrome recovery circuit but was not recovered, it shows that liberation was not a determinant for recovery. It means that the particles could not be recovered due to their ultrafine size making spiral gravity separation difficult.

9.1.2.7 Chromite Grain Size Distribution

One of the mineralogical parameters that was investigated was chromite grain size distribution with the grain size measured in equivalent sphere diameter (ESD). It was shown that 46.6% were in the <20µm ESD, 41% in the ≥20<60µm ESD, 10.2% in the ≥60<100µm ESD and only 2% in the ≥150<190µm ESD. In terms of size fractions, it was noted that the +106 µm fraction had a spread of grain sizes from <150µm to <20µm. This shows that the chromite grains of sizes 20µm to 100µm in the +106µm fraction conglomerated to form multi-grain particles of the size above 106µm. Similarly, there were 20µm, 60µm and 100µm grains in the -106+75µm with the similar pattern of conglomeration of chrome grains into bigger particles in the size fraction the grains were detected. The overall results show that the bulk of the chromite grains are in the -20µm size. This points to the difficulty of the recovery of chrome from this material since 20µm is exceedingly difficult to separate using conventional gravity methods. The other information that was derived from this analysis is that as the particles became smaller the chromite particles were becoming more planar in shape than the angular-spherical shape in the coarse fraction. The planar shape reduces the settling velocity of the chrome particles rendering them less amenable to efficient separation.

9.1.3 Separator Performance and Identification of significant factors

The separator units used in this study were a wide angle shallow M1T53 spiral, a Malvern L300 WHIMS belt magnetic separator and a Holman-Wilfley Model 800 shaking table separator and DOE results were used to determine parameters affecting separation of chromite ore tailings.

The following sections summarize the results on separator performance.

9.1.3.1 Spiral separator significant factors

Results from the DOE on spiral separation revealed that concentrate cutter position was the most significant factor for concentrate recovery and upgrade, or enrichment ratio followed by

spiral feed rate and then slurry density. However, the factors for recovery were opposite those for upgrade. As a result, intermediate level of the factors was chosen for the optimum spiral separation. The spiral separation settings chosen were slurry density 1.52t/m^3, feed rate 0.83t/h and concentrate cutter position 75mm.

9.1.3.2 Magnetic separator significant factors

The magnetic separator results revealed that the most significant factor for recovery and upgrade ratio was wash water flow followed by slurry feed rate. Belt speed was only significant for magnetic fraction grade and upgrade ratio. From these results, the chosen set of conditions were slurry density 1.38t/m^3, slurry flow rate 1.0 t/h, belt speed 0.5m/sec and wash/fluidization water 74.4ml/sec.

9.1.3.3 Shaking table separator significant factors

Shaking table results showed that the shaking table deck angle was the most significant factor for concentrate recovery. There was also an interaction effect between feed rate and deck angle factors. From the Taguchi main effect plots, the deck angle, feed rate and wash water were identified as main effect parameters for concentrate grade. For concentrate recovery, the only significant factors were deck angle and feed flow rate. The response surface plots showed that deck angle was the significant factor overall. The optimised conditions for the shaking table separation were slurry density 1.34t/m^3, feed rate 0.01428t/h (500ml/min slurry), wash water 140ml/sec and deck angle 4^o. All the factors and levels discussed in the above sections for each separation unit were chosen and applied in the full circuit tests whose results are presented in the next sections.

9.1.4 Full circuit Configurations

The results of the feed characterisation and separator performance were used to make the decision of where each separator unit was positioned in the flowsheet/circuit. The separator performance tests also helped to determine the optimum operating parameters for the full circuit test work. Two circuit options were proposed, and these are discussed in the following sections.

9.1.4.1 Circuit Configuration 1 (Spirals, Magnets, Screens and Shaking Tables)

The circuit Configuration 1 that comprised of a spiral, magnet, screen and shaking table produced three final products separately. Shaking table concentrate from spiral concentrate had

grade of 41.24% Cr_2O_3 at a recovery of 15.10%. The second shaking table concentrate from the recleaned shaking table middling had a grade of 37.99% Cr_2O_3 at a recovery of only 1.96%. The Shaking table concentrate from the magnetic concentration had a grade of 41.95%Cr_2O_3 at a recovery of 1.94%. The combined final concentrate grade was 40.59% Cr_2O_3 at a yield and recovery of 5.81% and 19.01%, respectively. The tailings grade for the full circuit was 8.52% Cr_2O_3 from a feed grade of 10.68% Cr_2O_3. The purpose of screening spiral concentrate at 106µm before shaking table concentration was to improve separation efficiency by narrowing particle size range.

9.1.4.2 Circuit Configuration 2 (Screens Spirals, Screens and Shaking Tables)

The Configuration 2 setup consisted of a split feed of +25 µm and -25µm streams separately processed from spiral stage down to shaking table. The separation of the particle sizes was meant to narrow the particles size range on both spirals and shaking table and improve efficiency. At the spiral stage, the +25µm concentrate analysed 12.49% Cr_2O_3 while middlings and tailings analysed 3.45% and 2.71% Cr_2O_3 respectively. The low grades of middlings and tailings indicated improved selectivity compared to unscreened feed in circuit configuration 1. The final shaking table concentrate from the coarse spiral concentrate had a grade of 41.51% Cr_2O_3 at a yield and recovery of 4.08% and 19.78%, respectively. The shaking table middlings produced a concentrate of grade 39.75%Cr_2O_3 at a yield and recovery of 1.86% and 5.56%, respectively.

The -25µm fraction produced a spiral concentrate of 14.37% Cr_2O_3, and middlings and tailings of 7.55%Cr_2O_3 and 8.83% Cr_2O_3 respectively. The shaking table final concentrate was of grade 35.05% Cr_2O_3 at a yield and recovery of 1.06% and 3.94%, respectively. The combined final concentrate analysed 40.07% Cr_2O_3 at an overall yield and recovery of 7.00% and 29.28%, respectively. The final tailings of the configuration 2 circuit had grade of 7.12% Cr_2O_3 from a feed of 8.26% Cr_2O_3. The +25µm fraction produced better results than the -25µm due to size effect, since ultrafine particles are difficult to separate using gravity methods.

The superior results of circuit configuration 2 was because concentrating feed on the spirals and shaking table separately produced a more efficient separation by reducing particle size effect range and amplifying the density effect. For this reason, the configuration 2 chosen as the circuit to have a techno-economic evaluation on as opposed to circuit configuration 1.

9.1.5 Techno-Economic Evaluation

A comparison of circuit 1 and 2 performance showed that circuit 2 was marginally better than circuit 1 in terms of yield and recovery as well as the final tailings grade. Because of this comparative difference, the techno-economic evaluation was done circuit 2 design. The design according to circuit 2 comprised of main processing units listed below:

- Spirals 320
- Shaking tables 52
- Cyclones 8
- Screens 6
- Cone thickeners 2
- Tailings thickener 1

The Capital Expenditure (CAPEX) on these pieces of main equipment and other ancillary units amounted to R718,376,073 and operating cost (OpEx) of R128,716,294 per annum. This plant design will produce 259 512 tons of metallurgical grade chrome per annum at a selling price of US$290.00 per ton. Using a Rand to US dollar exchange rate of 18.51% and a discount rate of 11.75%, the net present value NPV of the project over 5 years will be R2,550.5 million. This translates to a payback period of 10.6 months.

These experimental tests and the financial model show that the project is technically and economically viable. However, the amount of chrome remaining in the final tailings of this process is still substantial such that there is scope for other processing methods that can be investigated to further recover the ultrafine chrome missed by the gravity process investigated and presented in this work. The following section presents the recommendations from the results generated in this work as well as other opportunities outside the scope of this work all to develop comprehensive methods to recover the ultrafine chrome from the chrome and PGM tailings.

9.2 Recommendations

The following section lists some recommendations from this work to further advance the beneficiation knowledge of ultrafine chrome as well as the equipment settings. The following recommendations are areas that were either out of scope of the current work but showed some linkages with current research and need further investigation or they are areas investigated in

this work but need further probing to generate more data and knowledge in the same subject area. The following recommendations are made for further research:

9.2.1 Selective flocculation

In this research it was seen that recovery of chrome particles at finer particles size <25µm is exceedingly difficult. Only 4.87% of the chrome in the -25µm is recovered into the concentrate, while 64.23% is recovered into the middlings and 30.9% recovered into the tailings. The highest recovery of chrome was in the -106+75 µm fraction at 28.98% followed by 26.17% in the +106 µm fraction. This shows that recovery of chrome in the coarser size fractions is superior. Selective flocculation of the feed material prior to gravity separation on the spirals will improve the recovery since it can produce homogenous coagulation of the chrome particles. This work was outside the scope of this research and its investigation will enhance the recovery of the ultrafine chrome. There is literature published on the selective flocculation of chrome and can be is used to understand the behaviour of particles and enhance recovery of ultrafine particles.

9.2.2 Size range separation and Gangue oxide rejection

Results of this research have pointed to the benefit of improving recovery of chrome when narrow size range are processed separately. In this work treatment of the -25µm stream separately from the +25µm gave better performance than when no classification was done. Separating the feed into narrow size fractions (-25µm, -53+25µm, -106+53µm and +106µm) and determining the effective slurry density and feed rate ranges would add more knowledge towards understanding the beneficiation of ultrafine chrome.

The behaviour of the MgO, CaO, SiO_2, Al_2O_3 during gravity and magnetic separation need further studies as it was observed that MgO behaved differently on the shaking table compared to on the spiral. The focus on gangue rejection could be key to improving the effectiveness of ultrafine chrome tailings beneficiation.

9.2.3 Chrome flotation

The literature on effective size range of application of conventional mineral processing techniques has indicated that froth flotation has the potential to recover ultrafine down to 5µm size. Chrome flotation has not been extensively studied but with realization most of the chrome in this study is in the -25µm size fraction, chrome flotation tests would add more insight into

the extent to which recovery of chrome can reach if gravity and pneumatic processes are combined. The mineralogy of the feed material to this study has indicated that the chrome particles in the feed stream are 91% liberated. This means that any surface process like flotation can work on the particles since the surface to be modified by the reagents will be pure chrome mineral surface.

9.2.4 Two stage spiral separation

The spiral separation section of this study has indicated that the spiral products are classified according to size. The concentrate stream is the coarsest of the three and the tailings is the finest of the three while the middlings particle size is like the feed. This shows that the spiral can be used as a classifier. An investigation into the separation of chrome when all three spiral products are processed separately on another stage of spiral separation will improve the chrome separation since these will be near size streams. Investigation into the slurry density and feed rate suitable for each stream will provide some understanding on the potential of using spirals to upgrade the chrome grade close to target saleable level.

9.2.5 Modelling of the gravity circuit data

This work has generated substantial amount of data to form the basis of modelling. Choosing a mineral processing simulation software to model the scenarios of the chosen circuit will optimize the results and assist in refining the process parameters and even equipment positioning. Simulation packages like JKSimMet, ModSim and METSIM can be considered for use in this simulation of the process using data generated in this work.

LIST OF REFERENCES

Agacayak, T., Zedef, V., and Aydogan, S., *Beneficiation of low-grade chromite ores of abandoned mine at Topraktepe, Beysehir,* SW Turkey, Acta Montanistica Slovaca, Rocnik, 12, 2007, Cislo 4, pp323-327.

Abubakre, O.K., Muriana, R.A., and Nwokike, P.N., *Characterization and beneficiation of Anka Chromite ore using magnetic separation process***,** Journal of Minerals & Materials Characterization & Engineering, Vol 6, No 2, 2007, pp 143-150,**.**

Alaee, N., H., Sargheyni, J., Pezeshkan, M., and Kianoush, P**.,** *Design and optimization of a spiral separator for enhanced chromite recovery and sustainability,* Cleaner Engineering and Technology 24 (2025).

Al-Tigani, M.M.H., Awdekarim, A., Abdueldaem, A.A., and Seifelnasr, S, *Application of Response Surface Methodology on Beneficiation of Sudanese Chromite Ore via Pilot Plant Shaking Table Separator*, International Journal of Academic Multidisciplinary Research, Vol 4, Issue 5, May 2020, pp 63-73.

Ansari, M.I., *Fine particle processing – A difficult problem for engineers,* Proceedings: PROF-1997, pp. 93-102.

Ankireddy, P.R., Sudikondala, P., Mangadoddy, N., Tripathy, S.K., Yanamandra, R.M., *Comparative studies of experimental and numerical investigations of fluid flow and particle separation of high-gravity spiral concentrators*. Ind. Eng. Chem. Res. 63, 2024, pp 12177–12198.

Aras, A., and Taner, H.A., *Investigation of chromite ore beneficiation possibilities with different gravity concentrators,* The Mining -Geology Petroleum Engineering Bulletin, pp 127-134.

Atesok, G., Yildirim, I. and Celik, M.S. *Applicability of the Reichert spiral for cleaning bituminous and lignitic coals: a pilot study*. International journal of Mineral Processing 40 (1-2), 1993, pp 33-44.

Atiq, S., Hafeez, I., Khan, K., and Malik, M.A., *Beneficiation studies on the Low-grade chromite of Muslim Bagh, Balochistan, Pakistan*, Pak, J. Sci. Ind Res. 48(2), 2005, pp 86-89.

Banerjee, T.H., Sengupta, A.K., Sutaone, A.T., and Gundewar, C.S**.**, *Beneficiation practices in the Sukinda Valley area chromite deposits*, IBM, Nagpur, Proceedings of the International Seminar on Mineral Processing Technology-2006, Chennai, India pp.405–411.

Beklioglu, B. and Arol, A.I**.,** *Selective flocculation behaviour of chromite and serpentine*, Physicochemical Problems of Mineral Processing, 38, 2004 pp 103-112.

Boisvert, L., Sadeghi, M., Bazin, C*., Investigation of residence time and fluid volume in spiral concentrators.* Minerals. Engineering, 202, 2023.

Boisvert, L., Sadeghi, M., Rochefort, C., Bazin, C*., Axial or turn-by-turn particle recovery in a spiral concentrator.* CIM Journal 15, 2024, pp 45–58

Bornman, F., Foisy, R., and Naude, N**.,** *Spiral conditions for the recovery of ultra-fine particles*, IMPC 202: XXX International Mineral Processing Congress, Cape Town, South Africa, 18-22, Oct. 2020.

Boucher, D., Deng, Z., Leadbeater, T., Langlois, R., Waters, K.E., *Observation of iron ore beneficiation within a spiral concentrator by positron emission particle tracking of large (Ø=1440μm) and small (Ø=58μm) hematite and quartz tracers*. Chemical. Engineering Science. 140, 2016, pp 217–232.

Brożek, M., and Surowiak, A., *Effect of particle shape on jig separation efficiency*, Physicochemical Problems of Mineral Processing, 41, 2007, pp 397-413

Burt, R.O., and Mills, C**.,** *Gravity concentration Technology-Developments in Mineral Processing*, Vol. 5, , Elsevier, New York. 1984, pp 81-107.

Burt, R., *The role of gravity concentration in modern processing plants*, Minerals Engineering, Vol. 12, No. 11, 1999, pp. 1291-1300.

Burt, R.O., *Gravity Concentration***,** Tantalum Mining Corporation of Canada Ltd, 2005.

Can, I.B., Özsoy, B., and Ergün, S.L., *Developing an optimum beneficiation route for a low-grade chromite ore,* Physicochemical Problems of Mineral Processing, 55(4), 2019, pp 865-878.

Cicek, T., Cengizler, H., & Cocen, I., *An efficient process for the beneficiation of low-grade chromite ore*, Mineral Processing and Extractive Metallurgy, 119:3, 2010, pp 142-146.

Cicek, T., Cengizler, H., & Cocen, I., Engin, V.T., and Sen, S., *Technical and economic applicability study of centrifugal force gravity separator (MGS) to Kef chromite concentration plant*, Mineral processing and extractive metallurgy, 117:4, 2008, pp 248-255,.

Cicek, T and Cocen, I., *Gravimetric concentration of fine chromite tailings*, Innovation in Mineral and Coal processing, Belkema, Rotterdam, Netherlands, 1998.

Crause, R. (2013), *South African Inflation (2024*) (Online).
Available at: https://inflationcalc.co.za.

Dallaire, R., Laplante, A., and Elbrond, J., *Humphrey's spiral tolerance to feed variations*, Canadian Mining and Metallurgical Bulletin 71(796), 1978, pp 128-134.

Danacıoglu, N.∗ and Muluk, F.Z., *Taguchi techniques for 2^k fractional factorial experiments,* Hacettepe Journal of Mathematics and Statistics Volume 34, 2005, pp 83–93

Das, A. & Sarkar, B**.,** *Advanced gravity concentration of fine particles: A review***,** Mineral processing and extractive metallurgy review, 39:6., 2018 pp 359-394.

Das, S.K., *Quantitative mineralogical characterization of chrome ore beneficiation plant tailing and its beneficiated products*, International Journal of Minerals, Metallurgy and Materials. Volume 22, No 4, , 2015, pp 335–345.

Dawson, N.F**.,** *Experiences in the production of metallurgical and chemical grade UG2 chromite concentrates from PGM tailings streams*, The Journal of The South African Institute of Mining and Metallurgy, Volume 110, 2010, pp. 683–690.

De Andrade, A., Thornton, C., Mac Hunter, D. and Agenbag, J**.**, *Advances in Spiral Automation and Ultrafine Processing*, Engineering, Materials Science**,** 2014.

Drzymala, J., *Mineral processing: Foundations of theory and practice of metallurgy*, 1st English Edition, Oficyna, Wydawnicza PWr., 2007**.**

Durakovic, B., *Design of Experiments Application, Concepts, Examples: State of the Art,* Periodicals of Engineering and Natural Sciences 2303-4521 Vol 5, No 3, December 2017, pp 421–439

Dysert, L.R**.,** *Sharpen Your Cost Estimating Skills***,** Cost Engineering Vol.,45/No 6, June 2003.

Dworzanowski, M**.** *Optimizing the performance of wet magnetic separators,* Journal of The Southern African Institute of Mining and Metallurgy, Vol. 110, Nov 2010, pp. 643-653.

Falconer*,* A**.,** *Gravity separation: Old techniques/new methods,* Physical separation in Science and Engineering, Vol.12 No. 1, 2003, pp 31-48.

Gokarn, P., Ranjan, A., Nayak, C. R., and Murthy, Y.R**.,** *Sustainable development through beneficiation of low-grade chromite ores*, Tata Steel Limited Private Publication, 2015.

Guney, A., Onal, G., and Atmaca, T., *New aspect of chromite gravity tailings re-processing*, Minerals Engineering, Vol.14, No 11, 2001, pp 1527-1530.

Henderson, D.K., & McHunter, D.M., *A review of spiral technology for fine gravity beneficiation*, Internal communication, 2000.

Holtham, P.N., *Flow visualisation of secondary currents on spiral separators*., Minerals Engineering 3(3-4), 1990, pp 279-286.

Holtham, P.N., *Particle transport in gravity concentrators and Bagnold effect*, Minerals Engineering, 5(2), 1992, pp 205-221.

Honaker, R.Q., Forrest, W.R., *Advances in Gravity Concentration*. Society for Mining, Metallurgy, and Exploration, 2003.

Izerdem, D. and Ergun, S.L**.** *Size by size evaluation of the concentration process in spirals concentrators*, IMPC 2018, September 15-21, 2018, Moscow, Russia.

Jenkins, W., S., and Hayslip, G., O., *Removal of Silica from Samples of chrome ores from Canadian Refractories Limited, Montreal*, Mines Branch Investigation Report, 1965, IR65-34.

Jou, Y.T, Lin, W.T, Lee, W.C., and Yeh, T.M., *Integrating the Taguchi Method and Response Surface Methodology for Process Parameter Optimization of the Injection Moulding*, Applied Mathematics & Information Sciences 8, No 3, 2014, pp 1277-1285.

Kari, C., Kapure, G., and. Rao, S.M**.,** *Effect of Operating Parameters on the Performance of Spirals***,** Proceedings of the International Seminar on Mineral Processing Technology-, Chennai, India, 2006, pp. 316 – 319.

Karna, S.K., & Sahai, R., *An Overview on Taguchi Method*, International Journal of Engineering and Mathematical Sciences, Volume 1, June 2012, pp 11-17.

Khakmardan, S., Doodran, R.J., Shiray, A., and Shirazi, A., *Evaluation of chromite Recovery from shaking table tailings by Magnetic separation method*, Open Journal of Geology, 10, 2020, pp 1153-1163.

Khuri, A. I., *Response surface methodology and its applications in agricultural and food* sciences, Biometrics & Biostatistics International Journal, Volume 5, Issue 5, 2017.

Kinnaird, J.A. Kruger, F.D., Nex, P.A.M., and Cawthon, R.G**.** *Chromitites of the bushveld complex-Process of formation and PGE enrichment*, Economic geology research institute information Centre, No. 369, Dec 2002.

Majumder, A.K &. Barnwal, J.P., *Modelling of enhanced gravity concentrators-present status,* Mineral processing and extractive metallurgy review, 27:1, 2006, pp 61-86,.

Makgokgoa, M.E**.** *The Recovery of chromite from slimes using a shaking table*, Final Year project, Oct 2019.

Martín-Gil, A., Flores, O., *Predicting the skin friction's evolution in a forced turbulent channel flow*. Computational. Fluid dynamics, 284, 2024.

Maruli, M & Nheta, W. *Characterisation of South African Chromite Middle Group Seams,* Proceedings of the 6th World Congress on Mechanical, Chemical and Material Engineering (MCM'20), Virtual Conference – August 2020, DOI: 10.11159/mmme20.136.

Meng, L., Gao, S., Wei, D., Zhao, Q., Cui, B., Shen, Y., Song, Z., *Particulate flow modelling in a spiral separator by using the Eulerian multi-fluid VOF approach*. International. Journal of. Mineral. Science. Technology. 33, 2023, pp 251–263.

Mishra, B.K., and Tripathy, A., *A preliminary study of particle separation in spiral concentrators using DEM*, International Journal of Mineral Processing, 94 , 2010, pp192-195.

Montgomery, D. C., *Design and Analysis of Experiments,* Eighth Edition, John Wiley & Sons, Inc. 2013,

Mular, A.L., *Mineral Processing Equipment Costs and Preliminary Capital Cost Estimations*, The Canadian Institute of Mining and Metallurgy, Vol 25, 1982, pp 310-325.

Mulenga, F.K. and. Bwalya, M.M., *Application of the attainable region technique to the analysis of a full-scale mill in open circuit*, The Journal of The Southern African Institute of Mining and Metallurgy, Volume 115**,** August 2015, 729.

Murthy, Y.R., Tripathy, S., K and, Kumar, C.R**.,** *Chrome ore beneficiation challenges & opportunities – A review*, Minerals Engineering 24, 2011, pp 375–380.

Murthy, Y.R., and Tripathy, S.K., *Process optimisation of a chrome ore gravity concentration plant for sustainable development,* The journal of the Southern African Institute of Mining and Metallurgy, Vol 120, 2020, pp 261-268.

Nzeh, N. S., Popoola, P., Okanigbe, D., Adeosun, S., and Adeleke, A., *Physical beneficiation of heavy minerals-Part 1: A state-of-the-art literature review on gravity concentration techniques*. Heliyon 9, 2023.

Ozyurt, M., Cebeci, Y., and Ergun, S.L., *Recovery of chromite from concentrate plant tailings*, Scientific Mining Journal, 62(1), 2023, pp 17-21.

Ozcan, O., *Investigation of chromite recovery possibilities from coarse and fine plant tailings*, Scientific Mining Journal, 61(2), 2022 pp 69-81.

Palmer, M. and Vadeikis, C. *New developments in spirals and spiral plant operations*. Proceedings of the XXV International Mineral Processing Congress (IMPC) 2010. Australasian Institute of Mining and Metallurgy, Melbourne. 2010, pp. 1099–1108.

Periyasamy, S and Aravind, M., *Optimization od surface Grinding Process Parameters by Taguchi Method and Response Surface Methodology*, International journal of Engineering Research & Technology, Vol 3 Issue 5, May 2014, pp 1721-1727.

Peters, M.S and Timmerhaus, K.D., *Plant Design and Economics for Chemical Engineers,* Fourth Edition, McGraw-Hill, Inc, 1991.

Ramsaywok, P., Vermaak, M.K.G., and Viljoen, R**.,** *Case study: High-capacity spiral concentrators***,** The Journal of The Southern African Institute of Mining and Metallurgy, Vol. 110**,** November 2010, pp 637-642.

Rao, A.M., Rath, R.K., Mohanta. M.K., Dey, B., Sahoo, M., and Singh, R., *Beneficiation studies on low grade chromite ores using Multi Gravity Separator*, International Seminar on Mineral Processing Technology 2017, 1-3 February 2017, pp 76-80.

Rao, R.B., Das, B., and Sastri, S.R.S., *Improving grade of Indian chromite ores by High-gradient magnetic separation,* Magnetic and Electrical Separation, Vol.8, pp 175-183.

Ranga, S., Jaimini, M., Sharma, S., K., Chauhan, B. S., and Amit Kumar, A., *A Review on Design OF Experiments (DOE),* International Journal of Pharmaceutical and Chemical Sciences, Vol. 3 (1) Jan-Mar 2014, pp 216-224.

Rath, R.K., Dey, B., Mohanta, M.K., Prusty, L.K and Singh, R, *Recovery of chromite values from tailings of COB plant using Enhanced Gravity Concentrator*, International Seminar on Mineral Processing Technology, 2017, pp 644-649.

Raykundaliya, D.P & Shanubhogue, A., *Comparison Study; Taguchi Methodology vis-à-vis. Response Surface Methodology Though a Case Study of Accelerated Failure in Spin-on-Filter*, International Advanced Research Journal in Science, Engineering and Technology, Vol 2, Issue 3, March 2015.

Richards, R.G., and Palmer, M.K., *High-capacity gravity separators, A review of current Status,* Minerals Engineering, Vol. 10, No. 9 1997, pp. 973-982.

Richards, R.G., MacHunter, D.M., Gates, P.J., and Palmer, M.K**.,** *Gravity separation of ultrafine (-0.1mm) minerals using spiral separators***,** Minerals Engineering Vol. 13 No.1, 65-77, 2000**.**

Rodl, R.H., Prinzing, P., and Aichert, D., *Cost Estimating for Chemical Plants*, AACE Transactions, Vol. 29, Section B-1, 1985

Ross, V., Ramonotsi, M., and Marape, G., *A study on the recovery of fine chromite from UG2 tailings*, Minerals Engineering 187, 2022.

Roy, S., *Recovery improvement of fine magnetic particles by Floc magnetic separation*, Mineral processing and extractive metallurgy review, 33:3, 2012, pp 170–179,.

Seifelnassr, A.A.S., and. Tamam, T.A.K., *Flotation behaviour of Sudanese chromite ores,* Journal of Engineering Sciences, Assiut University, Vol. 39, No 3, May 2011, pp.649-661.

Sethabi, B. I., Popoola, A. P., and Tshabalala, L., *Evaluation of advanced gravity and magnetic concentration of a PGM tailings waste for Chromite recovery***,** Iran Journal of Chemical Engineering, Vol. 38, No. 2, 2019.

Shah, R.A., Akhtar, M., and Amin, M., *Studies on the effect of particle size on the upgrading of chromite from Dargai area (Pakstan), Part 1*, Pakistan J. Sci. Ind. Res., Vol. 17, Nos. 4-5, August-October 1974.

Singh, R., Bhattacharyya, K.K., and. Maulik, S.C**.,** *Gravity concentration of fines and ultra-fines,* Proceedings: PROF – 97, pp. 40-56.

Singh, R.K. Dey, S. Mohanta, M.K., & Das, A**.,** *Enhancing the utilization potential of a low-grade chromite ore through extensive physical separation***,** Separation Science and Technology, 49:12, 2014.pp-1937-1945.

Sivamohan, R. and Forssberg, E**.,** *The Problems of recovering very fine particles in mineral processing-A review*, International Journal of Mineral Processing, 28(3) May 1990, pp 247-288.

Sivamohan, R., and Forssberg, E., Principles of Spiral Concentration, International Journal of Mineral Processing, 15, 1985, pp 173-181.

State-Ease, *Handbook for Experimenters A concise collection of handy tips to help you set up and analyse your designed experiments,* Version 11.01, 2019.

Steenekamp, J.M.A., *The geology of the chromitite seams and their partings on Tharisa Mine***,** Private publication, 2015**.**

Subandrio, S, Dahani, W., Alghifar, M., and Purwiyono, T.T., *Enrichment of Chromite Sand Grade using Magnetic Separator*, Indonesia Malaysia Research Consortium Seminar, 2018, (IMRCS 2018), IOP Conf. Series: Material Science and Engineering 588 (2019).

Sudikondala, P., Mangadoddy, N., Kumar, M., Kumar Tripathy, S., Yanamandra, R.M., *CFD modelling of spiral concentrator- prediction of comprehensive fluid flow field and particle segregation*. Minerals Engineering, 2022, 183,

Surkov, A.V. Samykina, E. V., Eppelbaum, L.V. and Semenov, S.V**.** *The main reasons for Mineral loss in gravity dressing,* The Open Mineral Processing Journal, 2008, 1, pp 37-44.

Szpyrka, J., and Suponik, T., *Impact of spiral separator geometrical parameters on the density separation of various fine-grained materials*, E35 Web of Conferences 18, MEC, 2017, P1-4.

Towler, G., and Sinnott, R., (2022) *Chemical Engineering Design: Principles, Practices and Economics of Plant and Process Design*, Third Edition, Oxford: Elsevier, Available at: https://doi.org/10.1016/B978-0-12-821179-3.00007-8

Tribe, M.A., and Alpine, R.L.W*., Scale Economies and the "0.6 Rule",* Engineering Costs and Production Economics, 10 ,1986, pp 271-278.

Tripathy, S.K, Ramamurthy, Y., and Singh, V., *Recovery of Chromite Values from Plant tailings by Gravity Concentration,* Journal of Minerals & Materials Characterization & Engineering, 2011, Vol. 1 No1 pp. 13-25.

Tripathy, S.K, Ramamurthy, Y., Sahu, G.P., and Tathavadkar, V**.,** *Ultra-fine chromite concentration using spiral concentrator*, Proceedings of the XI International Seminar on Mineral Processing Technology, 2010, pp 144-150**.**

Tripathy, S.K. Murthy, Y.R. Suresh, N. and Banerjee, P.K., *Dry High Intensity magnetic separation in mineral industry-A review of present status and prospects***,** Mineral Processing and Extractive Metallurgy Review, 38:6, 2017, pp 339-265.

Tripathy, S.K., Murthy Y. R., Singh, V., Farrokhpay S., and Filippov L., O., *Improving the Quality of Ferruginous Chromite Concentrates Via Physical Separation Methods*, Minerals, 2019, 9, 667.

Tripathy, S.K., and Murthy Y. R., *Modelling and optimization of spiral concentrator for separation of ultrafine chromite*, Powder Technology, 221, 2021, pp 387-394.

Tripathy, S.K., Murthy Y. R., and Singh, V., *Characterisation and separation studies of Indian chromite beneficiation plant tailings*, International Journal of Minerals Processing 122, 2013 pp 47-53.

Tripathy, S.K., Murthy, Y., R, Sahu, G.P., Panda, L Singh, V. and Tathavadkar, V., *Influence of shaking table process parameters on concentration of chromite plant tailings*, Proceedings of the XI International Seminar on Mineral Processing Technology, 2010, pp 199–204.

Tripathy, S., K., Murthy, Y., R., Singh, V., Farrokhpay, S., and Filippov, L., O., *Improving the quality of Ferruginous Chromite Concentrates Via Physical Separation Methods*, Minerals 2019, 9, 667.

Ucbas, Y., Bozkurt, V., Bilir, K. and Ipek, H., *Separation of chromite from serpentine in Fine sizes using magnetic carrier*, Separation Science and Technology, 49:6, 2014, pp 946-956.

Van Amsterdam, M.F., (2018), *Factorial Techniques applied in Chemical Plant Cost Estimation: A Comparative Study based on Literature and Cases*, Master's Thesis, Delft University of Technology., Volume 22, Number 4, April 2015.

Wain, Y.A., *Updating the Lang Factor and Testing its Accuracy, Reliability and Precision as a Stochastic Cost Estimating Method,* PM World Journal Vol. III, Issue X – October 2014.

Wesseldijk, Q.I., Reuter, M.A., Bradshaw, D.J., and Harris, P.J., *The flotation behaviour of chromite with respect to the beneficiation of UG2 ore*, Minerals Engineering, Vol 12, No. 10, 1999, pp 1177-1184,.

Wills, B.A., and Finch, J.A. *Wills' Mineral Processing Technology-An introduction to the practical aspects of Ore treatment and Mineral Recovery,* Eighth Edition, Elsevier, New York, 2016**.**

Zhao, Y., Zhang, Y., Bao, S., Liu, T., Bian, Y., Liu, X., Moufang, *Separation factor of shaking table for vanadium pre-concentration from stone coal*, Separation and Purification Technology, 115, 2013, pp 92-99.

APPENDICES

APPENDIX A: SEM-EDS SPOT ANALYSES AND CR/FE RATIO

Test Feed +106µm					
	O	**Mg**	**Al**	**Cr**	**Fe**
EDS Point 1	27.09%	4.78%	8.24%	34.88%	24.98%
EDS Point 2	26.93%	4.78%	7.95%	35.75%	24.56%
EDS Point 3	26.93%	4.98%	8.21%	35.58%	24.28%
EDS Point 4	26.74%	4.85%	7.64%	36.65%	24.09%
EDS Point 5	26.45%	5.02%	7.31%	37.39%	23.81%
EDS Point 6	26.39%	4.95%	8.13%	37.08%	23.43%
EDS Point 7	26.71%	4.77%	8.07%	36.20%	24.22%
EDS Point 8	26.38%	4.92%	8.04%	36.41%	24.23%
EDS Point 9	25.99%	4.58%	7.31%	36.18%	25.92%
EDS Point 10	26.97%	5.09%	7.94%	36.30%	23.67%
EDS Point 11	26.72%	4.45%	7.52%	36.78%	24.50%
EDS Point 12	27.36%	5.21%	8.85%	33.93%	24.63%
EDS Point 13	26.62%	4.96%	7.22%	37.29%	23.89%
EDS Point 14	26.10%	4.90%	7.70%	36.69%	24.58%
EDS Point 15	24.29%	3.59%	4.69%	38.03%	29.37%
EDS Point 16	25.50%	3.53%	6.01%	37.81%	27.12%
EDS Point 17	26.66%	3.72%	6.87%	37.72%	25.00%
EDS Point 18	27.93%	4.52%	7.87%	36.73%	22.92%
EDS Point 19	26.88%	4.45%	7.75%	35.43%	25.46%
EDS Point 20	26.41%	3.94%	5.63%	37.22%	26.78%
Average concentration	26.55%	4.60%	7.45%	36.50%	24.87%
Cr/Fe ratio					**1:1.47**

Test Feed -106/+75µm					
	O	**Mg**	**Al**	**Cr**	**Fe**
EDS Point 1	26.37%	5.26%	8.69%	35.54%	24.11%
EDS Point 2	25.30%	5.05%	7.59%	38.79%	23.25%
EDS Point 3	24.26%	3.97%	7.00%	37.36%	27.38%
EDS Point 4	26.60%	5.21%	8.53%	35.69%	23.94%
EDS Point 5	24.98%	4.28%	8.00%	37.92%	24.80%
EDS Point 6	26.63%	4.93%	8.22%	35.63%	24.57%
EDS Point 7	25.64%	4.33%	7.47%	36.64%	25.89%
EDS Point 8	25.22%	5.45%	8.72%	36.71%	23.87%
EDS Point 9	26.38%	5.21%	8.56%	36.23%	23.60%
EDS Point 10	24.58%	4.22%	6.46%	38.35%	26.36%
EDS Point 11	25.70%	5.01%	7.56%	37.56%	24.14%
EDS Point 12	25.29%	4.75%	8.02%	36.33%	25.58%
EDS Point 13	26.77%	5.17%	8.62%	34.85%	24.57%
EDS Point 14	25.25%	4.28%	6.54%	37.74%	26.17%
EDS Point 15	26.26%	4.88%	8.22%	35.78%	24.84%
EDS Point 16	26.00%	5.05%	7.32%	36.93%	24.68%
EDS Point 17	25.86%	5.09%	8.40%	36.76%	23.86%
EDS Point 18	26.67%	4.18%	8.23%	37.43%	23.46%
EDS Point 19	24.29%	3.83%	6.07%	39.77%	26.02%
EDS Point 20	25.35%	4.83%	7.30%	37.68%	24.81%
Average concentration	25.67%	4.75%	7.78%	36.98%	24.80%
Cr:Fe ratio					**1:1.49**

Test Feed -75/+53µm					
	O	**Mg**	**Al**	**Cr**	**Fe**
EDS Point 1	27.07%	5.28%	8.75%	36.37%	22.50%
EDS Point 2	27.41%	5.09%	8.61%	34.56%	24.30%
EDS Point 3	25.54%	4.45%	8.81%	36.49%	24.69%
EDS Point 4	23.09%	2.70%	3.88%	38.79%	31.52%
EDS Point 5	26.18%	5.01%	8.43%	36.08%	24.26%
EDS Point 6	25.23%	3.90%	6.39%	35.43%	29.02%
EDS Point 7	26.66%	4.87%	8.07%	35.87%	24.50%
EDS Point 8	26.74%	4.74%	8.28%	34.99%	25.22%
EDS Point 9	26.35%	4.63%	8.28%	35.89%	24.82%
EDS Point 10	25.76%	4.80%	8.53%	37.41%	23.48%
EDS Point 11	26.21%	4.10%	8.48%	37.46%	23.73%
EDS Point 12	26.16%	5.00%	7.56%	37.14%	24.11%
EDS Point 13	26.76%	3.89%	8.66%	35.38%	25.29%
EDS Point 14	26.80%	4.88%	7.68%	36.65%	23.97%
EDS Point 15	27.19%	5.48%	9.08%	34.63%	23.59%
EDS Point 16	26.57%	4.77%	7.72%	36.01%	24.91%
EDS Point 17	26.82%	4.82%	8.00%	35.26%	25.08%
EDS Point 18	26.41%	4.77%	8.44%	36.09%	24.27%
EDS Point 19	27.02%	4.98%	8.73%	35.10%	24.14%
EDS Point 20	27.27%	4.84%	7.97%	36.15%	23.74%
Average concentration	26.36%	4.65%	8.02%	36.09%	24.86%
Cr:Fe ratio					**1:1.41**

Test Feed -53/+25µm					
	O	**Mg**	**Al**	**Cr**	**Fe**
EDS Point 1	26.79%	5.05%	8.25%	35.68%	23.77%
EDS Point 2	25.50%	3.26%	4.88%	35.79%	29.96%
EDS Point 3	26.43%	4.81%	8.43%	35.46%	24.45%
EDS Point 4	26.15%	3.88%	7.66%	37.69%	24.26%
EDS Point 5	28.63%	5.19%	8.26%	35.39%	22.13%
EDS Point 6	24.77%	3.16%	5.05%	35.48%	30.85%
EDS Point 7	26.78%	5.23%	8.83%	35.66%	23.21%
EDS Point 8	24.10%	3.00%	4.23%	37.83%	30.17%
EDS Point 9	27.02%	4.89%	7.45%	35.97%	24.16%
EDS Point 10	26.95%	4.92%	7.59%	37.28%	23.03%
EDS Point 11	23.84%	3.69%	5.83%	37.70%	28.24%
EDS Point 12	24.41%	3.06%	4.82%	39.42%	27.96%
EDS Point 13	26.77%	4.38%	7.65%	35.53%	25.34%
EDS Point 14	26.38%	4.59%	7.37%	34.60%	26.58%
EDS Point 15	27.15%	5.22%	8.72%	34.56%	23.86%
EDS Point 16	24.27%	2.95%	4.86%	39.65%	27.68%
EDS Point 17	27.73%	5.54%	8.80%	35.87%	21.72%
EDS Point 18	27.60%	4.74%	8.21%	34.68%	24.30%
EDS Point 19	26.61%	4.76%	7.74%	35.31%	25.09%
EDS Point 20	27.57%	4.68%	7.96%	35.32%	24.13%
Average concentration	26.27%	4.35%	7.13%	36.24%	25.54%
Cr:Fe ratio					**1:1.42**

Test Feed -25µm					
	O	**Mg**	**Al**	**Cr**	**Fe**
EDS Point 1	22.60%	3.20%	0.45%	38.39%	30.58%
EDS Point 2	26.53%	4.91%	0.31%	34.55%	25.32%
EDS Point 3	27.09%	4.91%	0.43%	36.15%	23.65%
EDS Point 4	25.87%	5.06%	0.50%	37.09%	24.08%
EDS Point 5	27.72%	4.36%	0.41%	36.31%	23.20%
EDS Point 6	25.86%	4.54%	0.39%	36.20%	26.25%
EDS Point 7	25.67%	4.90%	0.48%	35.96%	24.68%
EDS Point 8	25.87%	3.94%	0.48%	36.61%	26.46%
EDS Point 9	26.67%	4.84%	0.38%	36.95%	23.68%
EDS Point 10	27.47%	4.15%	0.39%	35.83%	25.57%
EDS Point 11	24.87%	4.16%	0.37%	40.10%	24.32%
EDS Point 12	27.85%	4.95%	0.41%	35.16%	24.05%
EDS Point 13	27.55%	5.13%	0.03%	35.46%	23.48%
EDS Point 14	26.99%	4.28%	0.48%	34.06%	26.68%
EDS Point 15	30.53%	4.93%	0.24%	33.07%	22.00%
EDS Point 16	27.93%	5.06%	0.39%	35.36%	23.24%
EDS Point 17	28.74%	5.68%	0.33%	35.58%	21.08%
EDS Point 18	28.37%	4.78%	0.33%	36.04%	22.98%
EDS Point 19	27.98%	4.90%	0.32%	35.45%	24.04%
EDS Point 20	27.55%	4.67%	0.01%	37.19%	22.90%
Average concentration	26.99%	4.67%	0.36%	36.08%	24.41%
Cr:Fe ratio					**1:1.48**

APPENDIX B: GRAIN SIZE DISTRIBUTION

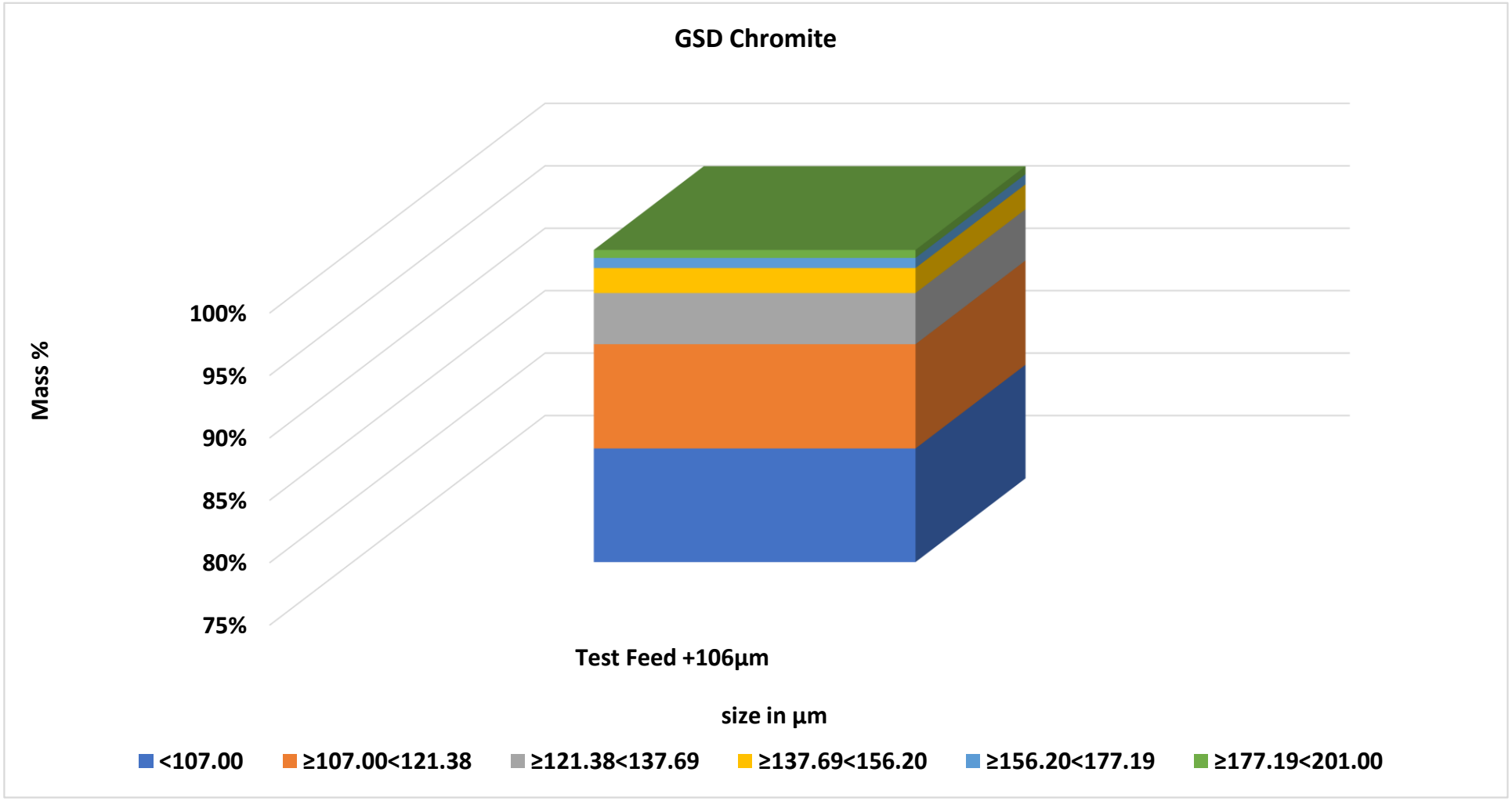

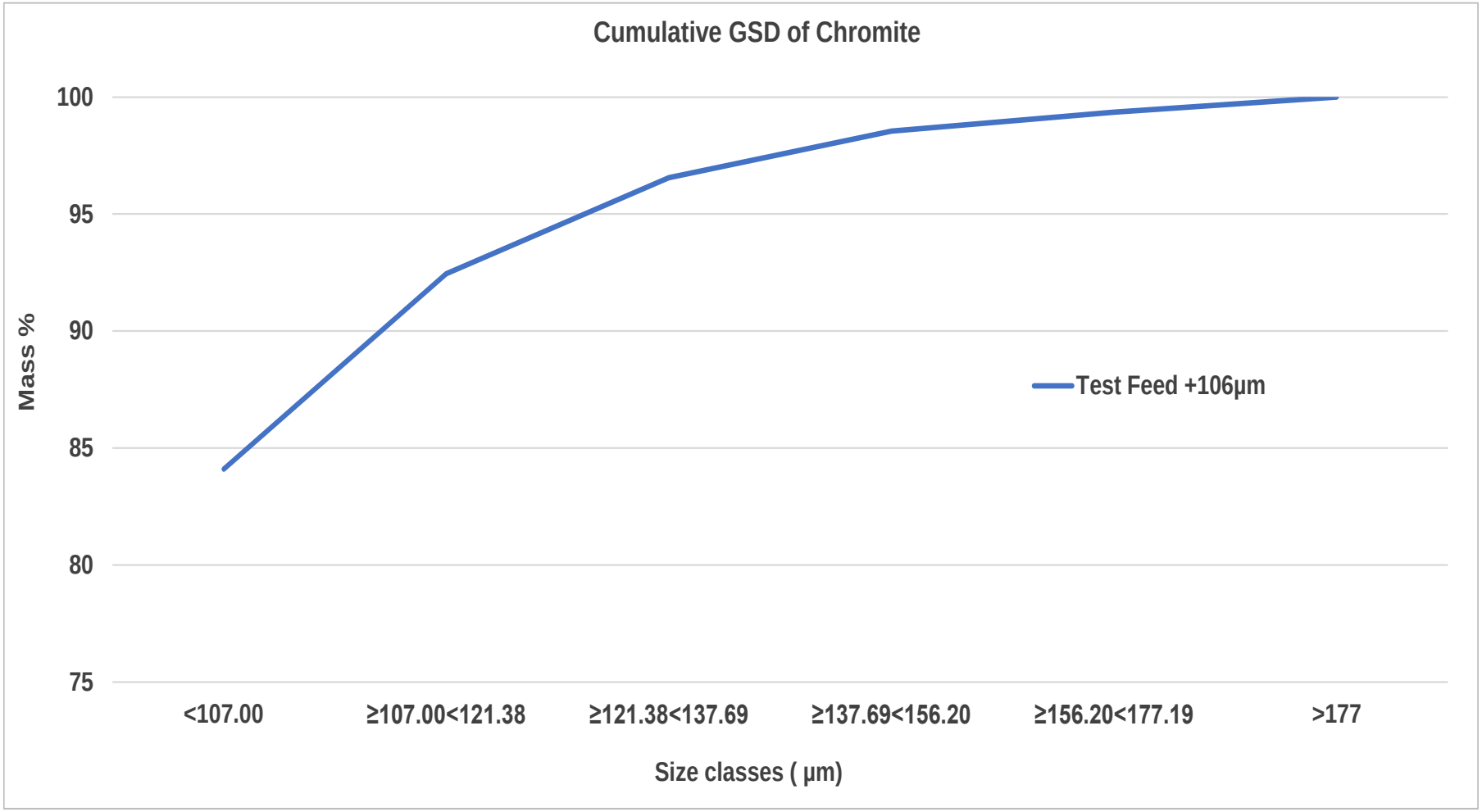
Cumulative GSD of Chromite
100
95
90
85
80
75
Mass %
Test Feed +106µm
<107.00
≥107.00<121.38
≥121.38<137.69
≥137.69<156.20
≥156.20<177.19
>177
Size classes (µm)

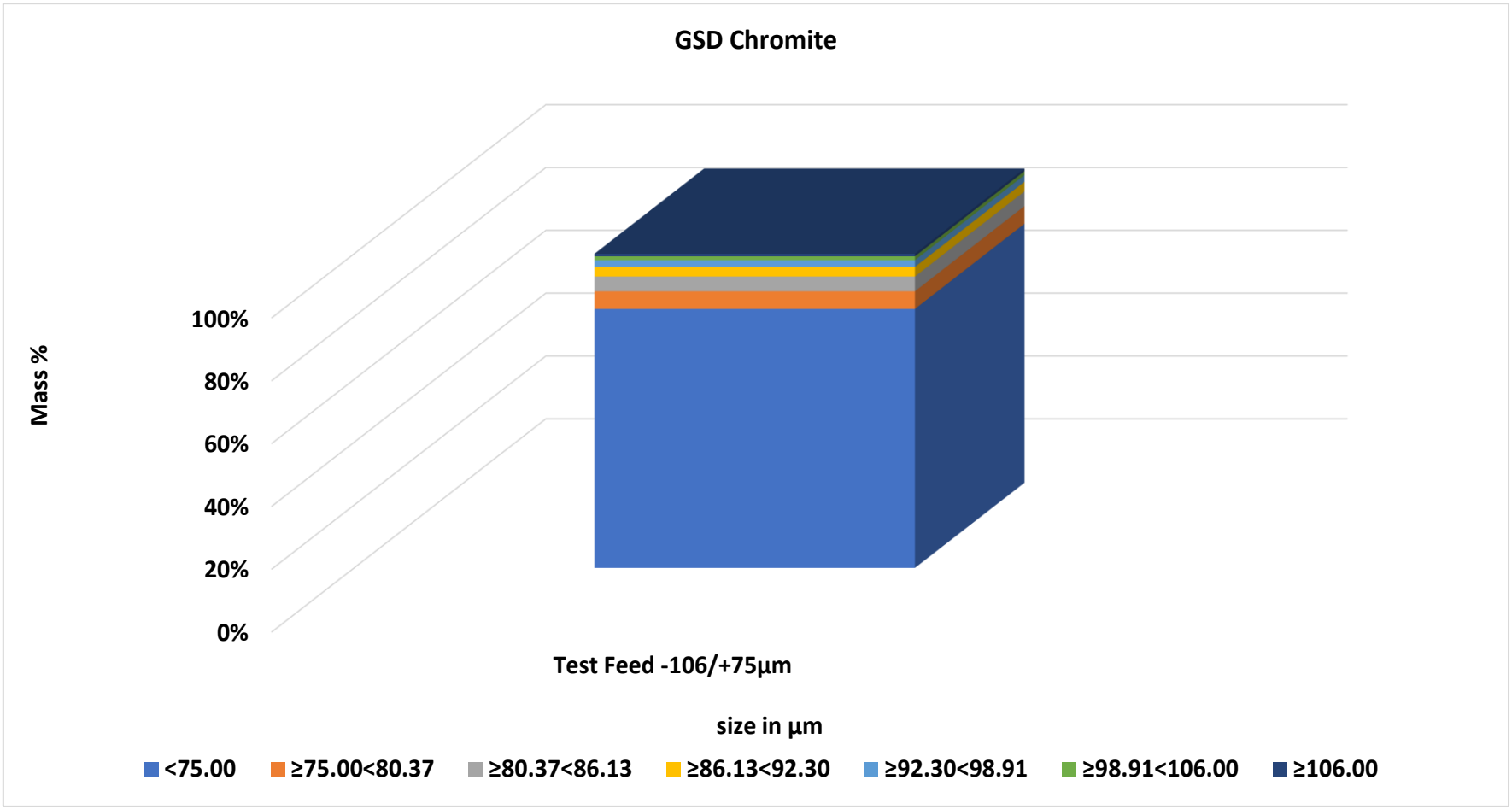
GSD Chromite
Mass %
100%
80%
60%
40%
20%
0%
Test Feed -106/+75µm
size in µm
<75.00
≥75.00<80.37
≥80.37<86.13
≥86.13<92.30
≥92.30<98.91
≥98.91<106.00
≥106.00

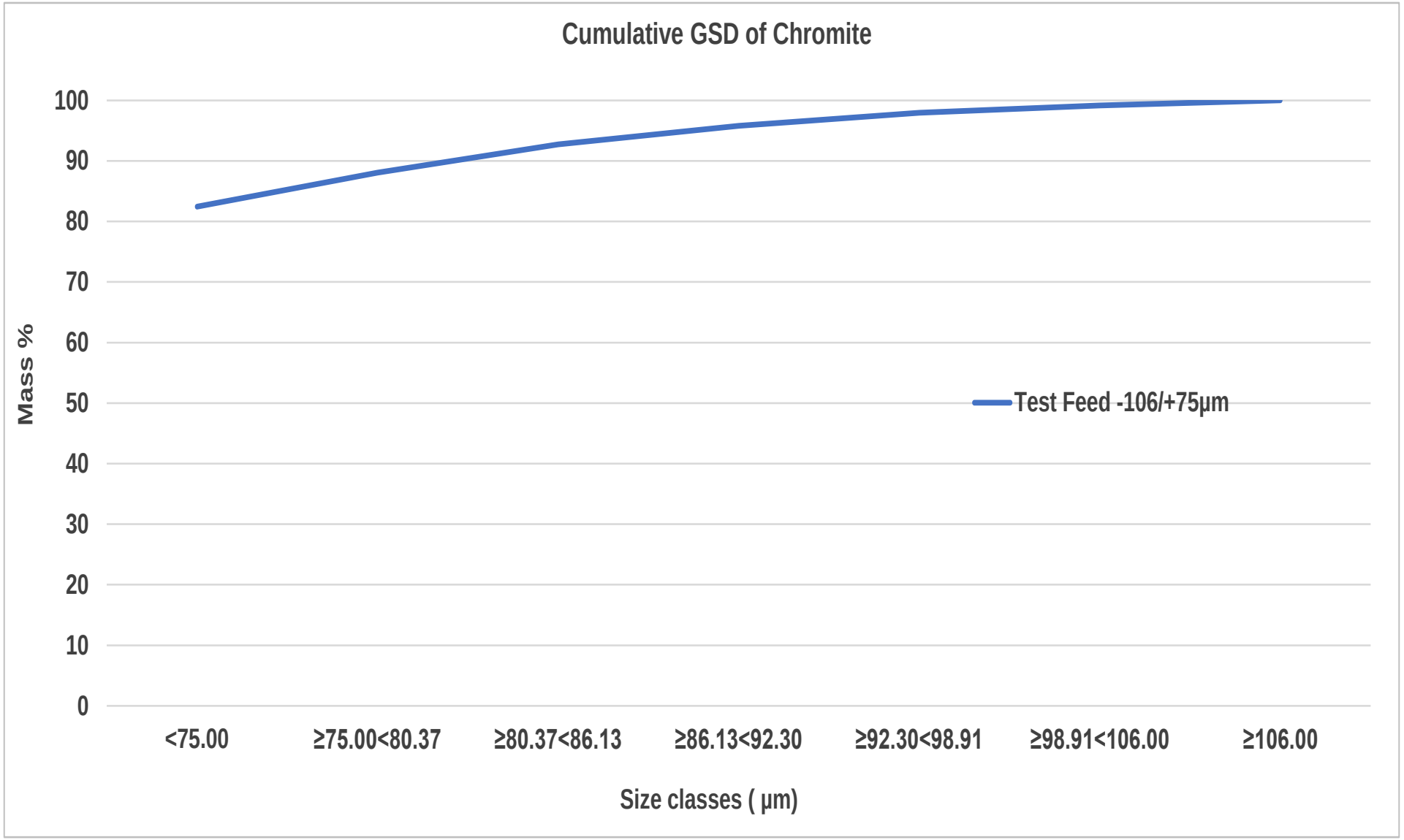
Cumulative GSD of Chromite
100
90
80
70
60
50
40
30
20
10
0
Mass %
Test Feed -106/+75µm
<75.00
≥75.00<80.37
≥80.37<86.13
≥86.13<92.30
≥92.30<98.91
≥98.91<106.00
≥106.00
Size classes (µm)

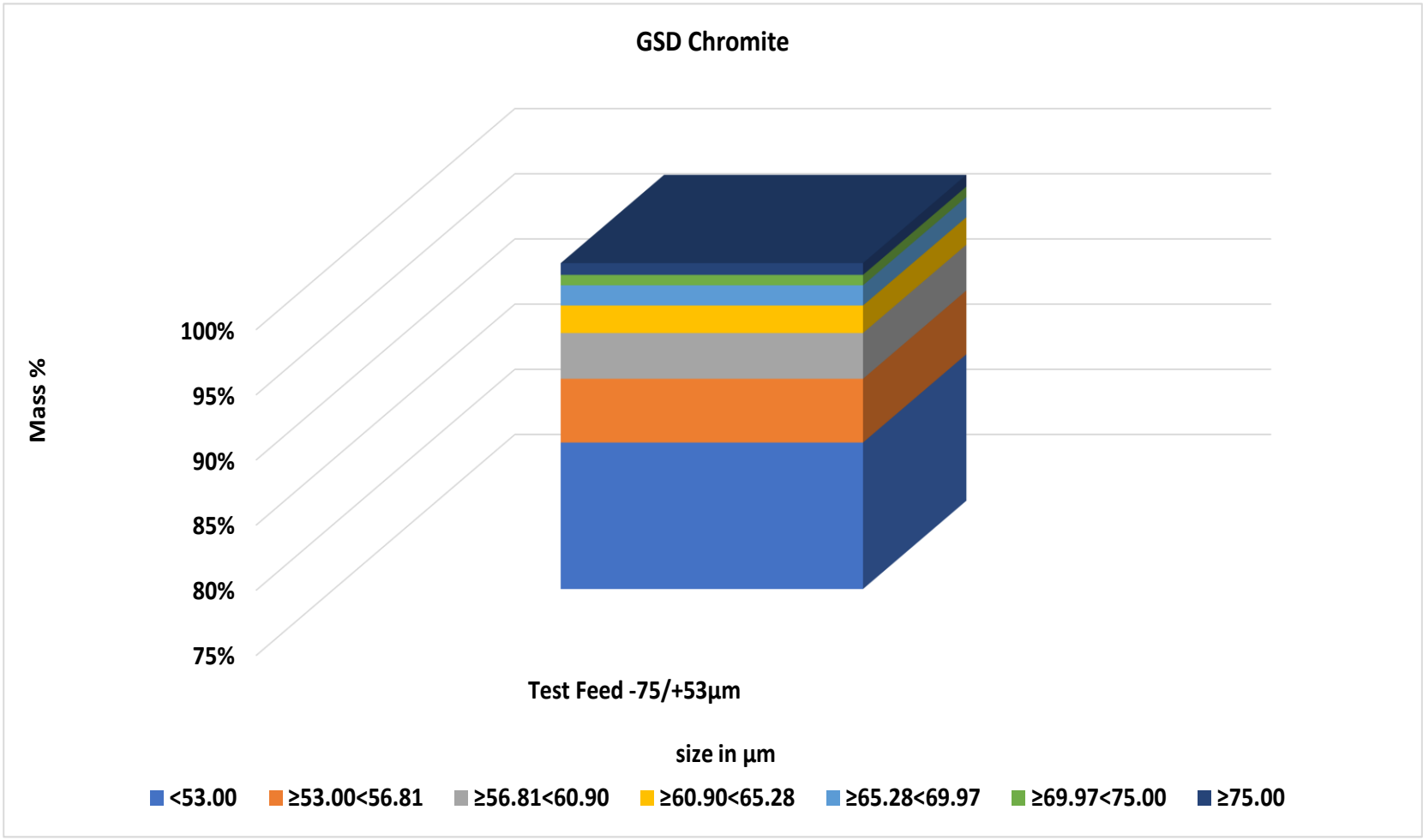
GSD Chromite
Mass %
100%
95%
90%
85%
80%
75%
Test Feed -75/+53µm
size in µm
<53.00
≥53.00<56.81
≥56.81<60.90
≥60.90<65.28
≥65.28<69.97
≥69.97<75.00
≥75.00

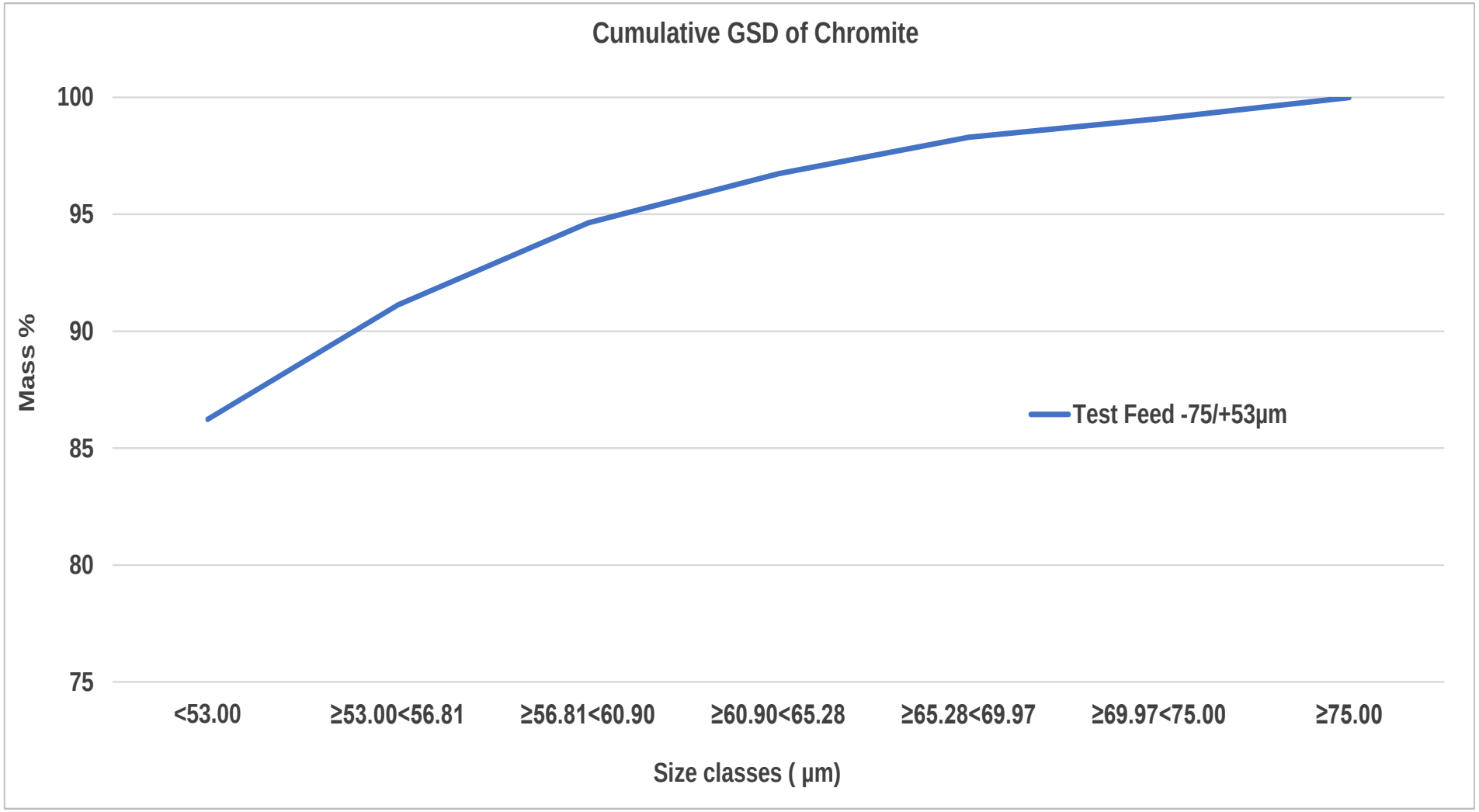
Cumulative GSD of Chromite
100
95
90
85
80
75
Mass %
Test Feed -75/+53µm
<53.00
≥53.00<56.81
≥56.81<60.90
≥60.90<65.28
≥65.28<69.97
≥69.97<75.00
≥75.00
Size classes (µm)

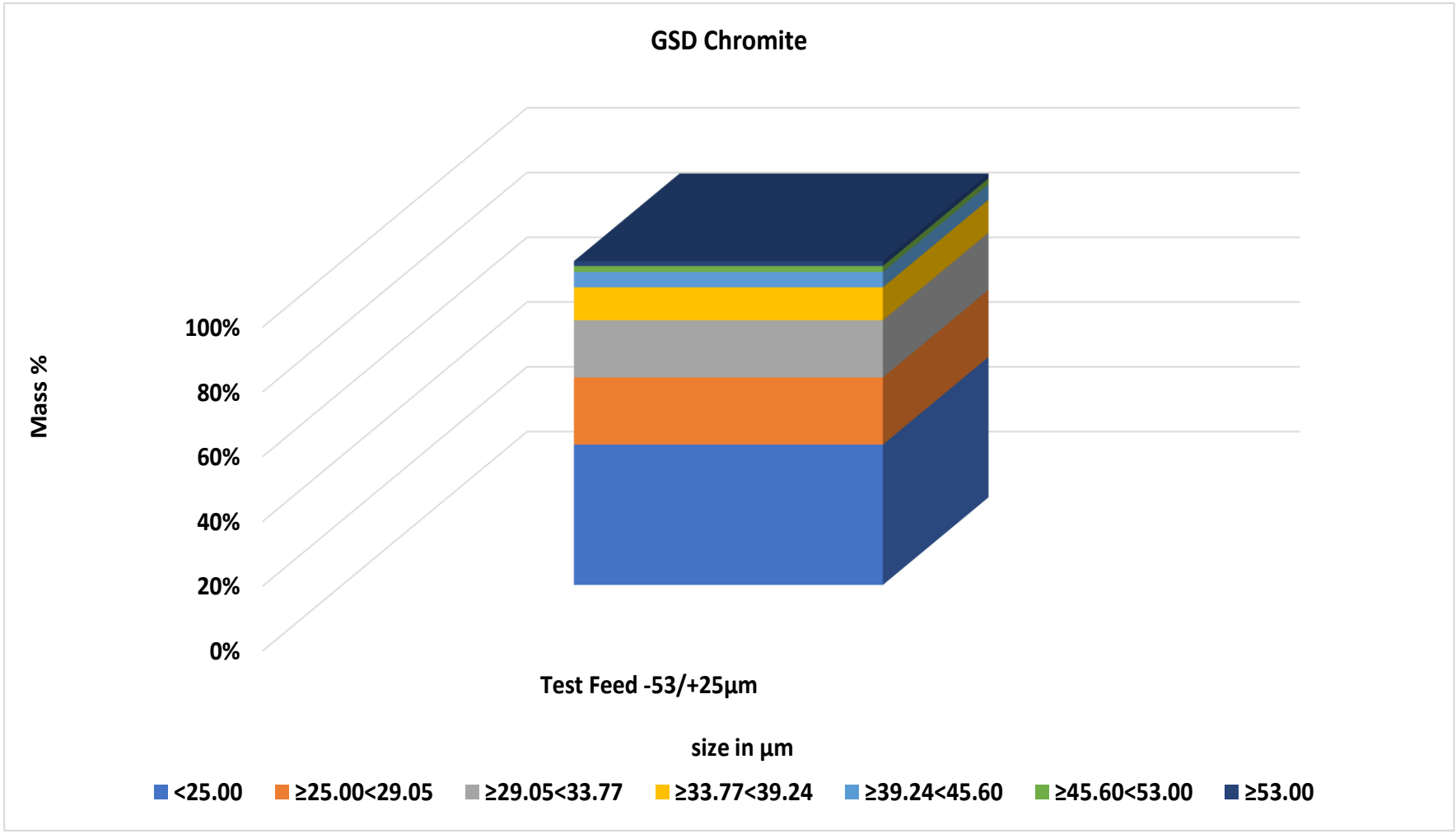
GSD Chromite
Mass %
100%
80%
60%
40%
20%
0%
Test Feed -53/+25µm
size in µm
<25.00
≥25.00<29.05
≥29.05<33.77
≥33.77<39.24
≥39.24<45.60
≥45.60<53.00
≥53.00

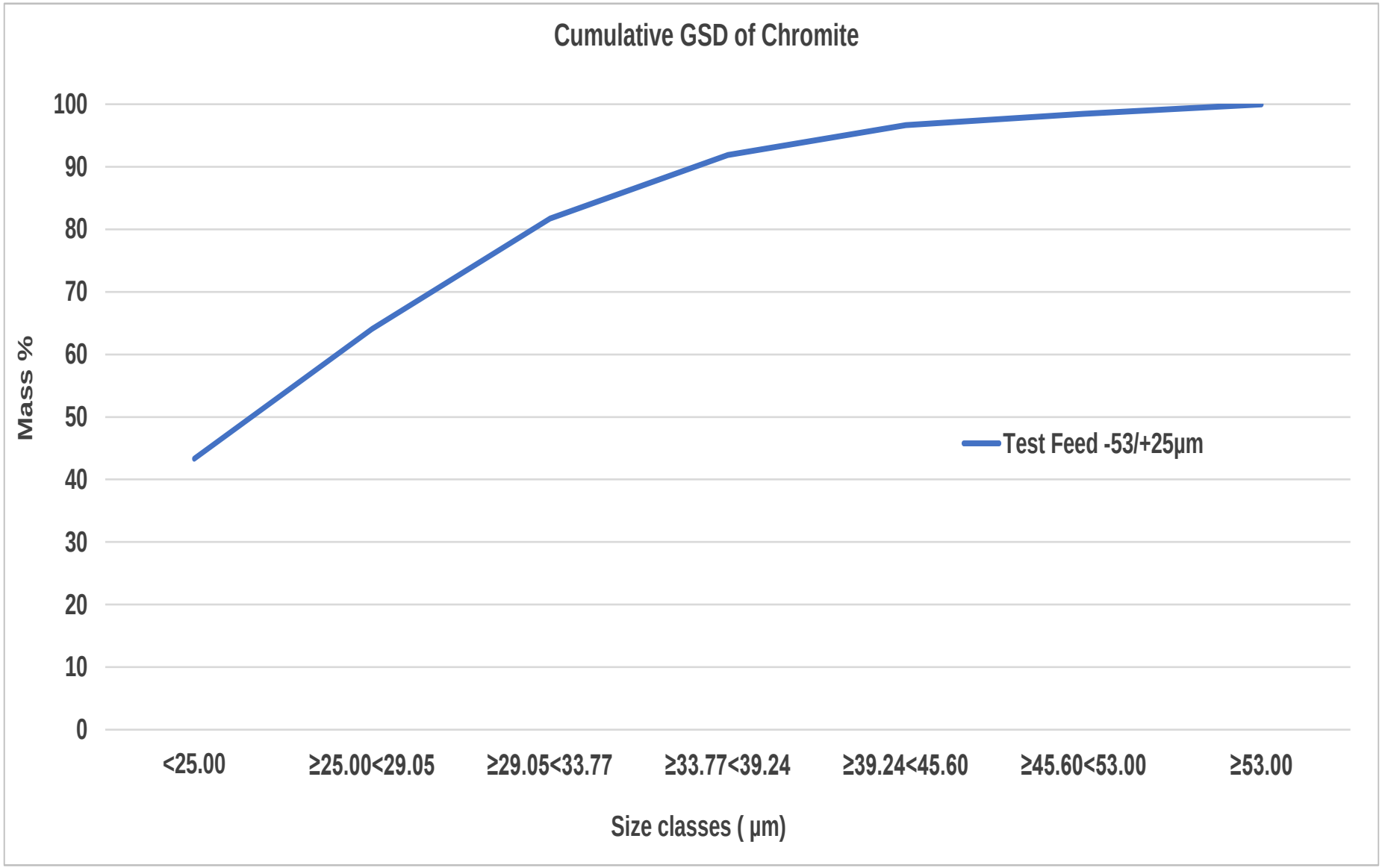
Cumulative GSD of Chromite
100
90
80
70
60
50
40
30
20
10
0
Mass %
Test Feed -53/+25µm
<25.00
≥25.00<29.05
≥29.05<33.77
≥33.77<39.24
≥39.24<45.60
≥45.60<53.00
≥53.00
Size classes (µm)

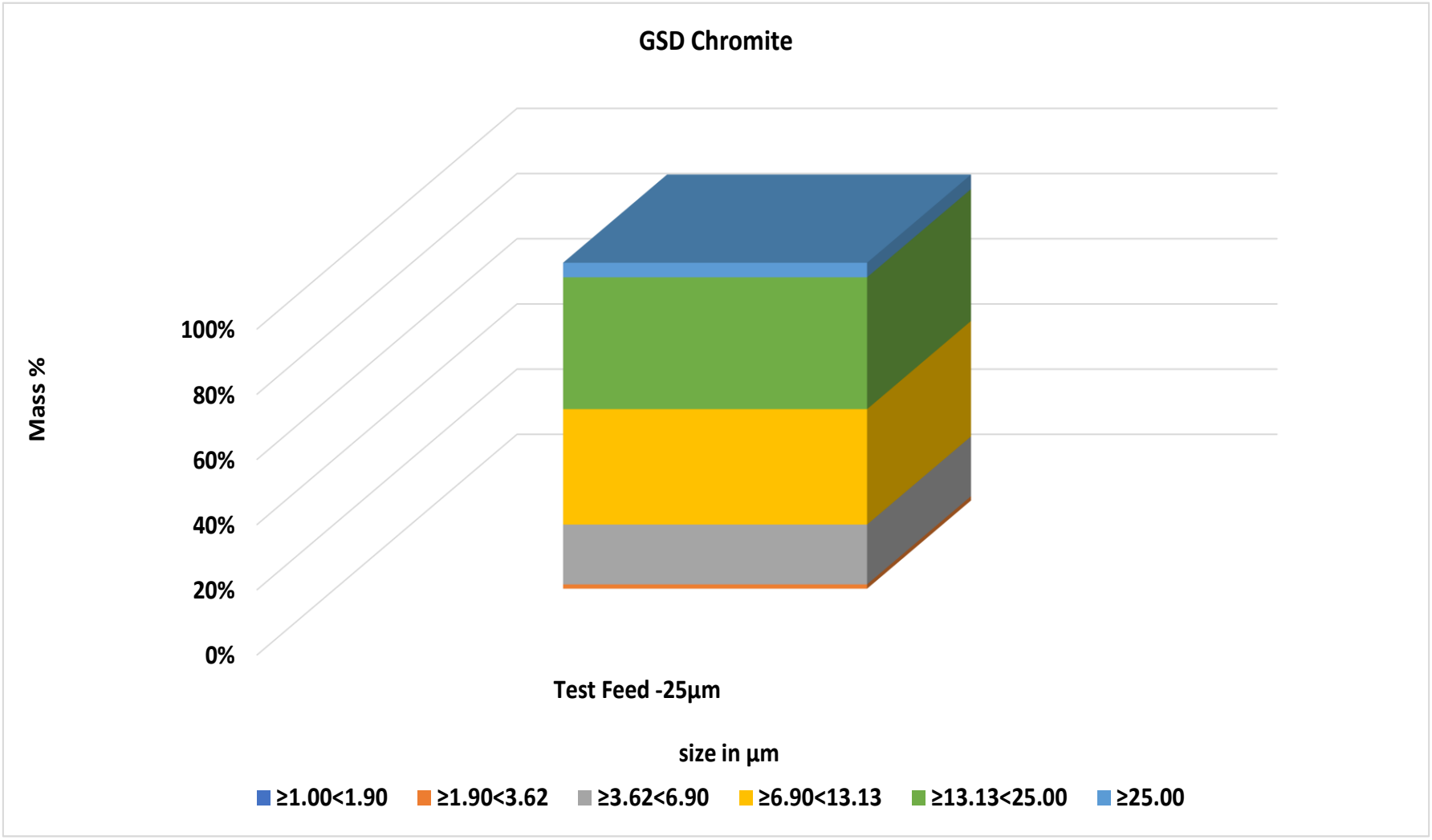
GSD Chromite
Mass %
100%
80%
60%
40%
20%
0%
Test Feed -25µm
size in µm
≥1.00<1.90
≥1.90<3.62
≥3.62<6.90
≥6.90<13.13
≥13.13<25.00
≥25.00

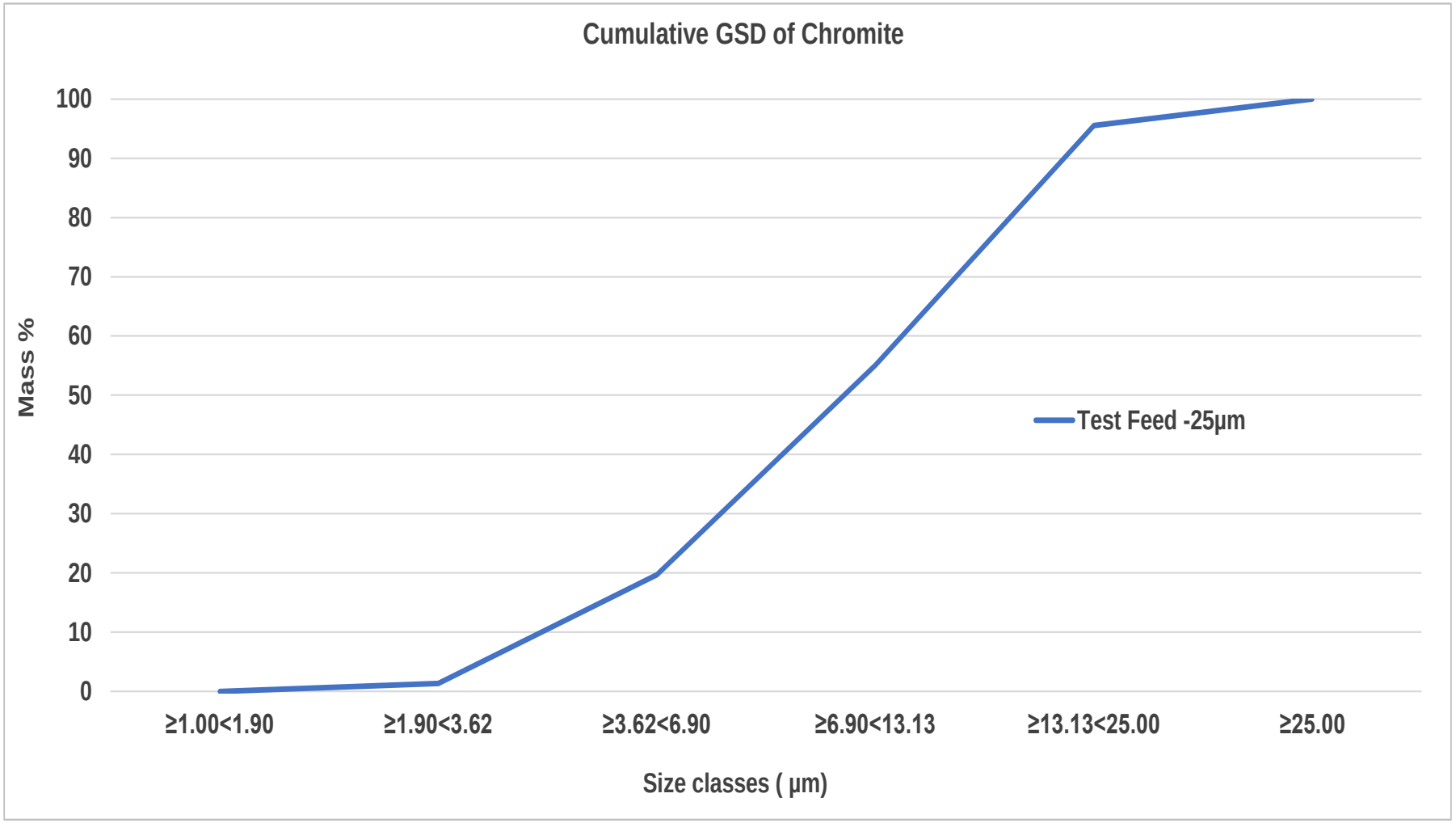
Cumulative GSD of Chromite
100
90
80
70
60
50
40
30
20
10
0
Mass %
Test Feed -25µm
≥1.00<1.90
≥1.90<3.62
≥3.62<6.90
≥6.90<13.13
≥13.13<25.00
≥25.00
Size classes (µm)

APPENDIX C: CONFIGURATION 1 CIRCUIT

Spiral separation

Run Code	Stream Name	% Mass Yield	% Cr_2O_3 Recovery	Cr_2O_3 %	FeO%	SiO_2 %	CaO %	Al_2O_3 %	MgO %
SP2023081201	Run 1 Spiral Feed	0.703	0.072	10.76	10.70	38.35	8.65	19.04	14.07
	Run 1 Spiral Concentrate	23.3	30.8	13.63	12.80	35.34	7.15	16.72	15.57
	Run 1 Spiral Middlings	48.7	43.5	9.20	9.78	39.52	9.12	19.72	13.76
	Run 1 Spiral Tailings	28.0	25.7	9.44	9.81	38.77	8.89	19.47	13.52
SP2023081202	Run 2 Spiral Feed	0.681	0.069	11.04	10.62	36.84	8.18	18.54	14.23
	Run 2 Spiral Concentrate	22.2	29.5	13.45	12.48	35.42	7.12	16.58	15.84
	Run 2 Spiral Middlings	49.1	43.8	9.02	9.33	39.06	8.99	19.45	13.29
	Run 2 Spiral Tailings	28.7	26.8	9.46	9.64	38.68	8.90	19.68	13.22
SP2023081203	Run 3 Spiral Feed	0.666	0.065	10.22	10.21	37.76	8.40	18.80	13.89
	Run 3 Spiral Concentrate	23.7	31.4	12.96	12.09	34.62	7.14	16.60	15.49
	Run 3 Spiral Middlings	48.4	42.9	9.09	9.08	38.21	9.18	19.64	13.58
	Run 3 Spiral Tailings	27.9	25.7	9.01	9.16	37.97	9.15	19.70	13.20

Magnetic Separation

	Magnetic Separation Batch 1	% Mass Yield	% Cr_2O_3 Recovery	Cr_2O_3 %	FeO%	SiO_2 %	CaO %	Al_2O_3 %	MgO%
SPMMG2023081301	Run 1 Mag Feed	0.823	7.7	9.16	9.88	45.96	10.44	21.19	14.71
	Run 1 Magnetics	8.1	17.5	20.33	18.95	33.68	5.01	14.65	18.47
	Run 1 Non-Magnetics	91.9	82.5	8.42	8.96	45.90	10.69	21.36	14.04
SPMMG2023081302	Run 2 Mag Feed	0.940	8.19	9.13	9.59	45.20	10.33	20.93	14.79
	Run 2 Magnetics	8.8	20.16	19.99	18.12	33.38	5.27	14.83	19.14
	Run 2 Non-Magnetics	91.2	79.84	7.62	8.34	46.34	10.73	21.40	13.53
SPMMG2023081303	Run 3 Mag Feed	0.796	7.15	9.08	9.57	43.22	9.13	18.90	13.21
	Run 3 Magnetics	8.5	18.94	20.06	18.31	32.11	4.38	13.23	17.33
	Run 3 Non-Magnetics	91.5	81.06	7.96	8.44	44.16	9.51	19.77	13.11
SPMMG2023081304	Run 4 Mag Feed	0.792	7.22	9.14	9.55	43.74	9.23	19.23	13.84
	Run 4 Magnetics	7.5	17.01	20.54	19.25	31.52	3.92	12.51	17.19
	Run 4 Non-Magnetics	92.5	82.99	8.17	8.88	46.32	10.37	21.24	13.80

	Magnetic Separation Batch 2	% Mass Yield	% Cr_2O_3 Recovery	Cr_2O_3 %	FeO%	SiO_2 %	CaO %	Al_2O_3 %	MgO %
SCVMG2023090201	Run 1 Scavenger Mag Feed	0.512	0.040	7.67	8.43	42.49	9.40	20.1	12.68
	Run 1 Scavenger Magnetics	18.7	26.5	11.09	10.66	38.60	8.01	18.6	13.85
	Run 1 Scavenger Non-Magnetics	81.3	73.5	7.06	7.55	43.15	10.18	21.0	12.59
SCVMG2023090202	Run 2 Scavenger Mag Feed	0.479	0.037	7.55	8.13	42.08	9.46	19.9	12.65
	Run 2 Scavenger Magnetics	17.2	24.4	10.95	10.36	37.71	7.85	18.0	13.95
	Run 2 Scavenger Non-Magnetics	82.8	75.6	7.03	7.58	41.94	9.48	19.9	11.98
SCVMG2023090203	Run 3 Scavenger Mag Feed	0.419	0.032	7.44	7.80	42.07	9.71	20.2	12.56
	Run 3 Scavenger Magnetics	18.6	26.9	11.04	10.46	38.08	7.99	18.1	14.02
	Run 3 Scavenger Non-Magnetics	81.4	73.1	6.83	7.48	43.09	10.22	20.8	12.39

	Magnetic Separation Batch 3	**% Mass Yield**	**% Cr_2O_3 Recovery**	**Cr_2O_3 %**	**FeO%**	**SiO2 %**	**CaO %**	**Al_2O_3 %**	**MgO%**
MGSPT2023090201	Run 1 Spiral Tail Mag Feed	0.92	0.076	8.42	8.96	41.33	9.48	19.8	13.0
	Run 1 Spiral Tail Magnetics	16.3	21.2	10.77	10.87	38.13	8.08	18.3	14.0
	Run 1 Spiral Tail Non-Magnetics	83.7	78.8	7.79	8.07	41.75	9.83	20.2	12.9
MGSPT2023090202	Run 2 Spiral Tail Mag Feed	0.87	0.071	8.51	8.70	40.88	9.12	19.5	13.0
	Run 2 Spiral Tail Magnetics	18.0	23.9	10.87	10.76	37.80	7.73	17.8	13.9
	Run 2 Spiral Tail Non-Magnetics	82.0	76.1	7.56	7.87	41.80	9.61	20.3	13.0
MGSPT2023090203	Run 3 Spiral Tail Mag Feed	1.01	0.084	8.30	8.95	42.45	9.78	20.7	13.3
	Run 3 Spiral Tail Magnetics	17.2	23.0	11.19	11.13	37.77	7.64	17.8	14.3
	Run 3 Spiral Tail Non-Magnetics	82.8	77.0	7.76	8.18	41.33	9.48	19.9	12.7

Shaking Table Separation

		% Mass Yield	% Cr_2O_3 Recovery	Cr_2O_3 %	FeO%	SiO_2 %	CaO %	Al_2O_3 %	MgO%
SPCST2023082201	Run 1 Shaking Table Feed	0.013	0.002	17.3	15.05	35.97	8.56	20.17	19.21
	Run 1 Shaking table Concentrate	30.9	66.8	37.7	25.84	11.61	2.09	18.82	17.19
	Run 1 Shaking Table Middlings	45.8	18.1	6.9	10.16	49.36	11.26	19.56	22.13
	Run 1 Shaking Table Tailings	23.3	15.1	11.3	11.15	45.06	12.27	24.56	17.50
SPCST2023082202	Run 2 Shaking Table Feed	0.012	0.002	16.8	14.84	39.89	9.60	21.66	20.25
	Run 2 Shaking table Concentrate	27.3	52.2	34.4	24.49	17.46	3.33	19.42	19.78
	Run 2 Shaking Table Middlings	36.3	21.6	10.7	11.85	47.89	11.25	20.88	22.83
	Run 2 Shaking Table Tailings	36.3	26.3	13.1	12.19	43.77	12.17	24.54	18.56
SPCST2023082501	Run 3 Shaking Table Feed	0.014	0.002	17.63	15.86	34.69	6.00	16.01	15.88
	Run 3 Shaking table Concentrate	21.54	56.78	44.13	28.85	3.89	0.94	16.80	11.72
	Run 3 Shaking Table Middlings	42.74	25.46	9.97	9.89	39.40	9.14	18.77	11.64
	Run 3 Shaking Table Tailings	35.73	17.76	8.32	10.30	43.10	8.42	15.52	16.52
SPCST2023082502	Run 4 Shaking Table Feed	0.012	0.002	17.63	15.86	34.69	6.00	16.01	15.88
	Run 4 Shaking table Concentrate	23.02	49.05	38.34	26.39	11.12	1.60	15.42	14.04
	Run 4 Shaking Table Middlings	41.58	31.46	13.61	14.27	38.17	7.67	17.83	16.17
	Run 4 Shaking Table Tailings	35.40	19.48	9.90	9.61	38.54	8.74	18.48	11.50

	Magnet Concentrate Batch 1	% Mass Yield	% Cr_2O_3 Recovery	Cr_2O_3 (%)	FeO%	SiO_2 %	CaO %	Al_2O_3 %	MgO %
SPMGST2023102101	Run 1 Shaking Table Feed	0.0133	0.0023	20.24	16.56	30.72	4.60	13.13	16.28
	Run 1 Shaking table Concentrate	11.13	26.57	41.55	27.30	2.55	0.40	16.47	9.56
	Run 1 Shaking Table Middlings	78.64	65.48	14.50	15.36	34.51	4.42	11.63	17.51
	Run 1 Shaking Table Tailings	10.23	7.95	13.53	14.48	34.54	7.11	16.76	13.52
SPMGST2023102102	Run 2 Shaking Table Feed	0.0148	0.0026	20.24	16.56	30.72	4.60	13.13	16.28
	Run 2 Shaking table Concentrate	10.36	23.52	39.80	25.79	2.25	0.48	15.99	9.10
	Run 2 Shaking Table Middlings	77.35	64.63	14.64	15.78	35.07	4.76	12.20	17.62
	Run 2 Shaking Table Tailings	12.30	11.86	16.90	16.47	33.60	7.03	16.31	16.54
SPMGST2023102103	Run 3 Shaking Table Feed	0.0130	0.0023	20.24	16.56	30.72	4.60	13.13	16.28
	Run 3 Shaking table Concentrate	9.06	22.92	44.51	29.19	2.83	0.83	18.26	11.35
	Run 3 Shaking Table Middlings	49.17	43.64	15.61	16.04	33.84	4.98	12.90	17.84
	Run 3 Shaking Table Tailings	41.77	33.44	14.08	14.74	36.96	8.95	18.19	15.88

	Spiral Concentrate Batch 3	% Mass Yield	% Cr_2O_3 Recovery	Cr_2O_3 (%)	FeO %	SiO_2	CaO%	Al_2O_3%	MgO%
SPCST2023082901	Run 1 Shaking Table Feed	0.014	0.00224	16.24	14.07	35.67	7.05	18.33	17.48
	Run 1 Shaking table Concentrate	11.36	30.04	42.77	27.98	2.44	0.57	18.17	11.58
	Run 1 Shaking Table Middlings	85.37	68.05	12.89	12.32	39.33	7.83	18.12	17.46
	Run 1 Shaking Table Tailings	3.27	1.92	9.48	9.89	42.51	9.92	21.10	14.79
SPCST2023082902	Run 2 Shaking Table Feed	0.014	0.00229	16.24	14.07	35.67	7.05	18.33	17.48
	Run 2 Shaking table Concentrate	9.95	25.51	42.66	27.76	1.51	0.60	18.75	11.35
	Run 2 Shaking Table Middlings	84.39	71.20	14.03	13.35	38.92	7.08	17.09	18.56
	Run 2 Shaking Table Tailings	5.66	3.29	9.66	9.79	41.01	9.69	21.11	14.57
SPCST2023082903	Run 3 Shaking Table Feed	0.013	0.00212	16.24	14.07	35.67	7.05	18.33	17.48
	Run 3 Shaking table Concentrate	9.91	25.57	42.14	27.42	1.47	0.63	18.53	11.06
	Run 3 Shaking Table Middlings	84.40	71.14	13.76	13.12	37.93	7.24	17.42	17.99
	Run 3 Shaking Table Tailings	5.69	3.29%	9.44	9.58	41.59	9.45	20.98	14.10

	Spiral Tail Mags Shaking Table Batch 1	% Mass Yield	% Cr_2O_3 Recovery	Cr_2O_3 (%)	FeO %	SiO_2	CaO%	Al_2O_3%	MgO%
SPTMgST2023102101	Run 1 Shaking Table Feed	0.015	0.002	11.84	12.22	40.15	7.67	18.01	14.48
	Run 1 Shaking table Concentrate	8.33	21.60	28.08	19.21	8.28	0.31	9.64	10.23
	Run 1 Shaking Table Middlings	65.08	53.32	8.87	10.52	42.91	8.34	17.73	14.63
	Run 1 Shaking Table Tailings	26.59	25.08	10.21	11.02	39.38	7.87	17.95	12.80
SPTMgST2023102102	Run 2 Shaking Table Feed	0.015	0.002	11.84	12.22	40.15	7.67	18.01	14.48
	Run 2 Shaking table Concentrate	9.46	29.05	34.27	24.32	14.22	1.12	13.34	14.89
	Run 2 Shaking Table Middlings	65.25	50.25	8.60	10.82	42.84	8.27	18.20	14.71
	Run 2 Shaking Table Tailings	25.29	20.70	9.14	10.71	40.85	8.15	18.89	13.04

	Spiral Tail Mags 1 Shaking Table Batch 2	% Mass Yield	% Cr_2O_3 Recovery	Cr_2O_3 (%)	FeO %	SiO2	CaO%	Al_2O_3%	MgO%
SPTMags2023111801	Run 1 Shaking Table Feed	0.013	0.00150	10.77	10.53	41.54	11.00	23.30	15.97
	Run 1 Shaking table Concentrate	8.78	26.42	36.02	22.91	14.63	2.04	15.99	16.90
	Run 1 Shaking Table Middlings	31.68	19.62	7.41	9.51	44.76	8.78	17.75	16.61
	Run 1 Shaking Table Tailings	59.54	53.96	10.84	10.55	41.24	10.78	22.23	14.90
SPTMags2023111802	Run 2 Shaking Table Feed	0.012	0.00146	10.77	10.53	41.54	11.00	23.30	15.97
	Run 2 Shaking table Concentrate	7.83	22.49	34.16	22.18	16.56	1.76	13.82	16.59
	Run 2 Shaking Table Middlings	34.05	23.75	8.29	9.67	44.69	9.18	18.72	16.24
	Run 2 Shaking Table Tailings	58.12	53.77	11.00	10.78	41.36	9.38	21.68	14.59

	Scavenger Mags Shaking Table Batch 1	% Mass Yield	% Cr_2O_3 Recovery	Cr_2O_3 (%)	FeO %	SiO_2	CaO%	Al_2O_3%	MgO%
SCAV Mg ST2023102101	Run 1 Shaking Table Feed			12.95	12.67	38.23	7.328	18.17	14.81
	Run 1 Shaking table Concentrate	7.28	18.75	28.41	22.12	19.32	1.91	13.60	16.33
	Run 1 Shaking Table Middlings	61.81	53.29	9.51	10.63	41.43	7.93	18.18	14.30
	Run 1 Shaking Table Tailings	30.91	27.96	9.98	10.94	40.25	7.83	18.68	13.25
SCAV Mg ST2023111801	Run 2 Shaking Table Feed			11.30	10.38	41.83	12.34	24.39	16.20
	Run2 Shaking table Concentrate	7.81	15.36	25.27	20.26	26.28	2.64	12.20	19.51
	Run 2 Shaking Table Middlings	29.06	26.52	11.73	11.26	40.78	12.28	23.09	17.09
	Run 2 Shaking Table Tailings	63.13	58.28	11.86	11.23	39.60	10.79	21.86	15.04

	Spiral Conc 1 S/Table Batch 3	% Mass Yield	% Cr_2O_3 Recovery	Cr_2O_3 (%)	FeO %	SiO_2	CaO%	Al_2O_3%	MgO%
SPConcST2023102101	Run 1 Shaking Table Feed	0.012768	0.002	16.54	14.61	34.25	5.77	15.48	14.93
	Run 1 Shaking table HG Concentrate	10.81	25.86	40.09	30.04	0.57	0.08	16.52	10.12
	Run 1 Shaking table LG Concentrate	22.46	31.64	23.60	26.49	9.36	0.65	14.84	13.66
	Run 1 Shaking Table Middlings	27.26	17.24	10.60	12.64	42.20	6.01	13.38	17.97
	Run 1 Shaking Table Tailings	39.47	25.26	10.72	11.23	41.38	8.79	19.44	13.91
SPConcST2023102102	Run 2 Shaking Table Feed	0.01278	0.002	16.54	14.61	34.25	5.77	15.48	14.93
	Run 2 Shaking table HG Concentrate	12.77	29.07	39.45	26.54	8.59	0.64	15.19	13.18
	Run 2 Shaking table LG Concentrate	26.95	38.25	24.60	29.75	0.63	0.08	16.37	9.96
	Run 2 Shaking Table Middlings	45.63	23.65	8.98	12.19	41.80	6.32	13.87	18.14
	Run 2 Shaking Table Tailings	14.65	9.04	10.69	10.64	41.08	8.43	18.97	13.17
SPConcST2023102103	Run 3 Shaking Table Feed	0.012204	0.002	16.54	14.61	34.25	5.77	15.48	14.93
	Run 3 Shaking table HG Concentrate	16.91	41.17	40.80	28.41	0.64	0.14	16.23	9.78
	Run 3 Shaking table LG Concentrate	8.46	13.34	26.45	25.17	12.56	0.84	13.84	14.65
	Run 3 Shaking Table Middlings	31.56	17.70	9.40	11.46	43.28	6.91	14.52	17.88
	Run 3 Shaking Table Tailings	43.07	27.79	10.82	10.94	40.20	8.24	18.59	13.19

Run Code	**-106 µm Spiral Conc 1 Shaking table Separation Batch 5**	**% Mass Yield**	**% Cr_2O_3 Recovery**	**Cr_2O_3 %**	**FeO%**	**SiO_2 %**	**CaO %**	**Al_2O_3 %**	**MgO %**
ST-106 2024011701	Run 1 Shaking Table Feed	0.0115	0.002	15.79	13.62	32.87	27.07	15.08	14.93
	Run 1 Shaking Table HG Concentrate	19.04	55.80	42.01	25.53	0.00	0.56	14.62	9.64
	Run 1 Shaking Table Middlings	51.05	25.44	7.14	9.47	43.18	32.35	13.70	17.72
	Run 1 Shaking Table Tailings	29.92	18.7	8.99	9.10	36.19	32.88	16.16	11.73
ST-106 2024011702	Run 2 Shaking Table Feed	0.0120	0.002	15.79	13.62	32.87	27.07	15.08	14.93
	Run 2 Shaking Table HG Concentrate	19.48	52.59	40.75	25.33	0.00	1.61	15.37	9.89
	Run 2 Shaking Table Middlings	50.40	28.96	8.67	11.00	41.59	28.18	12.90	17.64
	Run 2 Shaking Table Tailings	30.12	18.44	9.24	9.33	39.85	38.49	18.04	13.04
ST-106 2024011703	Run 3 Shaking Table Feed	0.0120	0.002	15.79	13.62	32.87	27.07	15.08	14.93
	Run 3 Shaking Table HG Concentrate	19.28	53.80	40.69	25.52	0.00	1.98	15.45	10.31
	Run 3 Shaking Table Middlings	50.20	26.56	7.71	9.51	42.96	33.21	13.96	17.80
	Run 3 Shaking Table Tailings	30.52	19.64	9.38	9.43	37.92	34.80	16.82	12.30

	Shaking Table Middlings (-106 SP Conc) Batch 1	**% Mass Yield**	**% Cr_2O_3 Recovery**	**Cr_2O_3 (%)**	**FeO %**	**SiO_2**	**CaO%**	**Al_2O_3%**	**MgO%**
ST Middlings 2024020101	Run 1 Shaking Table Feed	0.004632	0.0005	11.81	14.61	34.25	5.77	15.48	14.93
	Run 1 Shaking table HG Concentrate	26.42	14.55	25.43	30.04	0.57	0.08	16.52	10.12
	Run 1 Shaking table LG Concentrate	43.52	2.96	3.14	26.49	9.36	0.65	14.84	13.66
	Run 1 Shaking Table Middlings	18.13	3.21	8.18	12.64	42.20	6.01	13.38	17.97
	Run 1 Shaking Table Tailings	11.92	2.51	9.72	11.23	41.38	8.79	19.44	13.91
ST Middlings 2024020102	Shaking Table Feed			11.81	14.61	34.25	5.77	15.48	14.93
	Shaking Table Concentrate	15.88	54.49	37.99	26.54	8.59	0.64	15.19	13.18
	Shaking Table Middlings	71.67	33.86	5.23	24.70	12.46	1.88	15.65	12.31
	Shaking Table Tailings	12.45	11.65	10.36	10.64	41.08	8.43	18.97	13.17

APPENDIX D: CONFIGURATION 2 CIRCUIT

Plus 25 µm Spiral Separation Batch 3									
Run Code	**Density 1.52, 0,885 t/hr, Conc Cutter 1.5, Mids Cutter 4.**	**% Yield**	**Recovery %**	**Cr_2O_3 %**	**FeO%**	**SiO_2 %**	**CaO %**	**Al_2O_3 %**	**MgO %**
SP2023101101	Run 1 Spiral Feed	0.792	0.0617	7.45	9.35	45.23	8.39	18.45	14.77
	Run 1 Spiral Concentrate	44.73	75.17	13.08	13.18	38.88	5.77	14.56	16.87
	Run 1 Spiral Middlings	31.25	15.84	3.95	7.15	48.49	9.07	18.87	13.43
	Run 1 Spiral Tailings	24.02	9.00	2.92	5.85	50.24	10.71	22.10	12.34
SP2023101102	Run 2 Spiral Feed	0.752	0.0577	7.79	9.80	46.78	9.66	20.33	16.11
	Run 2 Spiral Concentrate	46.36	77.49	12.81	13.33	40.75	6.72	15.94	18.12
	Run 2 Spiral Middlings	31.40	14.73	3.60	6.98	50.36	11.02	21.81	13.83
	Run 2 Spiral Tailings	22.24	7.78	2.68	5.60	52.15	12.37	23.84	12.48
SP2023101103	Run 3 Spiral Feed	0.686	0.0509	7.41	9.50	45.61	8.84	18.92	15.16
	Run 3 Spiral Concentrate	47.44	79.79	12.48	12.98	39.74	6.41	15.56	17.05
	Run 3 Spiral Middlings	31.69	12.87	3.01	9.78	52.16	12.70	23.64	14.38
	Run 3 Spiral Tailings	20.87	7.34	2.61	5.47	51.86	12.72	25.03	12.43
SP2023101104	Run 4 Spiral Feed	0.733	0.0556	7.56	9.60	46.20	9.38	19.62	15.92
	Run 4 Spiral Concentrate	47.01	78.48	12.65	13.34	41.12	6.33	15.62	17.51
	Run 4 Spiral Middlings	32.10	14.06	3.32	6.52	51.38	11.86	22.86	14.30
	Run 4 Spiral Tailings	20.89	7.47	2.71	5.63	51.12	12.44	24.94	12.21
SP2023101105	Run 5 Spiral Feed	0.841	0.0607	7.60	9.41	47.39	10.30	21.18	16.19
	Run 5 Spiral Concentrate	40.27	71.27	12.76	12.81	41.46	7.66	17.73	19.09
	Run 5 Spiral Middlings	30.69	16.90	3.97	6.96	47.79	9.99	20.00	13.80
	Run 5 Spiral Tailings	29.04	11.82	2.94	5.98	50.59	11.56	22.94	12.78
SP2023101106	Run 6 Spiral Feed	0.767	0.0516	7.11	9.15	46.39	9.70	19.90	15.21
	Run 6 Spiral Concentrate	45.52	75.40	11.14	11.96	40.86	7.19	16.08	17.27
	Run 6 Spiral Middlings	31.41	16.30	3.49	6.63	50.46	11.18	21.58	14.04
	Run 6 Spiral Tailings	23.08	8.31	2.42	5.36	51.63	12.23	23.94	12.06

Run Code	-106 + 25 µm Spiral Conc Shaking Table Separation Batch 1	**% Mass Yield**	**% Cr_2O_3 Recovery**	**Cr_2O_3 %**	**FeO%**	**SiO_2 %**	**CaO %**	**Al_2O_3 %**	**MgO %**
ST2023110101	Run 1 Shaking Table Feed	0.012	0.00144	13.09	12.64	37.92	24.79	17.48	17.07
	Run 1 Shaking Table Concentrate	17.38	55.97	39.86	25.86	2.63	1.72	18.35	11.84
	Run 1 Shaking Table Middlings	52.52	34.25	8.07	10.68	44.87	29.33	15.45	20.79
	Run 1 Shaking Table Tailings	30.09	9.78	4.02	6.53	48.44	31.67	22.85	13.86
ST2023110102	Run 2 Shaking Table Feed	0.012	0.00148	13.09	12.64	37.92	7.57	17.48	17.07
	Run 2 Shaking Table Concentrate	16.46	55.40	42.43	27.13	2.28	0.56	17.22	11.44
	Run 2 Shaking Table Middlings	50.20	33.40	8.39	11.35	43.86	7.02	14.11	20.35
	Run 2 Shaking Table Tailings	33.33	11.19	4.23	6.76	46.74	10.94	21.08	13.30
ST2023110103	Run 3 Shaking Table Feed	0.012	0.00157	14.06	13.22	36.36	6.85	16.56	16.44
	Run 3 Shaking Table Concentrate	17.24	54.74	42.27	27.08	1.92	0.45	17.46	11.29
	Run 3 Shaking Table Middlings	49.29	33.70	9.10	11.65	43.21	7.22	14.29	20.60
	Run 3 Shaking Table Tailings	33.47	11.56	4.60	6.90	46.52	11.52	21.80	13.60

	-25 µm Spiral Separation Batch 3				10000				
Run Code	Stream Name	**% Mass Yield**	**% Cr Rec**	**Cr2O3 %**	**FeO%**	**SiO2 %**	**CaO %**	**Al2O3 %**	**MgO %**
SP2023101201	Run 1 Spiral Feed	0.138	0.0131	9.20	8.74	33.32	5.95	14.36	10.68
	Run 1 Spiral Concentrate	29.00	43.92	**14.36**	10.51	29.28	4.83	13.15	10.96
	Run 1 Spiral Middlings	30.39	25.75	8.04	7.89	33.28	6.01	14.03	10.09
	Run 1 Spiral Tailings	40.61	30.33	7.08	7.11	31.52	5.61	13.29	9.23
SP2023101202	Run 2 Spiral Feed	0.149	0.0129	9.55	8.78	31.57	5.70	13.67	10.30
	Run 2 Spiral Concentrate	23.96	40.35	**14.55**	9.10	25.80	4.24	11.61	9.23
	Run 2 Spiral Middlings	26.02	21.26	7.06	7.18	30.22	5.34	12.57	8.88
	Run 2 Spiral Tailings	50.0	38.38	6.63	6.74	30.06	5.34	12.35	8.40
SP2023101203	Run 3 Spiral Feed	0.151	0.0134	9.38	9.50	45.61	8.84	18.92	15.16
	Run 3 Spiral Concentrate	24.09	39.11	**14.36**	12.98	39.74	6.41	15.56	17.05

	Run 3 Spiral Middlings	25.99	22.18	7.55	9.78	52.16	12.70	23.64	14.38
	Run 3 Spiral Tails	49.92	38.70	6.86	5.47	51.86	12.72	25.03	12.43
SP2023101204	Run 4 Spiral Feed	0.171	0.0161	9.38	9.60	46.20	9.38	19.62	15.92
	Run 4 Spiral Concentrate	31.01	47.84	**14.48**	13.34	41.12	6.33	15.62	17.51
	Run 4 Spiral Middlings	24.21	19.46	7.55	6.52	51.38	11.86	22.86	14.30
	Run 4 Spiral Tailings	44.78	32.70	6.86	5.63	51.12	12.44	24.94	12.21
SP2023101205	Run 5 Spiral Feed	0.151	0.0135	9.38	9.41	47.39	10.30	21.18	16.19
	Run 5 Spiral Concentrate	24.09	39.4	**14.53**	12.81	41.46	7.66	17.73	19.09
	Run 5 Spiral Middlings	25.36	21.55	7.55	6.96	47.79	9.99	20.00	13.80
	Run 5 Spiral Tailings	50.5	39.0	6.86	5.98	50.59	11.56	22.94	12.78
SP2023101206	Run 6 Spiral Feed	0.134	0.0121	9.38	9.15	46.39	9.70	19.90	15.21
	Run 6 Spiral Concentrate	27.37	42.40	**13.94**	11.96	40.86	7.19	16.08	17.27
	Run 6 Spiral Middlings	29.43	24.68	7.55	6.63	50.46	11.18	21.58	14.04
	Run 6 Spiral Tailings	43.20	32.91	6.86	5.36	51.63	12.23	23.94	12.06

	-25 µm Spiral Conc Shaking Table Separation Batch 1				10000				
Run Code	Stream Name	**% Mass Yield**	**% Cr_2O_3 Recovery**	**Cr_2O_3 %**	**FeO%**	**SiO_2 %**	**CaO %**	**Al_2O_3 %**	**MgO %**
ST2023110101	Run 1 Shaking Table Feed	0.0117	0.0019	14.37	12.74	35.02	7.92	18.93	14.42
	Run 1 Shaking Table Concentrate	8.97	14.56	**35.56**	24.45	11.55	1.24	14.87	13.63
	Run 1 Shaking Table Middlings	60.93	72.02	14.44	12.65	34.90	7.90	18.83	14.38
	Run 1 Shaking Table Tailings	30.09	13.43	10.82	10.60	38.59	8.75	19.31	13.55
ST2023110102	Run 2 Shaking Table Feed	0.0118	0.0020	14.37	12.74	35.02	7.92	18.93	14.42
	Run 2 Shaking Table Concentrate	7.52	12.88	**34.11**	23.41	11.58	1.48	14.95	13.90
	Run 2 Shaking Table Middlings	59.15	72.00	14.47	12.67	34.31	7.28	17.68	13.77
	Run 2 Shaking Table Tailings	33.33	15.12	12.05	11.24	35.71	7.84	18.08	13.02

ST2023110103	Run 3 Shaking Table Feed	0.0118	0.0020	14.37	12.74	35.02	7.92	18.93	14.42
	Run 3 Shaking Table Concentrate	6.69	13.14	**37.55**	25.35	9.50	0.97	14.84	13.15
	Run 3 Shaking Table Middlings	59.84	73.69	14.83	12.95	34.33	7.36	18.24	14.52
	Run 3 Shaking Table Tailings	33.47	13.17	10.92	10.65	37.27	8.24	18.83	13.44

	-25 µm Spiral Conc Shaking Table Separation Batch 2				10000				
Run Code	Stream Name	**% Mass Yield**	**% Cr Rec**	**Cr_2O_3 %**	**FeO%**	**SiO_2 %**	**CaO %**	**Al_2O_3 %**	**MgO %**
ST-25m2023111801	Run 1 Shaking Table Feed	0.0182	0.0032	14.37	12.96	34.22	7.21	18.02	14.22
	Run 1 Shaking Table Concentrate	9.57	20.20	**37.13**	23.67	16.16	2.08	14.82	16.24
	Run 1 Shaking Table Middlings	48.84	45.79	16.49	12.76	35.66	8.39	18.57	14.39
	Run 1 Shaking Table Tailings	41.58	34.01	14.39	12.03	37.97	8.60	20.83	14.60
ST-25m2023111802	Run 2 Shaking Table Feed	0.0178	0.0030	14.37	12.96	34.22	7.21	18.02	14.22
	Run 2 Shaking Table Concentrate	9.58	19.94	**35.13**	22.22	16.46	2.48	15.04	15.93
	Run 2 Shaking Table Middlings	46.56	45.44	16.48	12.57	35.93	9.03	20.14	14.98
	Run 2 Shaking Table Tailings	43.86	34.62	13.33	11.08	39.01	12.53	24.05	15.66
ST-25m2023111803	Run 3 Shaking Table Feed	0.0180	0.0029	14.37	12.96	34.22	7.21	18.02	14.22
	Run 3 Shaking Table Concentrate	9.82	19.95	**32.90**	21.19	19.60	2.97	14.88	16.12
	Run 3 Shaking Table Middlings	44.76	43.76	15.83	12.35	36.67	10.11	22.07	15.40
	Run 3 Shaking Table Tailings	45.42	36.30	12.94	10.99	39.05	10.37	20.97	14.35

	-106 +25 µm Spiral Conc Shaking table Separation Batch 2				10000				
Run Code	**Stream Name**	**% Mass Yield**	**% Cr Rec**	**Cr2O3 %**	**FeO%**	**SiO2 %**	**CaO %**	**Al2O3 %**	**MgO %**
ST-106+25m2023111801	Run 1 Shaking Table Feed	0.0152	0.0019	13.41	12.32	39.66	9.79	21.06	18.29
	Run 1 Shaking Table Concentrate	46.80%	86.79%	**22.63**	16.68	29.61	6.49	16.53	21.05
	Run 1 Shaking Table Middlings	23.20%	6.26%	3.29	7.73	51.36	11.03	19.51	18.61
	Run 1 Shaking Table Tailings	29.99%	6.95%	2.83	5.44	53.75	26.81	33.94	16.14
ST-106+25m2023111802	Run 2 Shaking Table Feed	0.0146	0.0017	13.41	12.32	39.66	9.79	21.06	18.29
	Run 2 Shaking Table Concentrate	48.85%	87.75%	**20.55**	16.93	28.17	7.47	20.92	23.22
	Run 2 Shaking Table Middlings	21.88%	4.39%	2.30	6.39	54.66	22.73	27.34	20.53
	Run 2 Shaking Table Tailings	29.28%	7.85%	3.07	5.07	54.58	26.48	35.64	16.98
ST-106+25m2023111803	Run 3 Shaking Table Feed	0.0130	0.0018	13.41	12.32	39.66	9.79	21.06	18.29
	Run 3 Shaking Table Concentrate	54.61%	88.80%	**22.63**	16.68	29.61	6.49	16.53	21.05
	Run 3 Shaking Table Middlings	20.48%	4.22%	2.87	6.24	51.98	11.98	22.95	16.31
	Run 3 Shaking Table Tailings	24.91%	6.98%	3.90	6.30	48.55	11.09	21.91	13.61

Run Code	Minus 25 µm Spiral Conc Shaking Table Separation Batch 2	% Mass Yield	% Cr Rec	Cr2O3 %	FeO%	SiO2 %	CaO %	Al2O3 %	MgO %
ST-25m2024011501	Run 1 Shaking Table Feed	0.012	0.002	14.37	12.10	34.42	6.65	16.49	12.91
	Run 1 Shaking Table Concentrate	12.53%	26.65%	**28.01**	20.44	17.36	2.75	13.38	14.40
	Run 1 Shaking Table Middlings	74.13%	61.15%	10.86	10.67	36.09	7.00	16.82	12.61
	Run 1 Shaking Table Tailings	13.35%	12.20%	12.03	11.29	35.63	6.99	16.96	13.01

kl; /	-106 +25µm Spiral Conc 1 Shaking table Separation Batch 5	**% Mass Yield**	**% Cr Rec**	**Cr_2O_3 %**	**FeO%**	**SiO_2 %**	**CaO %**	**Al_2O_3 %**	**MgO %**
ST-106+25µm 2024011701	Run 1 Shaking Table Feed	0.0113	0.0013	13.41	12.14	35.09	5.96	14.75	14.77
	Run 1 Shaking Table Concentrate	18.60	63.32	39.90	24.93	0.00	0.37	15.20	9.85
	Run 1 Shaking Table Middlings	58.24	31.97	6.43	9.46	43.86	6.84	13.44	17.76
	Run 1 Shaking Table Tailings	23.17	4.71	2.38	4.90	47.85	11.20	20.51	11.78
ST-106 +25 µm 2024011702	Run 2 Shaking Table Feed	0.0111	0.0013	13.41	12.14	35.09	5.96	14.75	14.77
	Run 2 Shaking Table Concentrate	18.22	62.94	40.34	25.42	0.00	0.30	15.68	10.29
	Run 2 Shaking Table Middlings	58.13	31.73	6.37	9.41	44.75	7.25	13.98	17.98
	Run 2 Shaking Table Tailings	23.64	5.33	2.63	5.16	47.92	11.06	20.48	11.95
ST-106+25 µm 2024011703	Run 3 Shaking Table Feed	0.0108	0.0012	13.41	12.14	35.09	5.96	14.75	14.77
	Run 3 Shaking Table Concentrate	20.69	68.4	38.28	24.03	0.01	0.58	15.67	10.44
	Run 3 Shaking Table Middlings	54.39	25.44	5.41	8.75	45.62	7.34	13.71	18.06
	Run 3 Shaking Table Tailings	24.92	6.13	2.85	5.72	46.68	10.15	19.53	11.74

Run Code	Shaking Table Middlings Re-Cleaning	% Mass Yield	% Cr Rec	Cr2O3 %	FeO%	SiO2 %	CaO %	Al2O3 %	MgO %
ST-106+25 µm 2024020101	Ave +25 µm Reclean Shaking Table Feed			8.86	12.14	35.09	5.96	14.75	14.77
	Ave +25 µm Reclean Shaking Table Concentrate	15.34	46.60	39.75	24.93	0.15	0.37	15.20	9.85
	Ave +25 µm Reclean Shaking Table Middlings	61.35	46.90	10.00	9.46	43.86	6.84	13.44	17.76
	Ave +25 µm Reclean Shaking Table Tailings	23.31	6.15	3.65	4.90	47.85	11.20	20.51	11.78

APPENDIX E: TAILINGS PARTICLE MAPS.

+106µm Particle map

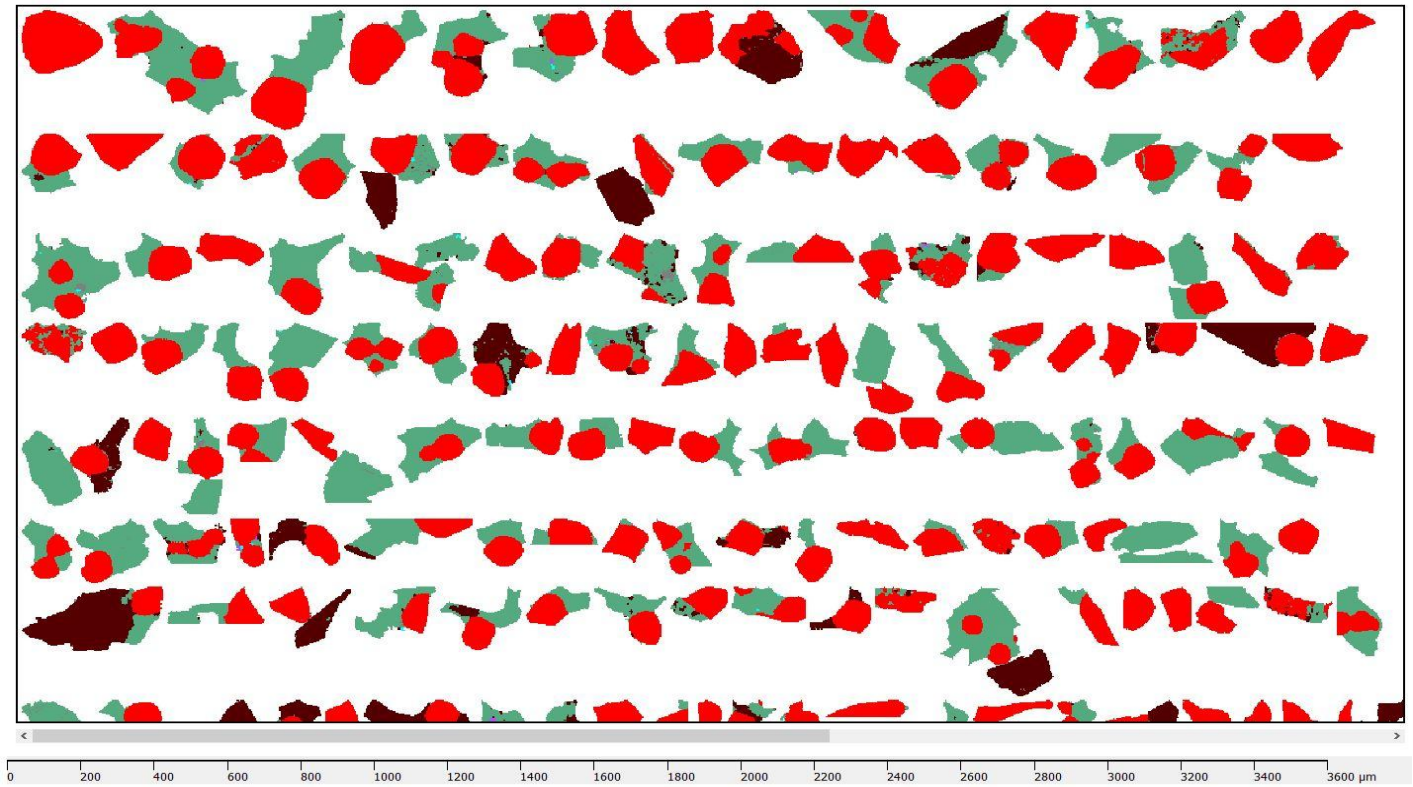

-106+75µm Particle Map

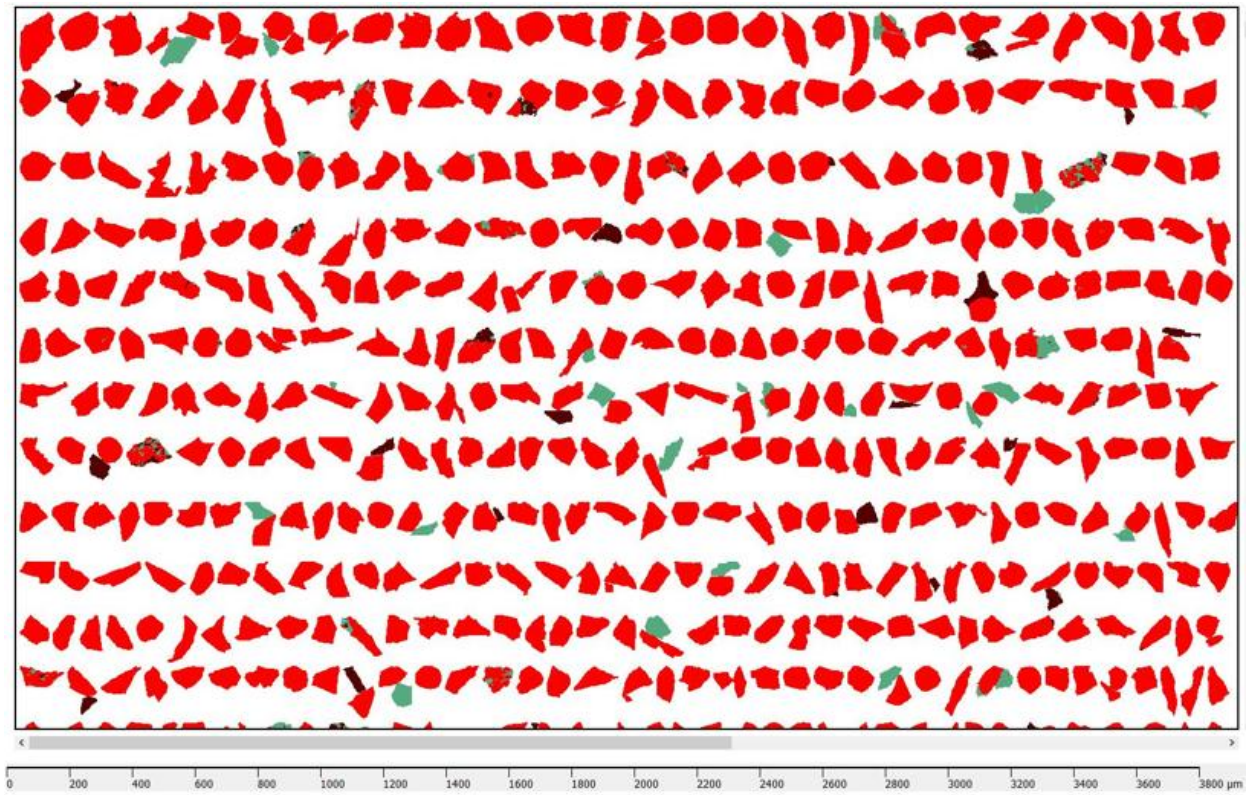

-75+53µm Particle Map

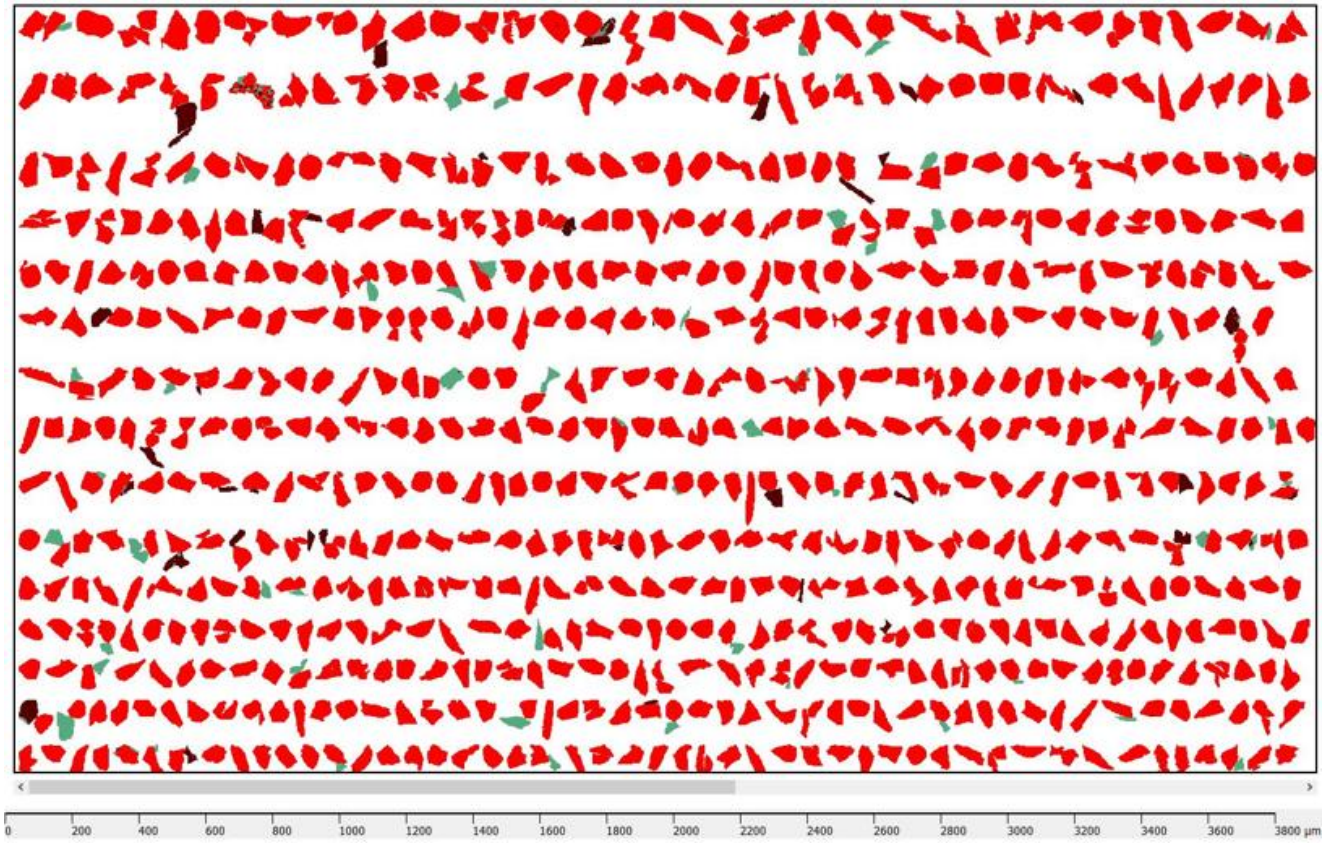

-53+25µm Particle Map

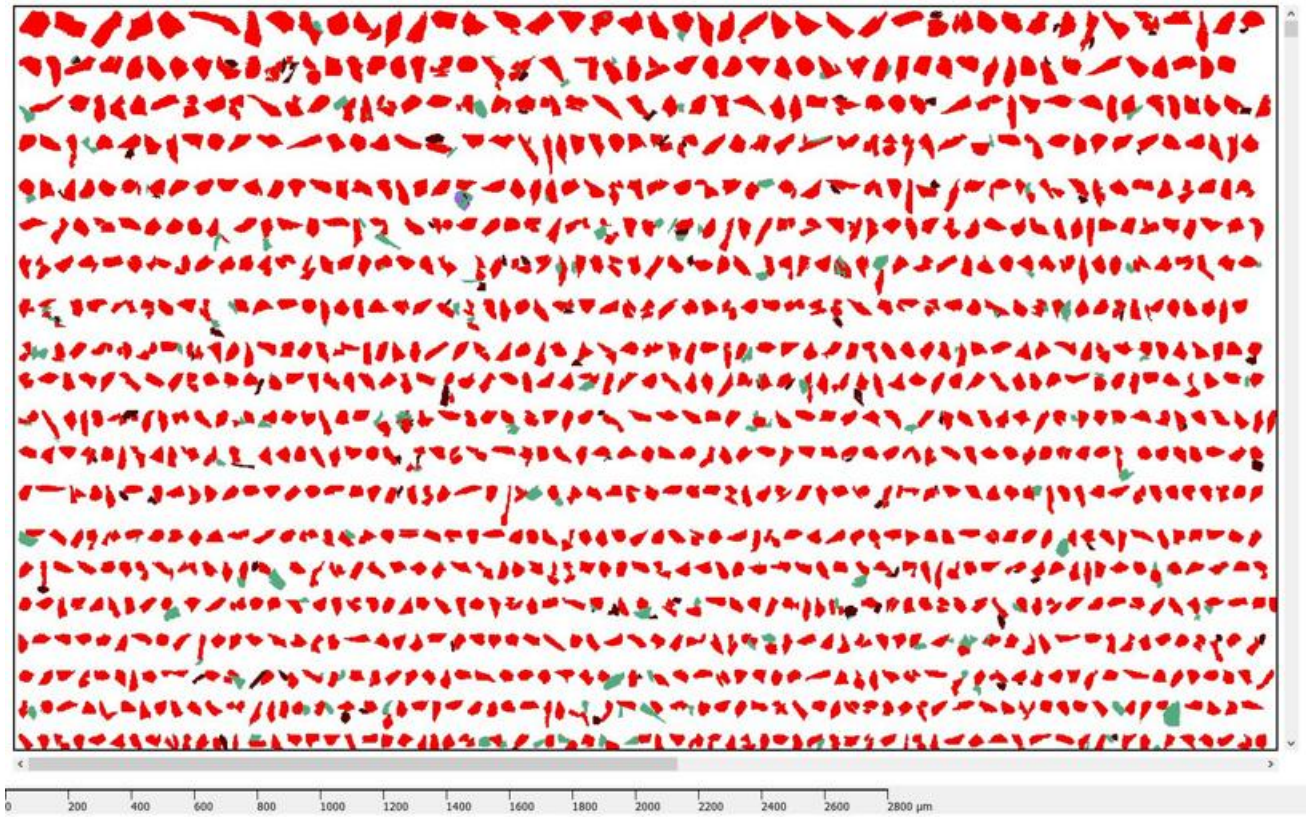

-25 µm Particle Map

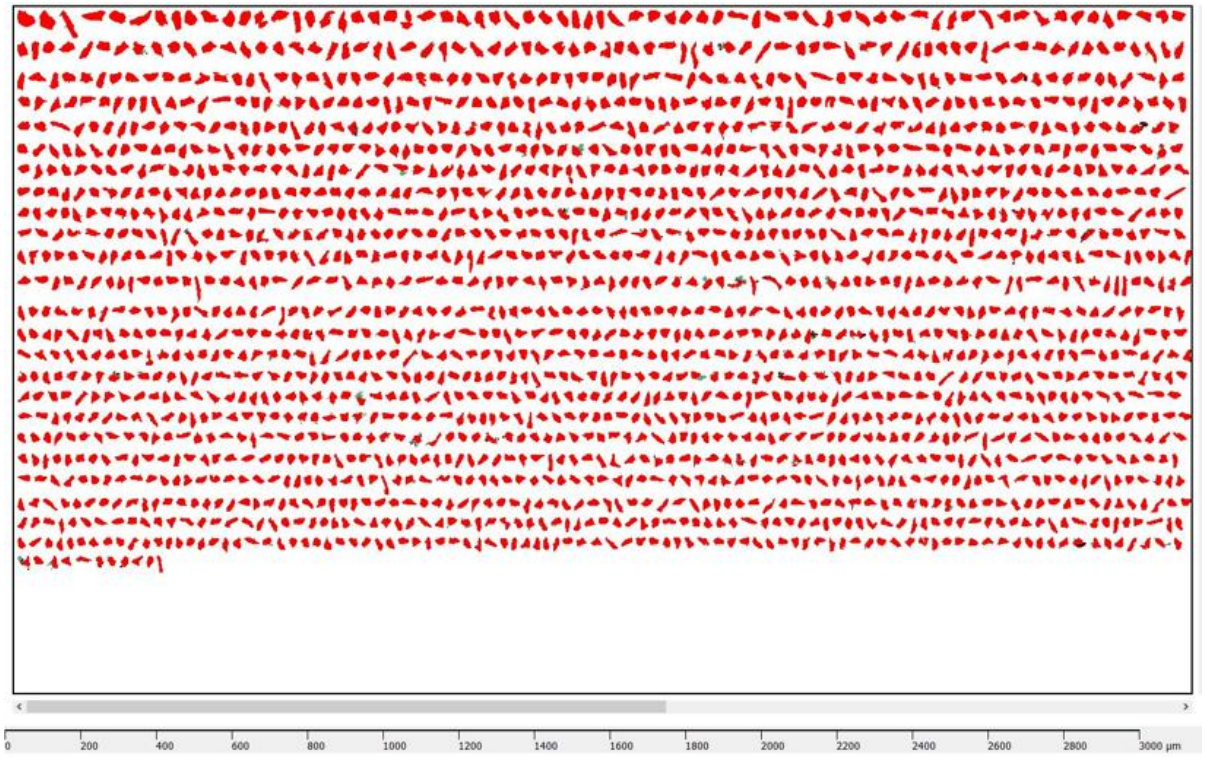

APPENDIX F: ANCILLARY METALLURGICAL AND ANALYTICAL EQUIPMENT AND INSTRUMENTS

		
Pneumatic filter pot for filtration	Rotary sample splitter	5110 ICP-OES
		
Ring Mill for pulverizing samples for wet chemical assay	Test sieves	Watson Marlow feed pump.

		
5 Turn -triple start spiral	Cutter position markers	Cutters and collection box.
		
Belt Magnet and piping.	Magnet feed trough	Magnet bed full of slurry..